C.3

LA-2827

LOS ALAMOS SCIENTIFIC LABORATORY
OF THE UNIVERSITY OF CALIFORNIA o LOS ALAMOS NEW MEXICO

MONTE CARLO CALCULATIONS OF THE EQUATION OF STATE OF SYSTEMS OF 12 AND 48 HARD CIRCLES

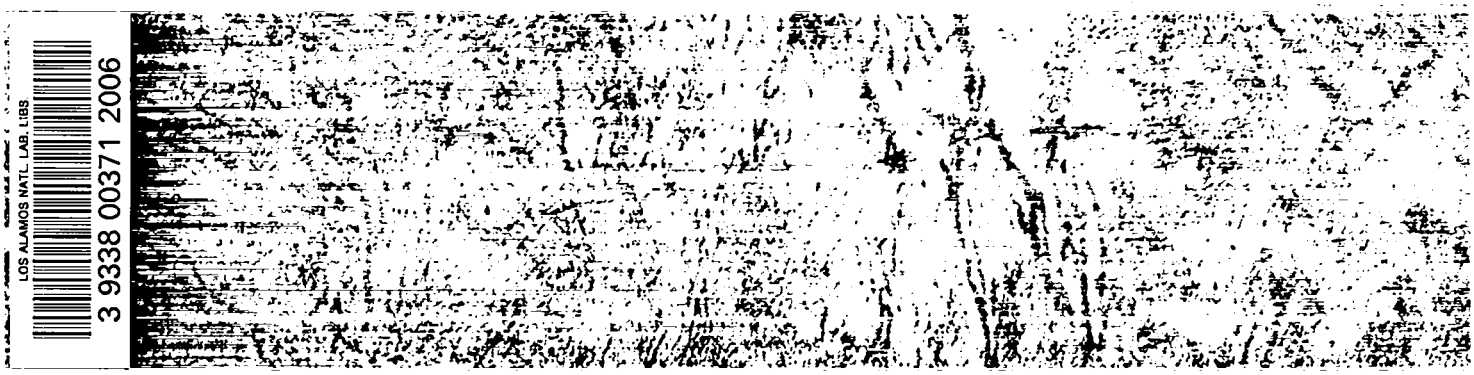

LEGAL NOTICE

Printed in USA. Price $4.00. Available from the

Office of Technical Services
U. S. Department of Commerce
Washington 25, D. C.

LA-2827
UC-34, PHYSICS
TID-4500 (20th Ed.)

LOS ALAMOS SCIENTIFIC LABORATORY
OF THE UNIVERSITY OF CALIFORNIA LOS ALAMOS NEW MEXICO

REPORT WRITTEN: September 1962

REPORT DISTRIBUTED: July 1, 1963

MONTE CARLO CALCULATIONS OF THE EQUATION OF STATE OF SYSTEMS OF 12 AND 48 HARD CIRCLES

by

W. W. Wood

Contract W-7405-ENG. 36 with the U. S. Atomic Energy Commission

ABSTRACT

This report presents Monte Carlo calculations of the equation of state of two systems of hard circles (two-dimensional hard spheres), one consisting of 12 molecules, the other of 48. Periodic boundary conditions are used in both cases.

The two-dimensional systems were considered in order to reduce "surface" effects for a given number of molecules, compared to three-dimensional systems, and in order to ascertain if certain phenomena appearing in previous calculations for three-dimensional systems (possibly indicative of the existence of a solid-fluid phase transition) would appear in the simpler two-dimensional systems. It seemed likely that such might be the case, the negative results of the pioneer Monte Carlo investigation of Metropolis et al., being somewhat suspect on the same grounds as those of Rosenbluth and Rosenbluth for three-dimensional hard spheres, where the behavior in question was not detected, presumably owing mostly to the rather slow computing machinery available at the time.

No such phenomena were found for the 12-molecule system. Except for certain trivial regions of configuration space, the Markov chains seemed to estimate adequately the over-all petit canonical ensemble pressure

throughout the entire density range. The calculated pressure was a monotonically decreasing function of the area, and agreed approximately with the free-volume pressure at high densities, and with the virial expansion at low densities, when account was taken of the theoretical N-dependence at both extremes.

The 48-molecule system gave qualitatively different results, except at the high and low density extremes where the behavior was as described for the smaller system. In the all-important mid-density region the Markov chains were unable to estimate the ensemble average owing to a severe compartmentalization of configuration space into two crystallographically distinct types of configurations. The first, or L, type is related to the familiar regular hexagonal configurations.

In the second, or H, type, two sub-classes could be distinguished. One consisted of configurations best described as irregular, with a stochastic behavior more or less like that expected for a fluid. The other sub-class of H-type configurations was derived from a defect-lattice of 49 molecules in the rectangular cell, one molecule being replaced by a hole. Within the latter configurations, diffusion occurred over a considerable range of densities by the hole-diffusion mechanism. At reduced areas τ in the interval 1.3 to 1.35 ($\tau = 1$ in the close-packed regular hexagonal configuration), the system only infrequently changed back and forth between configurations of L and H type; transitions between the two H subtypes were rather frequent. At $\tau < 1.3$, L-H transitions were not observed. However, the system could be stabilized in H-type configurations of the

defect type by means of "compression" from $\tau > 1.3$, the apparent pressure then considerably exceeding that of L-type configurations at the same reduced area. At $\tau > 1.4$ the L configurations and the defect type of H configurations progressively disappeared, as would be expected.

We conclude that while these phenomena, which are similar to those observed for three-dimensional hard spheres, may perhaps be the finite-system manifestation of the existence of a first-order phase transition in macroscopic systems, the present calculations certainly do not establish that such is the case. Calculations for considerably larger systems are necessary if the question is to be further investigated, as for example in the recent dynamical calculations of Alder and Wainwright for a system of 870 hard circles, in which they obtained a van der Waals loop in the equation of state.

Finally there is presented an extensive statistical analysis of the data reduction procedures required by the present petit canonical ensemble Monte Carlo method, in which the equation of state must be obtained by numerically differentiating the directly estimable "cumulative pair-distribution function." It is concluded that use of Markov chains convergent to isothermal-isobaric ensemble averages might be advantageous. This has been found to be feasible in some unpublished calculations for three-dimensional hard spheres.

PREFACE

This long-overdue report describes the calculations made at the Los Alamos Scientific Laboratory from 1958 up to the present on systems of twelve and forty-eight hard circles (i.e., two-dimensional hard spheres). The previously published results for three-dimensional hard spheres are briefly summarized, as well as some unpublished results.

It is a pleasure to express my appreciation to Dr. Berni J. Alder and Dr. Thomas E. Wainwright of the University of California Radiation Laboratory, Livermore, for many discussions in which ideas and calculational results were exchanged. I am also grateful to Professor Robert D. Richtmyer of New York University, for pointing out the utility of the Markov chain central limit theorem as a basis for the empirical statistical analysis. Above all I am indebted to Mr. Jack D. Jacobson for nearly all the calculator programs used in this investigation, as well as for the over-all supervision of the calculations.

W. W. Wood

September, 1962

TABLE OF CONTENTS

TABLE OF CONTENTS
(continued)

TABLE OF CONTENTS
(continued)

TABLE OF CONTENTS
(continued)

TABLE OF CONTENTS
(continued)

LIST OF FIGURES

LIST OF FIGURES
(continued)

LIST OF FIGURES
(continued)

LIST OF FIGURES
(continued)

LIST OF FIGURES
(continued)

LIST OF TABLES

LIST OF TABLES
(continued)

GLOSSARY OF SYMBOLS

We list here the more important symbols used in this report, along with the number of the section in which each is defined.

Symbol	Description	Section
a	Regular hexagonal lattice spacing.	2.3.3
$A(x)$	Unit step function.	2.1
$b(N)$	Unknown coefficient in Salsburg-Wood theory.	10.1
b_i	Estimate of β_i, q.v.	9.1
c	Coordination number of a close-packed configuration.	3.3.1.1
C	Determinant of matrix $(C_{\alpha\beta})$.	8.3
$C_i(N)$	i^{th} virial coefficient for a system of N molecules.	10.2
$(C_{\alpha\beta})$	Spatial correlation matrix of a sampled set of shell populations.	8.3
d	Diffusion parameter.	2.3.5
$D(x)$	Theoretical standard deviation of a stochastic variable x.	8.2.1
$E(x)$	Expected (mean) value of a stochastic variable x.	8.2.1
$f^{(1)}$	Degrees of freedom of $s^{(1)^2}$.	9.2.2.1
$f^{(2)}$	Degrees of freedom of $s^{(2)^2}$.	9.2.2.1
$f^{(12)}$	Degrees of freedom of $s^{(12)^2}$.	9.2.2.1
$G(\zeta)$	Ensemble average of $G(\zeta, \vec{r})$; i.e., the familiar cumulative pair-distribution function.	2.1
$G(\zeta, \vec{r})$	Cumulative pair-distribution function in configuration space.	2.1

GLOSSARY OF SYMBOLS
(Continued)

Symbol	Description	Section
$G(\zeta, t)$	$G(\zeta, \vec{r})$ at time step t of Markov chain realization.	2.2
$\tilde{G}(s, \alpha)$	The s^{th} time-smoothed observation of $G(\zeta, t)$ at $\zeta = \zeta_\alpha$.	2.3.4
$\overline{G}_t(\zeta)$	Over-all estimate of $G(\zeta)$ at time t. We will frequently abbreviate $\overline{G}_t(\zeta_\alpha)$ as $\overline{G}_t(\alpha)$.	2.2
$G_{1\alpha}, G_{2\alpha}$	Coefficients of skewness and excess of an observed set of shell populations of shell α.	8.5
$i(t)$	Molecule provisionally displaced at time t.	2.3.2
k	Boltzmann's constant.	2.1
K	The number of values ζ_α^2 , $\alpha = 1(1)K$, at which the c.d.f. is estimated.	2.3.4
L	The number of 2-molecule rectangular unit cells whose longer sides compose one edge of V.	3.1.4
M	The number of 2-molecule rectangular unit cells whose shorter sides compose one edge of V.	3.1.4
n	The number of time-smoothed observations.	8.2
N	The number of molecules in a hard-sphere (or hard-circle) system.	3.1.4
p	Thermodynamic pressure in the petit canonical ensemble.	2.1
$\hat{p}$	Pressure parameter of the isobaric-isothermal ensemble.	11.4
(p_{ij})	Fundamental transition probability matrix for a Markov chain.	2.3.2
$P_{N\hat{p}T}(V)$	Probability density of the fluctuating volume in the constant pressure ensemble.	11.4
$P(x)$	Cumulative probability function of a stochastic variable x.	---

GLOSSARY OF SYMBOLS
(Continued)

Symbol	Description	Section
r_{ij}	$\lvert\vec{r}_{ij}\rvert$.	1.1
$r^{(\alpha)}$	Mean-square successive-difference ratio statistic for a sequence of observed shell populations for shell α.	8.2.2
$\vec{r}$	The set of N vectors $\vec{r}_1, \vec{r}_2, \cdots, \vec{r}_N$.	2.1
$\vec{r}(t)$	$\vec{r}$ at time t.	2.2
$\vec{r}_i$	Two-component position-vector of molecule i.	2.1
$\vec{r}_{ij}$	$\vec{r}_j - \vec{r}_i$.	---
$R^{(\alpha)}$	Observed total number of runs in shell population of shell α.	8.2.1
$R_k^{(\alpha)}$	Number of runs of length k observed in shell population of shell α.	8.2.1
s^2	Estimate of σ^2 .	9.1
s_α^2	Sample variance of observed shell population for shell α.	8.2.2
$\hat{s}_\alpha^2$	Smoothed s_α^2 .	9.2.1
$s^{(1)^2}$	Within-shells estimate of σ^2 .	9.2.2.1
$s^{(2)^2}$	Estimate of σ^2 obtained from the variation of observed average shell populations about empirical regression curve.	9.2.2.1
$s^{(12)^2}$	Pooled estimate of σ^2 .	9.2.2.1
t	Markov chain "time".	1.1
T	Thermodynamic temperature.	---

GLOSSARY OF SYMBOLS
(Continued)

Symbol	Description	Section
u	Standardized normal deviate.	---
v	Volume (area) per molecule for hard-sphere (hard-circle) system.	1.2, 2.1
v_o	Volume (area) per molecule for face-centered cubic (regular hexagonal) close-packed hard spheres (circles).	1.2, 2.1
V	Volume (area) of system of N hard spheres (circles).	2.1, 3.1.1
w'_α	Weight factors.	9.2.1
x	Matrix of independent variables in regression analysis.	9.1
y	Least squares estimate of η .	9.1
Y	Column vector $(Y_1, Y_2, \cdots, Y_K)$ or $\overline{Y}_1, \overline{Y}_2, \cdots \overline{Y}_K)$.	9.1
$\overline{Y}_\alpha$	Sample mean of a set of observed shell populations $Y_{1\alpha}, Y_{2\alpha}, \cdots Y_{n\alpha}$.	8.2.2
$Y_{s\alpha}$	Observed shell population for shell α over the s^{th} time-smoothing interval.	7.4
$Z_N(V)$	Gibbs phase integral in configuration space.	2.1
β_i	Theoretical coefficient of α^i in approximating polynomial for η_α .	7.5
γ_i	Theoretical coefficient of α^i in approximating polynomial for $G(\zeta_\alpha)$.	7.5
δ	Maximum displacement parameter.	2.3.2
$\delta(x)$	Dirac delta function.	2.1
Δr^2	$\zeta^2_{\alpha+1} - \zeta^2_\alpha$.	2.3.4
Δt	Time-smoothing interval.	2.3.4

GLOSSARY OF SYMBOLS
(Continued)

Symbol	Description	Section
ζ	Argument of cumulative pair distribution function.	2.1, 2.4
η	Column vector of components η_α .	9.1
η_α	Theoretical shell population of shell α.	7.4
κ	Compressibility factor.	2.1
$\kappa^*(\tau; N)$	Free-volume equation of state with an arbitrarily appended $O(N^{-1})$ correction.	10.1
κ_{FV}	Free-volume approximation for compressibility factor.	3.3.1.2
$\kappa_{N,i}(\tau)$	Virial equation of state for a system of N molecules truncated to a polynomial of degree i in τ^{-1}.	10.2
ν	Degree of regression polynomial approximating η_α.	7.5
σ	Diameter of a hard-sphere or hard-circle molecule.	2.1
σ^2	Unknown scalar factor in φ.	9.1
τ	Reduced volume (area) per molecule in a system of hard spheres (circles).	1.2, 2.1
τ^*	Reduced area per molecule of a close-packed configuration.	3.3.1.1
φ	Theoretical shell population covariance matrix.	9.1
$\tilde{\varphi}$	φ/σ^2.	9.1

Chapter 1

INTRODUCTION

1.1 Preliminary Description of the Monte Carlo Method

The Monte Carlo method used in the calculations to be discussed in this report is essentially that orginally described by Metropolis, et al.[1] Its theoretical basis has been discussed in a number of papers,[2-5] so that it will suffice to recall here that it is a prescription for defining a stationary Markov chain with discrete states and discrete time whose time average converges stochastically to an ensemble average with a given weight function. In this report we will consider only the classical mechanical petit ensemble of Gibbs, whose weight function (unnormalized) is the usual Boltzmann factor. The desired ensemble averages are then estimated by the corresponding time averages over a particular realization or development of the chain carried out to a large number of time steps on a high-speed computing machine.

It will be convenient to adopt the following terminology: A system is specified when a space or class of possible states is defined. A (Markov) chain for such a system is specified when a stochastic matrix of

one-step transition probabilities between all pairs of these states is given. A realization (or development) of such a chain is a sequence of states actually traversed by the system in the course of a stochastic evolution according to these transition probabilities.

It must be emphasized that the "time" mentioned in the above description has no relation to any actual physical time (except the machine time involved in the development of the chain), nor does the motion of the state point bear any detailed relation to any actual dynamical motion of the molecular system. The procedure is a numerical method for estimating classical statistical mechanical ensemble averages, and indeed since it is a classical method (i.e., not quantum mechanical), the integrations over momentum variables involved in the ensemble averages can be performed analytically, so that as actually carried out for a system of N two-dimensional molecules the method is a random walk in the 2N-dimensional configuration space of the system.

The original investigation[1] reported calculations for a system of 224 hard spheres in two dimensions (hard circles), and subsequently Rosenbluth and Rosenbluth[6] considered systems of 256 three-dimensional hard spheres and 56 two-dimensional Lennard-Jones molecules. Our own work began with systems of 32 and 108 three-dimensional Lennard-Jones molecules.[2] From this point on, the term "hard sphere" unless further qualified will refer to the three-dimensional case; "hard circle," to the two-dimensional case.

In the meantime Alder and Wainwright[7] at the Livermore Laboratory, had devised their molecular-dynamical method and applied it to systems of

hard spheres. As the name implies, this method calculates thermodynamic functions (as well as some transport properties) by time-averaging over the actual dynamical phase-space trajectory of the molecular system, starting from a suitable initial state, and integrating the elementary Newtonian equations of motion over long enough times so as to attain dynamical equilibrium.

The Monte Carlo statistical mechanical method and the dynamical method, when applied to the same molecular system, ought to give the same thermodynamic results [at least to $O(N^{-1})$], if the quasi-ergodic hypothesis of statistical mechanics is correct. This hypothesis, though widely believed, has not been rigorously established,[8] so that comparison of results from the two methods is of some interest in itself.

The preliminary results of Alder and Wainwright for hard spheres, of which we were privately informed, in fact differed significantly from those of Rosenbluth and Rosenbluth,[6] and this naturally led us to adapt our then existing program for three-dimensional Lennard-Jones molecules[2] to calculate the equation of state of systems of 32, 108, and 256 hard spheres. The results indeed exhibited a behavior qualitatively different from that obtained by Rosenbluth and Rosenbluth,[6] which we attribute to their relatively slow computing machine (Maniac I); the phenomena in question (to be described below) are likely to appear only after a rather long "time".

Accordingly programs especially adapted to the hard-sphere system were prepared,[5] and a re-examination of the equation of state of hard

spheres by the Monte Carlo method was undertaken in collaboration with Alder and Wainwright's dynamical investigation. Preliminary results by both methods were published simultaneously[3,9] for systems of 32 and 108 molecules, as well as additional though still incomplete Monte Carlo results,[5] and a rather complete account of the molecular-dynamical results for systems of 4 to 500 molecules.[10]

1.2 Summary of Results for Three-Dimensional Hard Spheres

The hard-sphere equation of state calculations by the Monte Carlo method are summarized and compared with the molecular-dynamical results in Fig. 1.1, taken from Ref. 5. Also shown is the free-volume hard-sphere equation of state[11] and the five-term virial equation of state of Rosenbluth and Rosenbluth.[6] In Fig. 1.1 the abscissa τ is the ratio v/v_o where v is the volume per molecule, v_o is the face-centered cubic close-packed volume per molecule, and the other symbols have their usual significance: p is the pressure, T the temperature, k Boltzmann's constant.

Two branches of the equation of state are shown in Fig. 1.1 for $\tau \leq 1.6$. In the interval $1.52 < \tau \leq 1.60$ the branches arose from separately averaging the high and low plateaus of realizations having the typical appearance of Fig. 1.2 (also taken from Ref. 5). Similar secular fluctuations occurred in the molecular-dynamical results, and were treated in the same way.

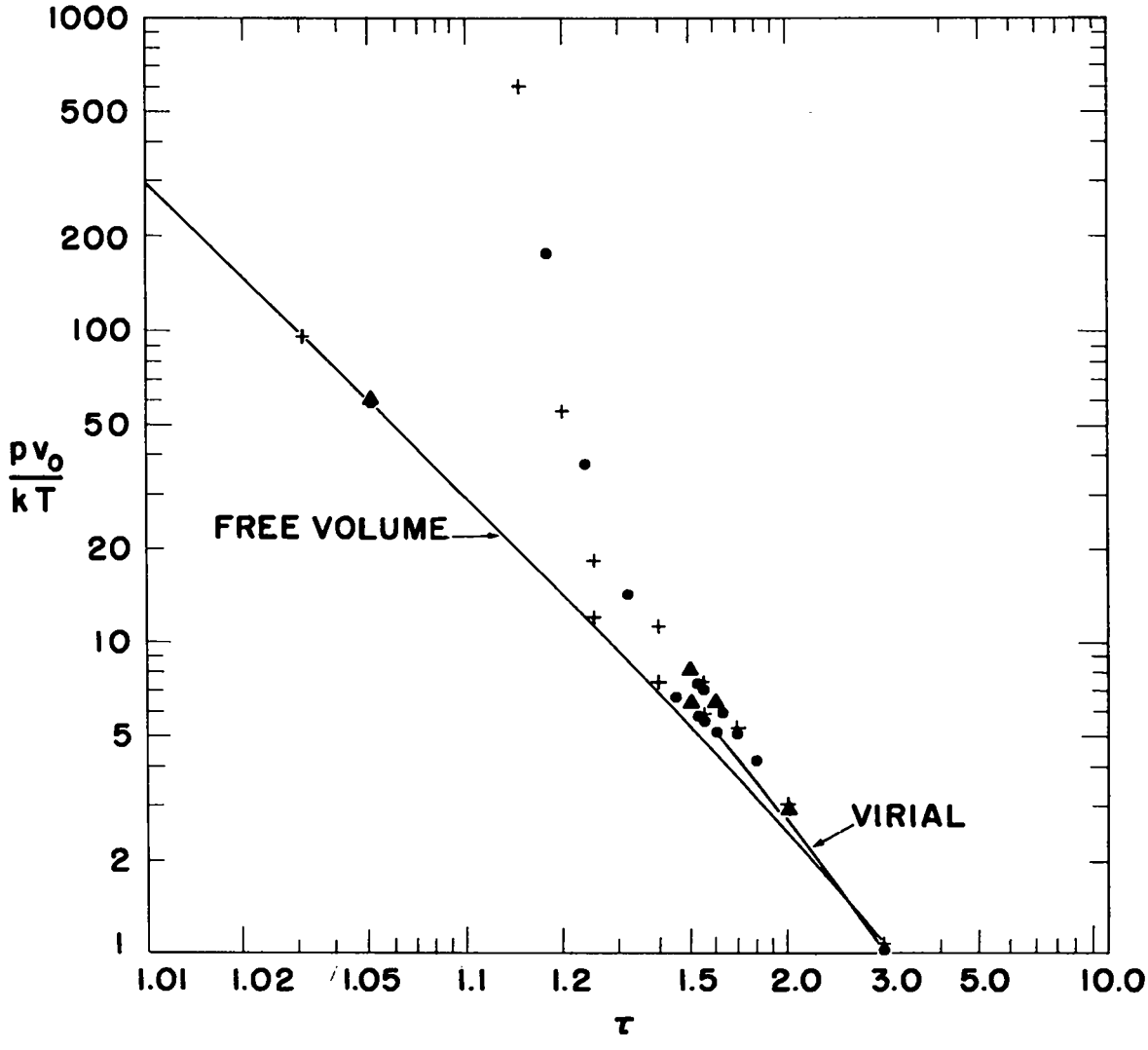

Fig. 1.1 The equation of state of hard spheres, as reported in Ref. 5: (●, ▲) Monte Carlo method for N = 32 and 256, respectively; (+) molecular dynamics, N = 32 (Ref. 9).

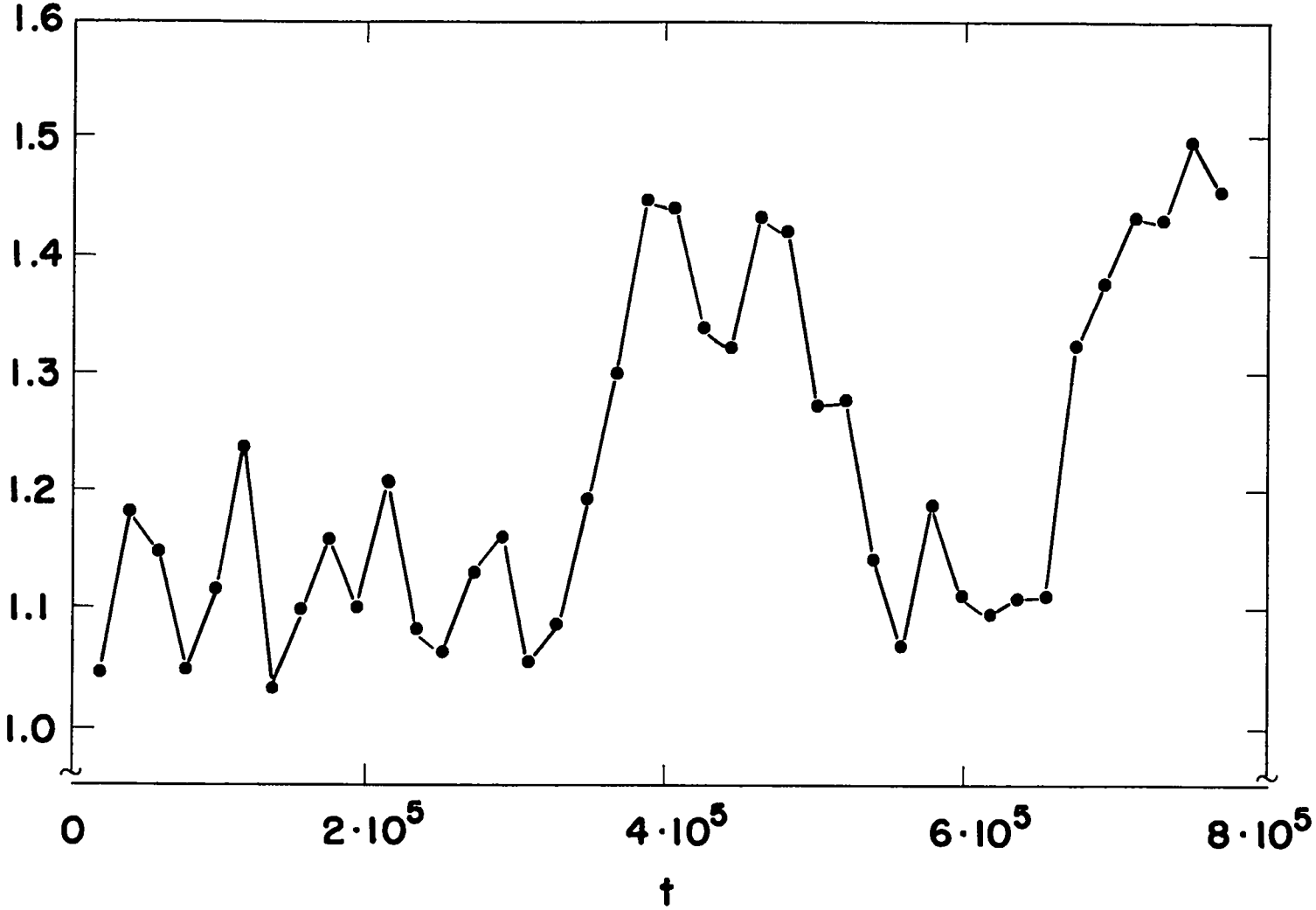

Fig. 1.2 Control chart for a typical realization of a Markov chain for a system of 32 hard spheres at $\tau = 1.55$. The ordinate is the time-smoothed cumulative pair-distribution function at a distance 1.026σ. The abscissa is the "time" or number of steps in the random walk, which began at the regular face-centered cubic lattice configuration.

1.2.1 "Hourglass" model of configuration space.

This behavior led us to the following visualization of the geometry of 3N-dimensional configuration space which is undoubtedly over-simplified but which affords a convenient model for the observed behavior, and which motivated much of the subsequent investigation. We imagine that at these densities the accessible region of phase space is essentially hourglass-shaped, and we label the two chambers of the hourglass L (low) and H (high) according to whether an average restricted to the particular chamber leads to a high or low pressure. This two-chamber description is suggested by the essentially two-level appearance of Fig. 1.2. The constriction of the hourglass is imagined to be relatively narrow, and to contain only a small fraction of the total accessible volume, as suggested by the abrupt and relatively infrequent shifts in level in Fig. 1.2. The state point representing the face-centered cubic lattice configuration (which is the usual starting point of the random walk) is deduced to be in chamber L from the fact that random walks begun from it typically show initially a low plateau (e.g., Fig. 1.2), in this interval of τ. In these terms the random walk of Fig. 1.2 can be summarized as roughly $3.5 \cdot 10^5$ steps in chamber L, $1.7 \cdot 10^5$ steps in chamber H, $1.3 \cdot 10^5$ steps in chamber L, then $1.1 \cdot 10^5$ steps in chamber H, after which the calculation was terminated.

Larger values of τ in the interval 1.52 to 1.6 seemed to lead to shorter low plateaus and longer high plateaus; at $\tau > 1.6$ there was seldom a noticeable low plateau. At smaller values of τ in this interval

the system tended to remain in chamber L for very long times; if it succeeded in reaching chamber H it also remained there for a long time. (These observations should be understood to apply to the 32-molecule system; very few calculations were performed with the larger systems in this range of reduced volumes.) These observations led us to conclude that as τ increases the hourglass connection widens, with the chambers probably becoming indistinguishable at $\tau > 1.6$. There is some suggestion that at $\tau = 1.6$ chamber H is probably much larger than chamber L. For τ near 1.52 the relative volumes are unknown, and the connection between them very constricted. For $\tau < 1.52$ neither the Monte Carlo nor the dynamical calculations observed the 32-molecule system to leave the L chamber, when the calculation was started from the face-centered cubic (f.c.c.) lattice.

We were naturally led to examine the geometrical structure of configurations sampled from the low and high plateaus of random walks in the interval $1.52 \leq \tau \leq 1.6$, though the number of configurations which could be investigated was rather small due to the difficulty of adequately visualizing the three-dimensional structures. Not unexpectedly, we found that configurations selected from a low plateau (i.e., according to our model, points in the L chamber of configuration space) were recognizably close to the f.c.c. lattice arrangement. Furthermore, we noted that diffusion (i.e., interchanges of neighboring molecules) was very rare, perhaps non-existent, throughout the duration of a L plateau. On the other hand, we were unable to recognize any particular regularity in

configurations sampled from high plateaus (i.e., points in the H chamber), during which considerable diffusion occurs.

The infrequent molecular interchanges within a L plateau indicate a revision of our model of configuration space to show N! chambers of type L, corresponding to the N! permutations of the molecules, with interconnections which are more constricted than the L-H connections. This is crudely indicated in Fig. 1.3 by showing two L chambers. Two H chambers are also shown, although one might be consistent with the observations for $1.52 < \tau \leq 1.6$, because at smaller values of τ they are expected to appear (see below). The H-H connection is shown wider than the L-H

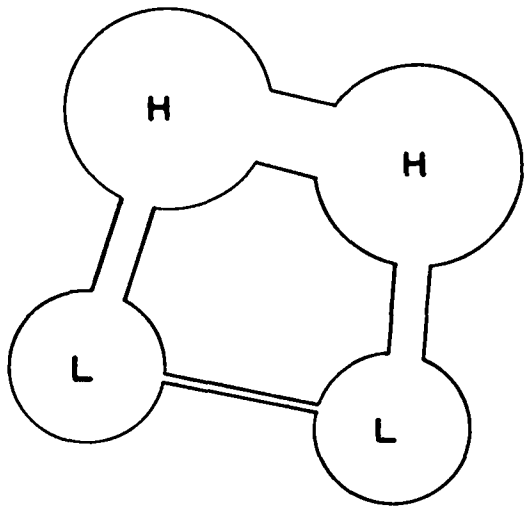

Fig. 1.3 A schematic diagram of the hourglass model 3N-dimensional configuration space of a system of hard spheres near $\tau = 1.55$.

connections, in agreement with the observations above.

It is obvious that for Markov chain realizations such as that of Fig. 1.2, the over-all time average, which should converge to the desired ensemble average, is in fact very poorly convergent. On the other hand, the average over a particular L or H plateau may be reasonably convergent, and if the plateau is sufficiently long this average is not too sensitive to uncertainities concerning the beginning and end of the plateau. According to our model (Fig. 1.3) such averages estimate ensemble averages restricted to the L or H chamber, which are evidently lower and upper bounds, respectively, to the complete average. Such, then, was the motivation leading to the double-valued equation of state of Fig. 1.1 in the interval $\tau = 1.52$ to 1.6.

1.2.2 Possible phase transition.

The properties of the L states outlined in the preceding section are strikingly similar to those usually associated with a solid crystalline phase: (1) approximately regular lattice (f.c.c.) structure; (2) inhibited diffusion. Similarly, the properties of the H states resemble those of a fluid: (1) irregular structure; (2) free diffusion; (3) higher pressures than L states at the same τ. Taken in conjunction with the considerable discussion which has been carried out in the statistical mechanical literature concerning the existence of a solid-fluid phase transition for systems of hard spheres, these observations naturally led us [3,9] to suggest them as tentative support for the existence of such a

phase transition. This interpretation was also strongly supported by the appearance of essentially the same phenomena in the Monte Carlo calculations[2] for three-dimensional Lennard-Jones molecules at a pressure and temperature in reasonable agreement with extrapolation of the experimental melting locus of argon. On the other hand, of course, it was possible to believe that these phenomena were artifacts of the small number of molecules which were used in the calculations, rather than characteristic of the behavior of macroscopic systems.

In addition to whether or not a first-order phase transition exists for hard spheres, there are also differences of opinion as to whether, if such a transition does exist, the exact petit canonical ensemble reduced pressure pv_o/kT should be a monotonically decreasing function of volume at fixed T and fixed finite N, or whether it might exhibit loops more or less similar to those of the van der Waals equation of state. The best discussion of this problem seems to be that of Hill.[12] The only cases in which exact calculations exist are for certain simple lattice gases with small N, where loops in fact do occur. It is thus of some interest to examine the possibilities on the basis of our simple configuration-space model (Fig. 1.3), again under the assumption that the connections have negligible volume. We denote the volumes of the L and H chambers by $\omega_L(\tau,N)$ and $\omega_H(\tau,N)$, and define three pressures: $p(\tau,N)$, the result of averaging over both types of chambers; $p_L(\tau,N)$, obtained from the L chambers alone; and $p_H(\tau,N)$, from the H chambers. The usual petit ensemble theory gives

$$p_L v_o/kT = N^{-1}(\partial\, \ell n\, \omega_L/\partial\tau)_N \quad ;$$

$$p_H v_o/kT = N^{-1}(\partial\ \ell n\ \omega_H/\partial\tau)_N \quad ;$$

$$pv_o/kT = N^{-1}\left[\partial\ \ell n\ (\omega_L + \omega_H)/\partial\tau\right]_N \quad .$$

The last equation can be written by use of the first two as

$$p = (1 - w)p_L + wp_H \quad ,$$

$$w = \omega_H/(\omega_L + \omega_H) \quad ,$$

giving the expected result that the over-all average pressure p is just the average of p_L and p_H weighted in proportion to their volumes ω_L and ω_H. Now consider the variation of τ at fixed N; on the right side of the above equation for p, the functions w, p_L, and p_H all vary. Let us suppose, as is intuitively plausible, that p_L and p_H are both monotonically decreasing functions of τ, as indicated in Fig. 1.4. Suppose in addition that the weight function w increases from values near zero to values near one, as τ increases over a small interval, as shown in the figure. If this increase is abrupt enough, it is clear that van der Waals loops will appear, as is most easily seen by considering the limiting case in which w approaches the unit step function (see figure). On the other hand, a more gradual increase in w can evidently result in a monotone p. Thus we see that either type of isotherm could result from our model.

Accepting for the moment this first-order phase-transition interpretation of the observations, let us consider the effect of increasing the number of molecules. For large enough N, and values of τ between the phase boundaries, we expect that a typical configuration should be

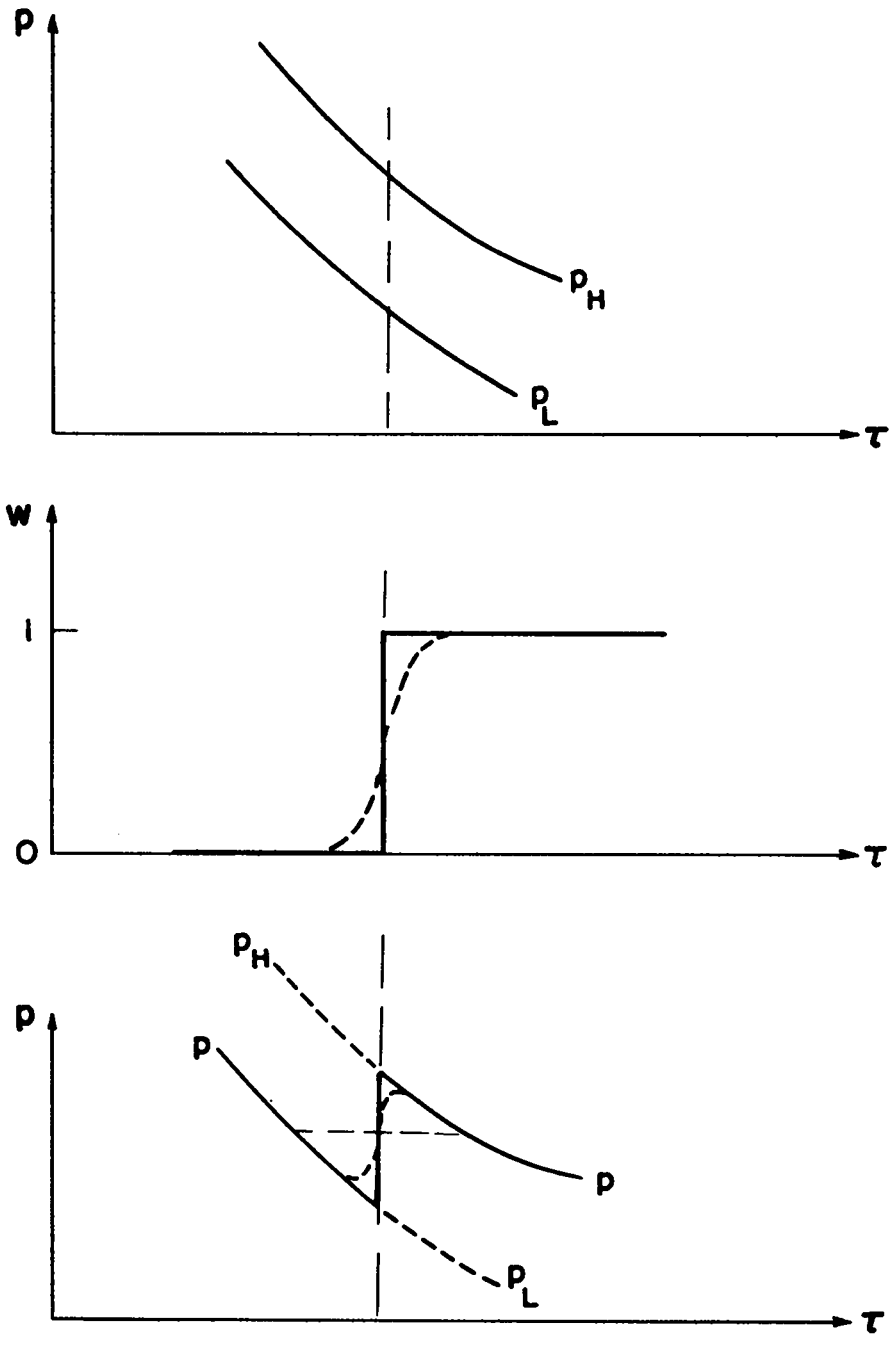

Fig. 1.4 A possible mechanism for the occurrence of van der Waals loops for the model of Fig. 1.3.

one of coexistent phases, some portions of the system being crystalline, others fluid. The failure to observe this in small systems can be reasonably interpreted as being due to large interfacial effects. Thus at larger values of N we would expect Fig. 1.3 to change. Regions of mixed L and H character should appear and be predominant except near the phase boundaries. Exactly how this will occur is not clear; a likely possibility is that the L-H connections expand and dominate the L and H regions.

1.2.3 "Extended fluid" branch of the equation of state.

As already suggested in Section 1.2.1, it seemed likely that the failure to observe H states in the realizations started from the f.c.c. lattice at $\tau < 1.52$ was due to constriction of the L-H connections, rather than to the complete disappearance of the H region of configuration space. The well-known phenomenon of supercooling of liquids below their freezing point, and the existence of "random close-packed" hard-sphere configurations[13] also influenced our thinking in this respect, as a result of which we devised the following "compression procedure" for obtaining starting configurations in the H region at reduced volumes below 1.52.

We begin with an arbitrarily chosen H state from a high plateau of a realization at $\tau > 1.52$. With the centers of the molecules fixed in the Monte Carlo cell, the molecular diameter is increased (i.e., τ is decreased) to a value at which the closest pair of molecules is just

in contact. The standard Monte Carlo random walk is then carried out from this starting point until one or the other member of this pair is successfully moved. The molecular diameter is then again increased until the closest pair (usually a different pair than in the previous step) is in contact, etc. In this way a sequence of configurations is obtained with decreasing reduced volumes; since the "compression" process is rather rapid (at least in the early stages) the state point was expected to remain with high probability in the H region. Such configurations were used as the starting point for the usual random walk realizations, and gave the points shown in Fig. 1.1 on the upper branch of the equation of state for $\tau < 1.52$. Without intending to prejudice the decision with respect to a first-order phase transition, we call this part of the upper branch the "extended fluid" branch of the equation of state.

It is a priori quite possible that at high densities H chambers of qualitatively different type (i.e., not equivalent under a permutation of the molecule labels) may be present, and their connections may become very constricted or non-existent. In such a case more than one upper branch of the equation of state may be present (at fixed small N). This might explain the possibly significant difference between the "extended fluid" points obtained by us and those obtained by Alder and Wainwright (Fig. 1.1), who used a similar but more gradual "compression" procedure.

Sample configurations from these extended fluid realizations at $\tau = 1.32$ and $\tau = 1.18$ were examined by constructing rather crude

three-dimensional models, and various two-dimensional projections. At $\tau \leq 1.32$ diffusion was absent, in contrast to the rather free diffusion at $\tau > 1.52$ already mentioned. (In terms of our model this implies N! regions of the H type, either disconnected or having very constricted connections.) The highest density ($\tau = 1.18$) configurations fluctuated very little, and were describable as rather distorted body-centered cubic arrangements, apparently quite different from the structure described by Alder and Wainwright[7] at about the same density (thus suggesting the presence of more than N! H regions of at least two non-equivalent types).

From Fig. 1.1 it is clear that the "extended fluid" branch of the equation of state has an apparent asymptote in rough agreement with Scott's[13] value of $\tau \approx 1.16$ for "dense random packing", but the agreement is most likely accidental, since one would hardly expect to duplicate "dense random packing" with as few as 32 molecules (no realizations were generated on this branch with $N > 32$).

1.3 Retreat to Hard Circles

The indications, described in the previous section, of a possible phase transition in systems of hard spheres led us to question whether similar phenomena might also be present in systems of hard circles and have been missed in the original investigation,[1] again due to the slowness of the calculators of that date (as well as to the relatively large number of molecules which was chosen). As far as statistical mechanical

theory is concerned, the situation for hard circles is the same as for hard spheres. The first-order phase transition has not been shown to exist, nor has it been shown not to exist. Only in the one-dimensional case, where the complete equation of state can be obtained analytically, is an exact answer known: in this case, there is no transition.

Aside from an investigation of the two-dimensional case as a question in its own right, there were important reasons of convenience for transferring our efforts to it. At that time the available calculators were IBM type 704, and it seemed to us that we had about reached the practical limit of the ability of calculators of that speed to attack the phase-transition problem in the three-dimensional systems. The over-all average of 32-molecule realizations like that of Fig. 1.2 clearly could not be determined; that realization, for example, required between four and five hours of machine time, and its over-all average (as distinct from the within-plateau averages) is essentially worthless. Without a determination of such over-all averages at a number of points in and near the possible transition region, the nature of the p-V isotherm even for the small system remains in question. Further, even if the equation of state for the 32-molecule system could be determined, and displayed, say, a van der Waals loop, the significance of this result for macroscopic systems would still be in doubt. Obviously, the inherent limitation of the method to very non-macroscopic numbers of molecules prevents one from even expecting to <u>prove</u> the existence of a first-order phase transition by such means. The most that can be expected is a

demonstration by calculations for larger systems ($N \sim 1000$, say) that the phenomena appear likely to persist as N increases. [For example, one can imagine that a van der Waals loop for small N might shrink as N increases in such a way as to produce a second-order transition for macroscopic systems ($N \to \infty$).]

As already mentioned, there is some reason to suspect that at larger values of N the statistical behavior may be less difficult (appearance of coexistent phases, rather than secular fluctuation between the two pure phases). However, larger values of N were already very time consuming outside the "transition" region, and could certainly not be expected to be less so inside it. Thus, an important reason for investigating two-dimensional systems was the fact that with calculationally feasible values of N (which are only slightly greater than in three-dimensions), the interfacial effects believed to be responsible for much of the difficulty should be considerably reduced.

An incidental advantage of the two-dimensional case is the greater ease with which the geometrical structure of sample configurations can be studied.

Accordingly, in 1958 we began the calculations which will be described in this report. Unfortunately, soon after most of the calculations were completed the investigation was put aside in favor of other unrelated problems, and only recently have we returned to the work of reducing the results to a form suitable for publication. Preliminary results were made available to Helfand, Frisch, and Lebowitz,[14] for comparison with their approximate analytical results.

Alder and Wainwright have also applied their dynamical method to hard circles, and in a recent paper[15] present an isotherm displaying a van der Waals loop for a system of 870 molecules.

In the meantime our own situation with respect to calculator speed has improved, with the availability of IBM-7090 and IBM-7030 machines. In the near future we will attempt to verify the molecular-dynamical result for a large system of hard circles. In this report we present Monte Carlo results for two small systems of 12 and 48 molecules, which are of some interest in their own right, and whose understanding ought to facilitate the investigation of larger systems.

A considerable effort has been made to develop data reduction methods which can give estimates of the precision of the equation of state results, as will be described.

Chapter 2

THE MONTE CARLO METHOD FOR SYSTEMS OF HARD CIRCLES

2.1 Derivation of the Equation of State

The petit canonical ensemble expression for the pressure of a system of hard circles in terms of the value of the radial distribution function at the molecular surface is well-known, but the usual derivation proceeds by way of an assumption of circular symmetry. This assumption is not exactly valid in our calculations owing to the finite number of molecules and to the particular boundary conditions which are used. For this reason we present here a derivation which avoids the symmetry assumption.

The Gibbs phase integral in configuration space for a system of N hard circles of diameter σ confined to an area V is

$$Z_N(V) = \int_V \cdots \int_V \prod_{(ij)} A(r_{ij} - \sigma)\, d\vec{r} \,. \tag{2.1}$$

The two-component vector giving the position of the center of molecule i is denoted by $\vec{r}_i$, while $\vec{r}$ denotes the set of all such positions $\{\vec{r}_1, \vec{r}_2, \cdots, \vec{r}_N\}$, and is a 2N-vector; r_{ij} is the magnitude of the

separation vector $\vec{r}_j - \vec{r}_i$ between molecules i and j; and (ij) stands for the set of all distinct molecular pairs. The function A(x) is the unit step function,

$$A(x) = \begin{cases} 0 \text{ if } x < 0 \ , \\ 1 \text{ if } x \geq 0 \ . \end{cases} \tag{2.2}$$

The thermodynamic pressure is defined by

$$\frac{pV}{NkT} = \frac{V}{N}\left(\frac{\partial \ \ell n \ Z_N}{\partial V}\right)_{T,N} \ , \tag{2.3}$$

where the variation of the area V is understood to take place with its shape (to be discussed in Chapter 3, along with the boundary conditions) held fixed. The symbols k and T as usual stand for the Boltzmann constant and the thermodynamic temperature.

If the dimensionless vectors

$$\vec{x}_i = V^{-\frac{1}{2}}\vec{r}_i \ ,$$

$$\vec{x} = \{\vec{x}_1, \vec{x}_2, \cdots, \vec{x}_N\} \ ,$$

$$x_{ij} = |\vec{x}_j - \vec{x}_i| \ ,$$

are introduced, (2.3) can be written

$$\frac{pV}{NkT} = 1 + \frac{V}{N}\left(\frac{\partial \ \ell n \ Z_N^*}{\partial V}\right)_{T,N} \ ,$$

with

$$Z_N^*(V) = \int_\omega \cdots \int_\omega \prod_{(ij)} A(V^{\frac{1}{2}}x_{ij} - \sigma)d\vec{r} \ ,$$

where ω is a fixed unit area whose shape is independent of V. Differentiation under the integral sign then gives

$$\frac{\partial \ell n\, Z_N^*}{\partial V} = \frac{1}{Z_N^*}\int_\omega \cdots \int_\omega \sum_{(k\ell)} \left[\prod_{(ij \neq k\ell)} A\left(V^{\frac{1}{2}} x_{ij} - \sigma\right)\right] \frac{\partial A\left(V^{\frac{1}{2}} x_{k\ell} - \sigma\right)}{\partial V} d\vec{x} \quad .$$

With use of the identities

$$\frac{dA(x)}{dx} = \delta(x)$$

and

$$A(x)\delta(x) = \delta(x) \quad ,$$

where $\delta(x)$ is Dirac's delta function, we obtain

$$\frac{\partial \ell n\, Z_N^*}{\partial V} = \frac{\sigma}{2VZ_N^*}\int_\omega \cdots \int_\omega \left[\prod_{(ij)} A\left(V^{\frac{1}{2}} x_{ij} - \sigma\right)\right] \left\{ \sum_{(ij)} \left[\frac{\partial A\left(\zeta - V^{\frac{1}{2}} x_{ij}\right)}{\partial \zeta} \right]_{\zeta=\sigma} \right\} d\vec{x} \quad .$$

Return to the original coordinates $\vec{r}_i$ gives

$$\frac{\partial \ell n\, Z_N^*}{\partial V} = \frac{\sigma}{2VZ_N}\int_V \cdots \int_V \left[\prod_{(ij)} A(r_{ij} - \sigma)\right] \left\{ \sum_{(ij)} \left[\frac{\partial A\left(\zeta - r_{ij}\right)}{\partial \zeta} \right]_{\zeta=\sigma} \right\} d\vec{r} \quad .$$

Next we introduce the cumulative pair-distribution function in configuration space

$$G(\zeta, \vec{r}) = \frac{2}{N} \sum_{(ij)} A(\zeta - r_{ij}) \quad , \tag{2.4}$$

in which the sum is evidently the number of molecular pairs whose distance between centers in configuration $\vec{r}$ is less than or equal to ζ, and the corresponding ensemble average

$$G(\zeta) = \frac{1}{Z_N}\int_V \cdots \int_V \left[\prod_{(ij)} A(r_{ij} - \sigma)\right] G(\zeta, \vec{r}) d\vec{r} \quad . \tag{2.5}$$

Then we obtain

$$\frac{\partial \ell n\ Z_N^*}{\partial V} = \frac{N\sigma}{4V}\left[\frac{\partial G(\zeta)}{\partial \zeta}\right]_{\zeta=\sigma} ,$$

by use of which (2.3) becomes

$$\frac{pV}{NkT} = 1 + \frac{\sigma}{4} G'(\sigma) \quad . \tag{2.6}$$

The prime denotes partial differentiation with respect to the argument ζ of $G(\zeta)$; the latter of course depends also on N and V.

Equation (2.6) is the desired result, expressed for convenience in terms of the derivative of the average cumulative pair-distribution function, rather than in terms of the radial distribution function because the latter cannot be directly calculated by the Monte Carlo method.

As indicated at the outset, no assumption of circular symmetry was necessary, and in fact the usual assumption of uniform singlet density was also avoided. Thus Eq. (2.6) applies, with the pressure definition of Eq. (2.3), also to crystalline phases in which the singlet density is not necessarily uniform (though in the case of systems with periodic boundary conditions, see Chapter 3, the singlet density is always uniform).

We will frequently find it convenient to use the symbol

$$\varkappa = pV/NkT \tag{2.7}$$

for the compressibility factor. We also define the area per molecule

$$v = V/N \quad ,$$

and define the hexagonal close-packed area per molecule

$$v_o = \sqrt{3}\ \sigma^2/2 \quad . \tag{2.8}$$

For coverings of the infinite plane by non-overlapping circles of diameter σ, it is known[16] that v_o is the smallest possible value of the area per molecule v. The reduced area τ is defined as

$$\tau = v/v_o \quad . \tag{2.9}$$

2.2 Estimation of the Equation of State

As indicated in Chapter 1, the average cumulative pair-distribution function $G(\zeta)$ defined by Eq. (2.5) is estimated by the Monte Carlo method as the time average of the configuration-space function $G(\zeta, \vec{r})$ over a realization of a suitable Markov chain in the space of the configuration states of the system. If we denote the configuration state attained by the realization at time t by $\vec{r}(t)$, and the corresponding value of $G(\zeta, \vec{r})$ by $\hat{G}(\zeta, t) = G[\zeta, \vec{r}(t)]$, then the resulting estimate of the petit ensemble average $G(\zeta)$ is

$$\overline{G}_t(\zeta) = \frac{1}{t} \sum_{t'=1}^{t} \hat{G}(\zeta, t') \rightarrow G(\zeta). \tag{2.10}$$

The arrow indicates the stochastic convergence of the Markov chain time average to the ensemble average as $t \rightarrow \infty$.

Thus, the essence of the method is the generation on a high speed computing machine of a sequence of configuration states, which sequence forms a realization of a Markov chain having this convergence property. For each state t' in the sequence, the function $\hat{G}(\zeta, t')$ and its running average $\overline{G}_{t'}(\zeta)$ are calculated for an appropriate set of values of ζ. The development is carried to an appropriately large value t of t',

whereupon the estimates $\overline{G}_t(\zeta)$ must be numerically differentiated to give $G'(\sigma)$, from which the compressibility factor $\varkappa$ is calculated from Eq. (2.6). The data reduction procedures involved are discussed in Chapters 7, 8, and 9.

2.3 Classification of Parameters

2.3.1 Parameters which specify the system: N, V(shape), and τ.

The basic parameters which define the physical hard-circle system, and thus the space of configuration states, are the number of molecules N, the area V (including its shape and boundary conditions), and the molecular diameter σ. The first two of these parameters are discussed in detail in Chapter 3. Together they determine $v = V/N$, while σ determines v_o by Eq. (2.8), the reduced area τ being then given by Eq. (2.9). It is convenient to reverse this procedure and specify the reduced area τ as a fundamental system parameter instead of the diameter σ.

2.3.2 Parameters which define the Markov chain: (p_{ij}) and δ.

The conditions on the stochastic matrix defining the Markov chain which suffice for the time averages of its realizations to converge stochastically to the corresponding petit ensemble averages have been discussed in detail elsewhere.[1-5] Briefly, the configuration states to be included in the ensemble averages must form a single ergodic class, and the elements of the stochastic matrix must satisfy a stationarity condition involving the Boltzmann factors for the states.

For the case of hard circles, the configuration states to be included ("accessible states") are ordinarily all those in which no "overlap" occurs, i.e., those in which all pairs (i, j) satisfy $r_{ij} \geq \sigma$. In exceptional cases (Section 1.2.1) only a subset of these states may be desired. If the one-step transition probability from state j to state k is p_{jk}, the stationarity condition for hard circles reduces to the reversibility or symmetry condition

$$p_{jk} = p_{kj} \quad .$$

The ergodicity condition requires that between any two "accessible states" j and k there be a non-zero transition probability in some finite number of steps.

The matrix which we used in the present calculations is the two-dimensional modification of the one used in the hard-sphere calculations.[5] Rather than write out its algebraic definition, we will describe the stochastic process by which the configuration state $\vec{r}(t + 1)$ at time $t + 1$ is generated from the state $\vec{r}(t)$ at time t. One of the N molecules is selected randomly and approximately uniformly; call this molecule i(t). The two cartesian coordinates of i(t) (giving the position $\vec{r}_{i(t)}(t)$ of this molecule at time t) are given provisional displacements random and uniform on a certain interval $(-\delta, \delta)$, the other molecules remaining in their positions at time t; call this provisional configuration $\vec{r}'(t)$. If $\vec{r}'(t)$ contains an overlap (i.e., if as a result of its provisional displacement, molecule i(t) has approached closer than the distance σ to another molecule), then i(t) is returned to its former

position, and the next state of the realization is identical to the previous state: $\vec{r}(t + 1) = \vec{r}(t)$. If $\vec{r}'(t)$ contains no overlap, then it becomes the next realized state: $\vec{r}(t + 1) = \vec{r}'(t)$.

The maximum displacement parameter δ, which appears in the above description (and is not to be confused with the Dirac delta function of Section 2.1), affects the rate of convergence of the stochastic process (i.e., the number of steps required on the average for a certain precision of the statistical averages), but not the existence of convergence toward the petit ensemble limit. The value of δ should in principle be chosen for optimum convergence. It is clear that both very small and very large values will lead to too gradual a motion of the state point in configuration space. In the hard-sphere case[5] a limited investigation of this optimization problem was made, on the basis of the intuitive criterion of maximizing the rectified trajectory of the state point. These results have been used as a rough guide in choosing δ during the hard-circle investigation.

It is evident that the above described Markov chains satisfy the sufficient conditions for convergence, assuming of course that the initial state at $t = 0$ is chosen to be an accessible state, except for one possibility. The latter is the case in which the prescription permits the state point to move between two disconnected (i.e., mutually inaccessible) regions of configuration space, depending on their separation relative to δ, as indicated schematically in Fig. 2.1 The figure is to be understood as a schematic projection of configuration space onto the

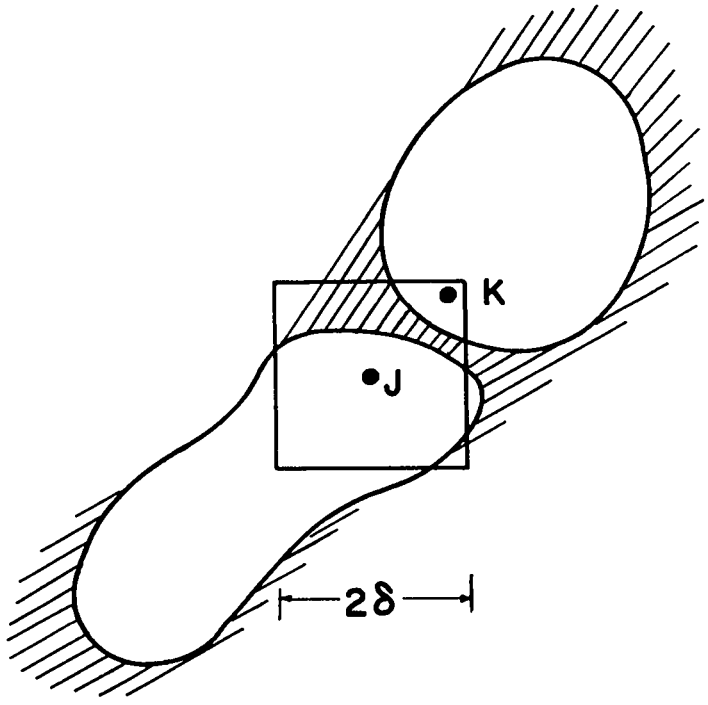

Fig. 2.1 A possible one-step transition between two dynamically inaccessible regions of configuration space.

two-dimensional space of a single molecule, with states j and k differing only in the position of this molecule. The square with state j as center is of edge 2δ, and consequently dynamically inaccessible states such as k can possibly be reached from j. Such situations are believed to be rare, since at densities where compartmentalization of configuration space is important the usual values of δ are expected to be small compared to the probable distance between mutually inaccessible regions.

2.3.3 Parameters which determine the realization: $\vec{r}(0)$ and the pseudorandom number sequence.

The realization which will be obtained on the computing machine is determined by the initial state $\vec{r}(0)$, and by the pseudorandom number sequence which is used to produce the pseudostochastic sequence of states. The initial configuration is usually a regular hexagonal arrangement of the molecules with the distance a between nearest-neighbor centers given by

$$a^2 = 2V/\sqrt{3}\,N \quad . \tag{2.11}$$

The random number sequence is discussed in Chapter 4.

2.3.4 Parameters which determine the observations made upon a realization: Δr^2, K, and Δt.

As seen in Section 2.1, for the determination of the equation of state of hard circles, the derivative of $G(\zeta)$ at $\zeta = \sigma$ is sufficient. The required numerical differentiation can accordingly be carried out using only observations of $\hat{G}(\zeta, t)$ near $\zeta = \sigma$. To date only such observations have been made, not because the radial distribution function over a wider range is without interest, but because this restriction permits a considerable increase in the speed with which the computer can generate the realization. This comes about because the calculations required to compute the observation $\hat{G}(\zeta, t)$ at each step can, if ζ is so restricted, be limited to just the interactions of the displaced molecule i(t) (Section 2.3.2) with its immediate neighbors.[5]

For convenience the set of values $\{\zeta_\alpha\}$, at which the observations are made, is chosen to be of the form

$$\zeta_\alpha^2 = \sigma^2 + \alpha\Delta r^2 \ , \ \alpha = 1,2,\cdots,K \quad , \tag{2.12}$$

where Δr^2 and K are suitably chosen parameters. They determine the fineness of detail and the range over which the cumulative pair-distribution function is observed. In principle they should be chosen so as to optimize statistically the results obtained in a given computation time. In practice they have been chosen somewhat haphazardly, in part on the basis of graphical differentiation techniques.

The realizations used in practice are much too long to allow the tabulation of the observations at each step of the random walk. Also, the running averages $\overline{G}_t(\zeta_\alpha)$ are too slowly varying to be convenient for the purpose of monitoring the progress of the realization. For this purpose we make coarse-grained or time-smoothed observations by averaging $\hat{G}(\zeta_\alpha, t)$ over successive groups of Δt steps each. Thus, our primary observations are

$$\tilde{G}(s,\alpha) = \frac{1}{\Delta t} \sum_{t'=(s-1)\Delta t+1}^{s\Delta t} \hat{G}(\zeta_\alpha,t'), \ \alpha = 1,2,\cdots,K, \ s = 1,2,\cdots \ . \tag{2.13}$$

The coarse-graining parameter Δt could also, in principle, be determined optimally on the basis of statistical considerations, but in practice it has also controlled intermittent dumping of data for restarting the calculation, and has been chosen on the basis of convenience in this respect.

The running averages $\overline{G}_t(\zeta_\alpha)$, which converge toward the desired ensemble averages, are of course easily obtained at times $t = s\Delta t$:

$$\overline{G}_{s\Delta t}(\zeta_\alpha) = \frac{1}{s} \sum_{s'=1}^{s} \tilde{G}(s',\alpha) \ . \tag{2.14}$$

2.3.5 A parameter which determines only the speed of the calculation: d.

The "diffusion distance" d is a parameter[5] which affects only the speed with which the computer generates the observations on a particular realization. Its value determines the number of neighbors of the displaced molecule i(t) (see Section 2.3.2) whose interactions with i(t) must be calculated at each time step. A small value of d leads to a small number of neighbors but more frequent updating of certain tables of these neighbors. The balancing of these two opposing effects leads to an optimum value of d. This was the subject of a limited investigation for the hard-sphere case,[5] in which a rather broad range of nearly optimum values was found. The values of this parameter in the present investigation were selected for the most part by analogy with the behavior of the three-dimensional case.

Chapter 3

PERIODIC BOUNDARY CONDITIONS, THE AREA V, AND THE NUMBER OF MOLECULES N

As in all our previous Monte Carlo investigations, we have used periodic boundary conditions in the belief that they probably afford the best means of approximating with a finite number of molecules the behavior of quasi-infinite thermodynamic systems.

3.1 Definitions

3.1.1 V must be a unit cell of a planar lattice.

The first requirement of these boundary conditions is that the area V must be a unit cell of some lattice which covers the plane. That is, given an area V of specified shape and dimensions, there must exist two linearly independent lattice vectors $\vec{\ell}_1$ and $\vec{\ell}_2$ having the following property. Let V_{mn}, with m and n any positive, negative, or zero integers, be the area obtained by applying to every point $\vec{R}$ of $V = V_{oo}$ the translation

$$\vec{R}_{mn}(\vec{R}) = \vec{R} + m\vec{\ell}_1 + n\vec{\ell}_2 \quad .$$

Then V is a proper unit cell if corresponding to any point $\vec{R}_o$ of the

plane there exists a unique pair of integers $m(\vec{R}_o)$ and $n(\vec{R}_o)$ such that $V_{m(\vec{R}_o),n(\vec{R}_o)}$ contains $\vec{R}_o$. It is immediately clear that this requirement alone considerably limits the shape of V. For example triangular shapes are excluded. Among the satisfactory shapes are evidently parallelograms (including rectangles) and certain hexagons; certain shapes with curvilinear boundaries would also be admissible.

This requirement being satsified, one next associates with each configuration of N hard-circle molecules in the area V the infinite configuration (covering of the plane by circles) of density [16] N/V obtained by applying the above translations to the finite configuration.

3.1.2 Summation conventions.

The set (ij) of molecular pairs over which the sums and products in Section 2.1 are taken for any configuration is then defined as follows. The index i runs over just the N molecules of the basic cell $V = V_{oo}$. The index j runs in principle over all the molecules in all the cells $V_{mn} \neq V_{oo}$, as well as over the values $j > i$ in V_{oo}. However, for the systems we will consider, the molecular diameter σ and the relevant values of the argument ζ of the cumulative pair-distribution function will always be small enough compared to the dimensions of V so that the equations are unaltered, with j restricted to its values in V_{oo} and to the molecules in the immediately adjacent cells. Owing to this extension of the range of the j subscript, the set (ij) now contains more than the $N(N - 1)/2$ distinct pairs obtained if both i and j were restricted

to just the molecules in V_{oo}. However, the independent variables which specify a configuration are still just the N position vectors $\vec{r}_i$ ranging over $V = V_{oo}$, and it is readily verified that the equations of Section 2.1 are unchanged.

3.1.3 Maximum packing density.

In the terminology of Section 2.3.1, a configuration has an overlap, and is thus not an allowed state during the random walk, if there is an overlap between any pair of molecules of the infinite system. And conversely any configuration which is an allowed state under the periodic boundary conditions corresponds to a non-overlapping covering of the infinite plane with a packing density equal to the density N/V of the finite system. Thus, a finite system with periodic boundary conditions cannot have a packing density greater than that possible for an infinite system.

As mentioned in Section 2.1, the maximum density for an infinite system is that of the familiar hexagonal close-packed arrangement, which has a volume per molecule equal to v_o, as given by Eq. (2.8). It is obvious that if we wish our finite system to approximate the behavior of nearly close-packed, quasi-infinite systems, we should choose V and N so that the area V is an N-molecule unit cell for the regular hexagonal lattice.

3.1.4 Unit cells for regular hexagonal lattice.

Figure 3.1 shows several unit cells containing one or two molecules, which themselves generate the regular hexagonal lattice, and from which larger composite unit cells can be constructed. Of the possible shapes, rectangles are computationally the most convenient. The smallest such unit cell contains two molecules, as shown in the figure, and has edges a and $\sqrt{3}$ a, where a is the nearest-neighbor distance. A rectangular array of LM such unit cells, with edges $\sqrt{3}$La and Ma, is accordingly a suitable cell with an area

$$V = \sqrt{3}LMa^2 \tag{3.1}$$

for a system of

$$N = 2LM \tag{3.2}$$

molecules. For both of the systems to be reported here, the area V is a rectangle with side-ratio $\sqrt{3}/2$, the ratio L/M being fixed at 2/3. The smaller of the two systems contains 12 molecules (L = 2, M = 3), the larger, 48 molecules (L = 4, M = 6); see Figs. 3.2 and 3.3. Both will be discussed in more detail in subsequent sections of this chapter.

3.1.5 Toroidal formulation.

An equivalent, often helpful, description of periodic boundary conditions for such rectangular areas is to regard the N molecules as moving on the surface of a torus, with a suitable definition of distance. The periodic boundary conditions are in fact sometimes called toroidal boundary conditions. In the above discussion we proceeded by the more

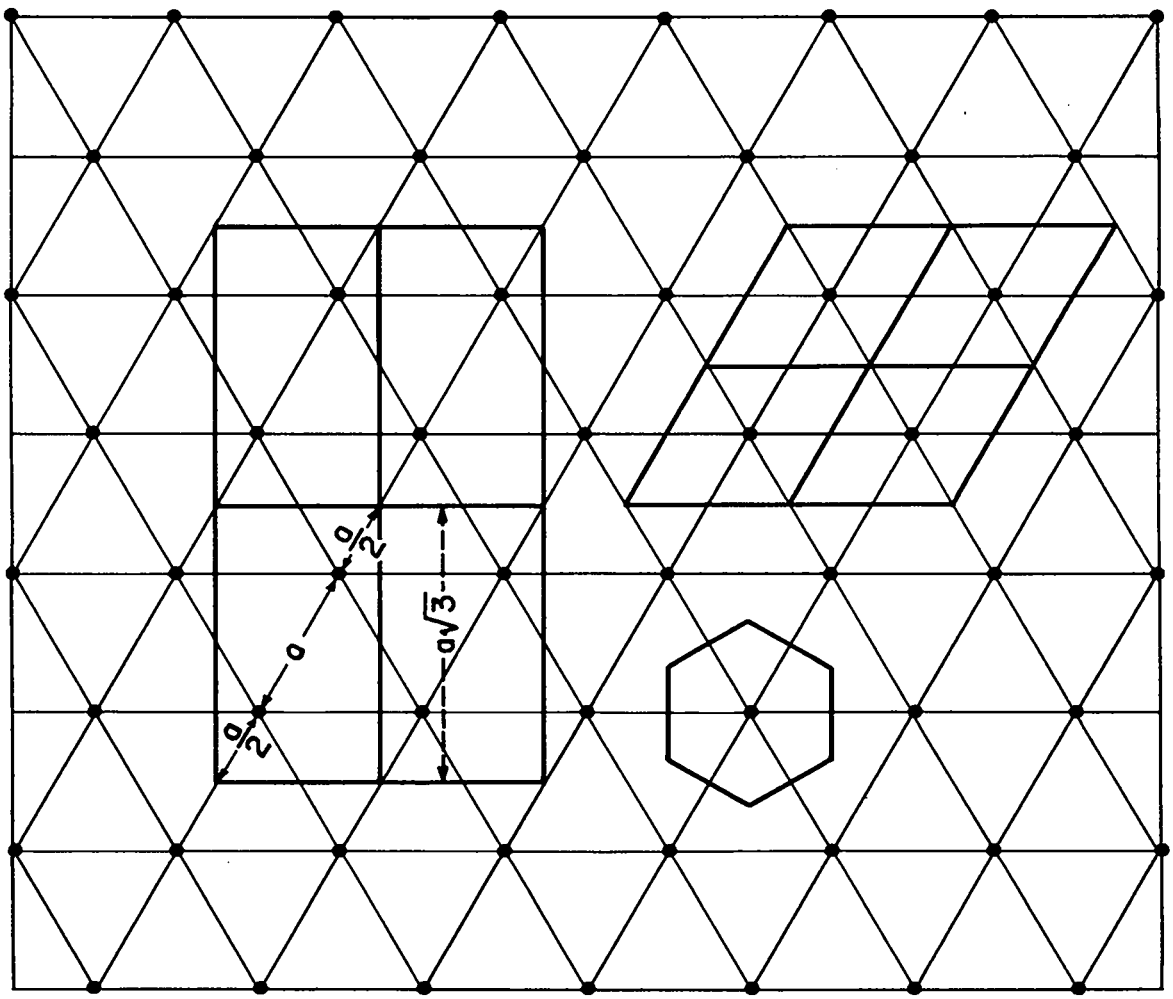

Fig. 3.1 Unit cells for the planar regular hexagonal lattice.

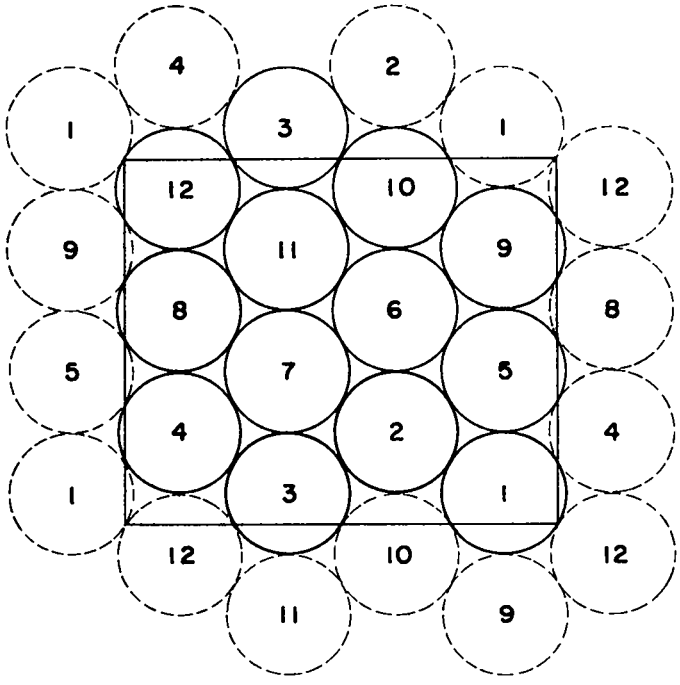

Fig. 3.2 The 12-molecule system in the regular hexagonal close-packed configuration, $\tau = 1$.

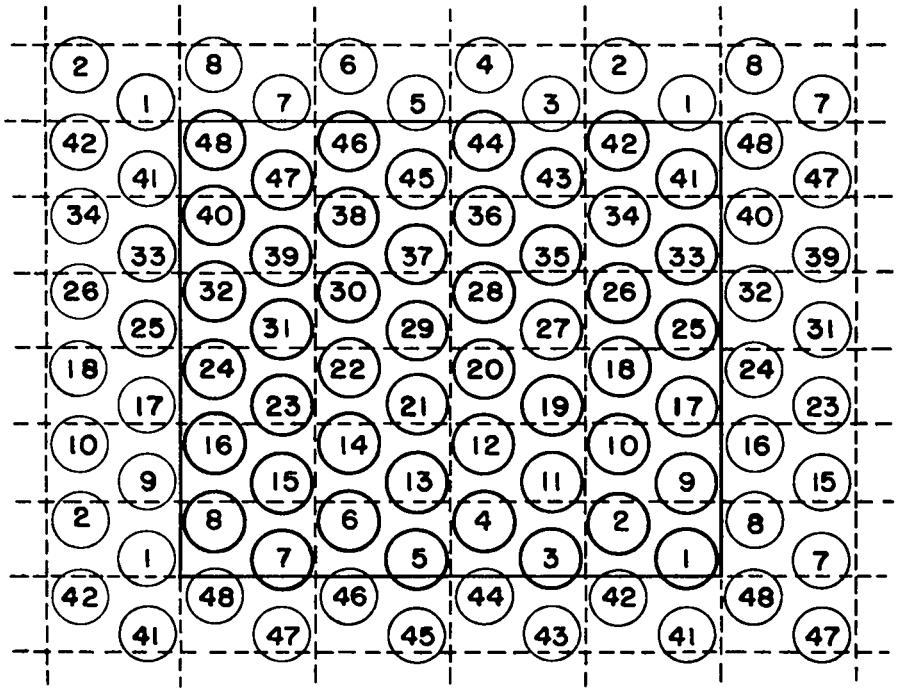

Fig. 3.3 The 48-molecule system in a regular hexagonal configuration.

cumbersome lattice definitions in order to more clearly establish the connection with quasi-infinite systems.

Finally it should be mentioned that during the random walk, a displacement of a molecule across the boundary of the cell $V = V_{oo}$ into an adjacent cell is allowed. However, under the above definitions the molecule simultaneously reappears in V at the opposite boundary, so that the number of molecules contained in V is conserved. (Note the greater simplicity of the toroidal formulation.)

3.1.6 Uniform singlet density; reduction of configuration space to 2(N - 1) dimensions.

Every configuration of a periodic system belongs to a two-dimensional continuum of equivalent configurations in which the relative positions $\vec{r}_{ij}$ are identical, corresponding to uniform translations around the torus. Due to this symmetry the singlet density of any periodic system is uniform. In addition the configuration space can be reduced to 2(N - 1) dimensions by introducing coordinates of the N - 1 molecules $i = 2,3,\cdots,N$ relative to molecule 1. The position $\vec{r}_1$ of molecule 1 then disappears from Eqs. (2.1) and (2.5), so that the integrations over $\vec{r}_1$ can be carried out to yield a factor V. This factor cancels from numerator and denominator of Eq. (2.5), with the result that the average cumulative pair-distribution function $G(\zeta)$ is expressed as the ensemble average for a system of N hard circle molecules having 2(N - 1) degrees of freedom, one molecule being held fixed at the origin.

The random walk of the Monte Carlo method can be modified to take place in this 2(N - 1)-dimensional space by simply holding one molecule fixed. In some recent calculations for Lennard-Jones molecules this has indeed been done, since in addition to slightly increasing the calculation speed [by a factor N/(N - 1)], the study of the geometrical structure of sample configurations is somewhat simplified.

3.2 Effect of Periodic Boundary Conditions and Finite N at Low Densities

Lebowitz and Percus[17] have recently investigated theoretically the dependence of the petit ensemble pressure on the number of molecules for systems with periodic boundary conditions. They showed that there are essentially two types of dependence of p on N at fixed v and T. One of these, which they call the "normal" dependence, arises from correction terms to the virial coefficients which are of the form of polynomials in N^{-1}. The second, or "anomalous" dependence on N is more complex, and arises from the area (for two-dimensional systems) dependence of the virial coefficients of large enough order for the corresponding Mayer clusters to wind at least once around the periodic torus. The latter dependence can be predominant for very small values of N.

For the rectangular systems with L/M = 2/3 the reduced area $\tau_c(\nu, N)$, below which the virial coefficient of order ν becomes area dependent, is given by

$$\tau_c(\nu, N) = 4\nu^2/3N. \qquad (3.3)$$

In Table 3.1 this critical reduced area is tabulated as a function of ν for the two systems of the present investigation. In the 12-molecule system, the second and third virial coefficient have a "normal" N-dependence (i.e., are volume independent) at all values of the reduced area, while the fourth virial coefficient becomes dependent on τ for $\tau < 1.78$. In the 48-molecule system, the second through the sixth coefficients have normal behavior, but the seventh virial coefficient is dependent on τ for $\tau < 1.36$.

TABLE 3.1 CRITICAL VALUES OF THE REDUCED AREAS FOR ANOMALOUS DEPENDENCE OF VIRIAL COEFFICIENTS C_ν

	$\tau_c(\nu, N)$	
ν	N = 12	N = 48
2	—	—
3	1	—
4	1.78	—
5	2.78	—
6	4	1
7	5.22	1.36
8	7.11	1.78
9	9	2.25
10	11.11	2.78

3.3 Effect of Periodic Boundary Conditions and Finite N at High Densities

3.3.1 Summary of Salsburg-Wood asymptotic analysis.

Complementing to a certain extent the results of Percus and Lebowitz discussed in Section 3.2, Salsburg and Wood[18] have recently established theoretically the behavior of the equation of state of finite periodic systems of hard circles or spheres in the high density limit.

3.3.1.1 Stable limiting configurations.

The fundamental assumption is that as the reduced area approaches from above a certain value τ^*, in a system of fixed shape and N, a closed region of the $2(N-1)$-dimensional configuration space of Section 3.1 contracts to a single point or limiting configuration $\vec{r}^*$. As a result at infinitesimal expansions from the reduced volume τ^* only configuration states which are infinitesimally close to the limiting configuration space point $\vec{r}^*$ are accessible from $\vec{r}^*$. Such a limiting configuration is said to be stable. No easily applicable sufficient condition for $\vec{r}^*$ to have this stability property was obtained, but a necessary condition on the coordination number c (defined as the average number of contacts per molecule) of the limiting configuration was shown to be

$$c \geq 4 - 2/N \quad . \tag{3.4}$$

In addition an obviously necessary condition is that the limiting configuration be close-packed, i.e., no molecule must be able to move with

the other molecules held fixed.

3.3.1.2 Free-volume equation of state is asymptotically correct.

Provided that the limiting configuration is stable, the following asymptotic expression for the petit ensemble equation of state restricted to configurations accessible from the limiting configuration was obtained:

$$\pi = \frac{pV}{NkT} = \frac{2(1 - N^{-1})\tau^*}{\tau - \tau^*} + O(1) \quad . \tag{3.5}$$

This result agrees, neglecting terms of $O(N^{-1})$ and $O(1)$ in $(\tau - \tau^*)$, with the free-volume equation of state[18] based on the same limiting configuration,

$$\pi_{FV} = \frac{\tau^{\frac{1}{2}}}{\tau^{\frac{1}{2}} - \tau^{*\frac{1}{2}}} \quad . \tag{3.6}$$

3.3.1.3 Difficulties for large N.

This asymptotic agreement with the free-volume approximation is the most interesting result of the Salsburg-Wood analysis. However, it still has to be regarded as an uncertain approximation as far as systems of thermodynamic size are concerned. This is because $\tau - \tau^*$ must be $O(N^{-\frac{1}{2}})$ if the states accessible from $\vec{r}^*$ are to be inaccessible from the permutations of $\vec{r}^*$ obtained by renumbering the molecules. The latter situation is necessary (though not sufficient) for the Salsburg-Wood derivation of Eq. (3.5). Such a range of expansion is uninterestingly small for thermodynamic values of N. There are intuitive reasons to believe that Eq. (3.5) is valid for such large systems, with $\tau^* = 1$, but this has not been proved.

3.3.2 Examples.

3.3.2.1 Stable regular hexagonal lattice.

The regular close-packed hexagonal configuration with $\tau^* = 1$ is undoubtedly an example of a stable limiting configuration, although a formal proof is lacking. In this case Eq. (3.6) becomes the usual free-volume equation of state, which should consequently usefully approximate the equation of state of finite systems at high density, provided that the hexagonal configuration is accessible to the system. And under the usual supposition that the vast majority of states of quasi-infinite systems at high density are close to the regular hexagonal configuration, Eq. (3.6) is hopefully a useful approximation for these systems also.

3.3.2.2 Unstable honeycomb lattice.

The close-packed honeycomb lattice configuration with $\tau^* = 1.5$, Fig. 3.4, is an example of an unstable limiting configuration (for all systems except those with very small values of N) whose coordination number (3) does not satisfy Eq.(3.4). Examination of the figure shows that by a coordinated rotation of the molecules in one of the hexagonal rings through one-twelfth of a revolution, the system reaches a configuration in which these molecules, as well as their nearest neighbors, all have considerable freedom of movement.

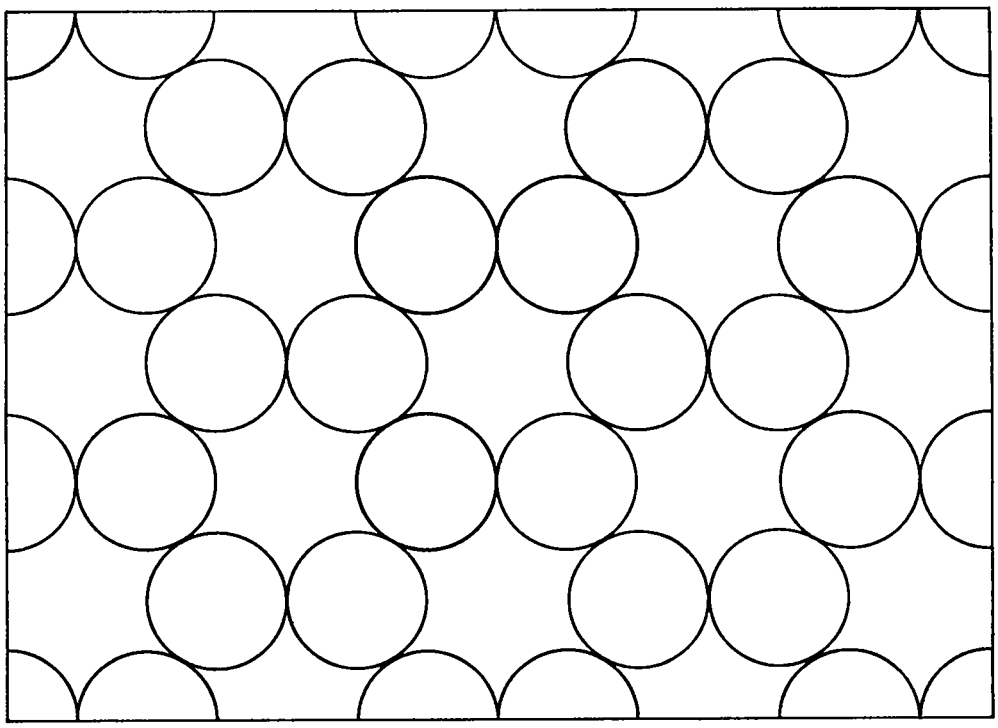

Fig. 3.4 The unstable close-packed ($\tau^* = 1.5$) honeycomb lattice of coordination number 3.

3.3.2.3 Unstable square lattice.

Another example of an unstable limiting configuration is the close-packed square lattice with $\tau^* = 1.154$, Fig. 3.5. Let us first consider this configuration under periodic boundary conditions in a square area $V = N\sigma^2$. We note immediately that the configuration is unstable in that any row of molecules (except that containing the fixed molecule) can be slipped horizontally around the torus by an arbitrary amount. If alternate rows are so displaced a distance of one hard-circle radius in the same direction, we arrive at a configuration in which the molecules within each row are still close-packed, but in which adjacent rows are

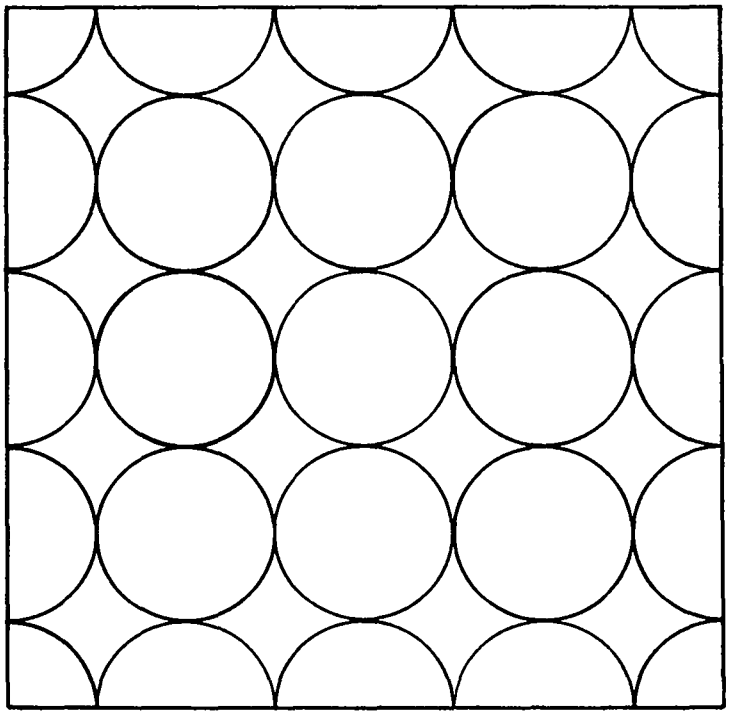

Fig. 3.5 The close-packed ($\tau^* = 1.154$) square lattice.

no longer in contact. Alternate molecules in each row can consequently be given small vertical displacements such that the configuration becomes one in which no molecules are in contact. Consequently the pressure obtained by averaging over states accessible from the close-packed square lattice is finite at $\tau = 1.154$. For sufficiently large N these states may be expected to include a preponderance of states which approximate a regular hexagonal arrangement of this density except for boundary defects. The pressure is then expected to approach approximately the usual ($\tau^* = 1$) free-volume value.

3.3.2.3.1 Effect of rigid boundaries. The preceding example shows that a configuration can be close-packed, satisfy Eq. (3.4), and still be unstable. Let us consider the same system with rigid wall boundary conditions. As far as we have been able to determine, this close-packed configuration is now stable at finite N. Consequently the equation of state under these conditions would be expected to approximate Eq. (3.6) with $\tau^* = 1.154$, for $\tau - \tau^* = O(N^{-\frac{1}{2}})$. However, the behavior of large systems at expansions greater than this would be quite different; as connections appear between the square lattice configuration and the approximately hexagonal configuration, the pressure can be expected to shift rapidly to the lower values characteristic of the latter configurations. Thus, one can argue that periodic boundary conditions are slightly advantageous since they allow the instability of such a close-packed configuration to manifest itself in finite systems.

3.3.3 Conclusion.

Comparing the Salsburg-Wood analysis with the hard-sphere Monte Carlo results of Fig. 1.1, we see that the approximate agreement of the high density points obtained from calculations started from the face-centered cubic lattice (the "solid" branch of the equation of state) is to be expected, and hopefully should be characteristic of much larger systems. The "extended fluid" branch for the 32-molecule system would be expected to be in approximate agreement with Eq. (3.6) with τ^* near 1.15. However, the significance of this curve is in doubt. It might be a small system

artifact; or it might be the small system manifestation of metastable randomly packed configurations of large systems.

The asymptotic N dependence given by Eq. (3.5) may be expected to be of some use in comparing Monte Carlo calculations for systems of different numbers of molecules, but its usefulness in this connection may be expected to be limited by our lack of knowledge of the N dependence of the O(1) term (see Chapter 10).

3.4 The 12-Molecule System

3.4.1 Surface molecules.

The twelve-molecule system defined in Section 3.1 was shown in Fig. 3.2 in its hexagonal close-packed configuration, $\tau = 1$. In a sense one can say that this system is almost all edge or "surface", although the term requires a special interpretation since under periodic boundary conditions there is no true one-dimensional surface (edge). However, considering any specific configuration such as Fig. 3.2, we see that if a surface molecule is defined to be one which has among its nearest neighbors one or more "image" molecules, i.e., one or more molecules contained in another unit cell V_{mn} in the notation of Section 3.1.1, then all except two molecules (numbers 6 and 7 in Fig. 3.2) are surface molecules.

Another way of characterizing the finiteness of the system is to note that, while in the regular hexagonal lattice arrangement the six nearest neighbors of each molecule are all distinct, there are only three distinct next-nearest neighbors, instead of six as would be the case in

a large system. For example, in Fig. 3.2 the six next-nearest neighbors of molecule 7 are molecules 5, 10, and 12, each being counted twice. In this respect the 12-molecule, two-dimensional system is similar to the 32-molecule, three-dimensional system.

3.4.2 Toroidal topology of lattice lines.

Still another characterization of rectangular periodic systems is obtained by considering the way in which the principal lattice planes, or lines in the present two-dimensional case, wind around the torus. The hexagonal lattice has three systems of such lines, which in Fig. 3.2 are at angles of 30°, 90°, and 150° with respect to the longer edge of the cell. The vertical lines are seen to form four distinct columns (rings), each of which contains three molecules. The inclined lattice lines, however, fall into a single class. Proceeding from molecule 1 along the 150° line, we find the sequence 1, 2, 7, 8, 9, 10, 3, 4, 5, 6, 11, 12, 1, ··· . That is, all twelve molecules are encountered before a repetition occurs. In geometrical terms, the 150° lattice lines of this system in the hexagonal lattice configuration form a single spiral around the torus.

3.4.3 Critical τ for diffusion; validity of free-volume equation of state.

In connection with the question of the reduced area range over which the assumptions of the Salsburg-Wood analysis are valid for this system, it is of interest to estimate the smallest value of τ at which the

configuration of Fig. 3.2 and one or more of its permuted arrangements (obtained from Fig. 3.2 by renumbering the molecules) are connected. The connecting path is probably one which we observed during the Monte Carlo calculations, but which might have been anticipated by study of Fig. 3.2. It corresponds to a fluctuation in which one of the above-mentioned columns of three molecules rotates one (or more) lattice distance around the torus. The value of τ required for this fluctuation is that at which one such column or ring has just sufficient room to rotate freely when the other three rings are tightly nested together, as shown in Fig. 3.6. In the 12-molecule system this requires $\tau \geq 1.136$. At smaller reduced areas the permuted lattice configurations are isolated from each other. It does not follow, of course, that the free-volume approximation is necessarily good for this system at all $\tau < 1.136$, since Eq. (3.5) is only an

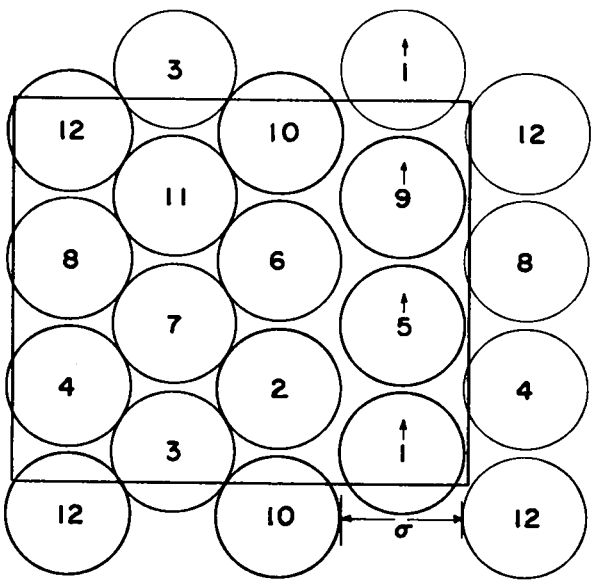

Fig. 3.6 High density diffusion mechanism, showing the presumably highest density path between permuted regular hexagonal configurations, just possible for the 12-molecule system at $\tau = 1.136$.

asymptotic expression valid at $\tau \to 1$.

On the other hand, it is possible that the free-volume approximation may indeed be useful for $\tau \approx 1.136$, since the probability of the above fluctuation is exactly zero at this minimum value of τ. At this and slightly larger reduced volumes, the configuration-space volume of the connecting paths is small, and the region of accessible space omitted in the Salsburg-Wood "polytope" estimate may be negligible. In order to form an idea of the rapidity with which the connections become larger as τ increases, we can calculate the reduced area at which the above rotation of a ring can take place with all other rings in their regular lattice locations. Under these conditions the fluctuation in question would appear to be fairly probable, corresponding to an appreciable connecting region. The required value of τ is $4/3$. Thus, the free-volume approximation is expected to break down at some smaller reduced area.

3.4.4 Alternative tetragonal (c = 4) lattice.

Figure 3.7 shows that this 12-molecule system is also compatible with a different regular lattice configuration which is a relative of the square lattice of Fig. 3.5. This lattice has a two-molecule rectangular unit cell of side ratio $3\sqrt{3}/4$, and is compatible with any rectangular area V based on the regular hexagonal lattice for which the ratio $L/M = 2/3$ (see Section 3.1). The lattice is close-packed at $\tau = 48/43 \approx 1.116$, and is probably stable since its coordination number 4

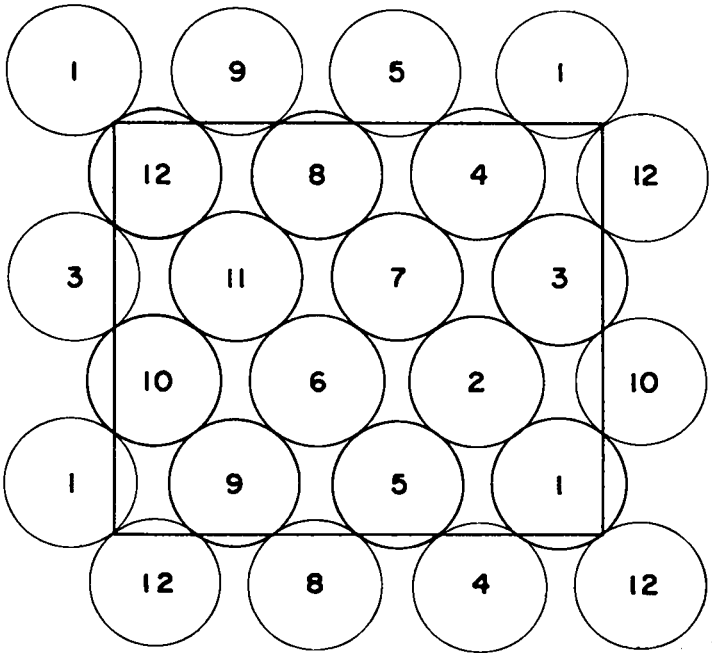

Fig. 3.7 A tetragonal close-packed ($\tau^* = 1.1163$) configuration which is compatible with the 12-molecule system, as shown, as well as the 48-molecule system.

satisfies Eq. (3.4), and in contrast to the square lattice, its lattice lines are not orthogonal. Consequently, in some interval of reduced area greater than 1.1163 this configuration is probably inaccessible from the regular hexagonal configuration. (Note that the close-packed reduced area of this $c = 4$ lattice is slightly smaller than the above estimate of the smallest reduced area at which the simplest permutations of the hexagonal arrangement are connected.)

For some interval of reduced area close to $\tau = 1.1163$, then, the equation of state obtained by averaging this system over the states accessible from the $c = 4$ configuration would accordingly be expected to approximate that given by Eq. (3.6) with $\tau^* = 1.1163$. For larger

reduced areas, however, the equation of state would be expected to shift toward the lower values characteristic of hexagonal configurations. For large systems Fig. 3.6 suggests this should occur at expansions where the inclined close-packed lines of molecules can slip along each other. For the 12-molecule system, however, this is not a possible mechanism, since the topology of these lattice lines is like that of the inclined lattice lines of the hexagonal configuration: each of the two systems contains a single class of all 12 molecules.

This configuration is mentioned in order to show the type of behavior which can appear in finite periodic systems. The structure of the arrangement, e. g., the angle between the lattice lines, depends on the ratio L/M, and one can be reasonably certain that for large systems it is of no statistical significance.

3.5 The 48-Molecule System

The regular hexagonal configuration of this system was shown in Fig. 3.3. The area V for this system can be regarded as being made up of four of those for the 12-molecule system. As a result any configuration of the latter has a corresponding analogue among the configurations of the 48-molecule system. Thus, many of the remarks already made in connection with the smaller system apply also to the larger one. In particular, the tetragonally coordinated lattice of Fig. 3.7 is also possible with the 48-molecule system.

Using the definition of surface molecule given in Section 3.4.1, exactly one-half of the molecules of this system are so characterized. In terms of the shell structure of the regular hexagonal lattice, all neighbors of any molecule are distinct through the fifth shell. The 30° and 150° lattice lines are found to decompose into two evenly divided classes each. The smallest value of τ at which one of the eight columnar rings of six molecules can rotate around the torus is 1.063, corresponding to the larger concentration of "free area" possible in the larger system. The value $\tau = 4/3$, at which this rotation is possible from the regular hexagonal configuration is, of course, independent of the size of the system.

The above description does not exhaust the possible structures obtainable with this system, as we shall see when we come to the discussion of the Monte Carlo results.

Chapter 4

THE CALCULATOR PROGRAM

All the calculations to be described in this report were performed on IBM Type 704 machines, using a two-dimensional adaptation of the hard-sphere program which has been described in detail elsewhere.[5] With this program a typical calculation time for one time-step of a realization is roughly 17 milliseconds.

4.1 Random Numbers

The pseudorandom numbers used for all realizations were those of a single sequence of 70-bit "middle square" numbers.[19] The cycle length of this sequence is unknown, but was found by suitable tests to be greater than four million. This is more than is required for any of the realizations to be described here. Except for this test for repetition, the sequence has not been further tested statistically. One-half (35 bits) of one of these numbers was used at each time step as follows: 9 bits to select the molecule to be moved; 12 bits for each of its two coordinate displacements; the remaining two bits were discarded.

4.2 Two Versions of the Program

Two slightly different codes were used, which we will designate as codes A and B. In code A, through an oversight, what amounts to a small low-order (less in magnitude than 2^{-17}, unit distance being the longer edge of the rectangular cell) noise was introduced into the displaced position $\vec{r}'_{i(t)}$ of the molecule which is moved at each time step t (Section 2.3.2). The effect of this noise is small as far as the Markov chain transition probability matrix is concerned, but at some point in any realization its presence changes the success - failure outcome of an attempted displacement for which this decision is borderline. Consequently the configuration at the next time step of the realization in which the noise is present differs from that in the same realization without noise. From that point on, of course, the two realizations are stochastically different. In the same way, two code A realizations which are identical except for their values of the diffusion parameter d (Section 2.3.5) will also differ, which would not normally be the case.

In code B this noise was accordingly removed. A number of realizations with identical parameters were run with both codes, and the results were found to be in statistical agreement, as expected. Such calculations accordingly can be regarded as replicate observations on the same system, in much the same way as variation of the initial configuration or the random number sequence can be used to produce replicate realizations for the same Markov chain, or as variation in the displacement

the same system averages.

4.3 Program Input and Output

The data required for input to the program are the parameters already discussed in Section 2.3: the system parameters, which are the reduced area τ and the integers L and M which determine V and N according to Eq. (3.1) and Eq. (3.2); the maximum displacement parameter δ which determines the Markov chain; and the observational parameters consisting of the time-smoothing interval Δt and the parameters Δr^2 and K which determine the detail and range of the observations of the cumulative pair distribution function. In addition the initial configuration can be provided; if none is given, the program positions the molecules on the regular hexagonal lattice. Finally the diffusion parameter d must be given.

The primary output of the program is the set of time-smoothed values $\tilde{G}(s, \alpha)$ of the cumulative pair-distribution function, as given by Eq. (2.13). These quantities, for $\alpha = 1(1)K$, are recorded on magnetic tape at the times $t = \Delta t, 2\Delta t, \cdots, s\Delta t, \cdots$, along with sufficient additional data to permit the realization to be restarted at these times, in case it is interrupted (for example, by a machine error). In particular the configurations $\vec{r}(t)$ at the above values of t are available on this output tape, which is preserved as the permanent record of each realization. This tape is used as input to various auxiliary programs which perform, for example the statistical reduction of the observations, as described

in Chapters 7, 8, and 9. Another such program can be used to plot the snapshot configurations $\vec{r}(t)$, available on the tape at time intervals Δt, on the SC-4020 microfilm printer-plotter.

Chapter 5

RESULTS FOR THE 12-MOLECULE SYSTEM

We generated 27 realizations of varying length for the system of 12 hard circles described in Section 3.4. The parameters and resulting compressibility factors are given in Table 5.1. The uncertainty estimates given for the compressibility factors were obtained by statistical techniques which will be described in Chapters 7, 8, and 9. Although they were formally obtained as estimates of the standard deviation of the estimated compressibility factors (whose distribution should be approximately normal), with more than 100 degrees of freedom in most cases, the statistical approximations involved are probably such as to make them too small. Thus, caution should be exercised in any statistical application such as confidence interval estimation.

As indicated by the appearance in Table 5.1 of just a single value of pV/NkT for each realization, we did not observe in this system of 12 hard circles the "jumpy" or "two-plateau" behavior which was exhibited by the hard-sphere systems as described in Chapter 1. This point is discussed in more detail in Section 5.1. Section 5.2 is devoted

TABLE 5.1 PARAMETERS AND COMPRESSIBILITY FACTORS

FOR THE SYSTEM OF 12 HARD CIRCLES
(see footnotes on following page)

Realization[a]	τ	$\frac{2\delta}{a-\sigma}$	K	n[b]	pV/NkT
A 1	1.025	2.4	18	99	76.84 ± 0.55
A 2	1.050	2.2	13	14	38.06 ± 0.38
A 3	1.075	2.4	12	19	26.42 ± 0.17
A 4	1.100	2.2	12	23	20.62 ± 0.09
A 5	1.150	2.2	12	24	14.25 ± 0.07
A 6	1.150	0.44	19	19	62.90 ± 0.87
A 7	1.200	2.2	11	11	11.20 ± 0.10
A 8	1.250	1.8	11	29	9.182 ± 0.063
A 9	1.250	2.03	19	15	9.262 ± 0.098
A10	1.290	2.2	13	16	8.405 ± 0.076
A11	1.300	2.2	10	29	8.328 ± 0.086
A12	1.350	2.3	11	32	7.423 ± 0.084
A13	1.400	2.0	11	24	6.857 ± 0.079
A14	1.450	2.3	10	42	6.272 ± 0.091
A15	1.475	2.3	11	44	6.214 ± 0.047
A16	1.500	2.5	11	42	6.033 ± 0.062
A17	1.500	2.4	11	76	5.909 ± 0.052
A18	1.500	2.5	11	30	6.008 ± 0.079
A19	1.525	2.5	11	38	5.788 ± 0.062
A20	1.550	2.5	11	39	5.524 ± 0.058
A21	1.600	2.3	10	99	5.229 ± 0.073
A22	1.700	2.5	10	23	4.660 ± 0.066
A23	1.800	2.5	9	24	4.066 ± 0.062
A24	2.000	2.5	8	16	3.372 ± 0.064
A25	2.500	2.9	11	18	2.459 ± 0.031
A26	3.000	2.8	11	23	2.030 ± 0.029
A27	3.900	3.0	8	26	1.674 ± 0.015

FOOTNOTES TO TABLE 5.1

a All realizations were generated using code A (see Section 4.2) with $\Delta t = 19\ 200$, except A1, A6, A9, and A21 for which code B with $\Delta t = 4\ 800$ was used. The value $\Delta r^2/a^2 = 12 \cdot 2^{-11}$ was used in all cases except A1 and A6, which had a value one-eighth as large, and A26, which had one-half the standard value. All realizations were started from the regular hexagonal lattice (Fig. 3.2) with the following exceptions: A6 and A9 were started from the tetragonal lattice of Fig. 3.7; A10 was started from a configuration generated by the "compression process" (see Section 5.1.2); A18 was started from a configuration obtained by Alder and Wainwright after 20 000 collisions along a dynamical trajectory started from the hexagonal lattice.

b This column gives the number of coarse-grained observations (of Δt steps each) used in estimating pV/NkT. On all realizations the first coarse-grained observation was not included, except for A9, where the first five such observations were omitted.

to the geometrical structures observed in this system. In Section 5.3 our qualitative conclusions with respect to this system are summarized. Discussion of the quantitative aspects of the equation of state results is postponed until after the calculations for the 48-molecule system and the data reduction techniques have been described.

5.1 Statistical Behavior

5.1.1 Regular lattice realizations.

Our principal objective in studying the 12-molecule hard-circle system was to see whether it would exhibit phenomena possibly indicative of the presence of a phase transition in large, quasi-infinite systems. Such indications might be of essentially two different types.

The first possibility is that it would be feasible to estimate the true ensemble average (over-all configurations accessible from the hexagonal lattice) over the entire density range. In this case the indication of a possible phase transition would take the form of an anomaly in the resulting p-v isotherm, presumably either a loop of the van der Waals type or a more or less horizontal inflection point. It might then also be possible to obtain a similarly complete equation of state for a significantly larger value of N, and thus perhaps to obtain some indication of the behavior of the anomaly with increasing N.

The second phenomenon which might be regarded as suggestive of a phase transition is the same "jumpy" or "two-plateau" behavior as was observed for hard spheres and described in Chapter 1. None of our

realizations of Markov chains for the 12-molecule system displayed such behavior. However, as we shall see, later calculations for the system of 48 hard circles did display this "jumpy" behavior at reduced areas in the interval 1.3 to 1.35. The calculations for the smaller system were almost all done before those of the larger one, so that at the time we had no particular reason to concentrate our attention in this interval of reduced area. As a result, for the 12-molecule system in this interval we have only realizations A11 and A12 at $\tau = 1.3$ and 1.35 respectively.

The "control charts" for the first three observed points $\tilde{G}(s, 1)$, $\tilde{G}(s, 2)$, and $\tilde{G}(s, 3)$ of the cumulative pair-distribution function for these two realizations are shown in Figs. 5.1 and 5.2. Even in retrospect, considering our later experience with the 48-molecule system, these control charts are not especially noteworthy, although that for realization A12 shows some indication of non-randomness in successive coarse-grained observations.

Thus, our calculations indicated that the ensemble averages over the accessible configurations of this system were being reasonably well estimated at all densities. It was accordingly possible to inquire about the presence of anomalies in the resulting isotherm which might, as already described, be indicative of a phase transition in large systems. In Fig. 5.3 the estimated reduced pressure pv_o/kT is plotted against the reduced area τ in the same logarithmic representation as used in Fig. 1.1 for hard spheres. Also shown are the virial equation of state, with neglect of terms of $O(\tau^{-5})$ as given by Metropolis, et al.,[1] and the usual

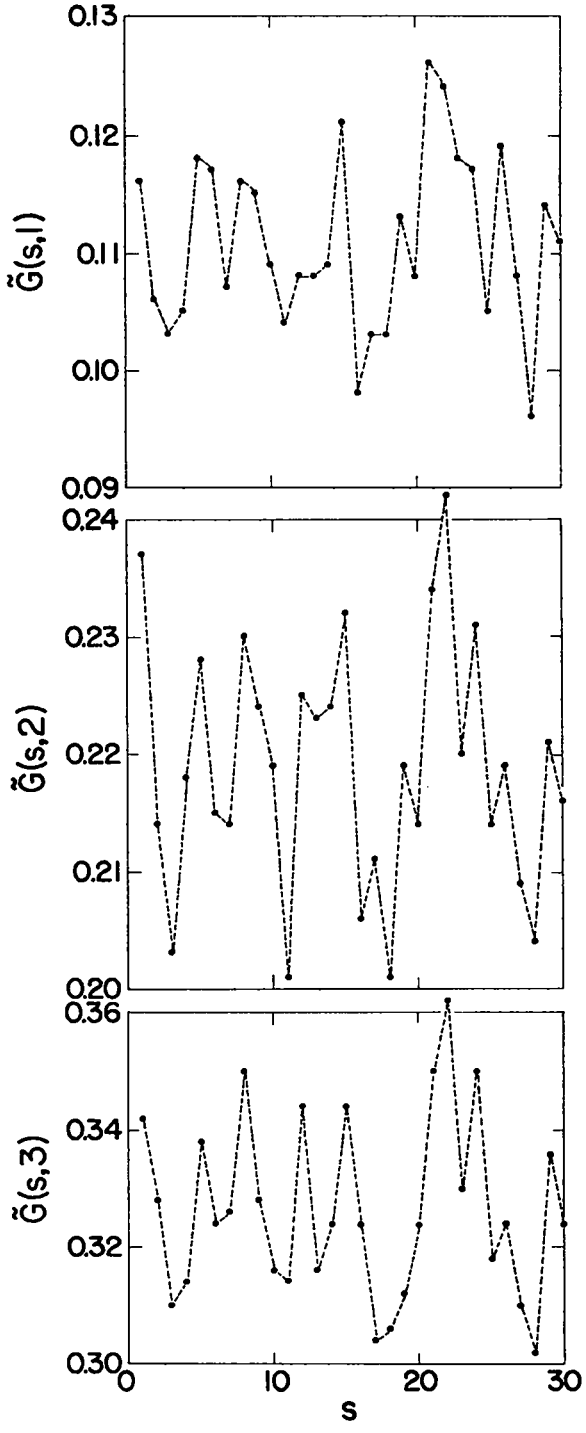

Fig. 5.1 Control charts for the first three cumulative distribution functions of realization A11 at $\tau = 1.3$.

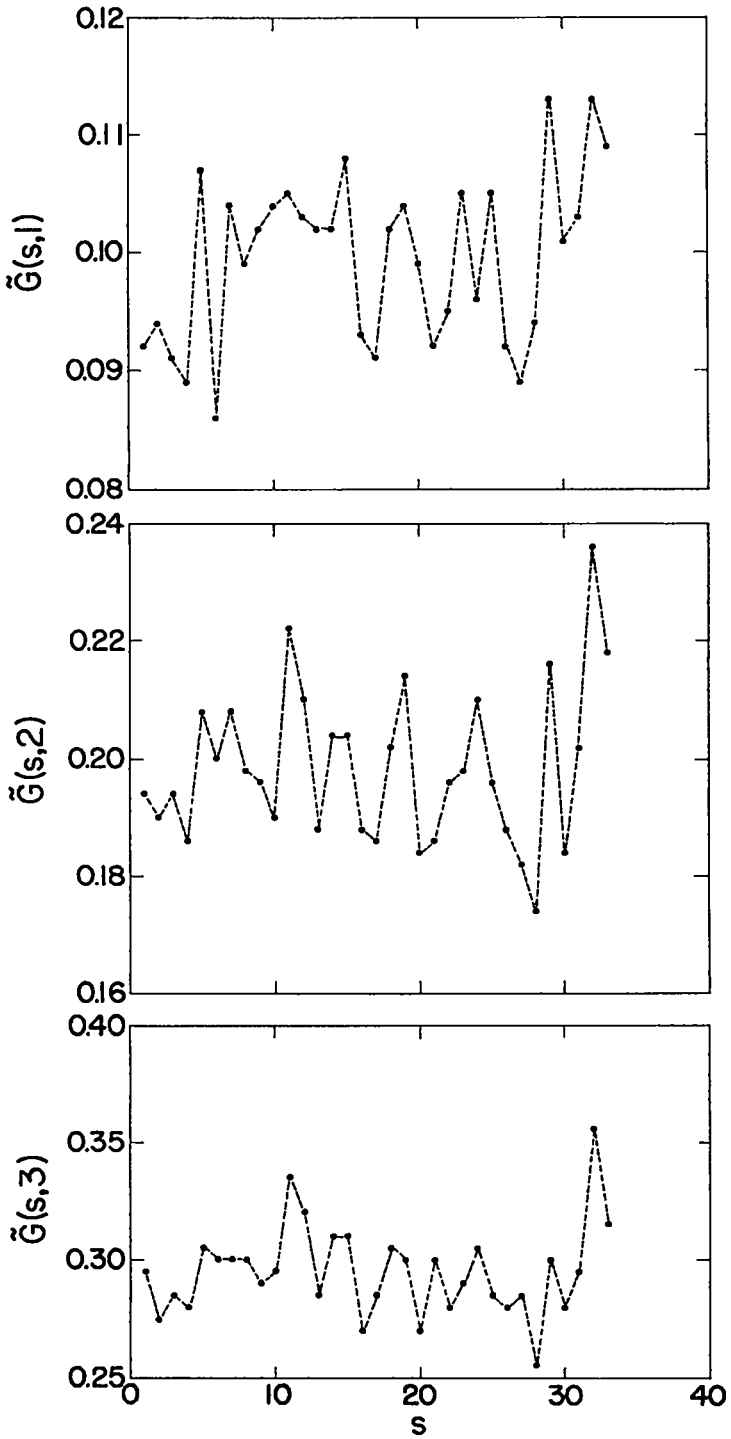

Fig. 5.2 Control charts for the first three cumulative distribution functions of realization A12 at $\tau = 1.35$.

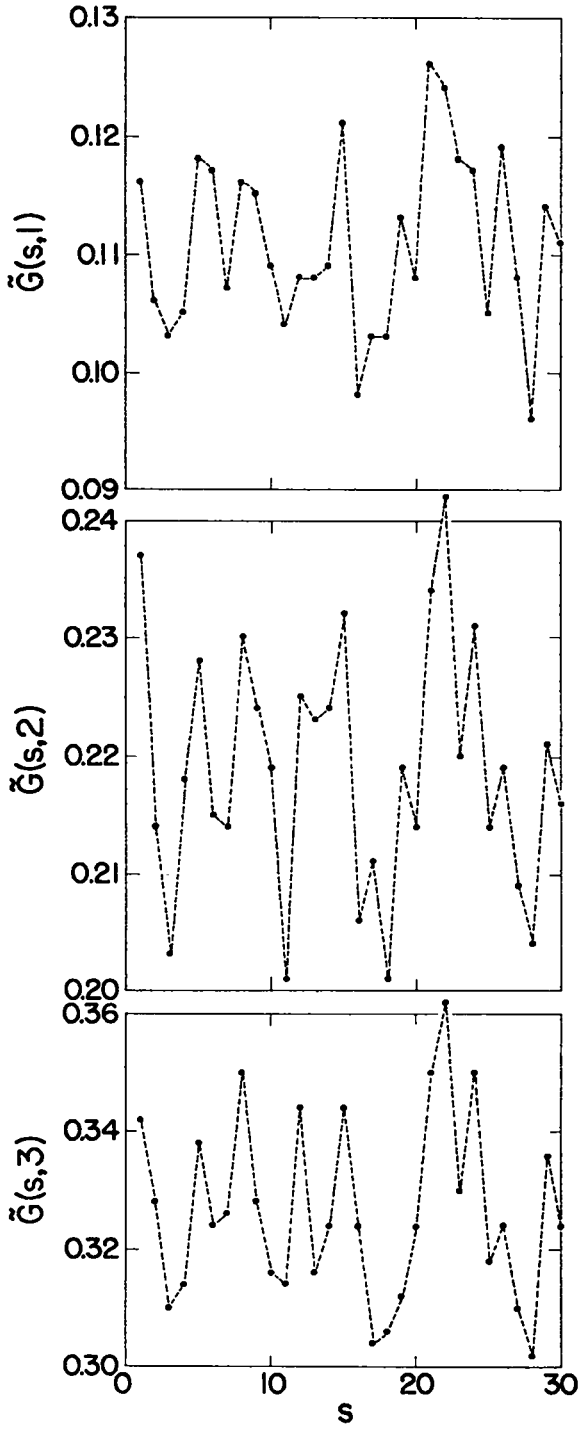

Fig. 5.1 Control charts for the first three cumulative distribution functions of realization All at $\tau = 1.3$.

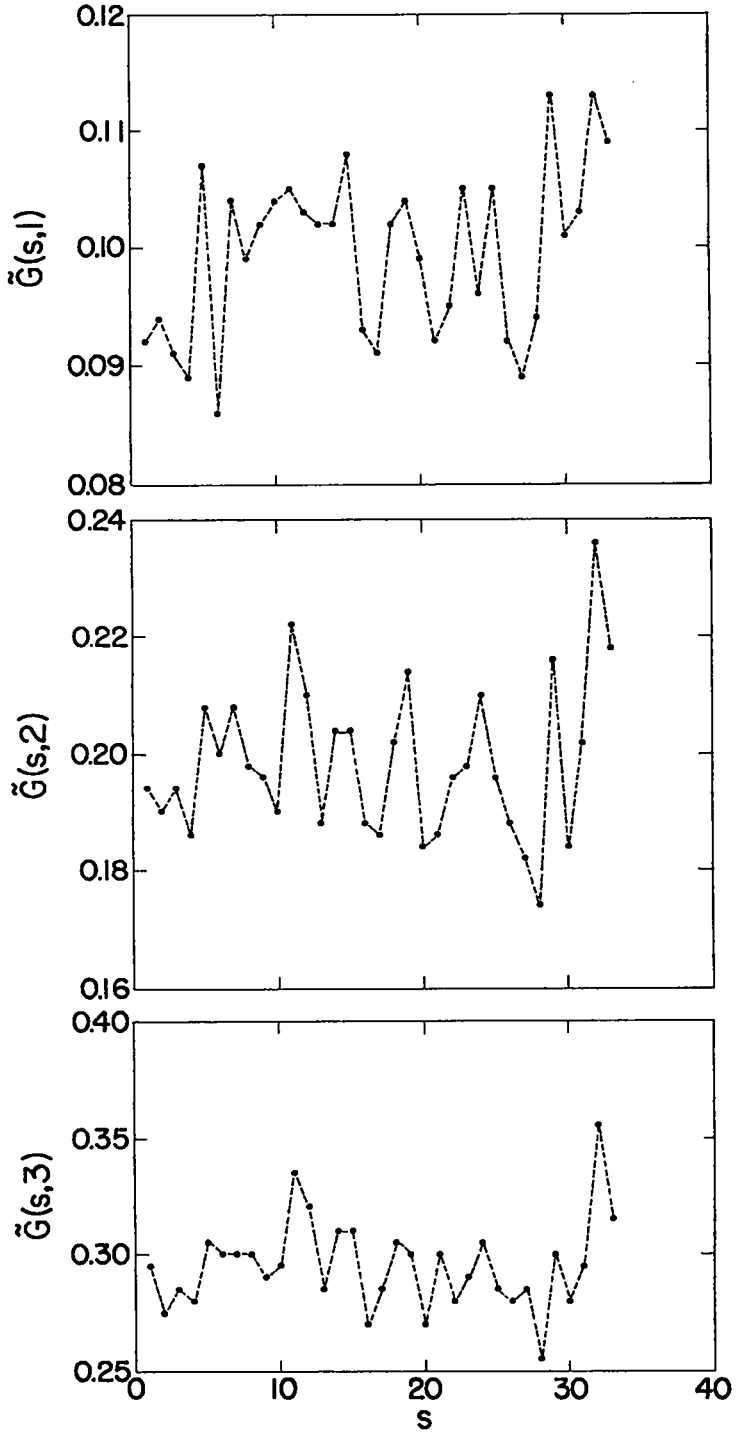

Fig. 5.2 Control charts for the first three cumulative distribution functions of realization A12 at $\tau = 1.35$.

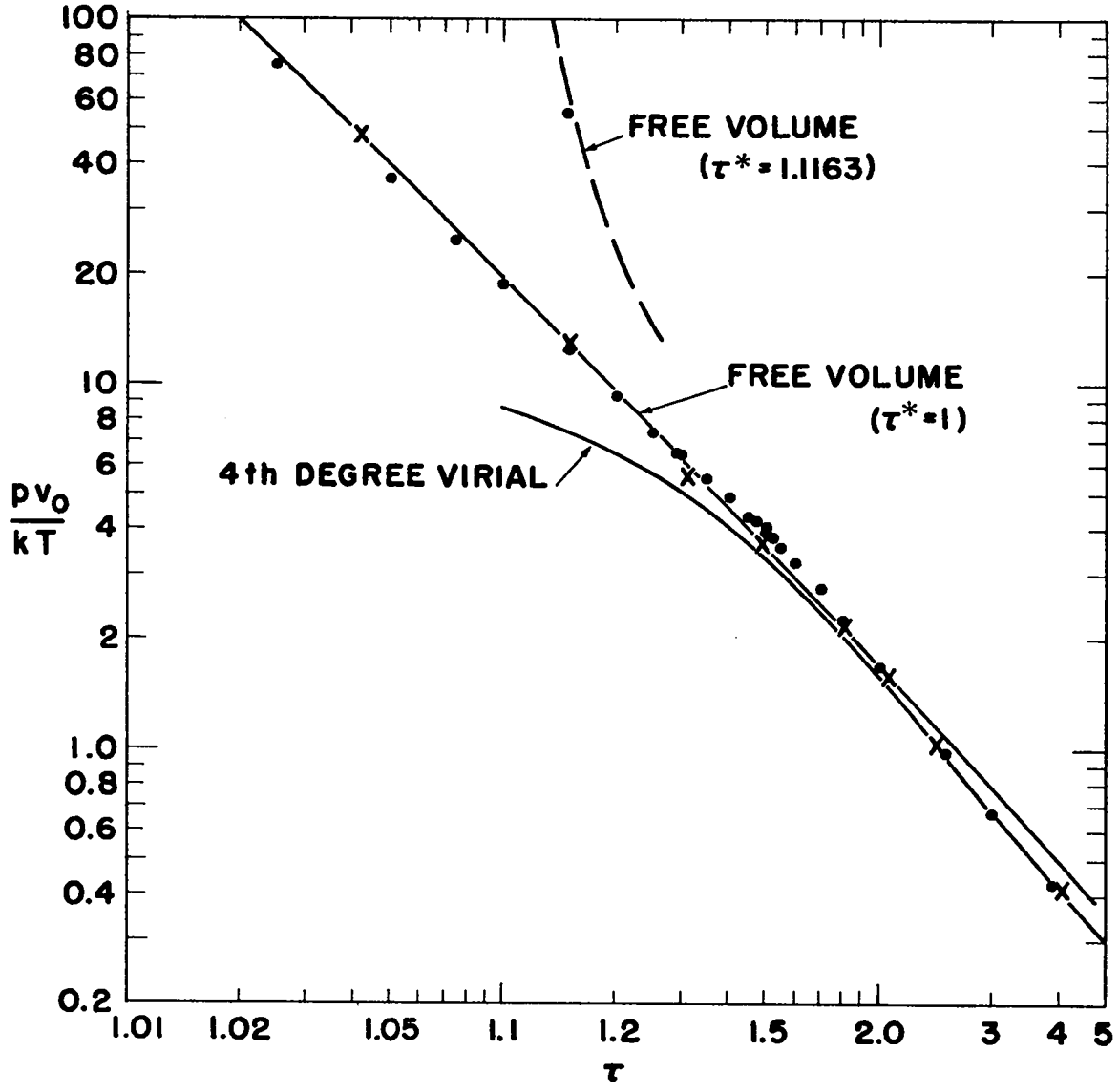

Fig. 5.3 The equation of state of the system of 12 hard circles as calculated by the Monte Carlo method in the present investigation (•). Also shown (x) are the results of Metropolis et al.[1] for 224 hard circles.

free-volume equation of state Eq. (3.6), with $\tau^* = 1$. (The free-volume curve for $\tau^* = 1.1163$ and the neighboring point for realization A6 are discussed in Section 5.2.4).

The results have the expected qualitative behavior at low and high densities. In the latter region the points lie slightly below the free-volume curve, by an amount which is in at least rough agreement with the N^{-1} term in Eq. (3.5). At low densities the Monte Carlo values approach agreement with the virial approximation; the scale of the figure is too small to show whether or not the difference is $O(N^{-1} \tau^{-1})$ as would be expected from the analysis of Lebowitz and Percus.

Furthermore, we note that all the points appear to lie on a reasonably smooth curve, including across the interval $\tau = 1.3$ to 1.35 in which, as already mentioned, the 48-molecule system will be seen to exhibt anomalous behavior. Figure 5.3 is in marked contrast to Fig. 1.1, where even if all the points in the interval $\tau = 1.5$-1.6 were ignored, and the entire "extended fluid" branch as well, the remaining points for the regular face-centered cubic lattice realizations would clearly indicate the presence of some sort of anomaly between $\tau = 1.5$ and 1.6. The Monte Carlo results for the 12-molecule system as plotted in Fig. 5.3 give no hint of any sort of anomaly which might suggest a phase transition for large systems, nor does Fig. 5.4 in which the mid-range data are shown in the usual linear representation.

Comparing (Figs. 5.3 and 5.4) the present results for 12 hard circles with those of the original investigation[1] of the system of 224

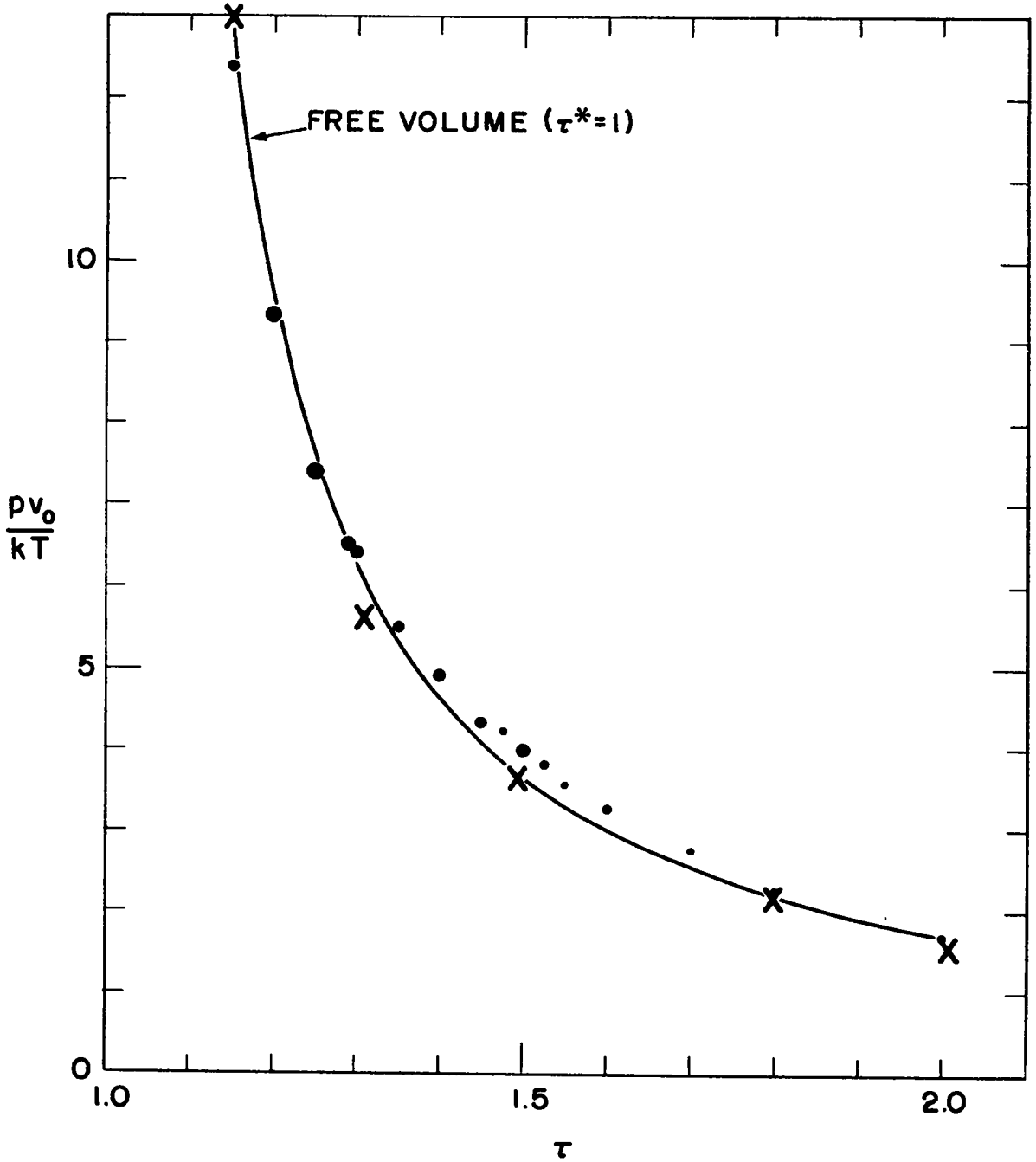

Fig. 5.4 Central portion of Fig. 5.3 replotted on a linear scale. The radii of the points (•) correspond approximately to the standard deviations given in Table 5.1.

hard circles, we note that there is approximate agreement at both low and high densities, as would be expected from the Lebowitz-Percus[17] and Salsburg-Wood[18] analyses. A more quantitative comparison at these two extremes will be made in Chapter 10.

The present results appear to be significantly higher than the previous ones in the mid-density range $\tau = 1.3$ to 1.5, say. Two explanations of this difference are possible. On the one hand, it is conceivable that the two systems, one of 12 molecules in a rectangular cell, the other of 224 molecules in a square cell, simply have appreciably different equations of state in this region. As will be seen when the behavior of the 48-molecule system is described, there is reason to suspect that such is indeed the case, but in quite a different fashion from that suggested by the results of Ref. 1.

The other possibility is that the random walks of Metropolis et al., because of the rather slow calculator available at the time, were not long enough for convergence; that is, their averages are too low due to "memory" of the initial regular configuration. In our opinion this latter possibility is quite likely since according to Metropolis et al.,[1] their random walks were all less than 22 400 steps long, only slightly exceeding the usual time-smoothing interval for our smaller systems. We ordinarily discard the first coarse-grained observation because it shows a tendency to fall below the over-all average, particularly in the mid-density range.

5.1.2 A single "compressor" experiment.

With the intention of seeing whether we could obtain an "extended fluid" branch of the 12-molecule equation of state distinct from that obtained by starting the realizations from the hexagonal lattice, we carried out one "compressor" experiment using the technique described in Section 1.2.3. The configuration selected was the last one in realization A16 at $\tau = 1.5$. It was "compressed" to $\tau = 1.29$, and the resulting configuration used as the starting point for realization A10. As shown in Figs. 5.3 and 5.4 the resulting reduced pressure is not significantly different from that expected for a realization begun at the regular hexagonal configuration.

At the time, this result was interpreted as additional support for the absence of any behavior indicative of a phase transition. However, our subsequent experience in studying the geometrical structure of both this and the larger system has suggested, as will be discussed in Section 5.2.2, that the parent configuration from realization A16 had a structure so close to the regular hexagonal configuration that the above result might have been expected.

At this point the investigation turned to the 48-molecule system, with results to be described in the next chapter. Recently the laboratory acquired the high-speed, electronic printer-plotter device (SC-4020) mentioned earlier, with which it has been feasible to make a much more thorough study of the geometrical structure of the hard-circle system than was possible using hand-plotting techniques. Accordingly, we

returned briefly to the 12-molecule system in order to study its geometrical character as a function of the reduced area τ, as will be discussed in the following section.

5.2 Geometrical Structure of the 12-Molecule System

5.2.1 Voronoi polygons.

In characterizing the geometry of irregular configurations sampled from the Markov chain realizations, we will find it convenient to employ the "Voronoi polygons" used by Rogers[16] in establishing his upper bound for the greatest possible packing density of hard spheres, and by Bernal[20] in his recent studies of the packing of hard spheres (in the three-dimensional case, of course, one has "Voronoi polyhedra" whose definition and properties are similar to those given below for two-dimensional systems).

In any configuration $\vec{r}$ of a system of N hard-circle molecules, there is one Voronoi polygon for each molecule i. It is defined as consisting of all those points of V (regarded as the surface of a torus) which are closer to $\vec{r}_i$ (the center of molecule i) than to the center of any other molecule. The boundaries of the polygon are evidently segments of some of the N - 1 perpendicular bisectors of the line segments $\vec{r}_{ij}$, $j = 1, 2, \cdots, N, \neq i$. From the definition it is easy to see that the N polygons are all convex and fit together so as to fill the area V.

In irregular configurations a convenient (for some purposes) definition of a "neighbor" of molecule i is any other molecule whose Voronoi polygon shares an edge with that of molecule i; the number of such

neighbors will be called the "Voronoi coordination number." These definitions are not always equivalent in the case of regular lattice configurations to the usual definitions of "nearest neighbor" and coordination number. For example, in the regular hexagonal configuration the definitions are equivalent, but in the tetragonal lattice of Fig. 3.7 there are six Voronoi neighbors, and only four nearest neighbors.

5.2.2 The "compressor" experiment.

Figure 5.5 shows the parent configuration, from realization A16 at $\tau = 1.5$, with which the compression was started, the configuration obtained after compression to $\tau = 1.29$, from which realization A10 began, and the last configuration ($t = 326\ 400$) of A10. In these and other figures of this type, the bonds connect "Voronoi neighbors" as defined in the preceding subsection. It should be mentioned in passing that they have been drawn in "by eye" and may be in error in borderline cases in which the shared edge is quite small or non-existent.

We note that the configuration before compression, Fig. 5.5a, is recognizably close to the regular hexagonal configuration (compare with Fig. 3.2); all molecules have Voronoi coordination number 6, and the bonds are not far from their regular lattice arrangement. Figure 5.5b, at the end of the compression, is still more so. Thus, the ensuing realization A10 would be expected to be statistically equivalent to one started from the usual lattice, as the resulting reduced pressure indicated (Section 5.1.2).

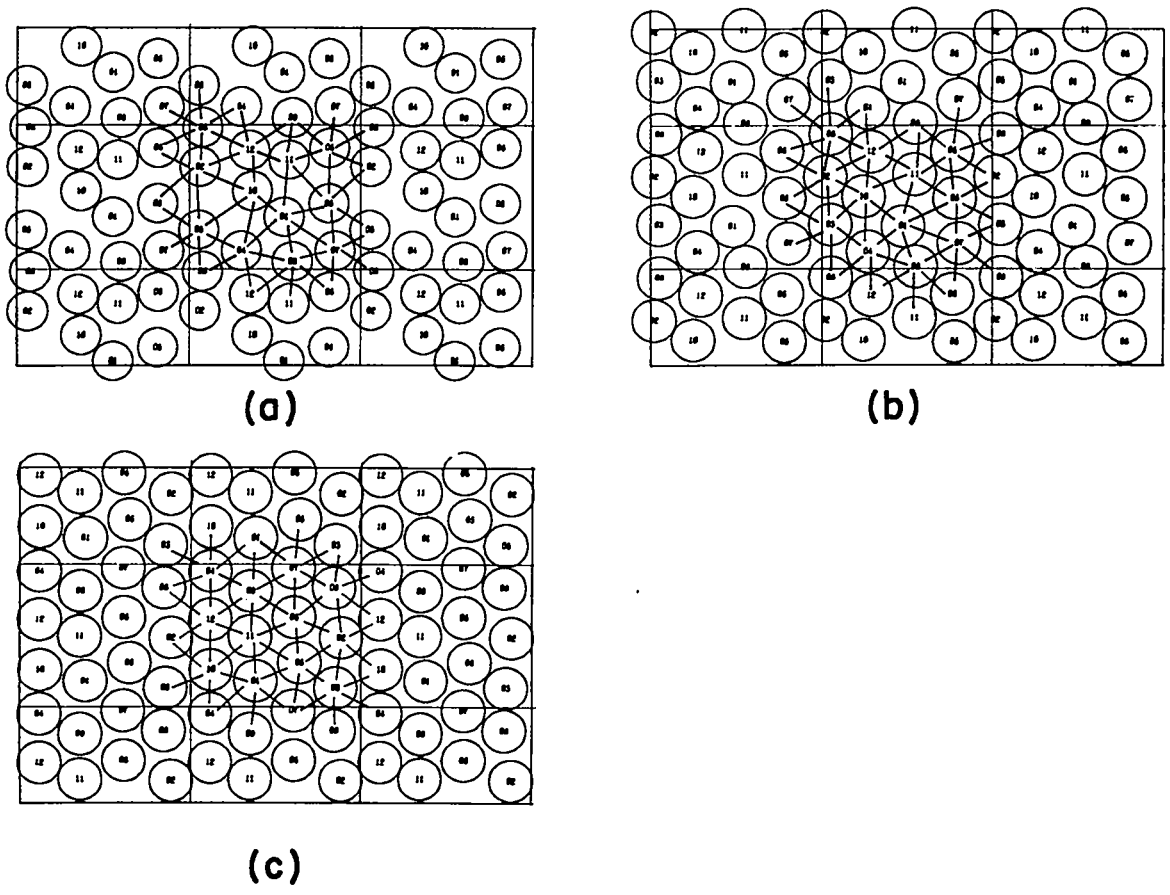

Fig. 5.5 Snapshots of realization A10 at $\tau = 1.29$ (compressor experiment).
(a) parent configuration from realization A16 at $\tau = 1.5$
(b) initial configuration of A10, obtained by compressing (a) to $\tau = 1.29$;
(c) final (t = 326 400) configuration of A10

The final configuration, Fig. 5.5c, is topologically equivalent to (b); the connectivity is identical, indicating that throughout this realization no "diffusion" of the molecules took place. (This conclusion is supported by an examination of all the intervening "snapshots" of this realization.)

5.2.3 Regular hexagonal realizations at $\tau < 1.3$.

All seven of these realizations (A1 through A5, A7, and A8) behaved like A10. The connectivity of the initial regular hexagonal lattice (in the Voronoi sense, Section 5.2.1) was preserved throughout with no molecular interchanges ("diffusion"). The longest of these realizations is A8 at $\tau = 1.250$ which was developed to 576 000 time steps. Thus, the structure of the 12-molecule system in the sampled region of configuration space at these densities is definitely crystalline-like. Furthermore, in terms of the Salsburg-Wood analysis, the state point has evidently remained over long "times" in the region of accessible configuration space associated with the initial hexagonal configuration even at expansions appreciably above $\tau = 1.136$, i.e., at expansions where the discussion of Section 3.4 shows that this configuration and some of its permutations are connected.

This may be interpreted as experimental evidence that such connections are extremely constricted and difficult to traverse in this range of density. Such a state of affairs is consistent with the further possibility that the volume of these connections is negligible in

comparison with the regions in the vicinity of the lattice configuration, but such is not necessarily the case. For example the situation indicated schematically in Fig. 5.6 would also account for the behavior of these realizations.

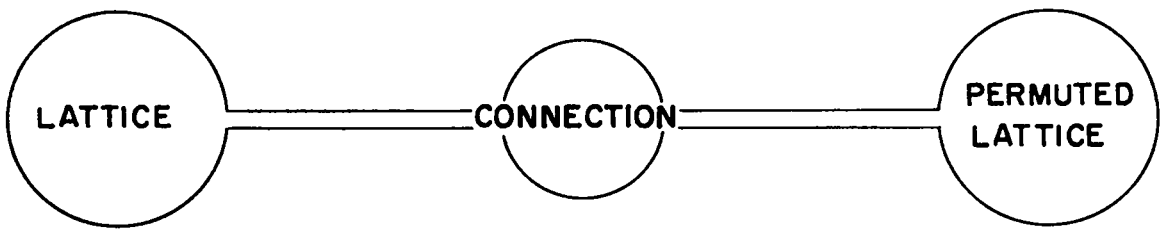

Fig. 5.6 Schematic example of a constricted connection between two lattice permutations, which has non-negligible volume.

5.2.4 Realizations started from the tetragonal lattice of Fig. 3.7.

In order to study the significance of the tetragonal lattice structure shown in Fig. 3.7 and discussed in Section 3.4.4, and in particular to investigate its relation in configuration space to the usual regular hexagonal lattice, we generated two realizations with this configuration as their starting points.

5.2.4.1 Realization A6 at $\tau = 1.15$.

This reduced area represents an expansion of about 3% above the close-packed value 1.1163 for this lattice. The development was carried to only t = 96 000, with all "snapshot" configurations exhibiting only insignificant deviations from the initial arrangement. This suggests, on the basis of the Salsburg-Wood analysis (Section 3.3) that the resulting reduced pressure ought to be in approximate agreement with the value calculated from the free-volume theory based on this lattice, i.e., from Eq. (3.6) with $\tau^* = 1.1163$. Figure 5.3 shows that such is indeed the case, the difference again being roughly as expected on the basis of the N^{-1} correction term in Eq. (3.5).

5.2.4.2 Realization A9 at $\tau = 1.25$.

Here the initial tetragonal configuration was found to be "unstable" with respect to transition to configurations of the usual hexagonal type. Figure 5.7 shows the "snapshots" at t = 0, 4 800, 9 600, and 14 400. By t = 14 400 the structure is seen to be a nearly perfect hexagonal arrangement for this system (compare Fig. 3.2). The arrangement remained unchanged (i.e., there was no "diffusion") throughout the remainder of this relization (t = 96 000).

5.2.4.3 Interpretation.

The behavior of realization A6 strongly suggests that at $\tau = 1.15$ the tetragonal lattice has a "pocket" or region of accessible states

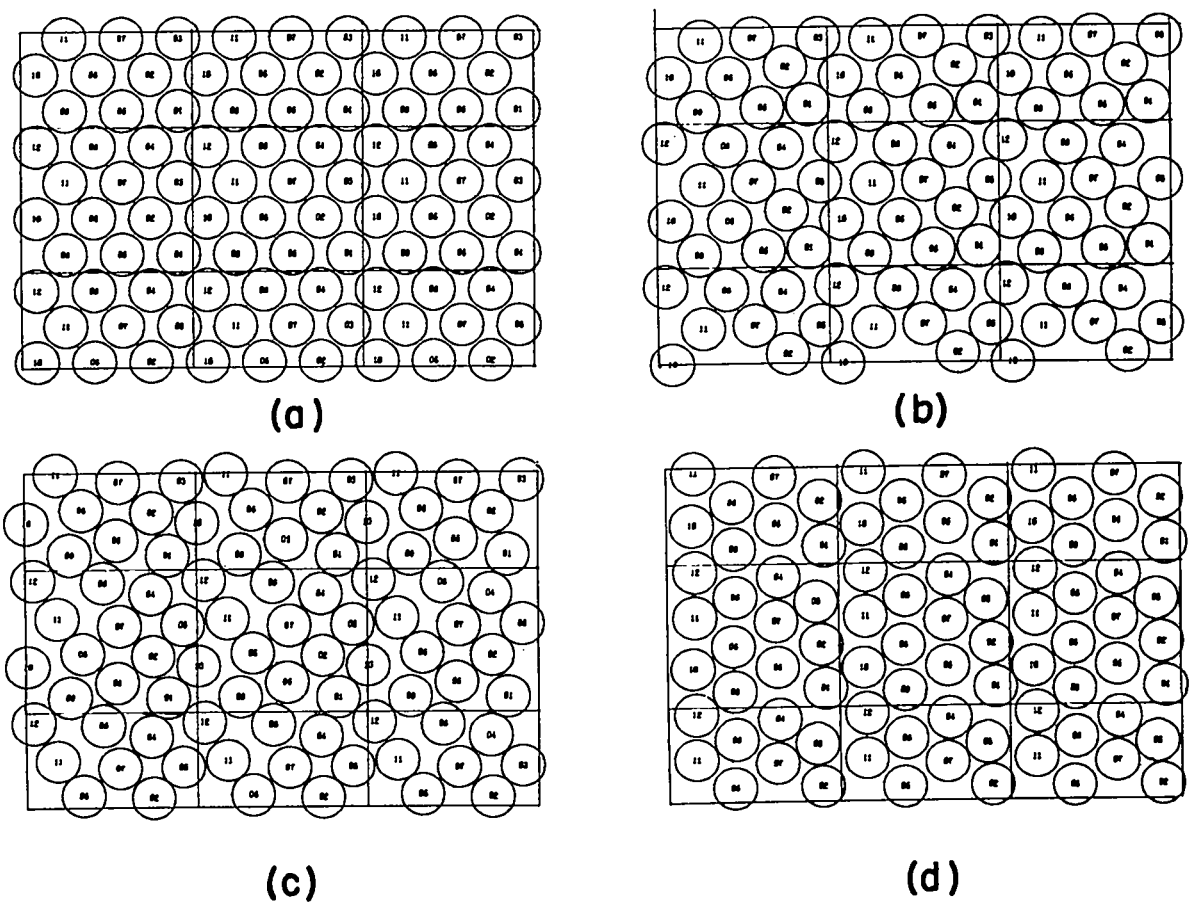

Fig. 5.7 Snapshots showing the relaxation of realizations A9 at $\tau = 1.25$ from the tetragonal lattice of Fig. 3.7 at t = 0 (a), through intermediate structures at t = 4 800 (b) and t = 9 600 (c), to the regular hexagonal structure at t = 14 400 (d).

which is at least effectively, if not actually, disconnected from the region around the regular hexagonal lattice. (The latter region is doubtlessly larger, since the volume of the tetragonal pocket must become zero at $\tau = 1.1163$.)

At $\tau = 1.25$, on the other hand, the rapid relaxation of realization A9 shows that the two lattice points are connected, and suggests that the "pocket" associated with the tetragonal lattice is no longer large compared to all its connections with other pockets. Thus, we are led to conclude that at $\tau = 1.25$ a pocket of hexagonal states is large compared to the volume of any other configuration space region that is easily accessible from the tetragonal configuration. At reduced areas greater than 1.25, we would expect the tetragonal configuration to be even more short-lived.

These inferences are all in agreement with our comments in Section 3.4 concerning the expected unimportance of the tetragonal type of configuration. In particular its stability character appears to be quite different from that of configurations on the "extended fluid" branch of the hard-sphere system ($N = 32$). The latter configurations were apparently very stable with respect to transition to nearly face-centered cubic configurations. The only reservation is that at this stage this interpretation is based on just one observation (A9) of definite instability, plus the more negative evidence of the non-appearance of tetragonal configurations in the other realizations at $\tau < 1.3$. We will return to this point as we discuss the realizations at larger reduced areas.

5.2.5 Realization All at $\tau = 1.3$.

Realization All at $\tau = 1.3$ is the highest density realization for the 12-molecule system in which different permutations of the regular hexagonal configuration were observed. Snapshots before and after the first such permutation are shown in Fig. 5.8, from which it is seen that during this interval of 19 200 steps the column of molecules 1, 5, and 9 experienced a net upward displacement around the torus of one lattice distance relative to the other molecules. This realization was developed to a total of 576 000 steps, during which two other displacements of the same type occurred.

This is the mechanism which was discussed in Section 3.4.3 as the probable first accessible path between permutations. It is noteworthy

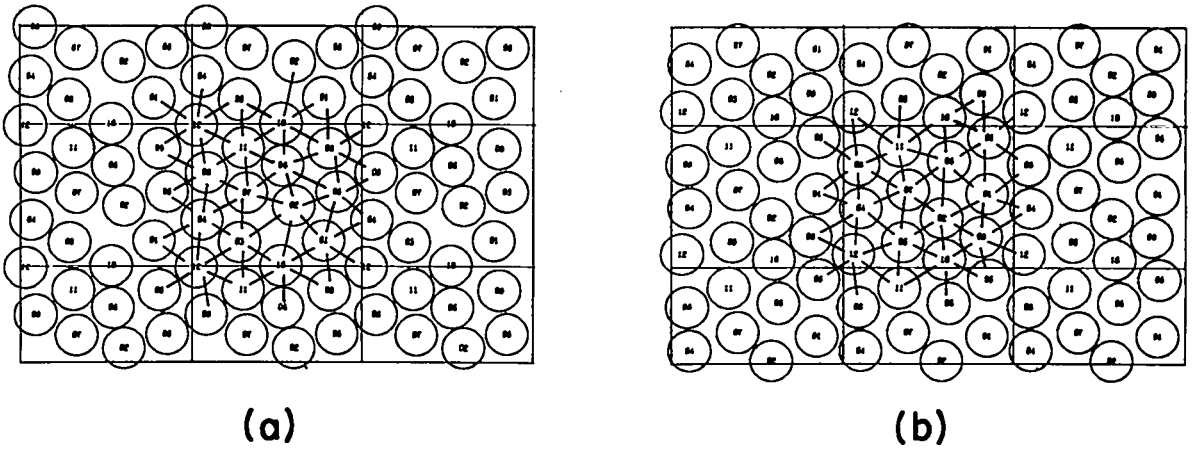

Fig. 5.8 Snapshots showing diffusion in realization All at $\tau = 1.3$, (a) t = 76 800 and (b), t = 96 000. Compare with Fig. 3.6.

that although it was there calculated that the path exists at $\tau \geq 1.136$, the present reduced area of 1.3 is the smallest at which it was observed, and furthermore this reduced area is rather close to the value $\tau = 4/3$ at which this rotation of the three-molecule columns is possible in the regular lattice configuration itself.

It is also significant that all the snapshots of this realization are recognizably close to the hexagonal lattice. Occasionally, molecules with coordination numbers of 5 and 7 (in the Voronoi sense) were noticed. The typical situation in which they appear is that sketched in Fig. 5.9. Hexagonal connectivity can be restored by a small relative motion which replaces bond BD by AC (dashed line).

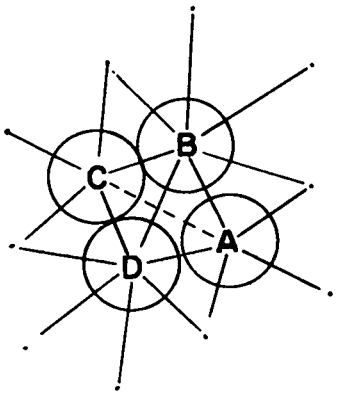

Fig. 5.9 The simplest occurrence (solid lines) of Voronoi coordination numbers 5 (molecules A and C) and 7 (B and D).

These observations are further evidence that in this system the connections between permutations of the regular hexagonal configuration are indeed very constricted at expansions appreciably greater than the reduced volume at which they first appear. In addition, as far as the simple mechanism of Fig. 3.6 is concerned, the connection itself probably possesses no "pocket" of the sort depicted in Fig. 5.6.

Figure 5.4 shows that just at this reduced area, where the system is first observed to make its way through this connection, the computed pressure crosses above the free-volume curve. In terms of the Salsburg-Wood analysis, at this density the contribution to the pressure of configurations neglected in the polytope approximation to accessible configuration space becomes comparable to the effect of the finite number of molecules (12) of this system. This would suggest, if substantiated for larger systems, that the free-volume pressure may indeed be a useful approximation at expansions greater than the range $O(N^{-\frac{1}{2}})$ required for the Salsburg-Wood demonstration.

5.2.6 Realization A12 at $\tau = 1.35$.

At this density additional types of motion between permuted hexagonal configurations were observed, and the extent of distortion from the regular arrangement increased, as would be expected. But in general the snapshot configurations were recognizable approximations to the regular hexagonal configuration, and the appearances of permutations were rare enough so that successive snapshots at intervals $\Delta t = 19\ 200$ could

be explained in terms of a simple motion of a small number of molecules. Examples, in addition to the columnar motion already described, were the one-step displacement of a staggered row of four molecules, such as the cycle 5 → 4 → 7 → 6 → 5 in Fig. 3.2, or a ring shift such as 6 → 10 → 11 → 7 → 6, also in Fig. 3.2.

The configuration at t = 614 400, Fig. 5.10, was exceptional. The arrangement can be made hexagonally connected, in the Voronoi sense, by replacing the bond 10-11 by 6-7, but the result is not the usual regular hexagonal configuration of Fig. 3.2. Instead it is a very close approximation to the tetragonal lattice of Fig. 3.7. (As a matter of fact, it was this snapshot which made us aware of the existence of this alternative lattice for systems with L/M = 2/3.) The following snapshot was

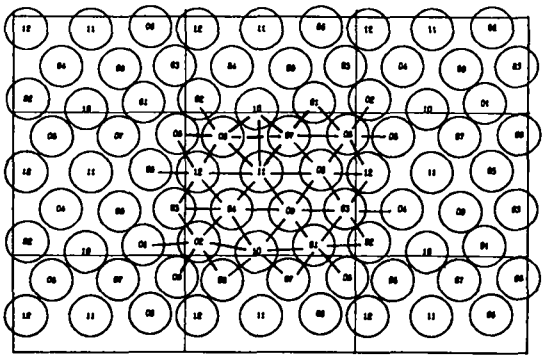

Fig. 5.10 Snapshot showing the occurrence of the tetragonal arrangement of Fig. 3.7 in realization A12 at τ = 1.35; t = 614 400.

again of the usual hexagonal type, indicating that the tetragonal arrangement probably does not posses a well-defined "pocket" of accessible configuration space at this reduced volume (see also Section 5.2.4).

5.2.7 Realizations at $\tau \geq 1.4$.

In realization A14, at $\tau = 1.4$, two of twenty-five snapshots had arrangements related to Fig. 3.7; most of the rest were recognizable approximations to the regular hexagonal lattice. At this density considerable distortion from the lattice was frequent, and considerable relative motion often occurred between successive snapshots ($\Delta t = 19\ 200$).

As τ increased from 1.4 to 1.6, the structures in which the regular hexagonal lattice was recognizable decreased in frequency, while those of irregular or random appearance increased. Occasional configurations of the tetragonal (Fig. 3.7) type appeared, but not very frequently. At $\tau = 1.5$ most configurations could still be classified as regular hexagonal types, e.g., Fig. 5.5a. Figure 5.11 shows four atypical configurations of realization A17 at this reduced area. At $\tau = 1.6$ the majority of the snapshots were best described as irregular or random.

When τ becomes as large as 2, the configurations become gas-like. Figure 5.12 shows some examples at $\tau = 2.5$ and 3.0.

5.2.8 Summary.

Our over-all impression from this examination of the geometrical structure of the system of 12 hard circles over the entire range of

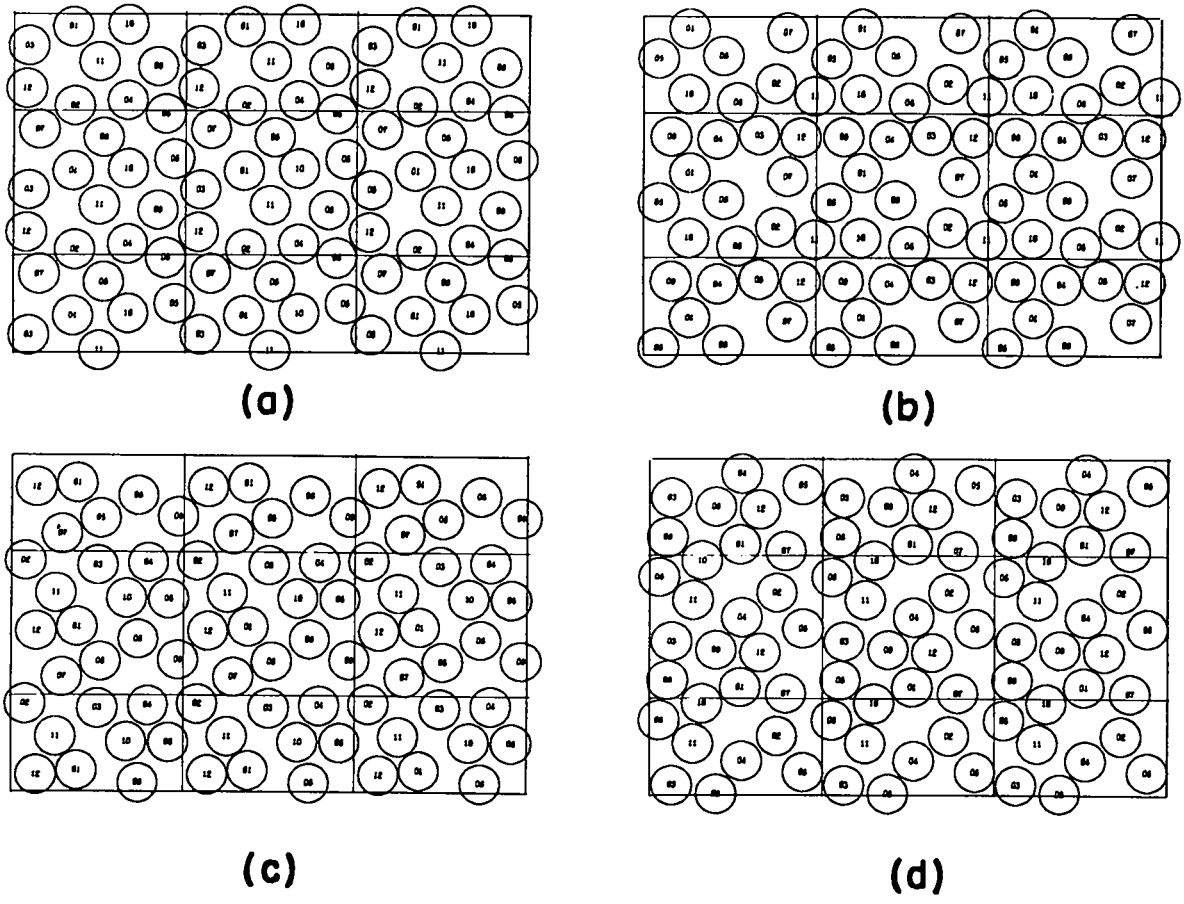

Fig. 5.11 Selected atypical configurations from realization A17 at $\tau = 1.5$.

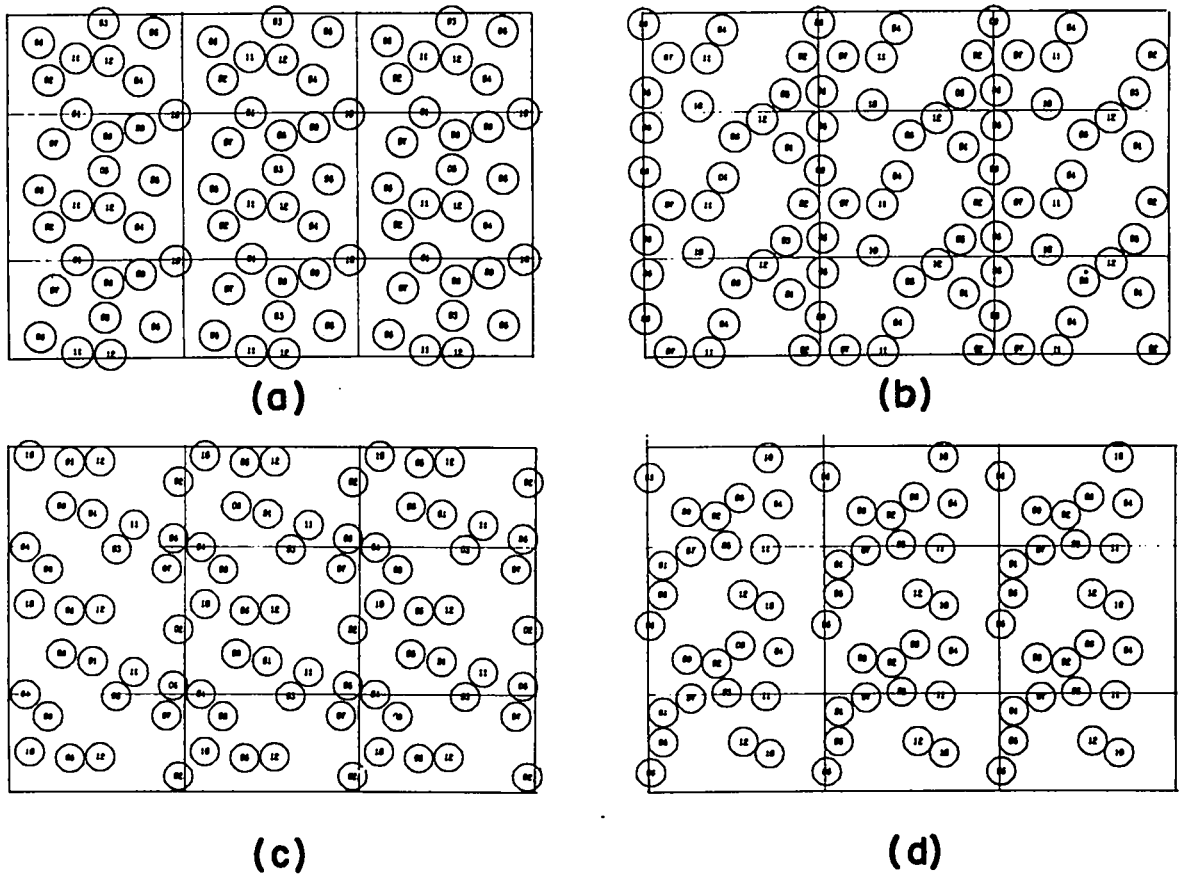

Fig. 5.12 Sample snapshots at $\tau = 2.5$ (a and b) and $\tau = 3.0$ (c and d).

interesting densities is one of gradual change from ordered hexagonal structure at high density to random structure at low density.

One of our main objectives in making this study was to see if structures in the intermediate density range would give any hint of a possible "extended-fluid" branch of the equation of state. We were guided in this connection by the results of our structural study of the 48-molecule system. This study will be described later in this report, but was carried out before that on the smaller system. Here it will suffice to mention in advance that in the 48-molecule system an "extended fluid" branch was found, and that it had a characteristic geometrical structure which was also quite evident at slightly larger reduced areas in realizations started from the regular hexagonal lattice. This structure, as we shall see, is not one which has an analogue in the 12-molecule system, but it seemed nevertheless probable that we might recognize any systematic occurrence of a structure that might have a similar role.

As the previous sections have indicated, no such characteristic structure was noticed in the small system. The only exceptional arrangement noticed was the tetragonal lattice of Figs. 3.7 and 5.10, which is not believed to be the basis of such a branch of the equation of state for the following reasons. First, at no reduced area is it a predominant or frequent structure in realizations started from the usual hexagonal arrangement. Second, it appears to be definitely unstable with respect to transition to hexagonal structures at $\tau \geq 1.25$. There appears to be a corresponding branch of the equation of state over a small range of

reduced areas above 1.1163, which agrees approximately with the free volume theory with $\tau^* = 1.1163$, as expected from the Salsburg-Wood analysis. However, this branch is expected to disappear with increasing N, and in any case it does not have the properties of an "extended fluid" branch.

Finally, we mention again that the system remains in the configuration space "pocket" associated with the initial hexagonal arrangement throughout quite long realizations at reduced areas up to 1.3, although connections with some of the permuted arrangements are known to appear in this system at $\tau = 1.136$.

5.3 Resume of the Results for the 12-Molecule System

Our main conclusion from our study of this small system is that it shows no behavior indicative of a phase transition in system of a large number of hard-circle molecules. The reasons for this conclusion are (1) the appearance of the calculated isotherm, shown in Figs. 5.3 and 5.4 and discussed in Section 5.1.1; (2) the absence of any "jumpy" or "two-plateau" behavior of the control charts; (3) the apparent absence of an "extended fluid" branch of the equation of state; (4) the gradual change in structure with increasing reduced area.

The third of these observations is indirect, being based on the failure to note any spontaneously appearing structure which seemed likely, on the basis of our experience with the 48-molecule system (see Section 5.2.8), to form a basis for an extended fluid branch. Further

"compression" experiments on the 12-molecule system could have been carried out starting with some of the less regular configurations noticed at $\tau \geq 1.4$, but this did not seem worthwhile in view of the probability of a negative result, as well as the rather tangential significance of a positive one, due to certain aspects of the behavior of the 48-molecule system which will be discussed subsequently.

The Monte Carlo pressures seem to approach agreement with the free volume approximation at high densities (Fig. 5.3) as suggested by the Salsburg-Wood analysis, a more precise correlation with the theoretical N-dependence being left for discussion along with results for the 48-molecule system. Comparison of the calculated pressure with the free-volume approximation suggests that the latter may be useful over a larger range of expansions than the $O(N^{-\frac{1}{2}})$ range required to localize the molecules in the strict sense demanded by the Salsburg-Wood asymptotic analysis.

At low densities the calculated pressures appear to approach agreement with the virial expansion (Fig. 5.3), a precise comparison with the theoretical N-dependence of Lebowitz and Percus again being left for later discussion.

Chapter 6

QUALITATIVE SURVEY OF REALIZATIONS FOR THE 48-MOLECULE SYSTEM

The system of 48 hard circles was discussed earlier in Section 3.5, and is shown in its regular hexagonal configuration in Fig. 3.3. For this system we generated 39 realizations, whose parameters and resulting compressibility factors are given in Table 6.1.

The compressibility factors are given here in order to facilitate the qualitative discussion of these realizations. The data reduction methods which were used to arrive at these estimates and their associated standard deviations (which follow the ± signs in the table) are discussed in Chapters 7, 8, and 9. As with the 12-molecule system, the reader is warned at this point that there is reason to expect the standard deviation estimates to be too optimistic.

The reduced pressures corresponding to the compressibility factors in Table 6.1 are plotted in Fig. 6.1 on the same logarithmic scales as used in Fig. 5.3 for the 12-molecule system and in Fig. 1.1 for hard spheres. Because of the small scale of this figure some of the points in the interval $\tau = 1.3\text{-}1.355$, and also most replicated points, are omitted.

TABLE 6.1 PARAMETERS AND COMPRESSIBILITY FACTORS FOR THE SYSTEM OF 48 HARD CIRCLES

Realization	τ	Code[a]	Initial Config.[b]	$\frac{2\delta}{a-\sigma}$	$-\log_2 \frac{\Delta r^2}{48a^2}$	K	n[c]	Observations[d]	$\frac{pV}{NkT}$
B 1	1.025	A	L	2.3	15	18	160	2-160	80.399 ± 0.292
B 2	1.025	B	L	2.3	15	18	100	2-100	80.315 ± 0.366
B 3	1.025	B	L	2.4	16	18	121	2-121	80.664 ± 0.354
B 4	1.025	A	L	2.4	16	18	100	2-100	80.962 ± 0.388
B 5	1.040	B	L	2.4	16	18	100	2-100	50.995 ± 0.215
B 6	1.074	B	C	1.5	16	17	99	2-99	97.199 ± 0.737
B 7	1.075	A	L	2.4	13	12	38	2-38	28.216 ± 0.158
B 8	1.075	B	L	2.4	15	19	50	2-50	28.301 ± 0.146
B 9	1.124	A	C	1.6	13	12	21	2-21	29.042 ± 0.208
B10	1.124	B	C	1.6	15	19	58	2-58	29.388 ± 0.237
B11	1.125	A	L	2.3	13	12	33	2-33	17.666 ± 0.084
B12	1.150	B	L4	0.44	16	18	40	6-40	42.587 ± 0.254
B13	1.169	A	C	1.8	13	11	33	2-33	18.545 ± 0.104
B14	1.240	A	L	2.2	13	11	100	2-100	10.277 ± 0.039
B15	1.250	B	L4	2.03	13	19	13	—	—
B16	1.254	A	C	2.0	13	11	75	2-75	11.645 ± 0.051
B17	1.275	A	L	2.2	13	13	101	2-101	9.280 ± 0.035
B18	1.290	A	C	2.3	13	13	50	2-50	8.886 ± 0.039
B19	1.300	B	L	2.4	13	17	150	2-80	8.747 ± 0.036
								81-150	10.484 ± 0.089
								120-150	10.732 ± 0.137
B20	1.316	A	C	2.3	13	13	82	2-19	10.017 ± 0.100
								20-39	8.520 ± 0.068
								40-82	9.941 ± 0.094
B21	1.325	A	L	2.3	13	11	95	2-95	8.583 ± 0.061
B22	1.330	A	L	2.2	13	10	95	1-14	8.359 ± 0.102
								15-26	9.964 ± 0.056
								86-95	8.236 ± 0.060
B23	1.340	A	L	2.2	13	10	141	58-78	8.282 ± 0.098
								102-141	9.370 ± 0.082
B24	1.350	A	L	2.2	13	12	27	2-27	9.238 ± 0.075
B25	1.350	A	L	2.0	13	12	70	1-16	8.174 ± 0.065
								28-40	10.050 ± 0.136
B26	1.350	B	L	2.2	13	12	71	2-71	9.374 ± 0.056
								42-71	9.674 ± 0.122
B27	1.355	A	L	2.3	13	12	49	2-49	8.941 ± 0.064
B28	1.375	A	L	2.2	13	12	92	2-92	8.667 ± 0.047
B29	1.400	A	L	2.2	13	9	90	2-90	8.080 ± 0.053
B30	1.500	A	L	2.0	13	11	47	2-47	6.675 ± 0.065
B31	1.500	B	L	2.2	13	14	151	2-151	6.545 ± 0.032
B32	1.650	A	L	2.5	13	10	38	2-38	5.099 ± 0.042
B33	1.750	A	L	2.5	13	9	41	2-41	4.427 ± 0.036
B34	2.000	A	L	2.6	13	8	50	2-50	3.384 ± 0.027
B35	2.400	A	L	2.9	13	8	22	2-22	2.597 ± 0.026
B36	3.000	A	L	2.9	13	7	51	2-51	2.063 ± 0.012
B37	3.900	A	L	3.0	13	7	27	2-27	1.6766 ± 0.0103
B38	3.900	B	L	2.2	13	14	50	2-50	1.6976 ± 0.0056
B39	3.900	B	L	11.2	13	14	50	2-50	1.6960 ± 0.0055

FOOTNOTES TO TABLE 6.1

a See Section 4.2.

b L = regular hexagonal configuration (Fig. 3.3)
C = configuration obtained by "compressor" technique. See detailed discussion of the realization in the text.
L4 = tetragonal configuration (Fig. 3.7)

c This column gives the total number of coarse-grained observations, each of $\Delta t = 19\ 200$ time steps, in the realization. The total length of the realization is $t = 19\ 200\ n$.

d This column gives the range of s over which the coarse-grained ($\Delta t = 19\ 200$) observations $\tilde{G}(s, \alpha)$ were averaged and differentiated to obtain the quoted estimate of the compressibility factor and its standard deviation.

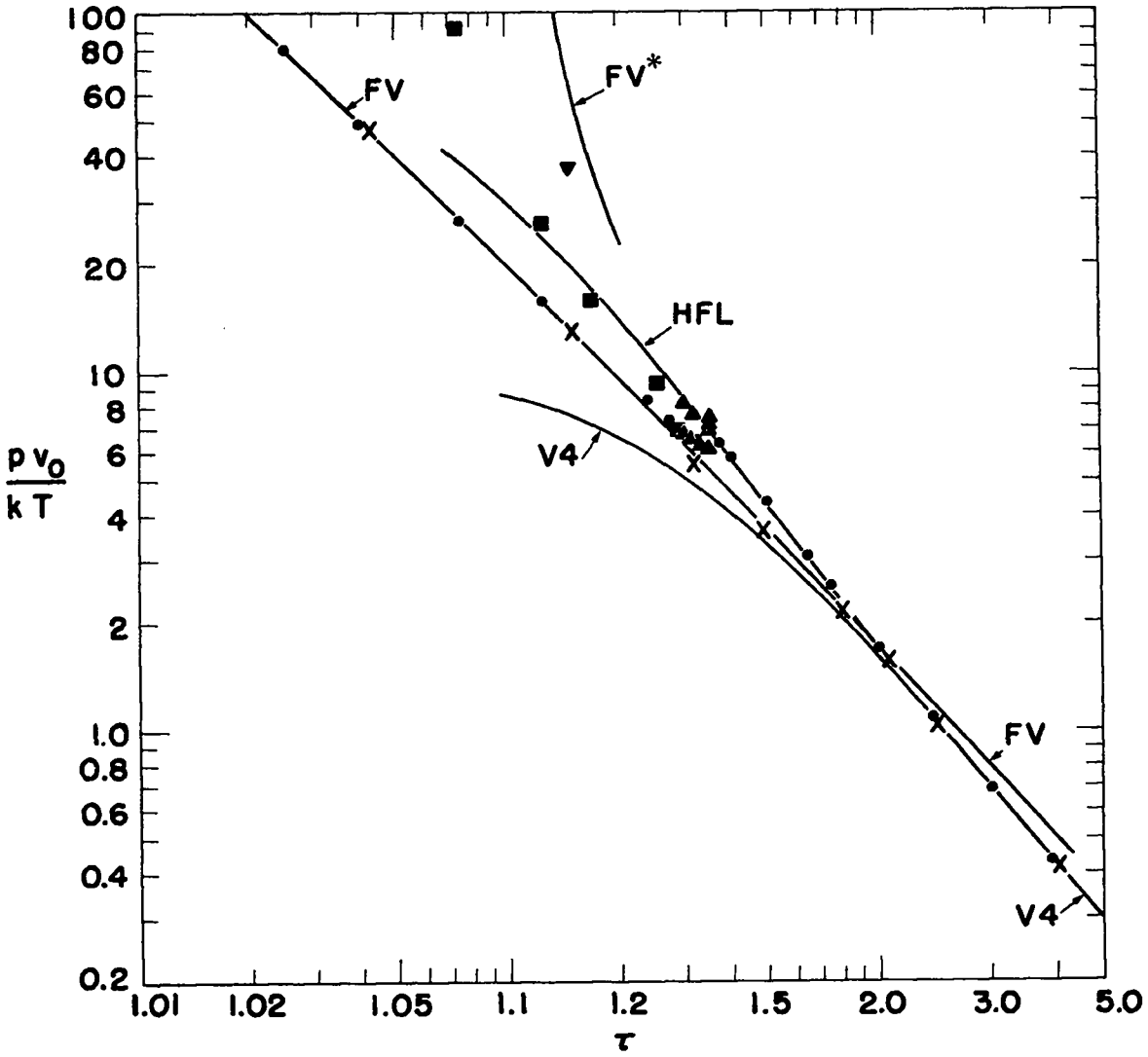

Fig. 6.1 Monte Carlo results for the system of 48 hard circles. ●: completely averaged realizations started from the regular hexagonal lattice. ■: realizations started from "compressed" initial configurations, again completely averaged. ▲: "plateau" estimates in incompletely averaged realizations. ▼: a realization whose initial configuration was the tetragonal lattice of Fig. 3.7. x: Metropolis et al.[1] for their system of 224 hard circles. Curves shown are FV, the usual free-volume theory, Eq. (3.6) with $\tau^* = 1$; FV*, Eq. (3.6) with $\tau^* = 1.1163$; V4, the virial expansion for $N = \infty$ with neglect of terms of $O(\tau^{-5})$ as given in Ref. 1; HFL, the scaled-particle approximation of Ref. 14.

In Fig. 6.2 the reduced pressures in the range $\tau = 1.2\text{-}1.5$ are replotted on the usual linear scale. Here the scale is large enough to show all the points, as well as to indicate the estimated precision.

It will be immediately noticed that Figs. 6.1 and 6.2 indicate a double-valued pressure curve for $\tau \leq 1.35$. This happens in exactly the same way as in the hard-sphere investigation (Chapter 1). In the interval $\tau = 1.30\text{-}1.35$ the realizations show a "jumpy" or "two-plateau" behavior. At $\tau < 1.30$ the higher pressure curve arises by application of the "compressor" technique (Section 1.2.3); as before, it will be called the "extended fluid" branch of the equation of state.

Reserving a quantitative discussion until a subsequent chapter, we note that in Fig. 6.1 the points obtained from the regular hexagonal realizations at high density agree quite well with the free volume theory. Comparing with Fig. 5.3 for the 12-molecule system, we note that the agreement is appreciably improved with the larger system, as would be expected from the Salsburg-Wood analysis, Eq. (3.6). At the low density end of the curve the Monte Carlo points approach agreement with the truncated virial expansion. We also note in Figs. 6.1 and 6.2 that the scaled-particle approximation of Helfand, Frisch and Lebowitz[14] agrees quite well with the entire ($\tau > 1.3$) "fluid branch" of the Monte Carlo results, as these authors pointed out on the basis of the preliminary version of the present data.

Also shown in Figs. 6.1 and 6.2 are the points obtained by Metropolis et al.[1] in their original Monte Carlo investigation of a system of 224 hard circles in a square area V. As with our 12-molecule system, these

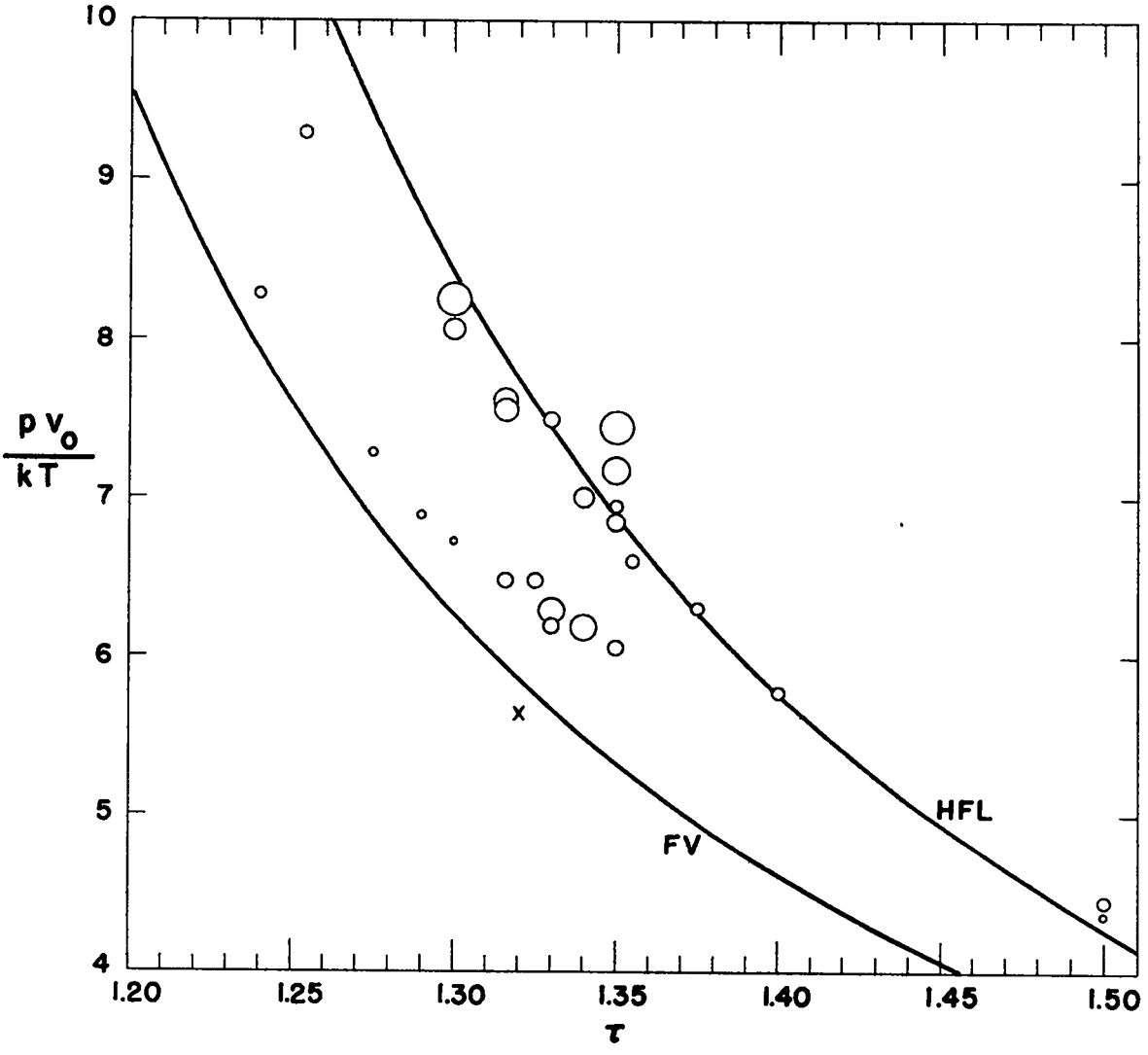

Fig. 6.2 The Monte Carlo results for the 48-molecule system for $\tau = 1.2$-1.5, plotted on a linear scale. All points of Table 6.1 are shown as circles whose radii correspond to the tabulated standard deviation. The curve labels are the same as in Fig. 6.1, and x again indicates a result from Metropolis et al.[1]

early results are in approximate agreement with the present 48-molecule results at low densities, and also with the present regular-hexagonal branch of the equation of state at high densities. Both of these approximate coincidences are, of course, to be expected on the basis of the low density analysis of Lebowitz and Percus[17] and the high density analysis of Salsburg and Wood.[18] A somewhat more quantitative comparison will be made in Chapter 10.

In the mid-density interval $\tau = 1.3$-1.5, these early Monte Carlo results lie below both branches of the 48-molecule equation of state. As in Chapter 5, we again attribute this primarily to the random walks of Metropolis et al. being much too short, as will become evident when the present Markov chain realizations in this interval, particularly for $1.3 \leq \tau \leq 1.35$, are described in detail (Sections 6.1.2 and 6.1.3). However, it must be emphasized that the long-time behavior of Markov chain realizations for the 224-molecule system would by no means necessarily be identical with that of the 48-molecule system to be described in this chapter. Indeed we will see that the particular size (N) and shape (V) of the present system apparently have considerable influence on its statistical behavior in this mid-density interval. Thus, although we incline to the belief that sufficiently long realizations for the 224-molecule system would show a two-plateau behavior similar to that of the 48-molecule system, it is important to label this statement as a conjecture. It derives significant support from the quite similar behavior observed in the various investigations[3,5,6,9,10] of three-dimensional hard sphere systems.

In the remainder of this chapter we will discuss qualitatively the behavior of these realizations for the 48-molecule system on the basis of

their statistical control charts, their estimates of the pressure, and their geometrical structure. We will begin with the realizations whose initial configuration is the regular hexagonal lattice, and we will proceed from the highest densities down through the interval $\tau = 1.30$-1.35 in which the "jumpy" behavior is observed, then on through the lowest density realizations. Next the "extended-fluid" branch is discussed, but following the "compression" process from low to high density. Finally the two realizations begun from the tetragonal lattice (Fig. 3.7) are discussed, after which the chapter ends with a summary and interpretation of these results.

6.1 Regular Lattice Realizations

In this section we discuss in order of decreasing density the realizations begun from the regular hexagonal lattice, as well as realizations B18 and B20 which were started from "compressed" configurations, but whose behavior resembles that of regular hexagonal realizations at the same density.

6.1.1 $\tau < 1.3$, "Crystalline" realizations.

At reduced areas less than 1.3, realizations B1 through B5, B7, B8, B11, B14, and B17 had the regular hexagonal configuration of Fig. 3.3 as their starting points. Realization B18 at $\tau = 1.29$ was begun from a configuration obtained by "compressing" one selected from an apparent L plateau of realization B23. This was done as part of an experiment which

employed the compression procedure as a diagnostic tool in distinguishing L and H plateaus in realizations where the plateaus are not very well defined (see Section 6.1.2.2). As seen from Figs. 6.1 and 6.2, the pressure estimate obtained from B18 indeed falls nicely on the "crystalline" branch of the equation of state determined by the regular hexagonal realizations in the neighborhood of $\tau = 1.29$.

In all of these realizations the initial configuration was maintained throughout the entire realization except for net displacements small compared to the nearest-neighbor distance. That is, in this density range we observed no "diffusion" (no molecular interchanges) in these initially regular hexagonal realizations. Furthermore, the Voronoi connectivity of the sampled "snapshot" configurations was predominantly that of the regular hexagonal lattice. At $\tau = 1.24$-1.29 a few configurations were noticed in which isolated groups of four molecules displayed the simple pentagonal-heptagonal connectivity of Fig. 5.9.

The control charts for these realizations exhibit no notable anomalies, their appearance being qualitatively similar to that of the L plateau of B19 to be discussed below.

Figures 6.1 and 6.2 show that the pressure estimates obtained from these realizations agree well with the free-volume theory at high densities, with the discrepancy gradually increasing with τ.

6.1.2 $\tau = 1.3$-1.355, "Jumpy" realizations.

In this reduced area interval we have realizations B19 through B26, all of which were started from the regular hexagonal lattice except B20

at $\tau = 1.316$. The initial configuration of the latter was obtained by the "compression" procedure, but it is convenient to discuss this realization along with the others in this density range since its behavior is qualitatively the same.

Most of these realizations showed "jumpy" or "two-plateau" control charts reminiscent of those for the hard-sphere systems (Chapter 1). In the following subsections each of the realizations in this interval is discussed individually. As a framework for the discussion it will be convenient to employ the terminology of the "hourglass" model of configuration space (Section 1.2.1). Let us emphasize, however, that by so doing we by no means intend to prejudice a decision in favor of interpreting the observed behavior as indicating a first-order phase transition.

6.1.2.1 Realization B19 at $\tau = 1.3$.

The control charts for the observations of the first three cumulative pair-distribution functions $\tilde{G}(s, \alpha)$, $\alpha = 1, 2, 3$, obtained from this realization are shown in Fig. 6.3. Because of the length of this realization the time-smoothing parameter Δt used in the figure is twice it usual value. On the other hand, the "snapshots" to be discussed below were taken at the usual interval $\Delta t = 19\ 200$, corresponding to the entries in Table 6.1. In the discussion, therefore, we will number the snapshots with index s' on the latter basis, i. e., snapshot s' shows the configuration of the system at $t = 19\ 200\ s'$. This configuration

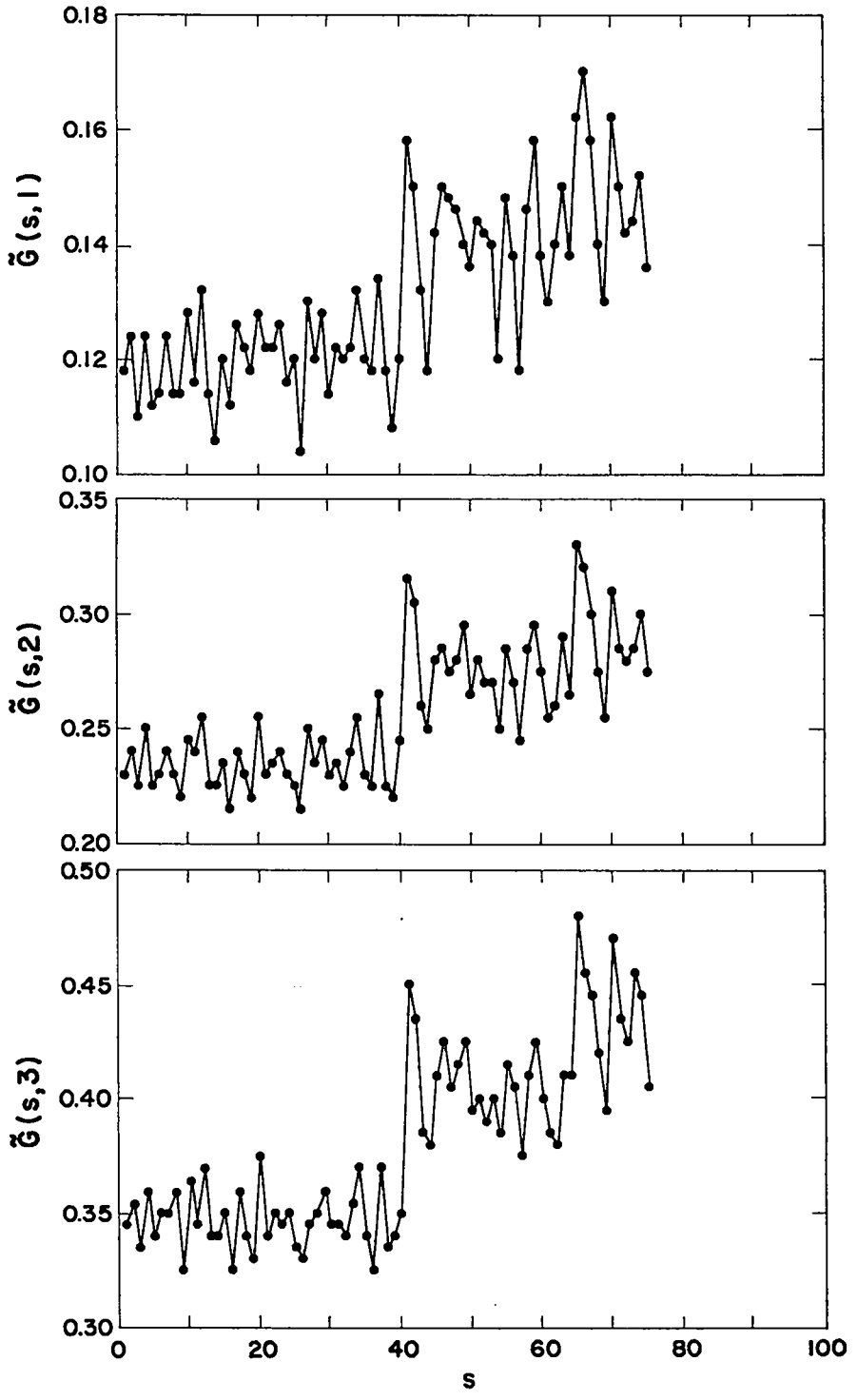

Fig. 6.3 The first three control charts for realization B19 at $\tau = 1.3$; $\Delta t = 38\,400$.

occurs in the middle of time-smoothing interval $s = (s' + 1)/2$ of Fig. 6.3 if s' is odd, and at the end of interval $s'/2$ if s' is even.

The "jump" or shift in level in Fig. 6.3 for $s > 40$ ($s' > 80$, $t > 1\ 536\ 000$) is especially striking and naturally led us to average configurations with $t \leq 1\ 536\ 000$ as a "L plateau", and those for $t > 1\ 536\ 000$ as a "H plateau".

6.1.2.1.1 The L plateau. This plateau exhibits properties which are a continuation of those of regular hexagonal realizations at higher density (Section 6.1.1), not only with respect to its control charts, but also with respect to its estimate of reduced pressure, as well as with respect to its geometrical structure. The reduced pressure obtained from this L plateau is the lowest of the points shown in Figs. 6.1 and 6.2 at $\tau = 1.30$, and clearly is in reasonable agreement with extrapolation of the points obtained from regular hexagonal realizations at higher density.

The geometrical structures of snapshots 1 through 79 were almost all describable as slightly distorted versions of the regular hexagonal arrangement of Fig. 3.3. Snapshot 19 at $t = 364\ 800$, shown in Fig. 6.4a was perhaps the most distorted configuration observed during this plateau. In this configuration we count eight molecules with pentagonal Voronoi coordination, and eight with heptagonal coordination. In order to restore the original connectivity of the regular lattice, ten diagonal bond replacements like that of Fig. 5.9 are required, as indicated by the broken lines in the figure. This is actually what happens on the

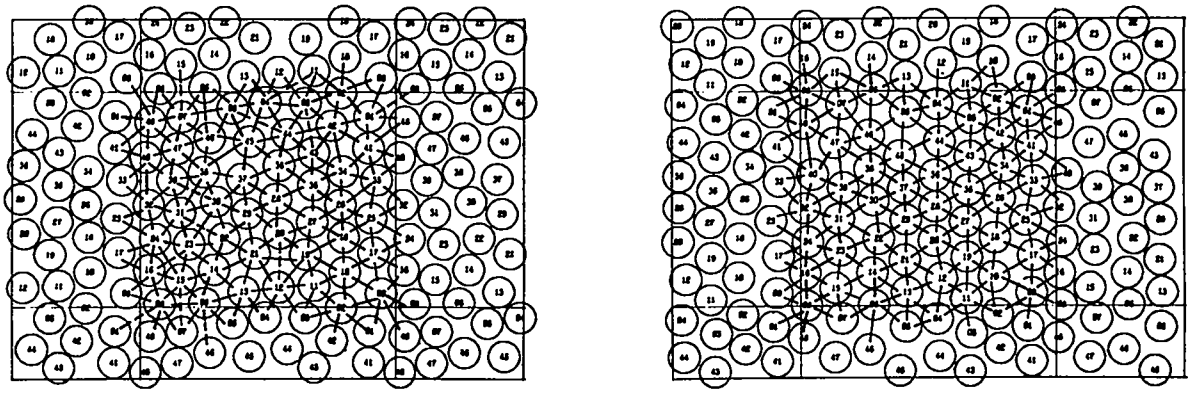

Fig. 6.4 Snapshots from realization B19 at $\tau = 1.3$, showing the relaxation of an atypically distorted, L-plateau configuration (a), t = 364 800, to a more typically regular hexagonal configuration (b), t = 384 000.

next snapshot (Fig. 6.4b, $s' = 20$, t = 384 000), in which the previous distortion has relaxed to restore exactly the original connectivity. Note also that the relaxed configuration is quite close to a regular hexagonal arrangement; it is much more typical of the L-plateau snapshots than is Fig. 6.4a.

Snapshots 21 through 66 showed the hexagonal lattice arrangement to be approximately preserved, with only minor connectivity perturbations of the type shown in Fig. 5.9.

Between snapshots 66 and 68, however, the two columns (5, 13, 21, 29, 37, 45) and (6, 14, 22, 30, 38, 46) moved downwards one lattice step around the torus (see the discussion of this type of motion in Sections 3.4.3, 3.5, and 5.2.5). The intermediate snapshot 67, Fig. 6.5a, is of

interest in that it shows this displacement almost precisely in mid-course. In this configuration there are four molecules with pentagonal Voronoi coordination, and four with heptagonal coordination. The six dotted bond substitutions return the system to the connectivity of snapshot 20 (Fig. 6.4b), whose connectivity is that of the immediately preceding snapshot 66 which is not reproduced here. The six dashed bond substitutions shown in Fig. 6.5a yield the connectivity of the next snapshot 68, Fig. 6.5b. The latter is again a close approximation to the regular hexagonal lattice, but one in which the above-mentioned two columns of six molecules each have moved down one step.

Snapshots 69 through 79 showed only minor distortions of the configuration shown in Fig. 6.5b. The final snapshot of the L plateau

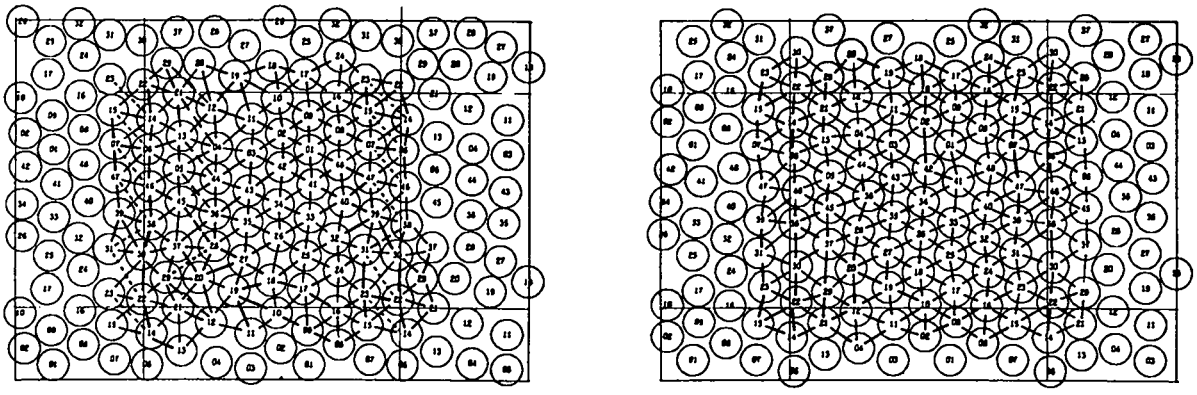

Fig. 6.5 Snapshots 67 (a) and 68 (b), taken at t = 1 286 400 and t = 1 305 600, from the L plateau of realization B19 at $\tau = 1.3$

(Fig. 6.6a, $s' = 80$, $t = 1\ 536\ 000$), however, is atypical of the L class of states, and indicates that the transition to the H region of configuration space, which is first signaled in the control charts by the point for $s = 41$, corresponding to $s' = 81$ and 82, actually occurred somewhat before $s' = 80$, $t = 1\ 536\ 000$. Thus, this snapshot is associated with the H plateau, although the corresponding coarse-grained observation falls in the L plateau.

6.1.2.1.2 The H plateau. The next three snapshots, $s' = 81$, 82, and 83, are shown in Figs. 6.6b through d. All four of these Fig. 6.6 configurations are perhaps best described as irregular. In each case a number of molecules have non-hexagonal Voronoi coordination, and although portions of the system show local order, the over-all structure seems to lack any regular character.

However, the next snapshot ($s' = 84$, $t = 1\ 612\ 800$), shown in Fig. 6.7a, is (to us, at least) a most surprising arrangement. It is an approximately hexagonal arrangement of the 48 molecules into 7 rows of 7 molecules each, except for one row which contains a hole instead of a 49th molecule! We assign molecules to rows as follows:

21	12	19	10	hole	16	21
14	13	4	11	2	9	8
6	44	3	42	1	48	7
46	5	36	43	41	40	47
38	45	35	34	33	32	39
30	37	28	26	25	24	31
22	29	20	27	18	17	23.

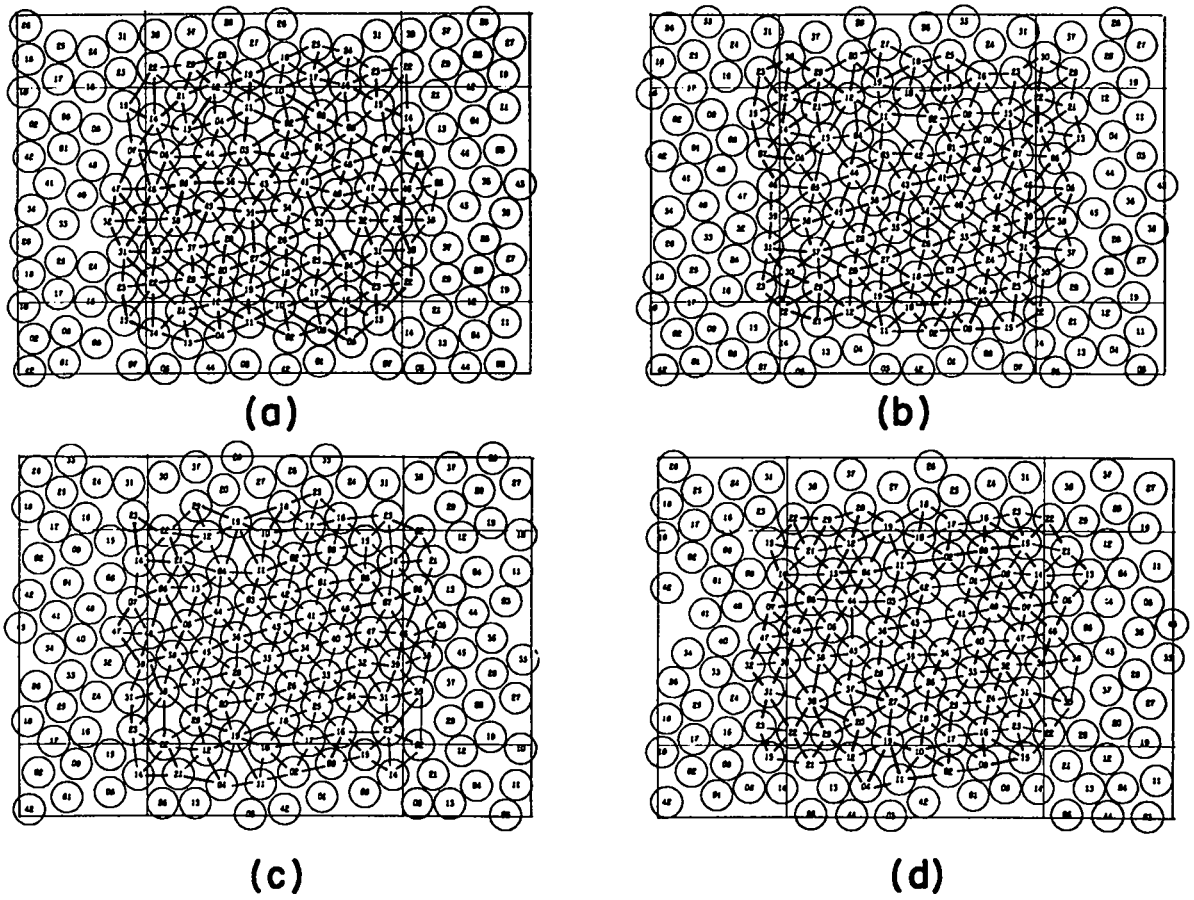

Fig. 6.6 Snapshots 80 through 83, (a) through (d) respectively, of irregular configurations at the beginning of the H plateau in realization B19 at $\tau = 1.3$.

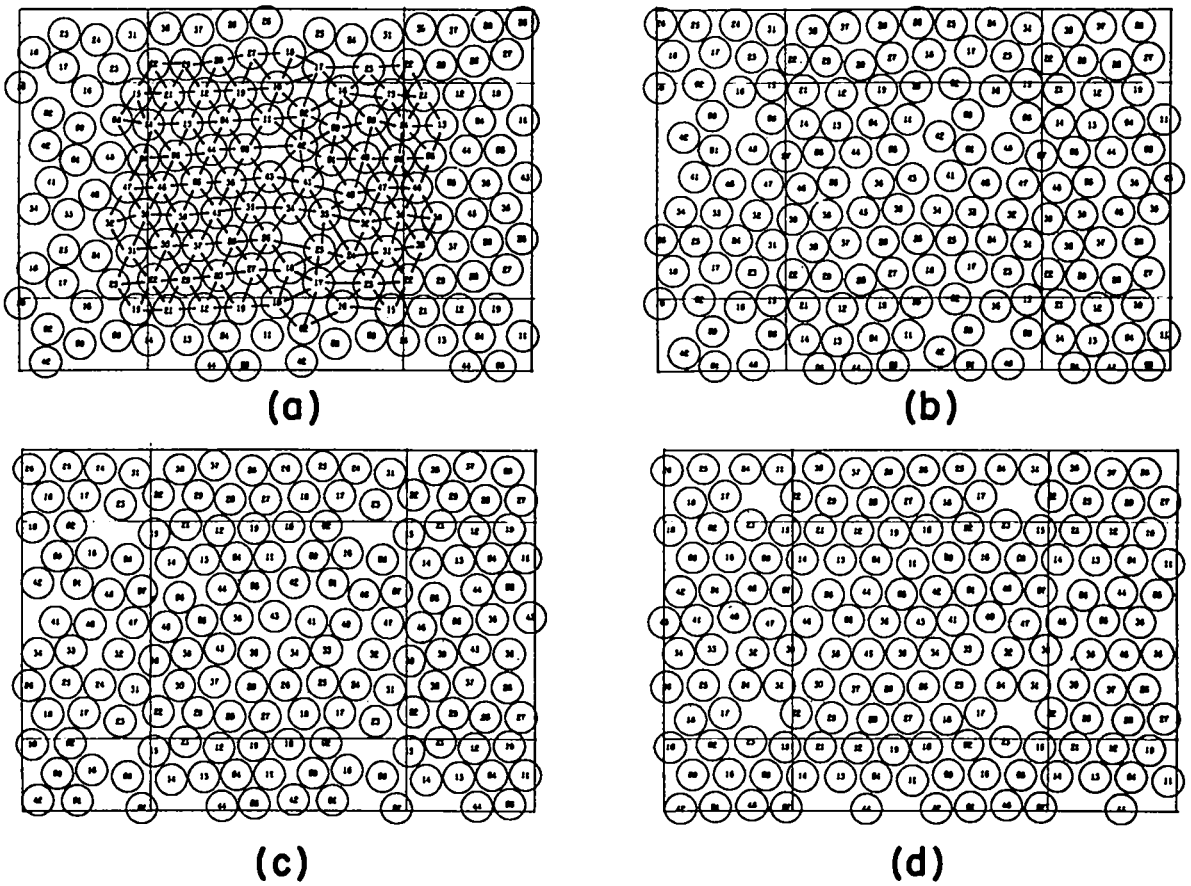

Fig. 6.7a-d Snapshots 84 through 87 from the H plateau of realization B19 at $\tau = 1.3$, showing occurrence of "7X7" structures.

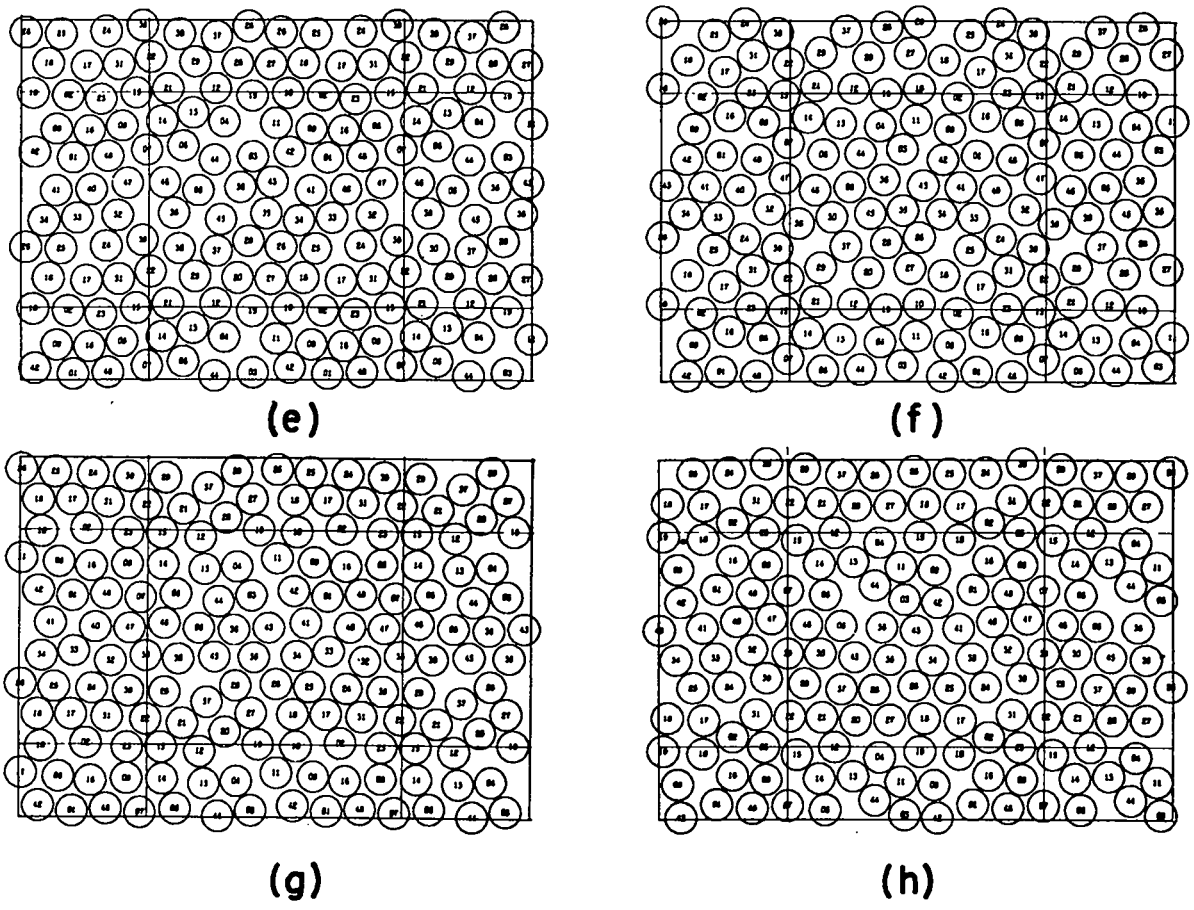

Fig. 6.7e-h Snapshots 88 through 91 from the H plateau of realization B19 at $\tau = 1.30$.

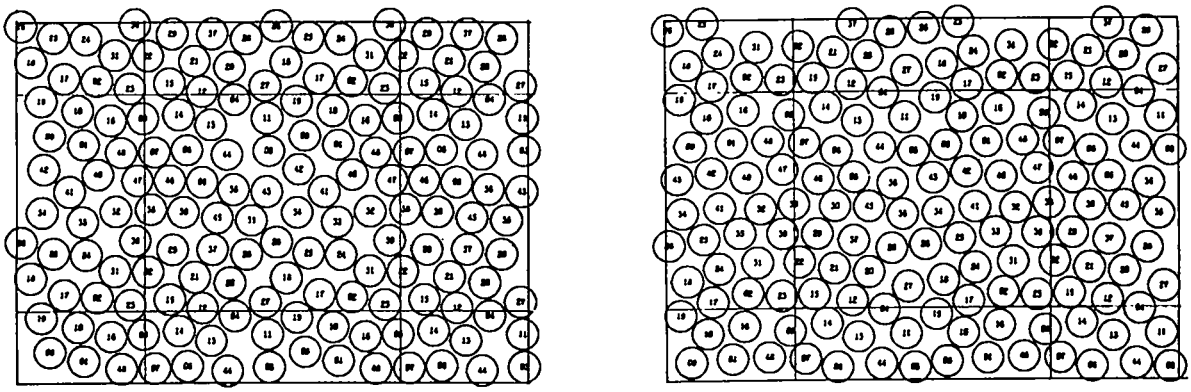

Fig. 6.7i-j Snapshots 92 through 93 from the H plateau of realization B19 at $\tau = 1.30$.

Most of the molecules have hexagonal Voronoi coordination; there are two with coordination number 5 and two with coordination number 7. The arrangement is nearly hexagonal, but differs from the standard one of Figs. 3.3 and 6.5b, for example, in that its lattice lines are approximately at 0°, 60°, and 120° instead of the usual 30°, 90°, and 150°. Arrangements of this kind will be frequently encountered, and it will be convenient to designate them as "7X7" configurations, reserving the term "regular hexagonal configuration" to designate, as before, configurations similar to Fig. 3.3.

The presence of the hole naturally leads to considerable mobility of the "7X7" structure by the usual mechanism of hole diffusion, as shown in the following 9 snapshots, Figs. 6.7b-j. It is noteworthy that

in most cases one or two molecule-hole interchanges (symbolized by molecule ⇄ hole) suffice to account for the gross differences between consecutive pairs of these snapshots. Thus, between snapshots 84 and 85 we assign the step 2 ⇄ hole; between 85 and 86, 9 ⇄ hole and 16 ⇄ hole; between 86 and 87, 23 ⇄ hole; between 87 and 88, 31 ⇄ hole and 39 ⇄ hole. Between snapshots 88 and 89 the events are 38 ⇄ hole and 30 ⇄ hole, with the latter configuration displaying noticeable irregularity in the "7X7" structure. By the time of snapshot 90, Fig. 6.7g, the events 29 ⇄ hole, 21 ⇄ hole, 12 ⇄ hole have occurred and in addition the pair of molecules 37 and 20 look as if they were moving down into the hole between molecules 12 and 19. However, the next snapshot, Fig. 6.7h, indicates that this did not happen; rather this pair apparently moved back up into their own rows, and molecule 4 moved up into the hole.

In Fig. 6.7i, snapshot 92, there is enough distortion in the "7X7" structure to result in considerable arbitrariness in any assignment of molecules to rows. By the time of the next snapshot, Fig. 6.7j, most of the distortion has disappeared. Nevertheless, the most plausible row assignment for this configuration, when compared with snapshot 91, implies that during the intervening 38 400 time steps the staggered column of seven molecules (10, 9, 42, 41, 33, 24, 17) rotated one row downwards around the torus, with the hole remaining in row (14, 13, 11, 9 or 10, 16, 8).

Snapshots 94 through 128, not reproduced here, continued to exhibit well-defined "7X7" structures, after which irregular configurations such as shown in Figs. 6.8, 6.9, and 6.10 reappear interspersed with

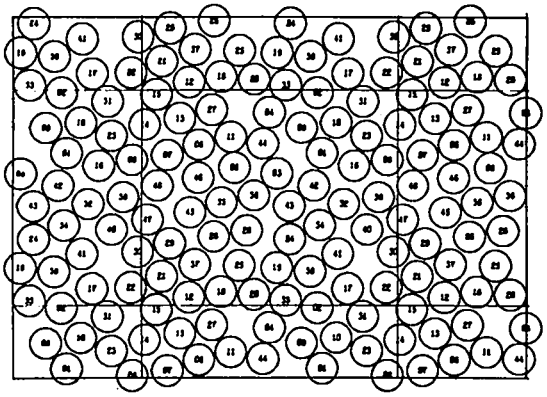

6.8

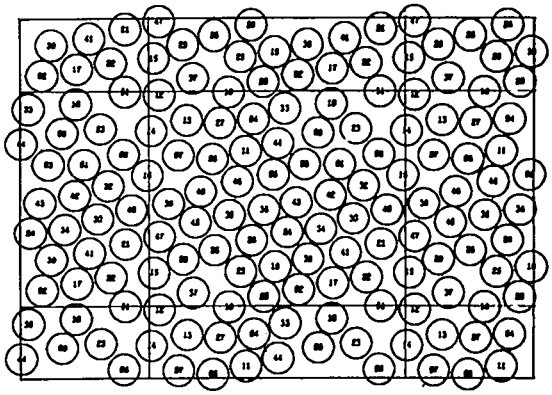

6.9

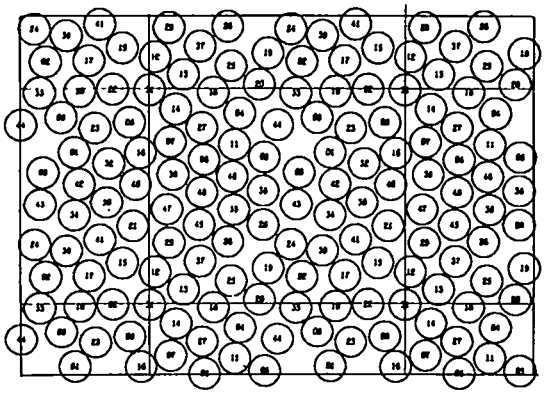

6.10

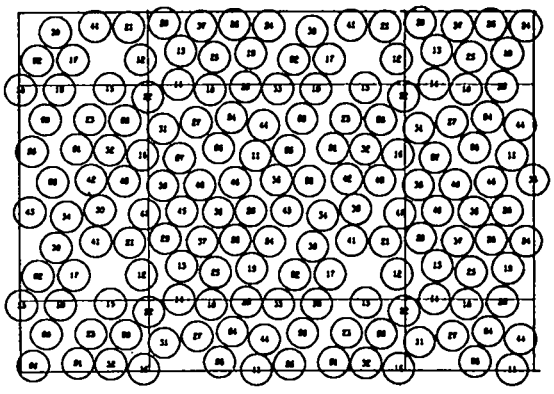

6.11

Figs. 6.8-6.11 Snapshots 132, 136, 140, and 143 from the latter part of H plateau of realization B19 at $\tau = 1.3$, displaying both irregular and "7X7" structures.

well-defined "7X7" structures such as Fig. 6.11. There is a noticeable tendency for the irregular snapshots to be associated with abnormally high coarse-grained observations $\tilde{G}(s, \alpha)$ in Fig. 6.3. As a result the last portion of this H plateau, in which such configurations seem to be more frequent, leads to a somewhat larger estimate of the compressibility factor (the third entry for this realization in Table 6.1) than that obtained from the H plateau as a whole. The difference serves as an illustration of the uncertainity in such estimates due to the non-random character of these observations. Figures 6.1 and 6.2 show that either of these two reduced pressures obtained from this H plateau (as well as the H-plateau estimates for other realizations yet to be discussed in the interval $\tau = 1.3$-1.35) can be regarded as a reasonable extrapolation of the values obtained from completely averaged realizations at $\tau > 1.35$.

Section 6.2 is devoted to a discussion of the properties of the "7X7" structure which we have just seen to be so characteristic of the H plateau of the present realization. Here it is of some interest to display the net displacements of the molecules between snapshot 79, the last one of the regular hexagonal lattice type, and snapshot 84, the first of the "7X7" type. In Fig. 6.12 the circles represent the molecules in the latter configuration with their numbers omitted, while the slightly distorted hexagonal lattice is the Voronoi lattice of snapshot 79. The vectors show the net displacement of each molecule over the 96 000 time steps between these two configurations.

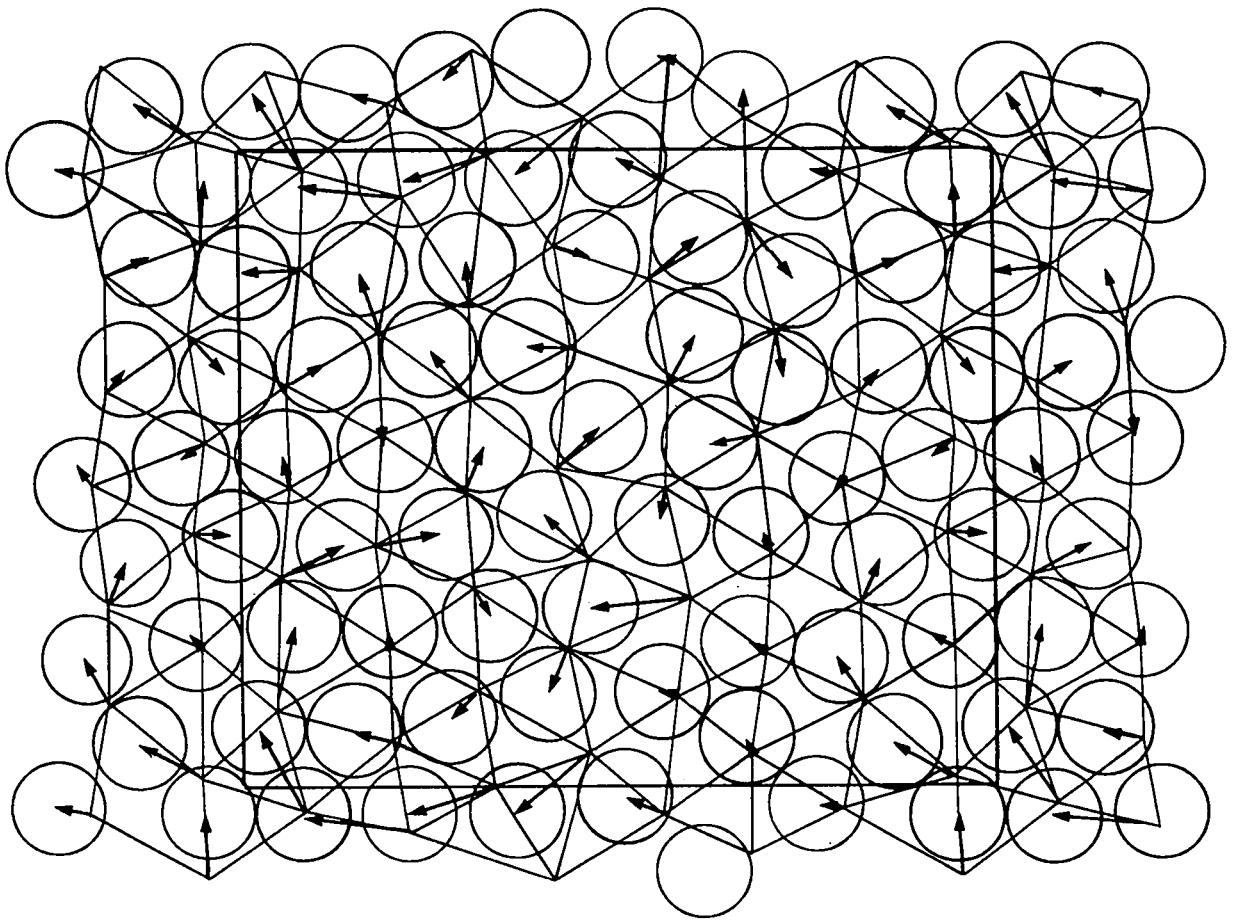

Fig. 6.12 Net molecular displacements between last "regular hexagonal" and first "7x7" configurations (snapshots 79 and 84) of realization B19 at $\tau = 1.3$.

6.1.2.1.3 Summary. At this point we will summarize our observations on this realization in terms of the hourglass model of configuration space.

The L region of configuration space evidently has the following properties: (1). It contains the regular hexagonal lattice point. (2). A typical configuration from this region shows only slight distortions from the regular lattice. (3). "Diffusion" or molecular interchange is still infrequent in this region at $\tau = 1.3$. When it does occur, the mechanism is the columnar rotation around the torus discussed in Sections 3.4, 3.5, and 6.1.2.1.1. (4). It seems fair to describe these configurations as being of the "perfect crystal" type.

The H region of configuration space for this system has more complicated character. Structures of two different types are found, namely the "7X7" structure which predominates in this realization, and the irregular structures such as Figs. 6.6, 6.8, 6.9, and 6.10. The latter type perhaps correspond, on the average, to somewhat higher values of the cumulative pair distribution function. There is the intriguing possibility that at this density, at least, the irregular configurations may represent the connection between the L region of regular hexagonal configurations and the "H-proper" region of "7X7" structures. This conjecture is based mostly upon the chronological occurrence of the irregular arrangements between those of the other two types. One can also, by staring long enough at irregular configurations such as Fig. 6.6, convince oneself that they are actually structurally intermediate between

the two "pure" types; that is, that they are mixtures of the latter. But with so few molecules, and with the "pure" structures differing mostly just in orientation, this impression seems too subjective to be given much confidence.

At this density, and at this point in our discussion, it is clear that it would be premature indeed to characterize the H states as being "fluid" in character. Diffusion is indeed relatively free, especially in the "7X7" structures, but it is evident that the latter have more nearly the character of imperfect crystals. The irregular structures may be more fluid-like in their properties, but in this realization they are a distinctive feature of the H plateau but not the predominant one.

6.1.2.2 Realization B20 at $\tau = 1.316$.

The control charts for this realization are shown in Fig. 6.13. As indicated in Table 6.1, they were interpreted in terms of three plateaus: coarse-grained observations s = 2-19 as a H plateau, 20-39 as a L plateau, 40-82 as another H plateau.

The realization began in the H region because its initial configuration was obtained by compressing a configuration taken from a H plateau of realization B23 at $\tau = 1.34$. Actually, at the time when this was done, our intention was to use the compression process as a sort of diagnostic technique to test for the presence of the H plateau in realization B23. As we shall later see in the discussion of the latter realization, its plateaus are not especially well defined and we were

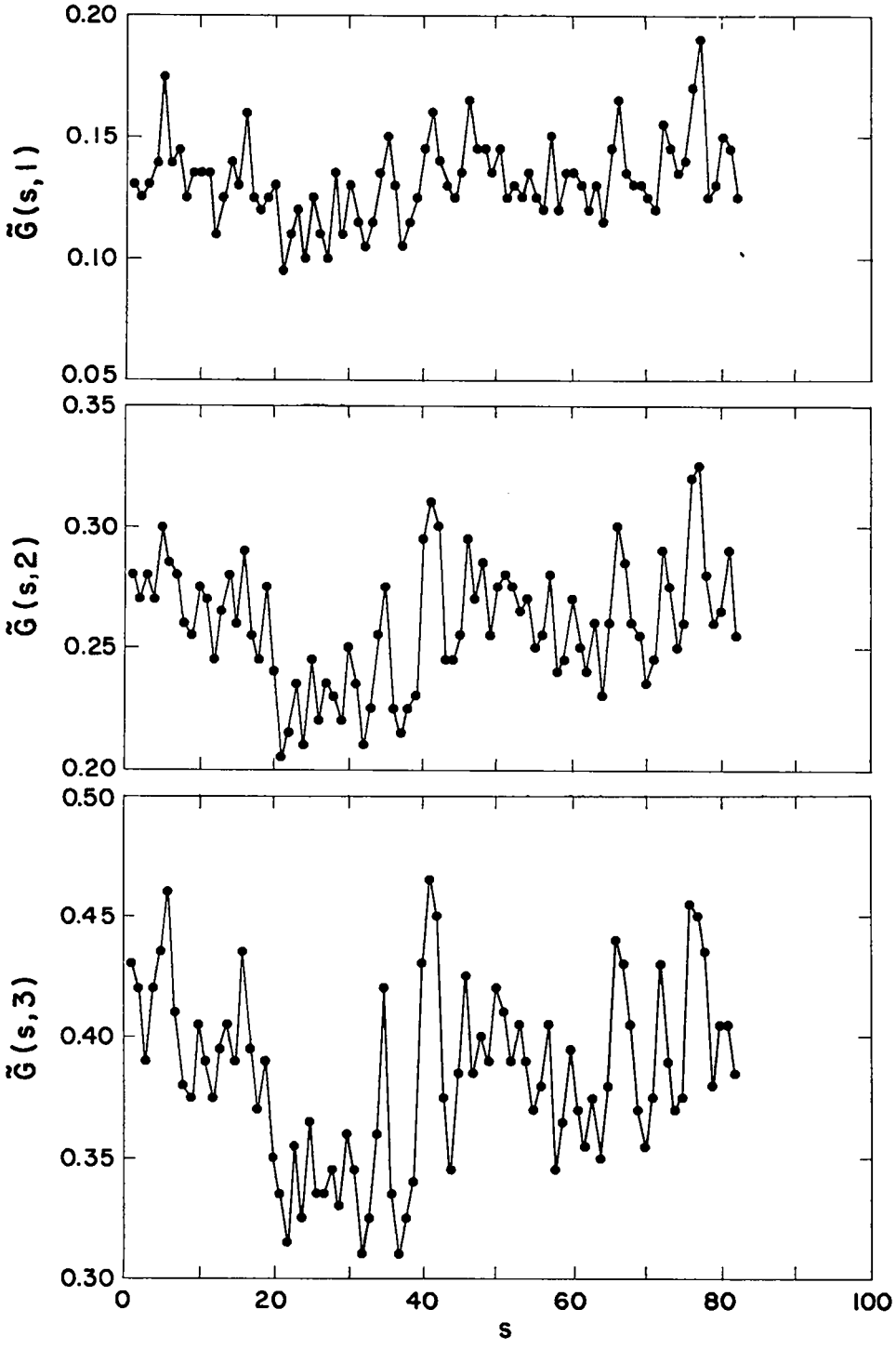

Fig. 6.13 The first three control charts for realization B20 at $\tau = 1.316$; $\Delta t = 19\ 200$.

not sure, on the basis of the control charts alone, that a subdivision into plateaus was proper. At the time we did not have the high speed microfilm plotting device with which we have since acquired experience in correlating the control chart behavior with the geometrical structure of the system. On the other hand, the existence of an "extended fluid" branch of the equation of state of the 48-molecule system had already been established (see Section 6.3), so that it occurred to us to use the approximately "adiabatic" character of the compression procedure to test for a qualitative difference between two configurations, as suggested by the control charts. In realization B23 the charts suggested that observation s = 38 (with Δt = 19 200) might belong to a L plateau, while the following point s = 39 might be the first of a H plateau. The final configuration of each of these time-smoothing intervals was accordingly selected as the starting point of a compression process.

Actually, the choice of the first of these, as a configuration with which to begin a compression which was expected to take place in the L region of configuration space, was a poor one, since the L → H transition might easily have happened near the end of coarse-graining interval s = 38 and still allowed this interval to give observations $\tilde{G}(s, \alpha)$ characteristic of the L region. Fortunately, however, the selected configuration was indeed of the L type, as indicated by its structure interpreted in the light of our subsequent experience, and also by the resulting realization B18 which began from this configuration after compression to τ = 1.29 (see Section 6.1.1).

6.1.2.2.1 The first H plateau. The s = 39 configuration of realization B23, shown in Fig. 6.14a, after compression to $\tau = 1.316$ as mentioned above, was used as the initial configuration (Fig. 6.14b) of the present realization. Both of these configurations are of the type described as "irregular" in our discussion of realization B19 at $\tau = 1.3$. This character was maintained through snapshots 1 through 4, which are not reproduced here. Figure 6.15 shows snapshots 5, 6, and 7, during which the system changes from this irregular arrangement to the same "7X7" structure previously described in Section 6.1.2.1.2.

Snapshots 8 through 15, the last being shown in Fig. 6.16a, were all well-defined "7X7" structures and displayed the same hole diffusion as discussed in connection with B19. Snapshot 16, Fig. 6.16b, shows

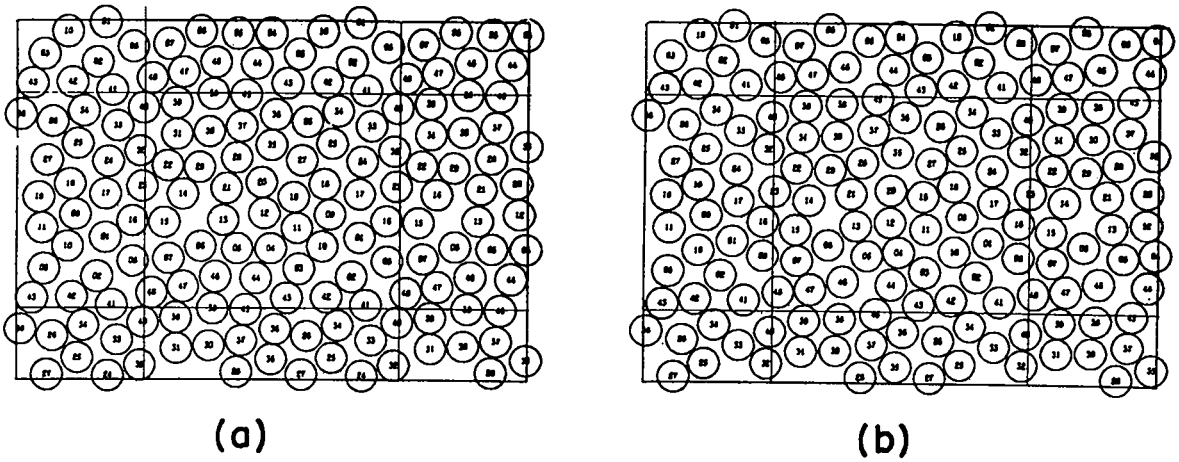

Fig. 6.14 Genesis of the initial configuration of realization B20 at $\tau = 1.316$. In (a) is shown the configuration of realization B23, $\tau = 1.34$, at t = 748 800. After compression to $\tau = 1.316$ it was used as the initial configuration (b) of B20.

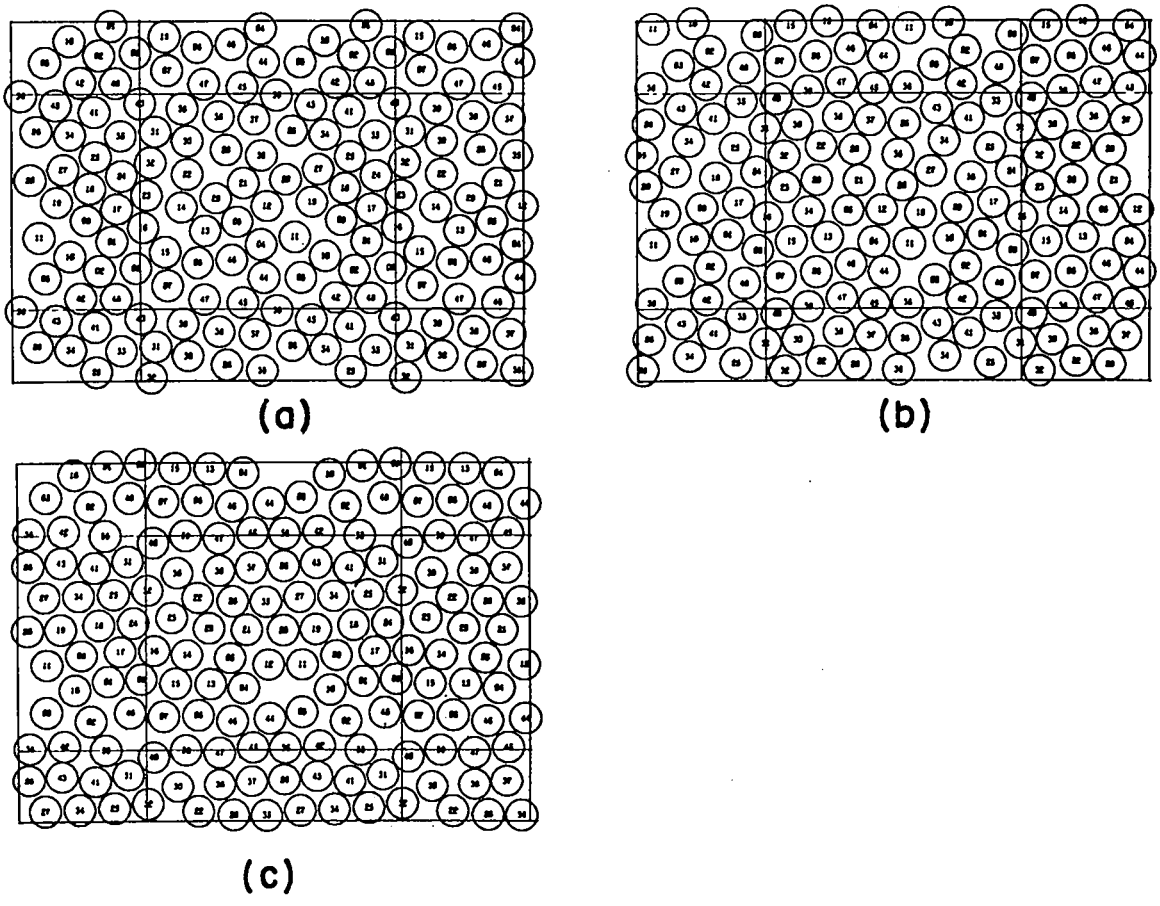

Fig. 6.15 Snapshots 5 (a), 6 (b), and 7 (c) from realization B20 at $\tau = 1.316$, showing the transition from "irregular" to "7X7" arrangement during the first H plateau.

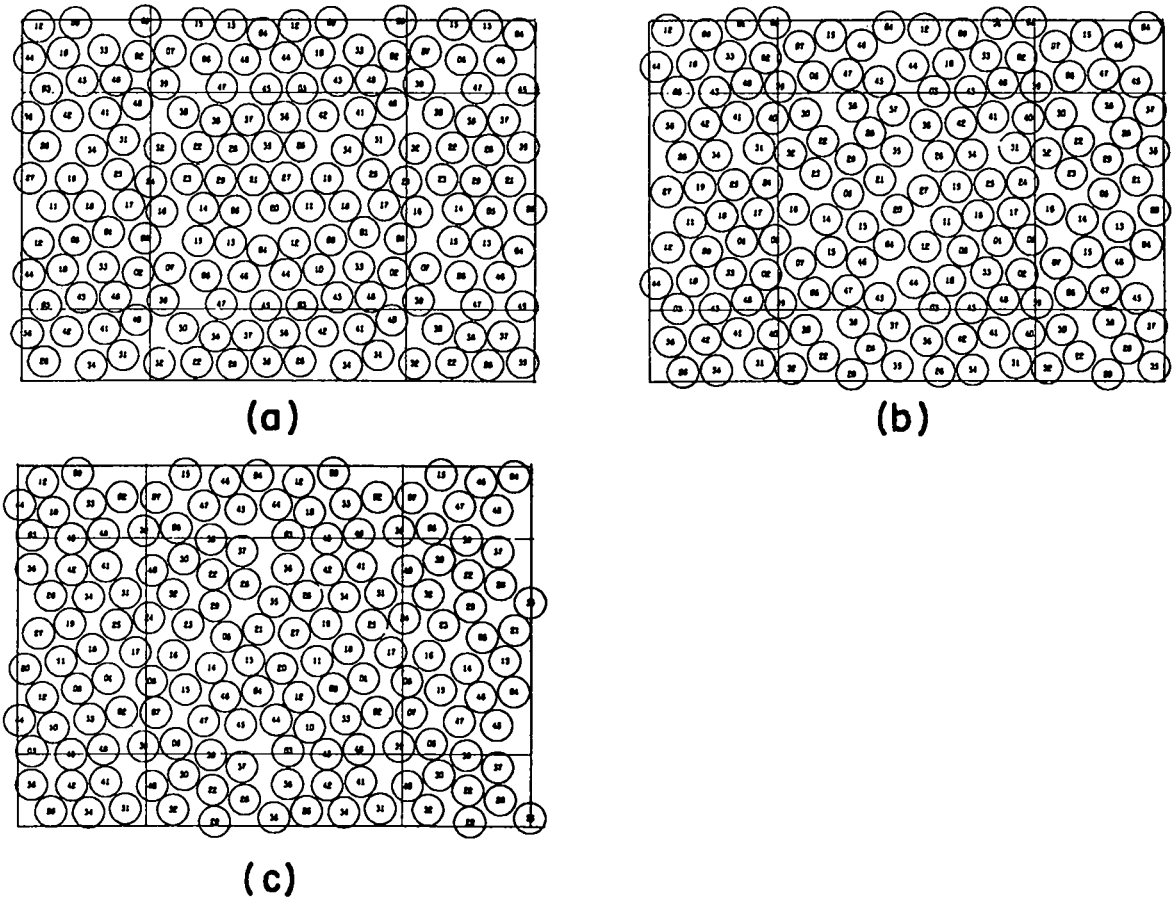

Fig. 6.16 Snapshots 15 (a), 16 (b), and 17 (c) taken at the terminus of the first H plateau of realization B20 at $\tau = 1.316$.

considerable distortion in the "7X7" structure. Indeed the arrangement might almost be described as irregular (note also that the associated points in Fig. 6.13 are comparatively high). The next snapshot, Fig. 6.16c, shows somewhat less distortion, but comparison with snapshot 15 shows that it still differs appreciably from the more regular examples of the "7X7" arrangement.

Figure 6.17 shows the next two snapshots. The first of these, at s = 18, resembles its predecessor (Fig. 6.16c) in being an appreciably distorted "7X7" arrangement. The second, at s = 19, is very different: the arrangement is that of the regular lattice. Thus, we conclude that between these two snapshots the system left the H region of configuration space and entered the L region. Since the control charts indicate that

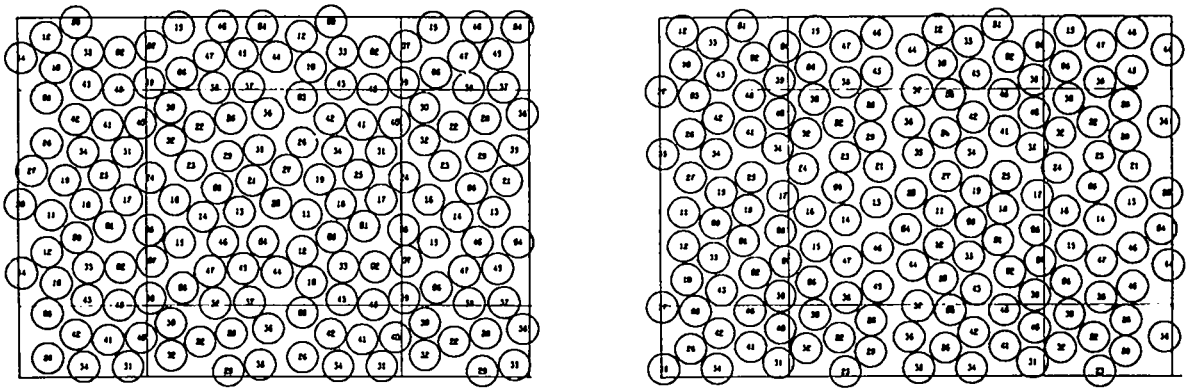

Fig. 6.17 Snapshots 18 (a) and 19 (b) from realization B20 at τ = 1.316, illustrating the H → L transition.

the s = 19 coarse-grained observation belongs to the L plateau, this transition presumably occurred near the end of this group of 19 200 configurations.

6.1.2.2.2 The L plateau. As indicated in Table 6.1, we treated observations s = 20 through 39 as a L plateau, although the point s = 35 was clearly anomalous (see Fig. 6.13). And indeed snapshots 20 through 34, the last of which is shown as Fig. 6.18a, were all typical L-type configurations, that is, arrangements in which the basic regular hexagonal lattice is easily recognizable. Furthermore, during this time no "diffusion" occurred (compare Figs. 6.17b and 6.18a).

The configuration at s = 35 (Fig. 6.18b), however, is of the irregular type, while the next snapshot, Fig. 6.18c, is again of the regular hexagonal type. Thus, we interpret the observations as indicating a brief excursion of the system into the H region of configuration space (or into the connections between L and H, if the H region proper is regarded as consisting of "7X7" structures, and the irregular configurations as the connections between L and H). Comparison of Figs. 6.18a and 6.18c shows that this excursion accomplished the following sequence of nearest neighbor displacements: 24 → 5 → 13 → 20 → 11 → 12 → 10 → 3 → 26 → 34 → 25 → 31 → 24.

In the remaining snapshots of the L plateau, the last of which is shown in Fig. 6.19a, the regular hexagonal arrangement of snapshot 36 (Fig. 6.18c) is preserved.

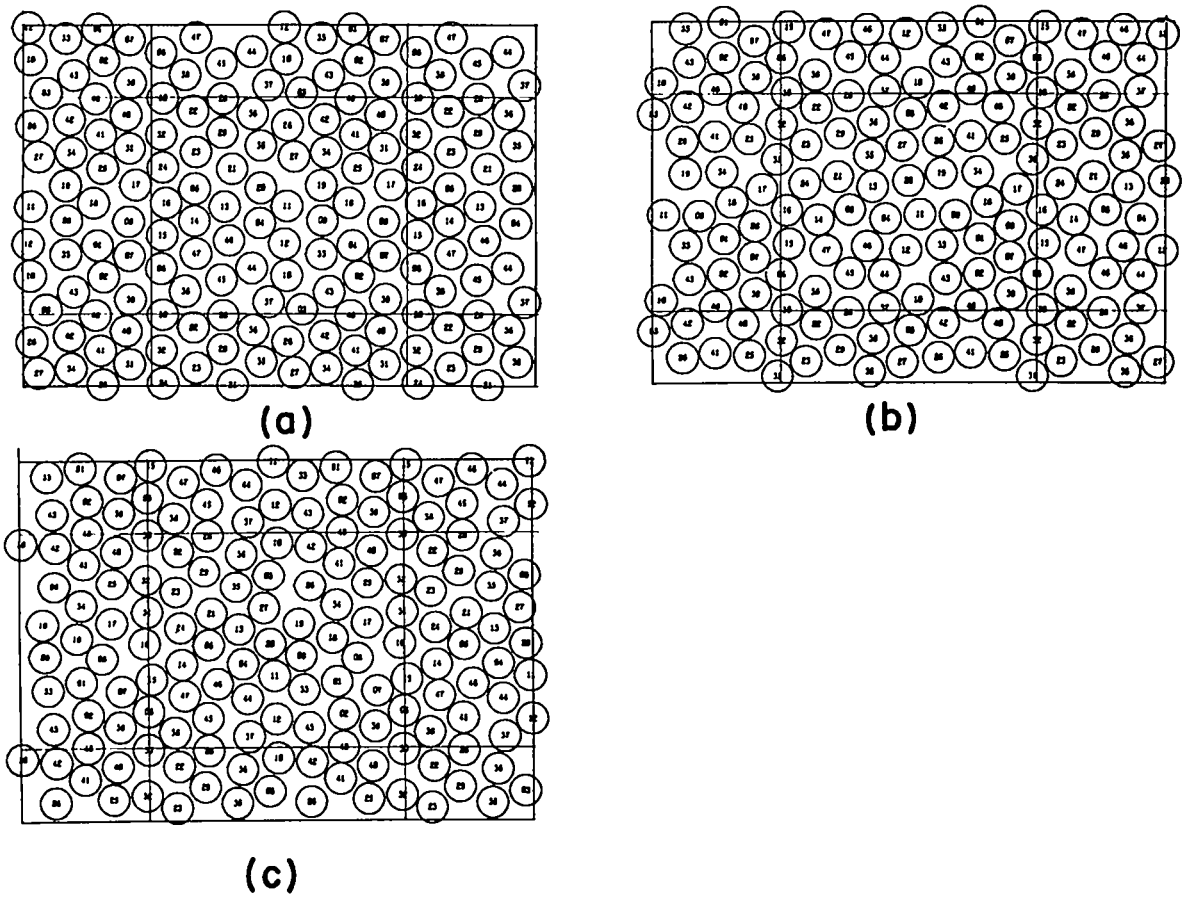

Fig. 6.18 Snapshots 34 (a), 35 (b), and 36 (c) from realization B20 at $\tau = 1.316$, showing a brief excursion to "irregular" states during the L plateau.

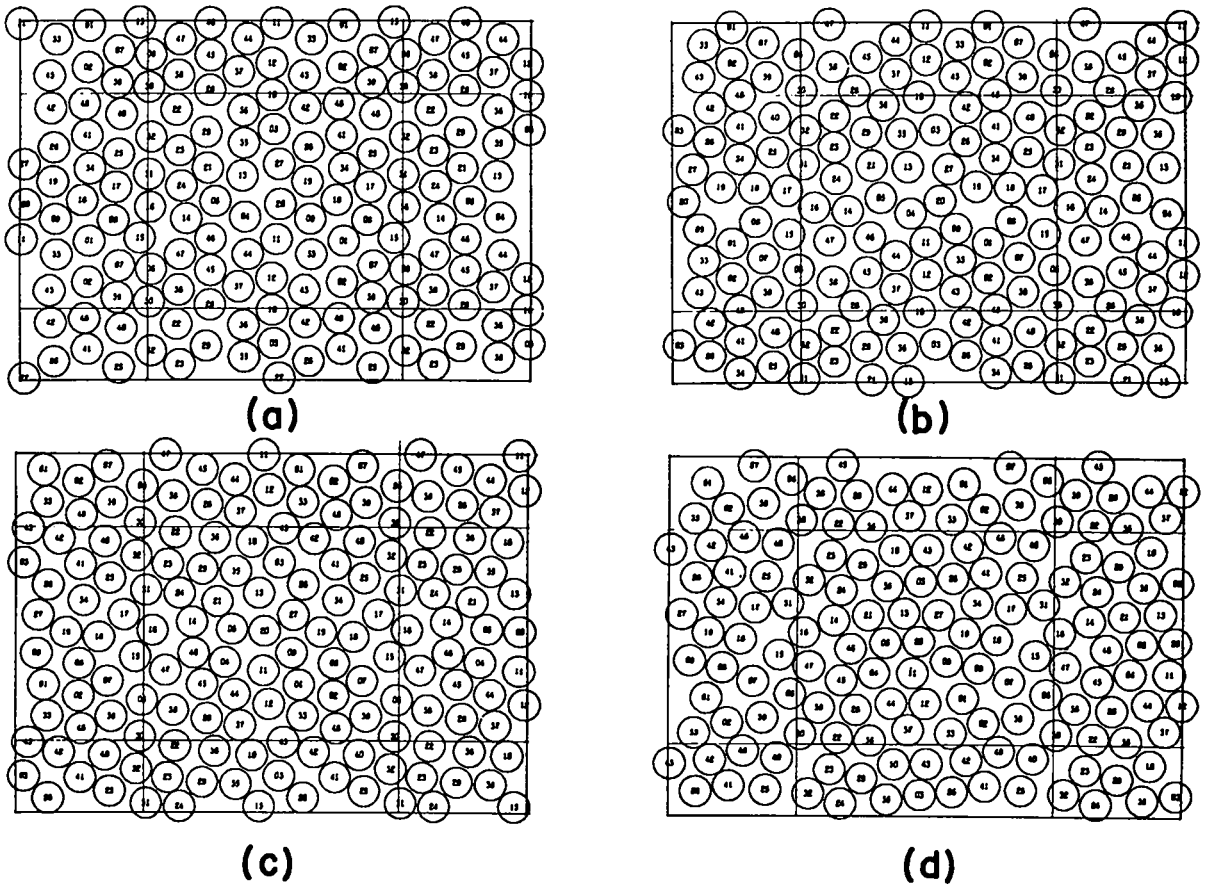

Fig. 6.19a-d Snapshots 39 through 42 of realization B20 at $\tau = 1.316$, showing the L- to H-plateau transition.

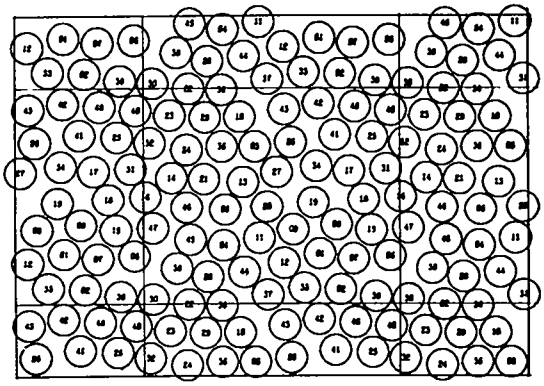

(e)

Fig. 6.19e Snapshot 43 of realization B20 at $\tau = 1.316$.

Figures 6.1 and 6.2 show that, just as in the case of the L-plateau reduced pressure of realization B19, the reduced pressure estimated from this short L plateau lies on a smooth continuation of the curve obtained from regular lattice realizations at higher density.

6.1.2.2.3 The second H plateau. As indicated in Table 6.1, the observations from s = 40 until the end of the realization at s = 82 were treated as a H plateau. The geometric structures during the transition from the preceding L plateau are shown in Fig. 6.19. Again configurations of irregular structure (snapshots 40 and 41) are observed between the last regular hexagonal structure (snapshot 39) and those of "7X7" type (snapshots 42 and, especially, 43). Of the remaining 40 snapshots

most were of "7X7" type; some (notably 71 through 76) were irregular. None were of the regular hexagonal (i.e., L) type.

Table 6.1 and Fig. 6.2 show that the reduced pressures estimated from the two H plateaus of this realization are in quite good agreement, and also, as in the case of the H-plateau estimates at $\tau = 1.3$, represent a reasonable continuation of the "fluid" branch of the equation of state from lower densities.

6.1.2.2.4 Summary. Our observations, and the interpretations derived therefrom, on this realization are very similar to those on realization B19 at $\tau = 1.3$. The occurrence of the H → L transition is perhaps the principal additional point of interest. In the present case, the correlation between irregular structure and high control-chart points within H plateaus is somewhat less marked than in the $\tau = 1.3$ realization. On the other hand, the interpretation of the irregular structures as constituting the L-H connections, the H region being principally of the "7X7" type, receives some additional support. The irregular structures are observed frequently enough to make it somewhat questionable to assign them a negligible statistical weight. Aside from this question of the appropriateness of treating the irregular and "7X7" structures as a single class, the observed geometrical structures definitely support the plateau assignments given for this realization in Table 6.1 (except, of course, for the $s = 35$ excursion within the set $s = 20$-39, which was evident from the control charts and ignored as a matter of crude approximation).

6.1.2.3 Realization B21 at $\tau = 1.325$.

This realization was started from the usual regular hexagonal lattice. The control charts, Fig. 6.20, are in marked contrast with those for the two immediately preceding realizations at $\tau = 1.3$ and 1.316, in that no well-defined two-plateau structure is apparent. Comparison of the values of $\tilde{G}(s, 3)$ for these realizations (all three have the same value of Δr^2) shows that most of the points for the present realization are in the range expected for the L region of configuration space, with only occasional brief upward excursions into the range expected for the H region. Consequently, as indicated in Table 6.1, the entire realization was averaged, and as would be expected from the remarks of the previous sentence, the resulting reduced pressure lies in Figs. 6.1 and 6.2 approximately on the "L" or "crystalline" equation of state as extrapolated from the regular hexagonal lattice realizations at $\tau < 1.3$ and from the L plateau estimates at $\tau = 1.3$ and 1.316.

Study of the snapshot configurations substantiates this interpretation in some detail. Of the 95 snapshots taken at the usual interval $\Delta t = 19\ 200$, 75 were unambiguously classifiable as definitely of the regular hexagonal type, five had well-defined "7X7" structures, and the rest were either notably distorted but recognizable versions of the regular hexagonal arrangement, or were of the irregular type discussed with the preceding realizations.

There were a number of instances in which permutations of approximately regular hexagonal structures occurred within one or two snapshot

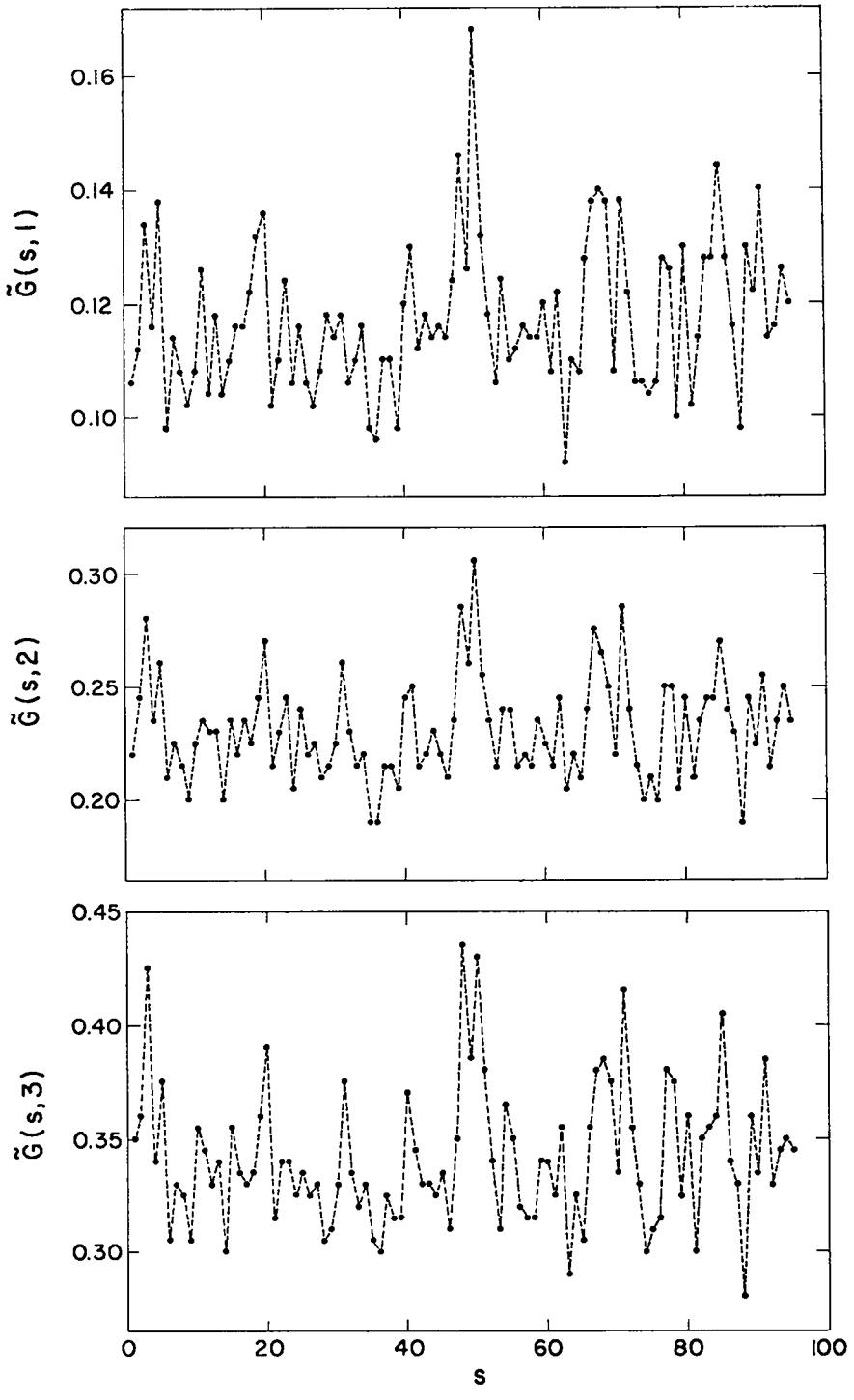

Fig. 6.20 The first three control charts for realization B21 at $\tau = 1.325$; $\Delta t = 19\ 200$.

intervals without observation of any gross departure from "L" type arrangements. For example, snapshots 1 and 3 both had well-defined regular hexagonal structures, but during the intervening 38 400 time steps one column of six molecules rotated one lattice step around the torus. The intermediate snapshot 2 showed a fairly distorted but recognizably regular hexagonal arrangement. The value of $\tilde{G}(3, 3)$ in Fig. 6.20 suggests that a brief excursion into the H region may have occurred, but if so, the snapshot interval is too long to detect it. Other, somewhat more complicated, displacements around the torus occurred, as well as an amusing sequence of three consecutive snapshots showing a ring-around-the-rosey rotation of the six nearest neighbors of one molecule through approximately 60°. All these motions in configuration space seemed to take place by way of L-L connections rather than by way of $L \rightarrow H \rightarrow L'$, as far as our snapshot time resolution and the diffuse definitions of these regions and their associated connections permit us to state.

On the other hand, the pronounced upward excursion in the control charts (Fig. 6.20) in the neighborhood of $s = 50$ was definitely associated with appearance of "irregular" structures, as shown in the sequence of snapshots 46 through 52 in Fig. 6.21. The first of these, snapshot 46, is a reasonably typical example of a L-region state, exhibiting only slight displacements from the regular hexagonal lattice. The next snapshot is more interesting. The structure is almost hexagonal, but the only plausible assignments of molecules into columns produce, instead of the eight columns of six molecules each characterizing regular hexagonal arrangements,

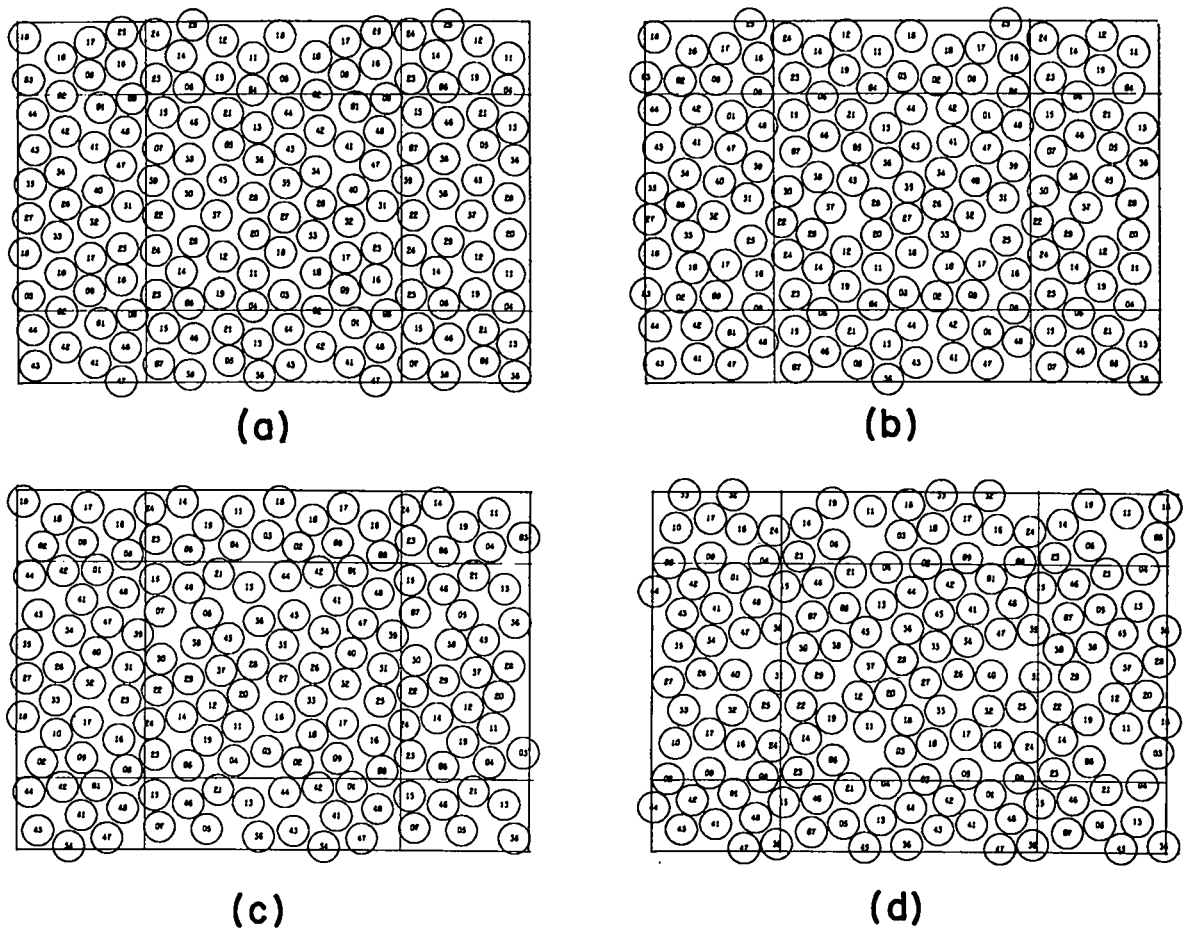

Fig. 6.21a-d Snapshots 46 through 49 from realization B21 at $\tau = 1.325$, showing an excursion into "irregular" states.

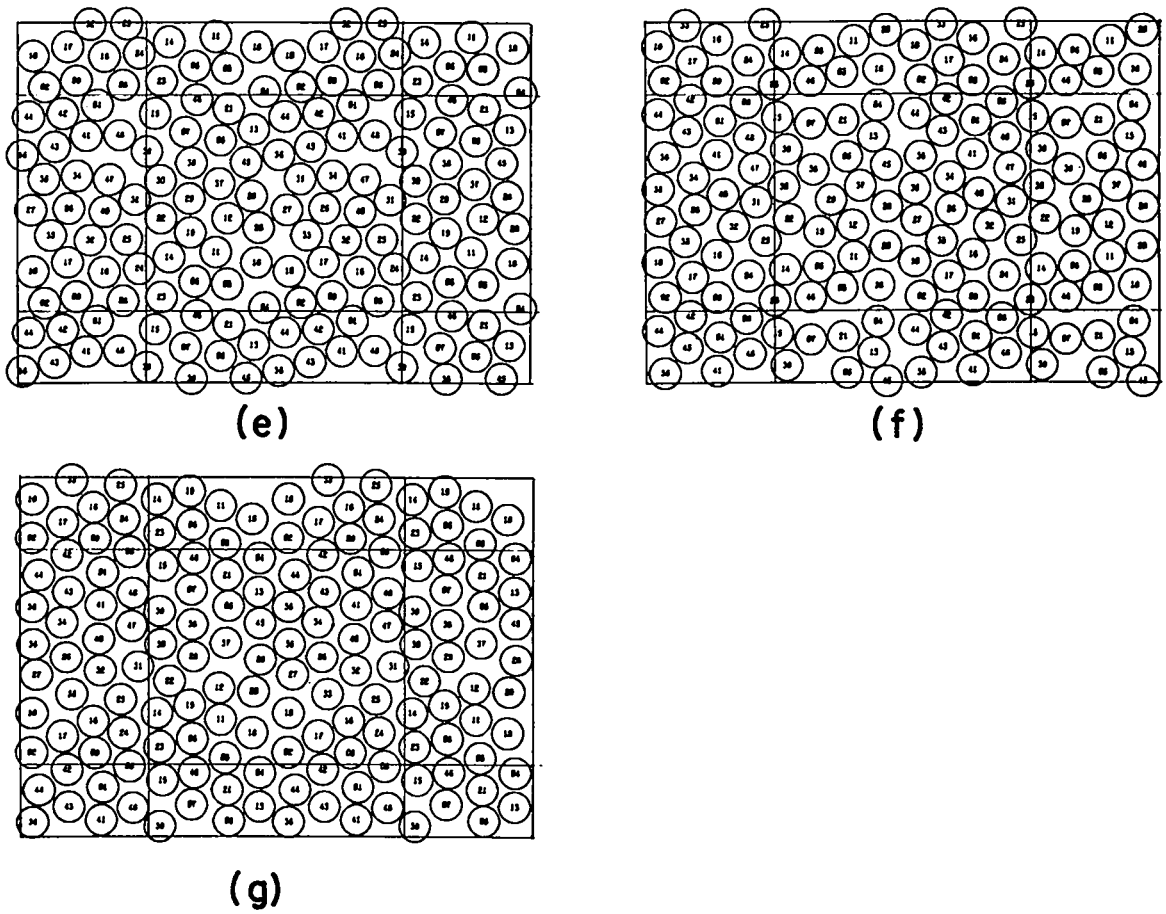

Fig. 6.21e-g Snapshots 50 through 52 from realization B21 at $\tau = 1.325$.

one column of seven molecules (42, 41, 34, 26, 33, 10, 2) and one column of five molecules plus one hole (21, 5, 45, hole, 12, 19) or (6, 46, 38, hole, 29, 14). That is, this configuration contains one vacancy and one interstitial. It is one of the few such examples which we have noticed in our hard-circle calculations. Snapshots 48 through 51 exhibit various irregular structures in which hints of both the regular hexagonal and "7X7" arrangements can be detected. The last snapshot, 52, of this sequence shows the system back in a nearly regular hexagonal configuration, but one differing from the initial snapshot, 46, of this sequence by a number of molecular interchanges.

During the less obvious upward excursion in Fig. 6.20 near s = 70, well-defined "7X7" structures were observed, as shown in the snapshots 65 through 72, Fig. 6.22. In addition to the quite pretty examples of "7X7" structures provided by snapshots 68 and 69, this sequence also displays in snapshot 71 what is perhaps our best example of a mixed structure.

Compared to the neighboring higher density realizations B19 and B20, this realization is noteworthy for its brief residence times in the H region. Indeed without the evidence provided by the snapshots we would not be certain that excursions into the H region had actually occurred. The over-all average evidently contains some H-region contribution, which can be invoked to explain the slightly high value of the reduced pressure estimate (Fig. 6.2) compared to adjacent L points.

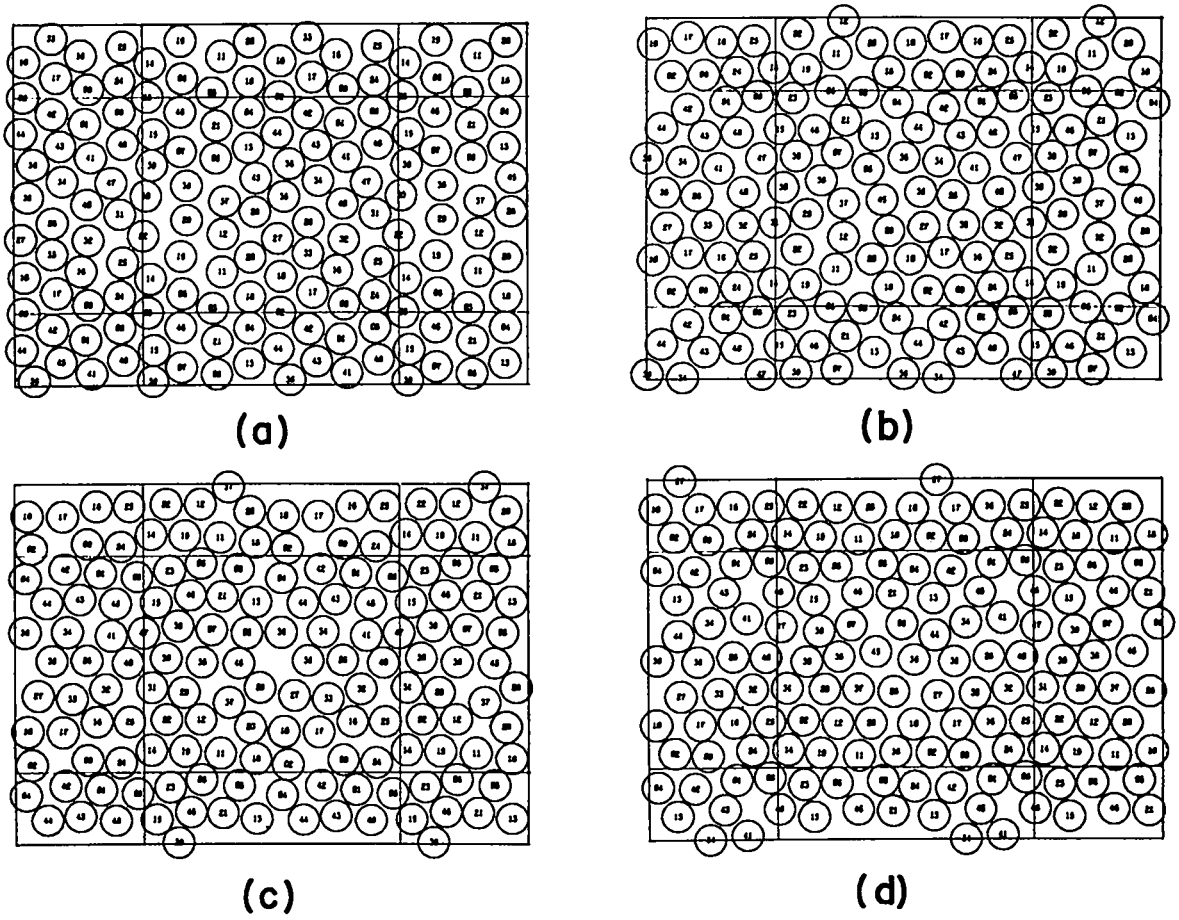

Fig. 6.22a-d Snapshots 65 through 68 from realization B21 at $\tau = 1.325$.

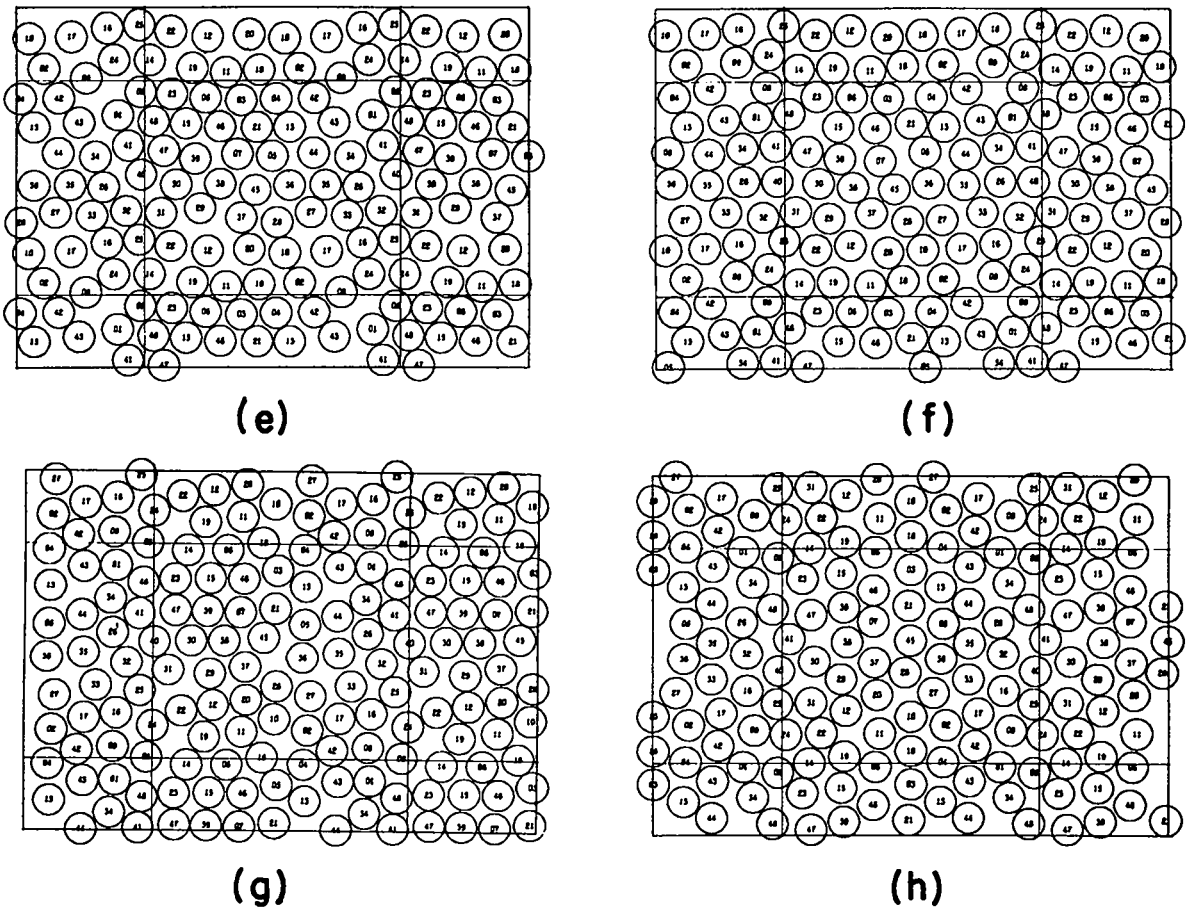

Fig. 6.22e-h Snapshots 69 through 72 from realization B21 at $\tau = 1.325$

6.1.2.4 Realization B22 at $\tau = 1.33$.

This realization was also started from the regular hexagonal lattice. Its control charts are shown in Fig. 6.23. As indicated in Table 6.1, only short sections of this realization were averaged, viz., s = 1-14 as a L plateau, 15-26 as a H plateau, 86-95 as a second L plateau. Figure 6.2 shows that the two L-plateau estimates are in reasonable agreement with each other, and with the extension of the L or "crystalline" equation of state from higher densities. Similarly, the H-plateau estimate is in approximate agreement with the "fluid" branch of the equation of state as determined by other H-plateau points and by non-jumpy realizations at $\tau > 1.35$.

As will be seen from the remaining discussion of this realization, examination of the snapshot configurations substantiates the above L-plateau classifications, but suggests that the H-plateau classification should be regarded with a certain reserve. We will describe the snapshots by type, rather than by reproducing them here, since the various observed structures are all quite well exemplified among the snapshots presented for the previously discussed realizations in this density range.

Snapshots 1 through 14, corresponding to the first L plateau, indeed showed the regular hexagonal type of structure which we associate with the L region of configuration space. In Fig. 6.23 the points for s = 9 lie well above the others in this plateau. Snapshots 8 and 9, which precede and terminate this time-smoothing interval were noticeably

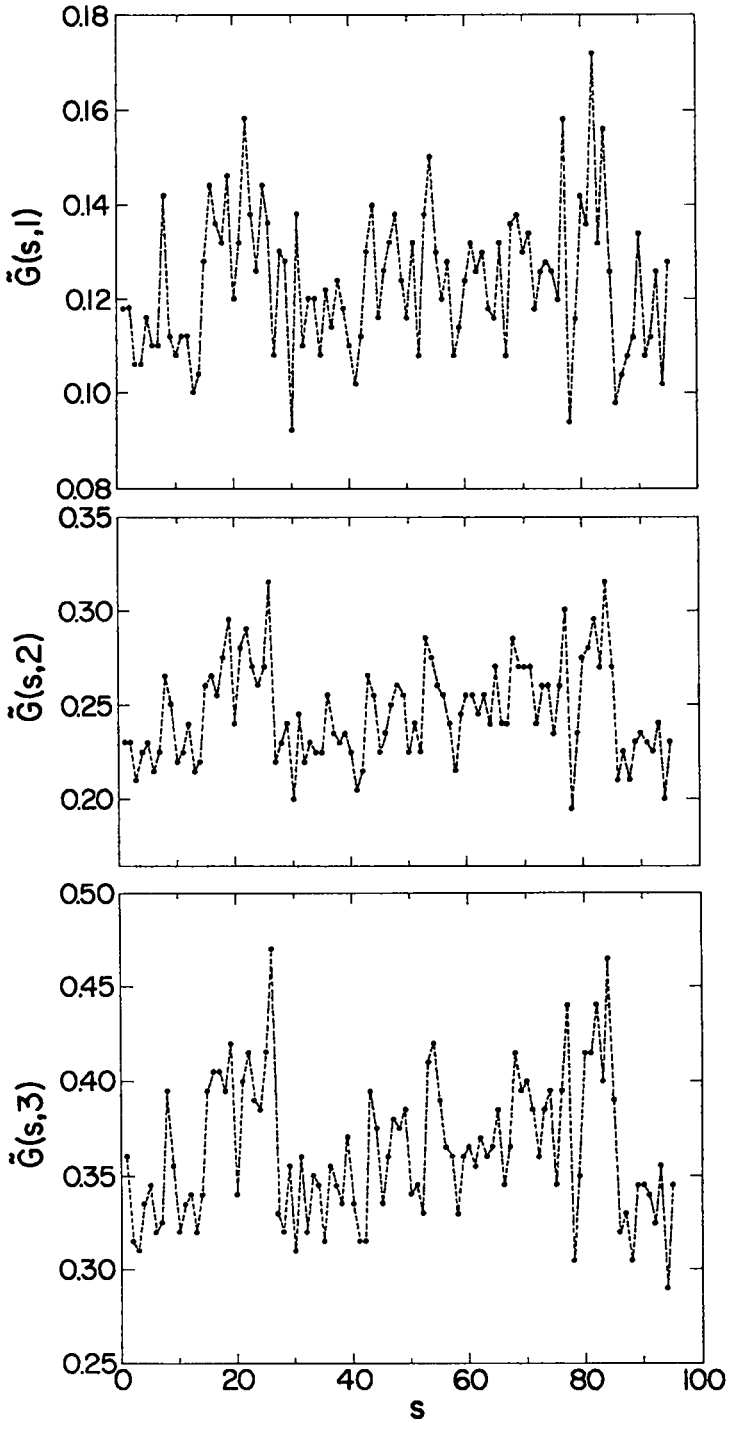

Fig. 6.23 The first three control charts for realization B22 at $\tau = 1.33$; $\Delta t = 19\ 200$.

distorted, but still of the L type. No diffusion was observed during this L plateau; that is, snapshots 0 through 14 all display the same permutation of the regular hexagonal lattice. Thus, the observed structures definitely support our classifying these observations as a L plateau. The upward excursion at s = 9 may have been due to undetected irregular configurations between snapshots 8 and 9, but the fact that no molecular interchanges seem to have occurred between these snapshots suggests that no great departure from regular hexagonal or L-type structures is likely to have taken place.

As already mentioned, points s = 15-26 were averaged as a H plateau. We classified the associated snapshots, in the same terminology as used for the previous realizations, as follows: Snapshots 15 through 18 were of the irregular type; 16 and 18, in particular, suggested description as mixtures of regular hexagonal and "7X7" structures. Snapshots 19, 20, and 21, particularly the first two, were good examples of "7X7" structures. In this connection it is interesting to note that from the points for s = 20 in Fig. 6.23, one might have guessed that the configurations during this time-smoothing interval were of the regular hexagonal type. The snapshots make it almost certain that they were not, and as we shall see from the later points of this realization, at this density any one time-smoothed observation over a sequence of "7X7" configurations may well have a value $\tilde{G}$ that could also be typical of a sequence of regular hexagonal states. Snapshots 22 through 25 were again of the irregular type. Snapshot 26, showing the last configuration of this H plateau, was

best described as another of our rare observations of the occurrence of a vacancy-interstitial combination in an otherwise regular hexagonal arrangement (Section 6.1.2.3 and Fig. 6.21b).

Snapshots 27 through 43 were again regular hexagonal structures (the last being appreciably distorted), indicating that the observations s = 27-43 could have been averaged to obtain an additional L-plateau estimate of reduced pressure. The control charts indicate that such an estimate would be in reasonable agreement with the existing two. Here again, no diffusion was noticed during these configurations.

Snapshots 44 through 67 were all of the "7X7" type except for snapshot 54, which was better described as irregular (which fact is probably associated with the upward control-chart excursion at this point). Thus, we note that we might well have averaged observations s = 44-67 to obtain a reduced pressure estimate which would, on the basis of the snapshots, be ascribed to a more-or-less well-defined "7X7" region of configuration space. Figure 6.23 shows that this estimate would be intermediate between the previously discussed L- and H-plateau estimates, the latter of which evidently contains an appreciable contribution from irregular structures. This behavior may be interpreted as a further indication that we should either distinguish two H regions of different structure, with the irregular region tending to have higher values of $\tilde{G}$ than the "7X7" region, or else we should consider the irregular structures as constituting the connections between regular hexagonal L states and "7X7" H states. As already mentioned this is mainly a matter

of terminology, since the irregular structures are observed frequently enough to require them to have non-negligible statistical weight. These remarks constitute the qualification made at the beginning of this subsection with respect to treating observations s = 15-26 as the only H plateau in this realization.

Continuing the point-by-point correlation of the snapshots with the control charts, we classified snapshots 68 through 71 as irregular, 72 as "7X7", 73 and 74 as irregular, 75 as a rather distorted "7X7" arrangement, and 76 as irregular. Again we note that irregular states seem to have larger values of $\tilde{G}$ than "7X7" states, on the average.

Snapshot 77 showed a return to regular hexagonal structure, the first since s = 43. The corresponding control chart point s = 77 suggests that a majority of the states during that time-smoothing interval must have been irregular. Snapshots 78 and 79 also displayed regular hexagonal arrangements, which correlates well with the pronounced downward control-chart excursion at s = 78. Snapshot 80 was another case of a regular hexagonal arrangement with a vacancy and interstitial. Snapshots 81 through 84 were again irregular (note the associated large $\tilde{G}$). Snapshot 85 was a rather distorted regular hexagonal configuration.

Finally, snapshots 86 through 95 were regular hexagonal structures, consistent with their position in the control charts, and with our treating them as a L plateau. No diffusion was observed in this rather short L plateau.

In summary, this realization is perhaps chiefly notable for the already discussed strong suggestion that three regions of configuration space should be distinguished, rather than two. Compared with the slightly higher-density realization B21 at $\tau = 1.325$, it shows much longer residence times in irregular and, especially, in "7X7" configurations.

6.1.2.5 Realization B23 at $\tau = 1.34$.

The control charts are shown in Fig. 6.24, where the time-smoothing interval has again been doubled. They suggest a rough classification into four plateaus: s = 1-19 as L, 20-29 as H, 30-51 as L, 52-end as H.

The snapshots confirmed this classification, except to associate the upward excursions at s = 8 and s = 40 with the occurence of irregular configurations, and the downward excursion at s = 66-67 with the occurence of regular hexagonal configurations.

However, as indicated in Table 6.1, only two sequences were averaged. On the scale of Fig. 6.24 they are (approximately, since one point in the figure corresponds to two actual observations with $\Delta t = 19\ 200$) s = 29-39 as a L plateau, and 52-end as a H plateau. In Fig. 6.2 the corresponding reduced pressures fall as expected.

As would be expected, with increasing values of τ the range of distortions observed in basically regular hexagonal (L-type) configurations increases. Diffusion is noticeably more frequent but at the present density is still rare enough in the L region of configuration space so that, at the interval $\Delta t = 19\ 200$, successive snapshots usually show the same

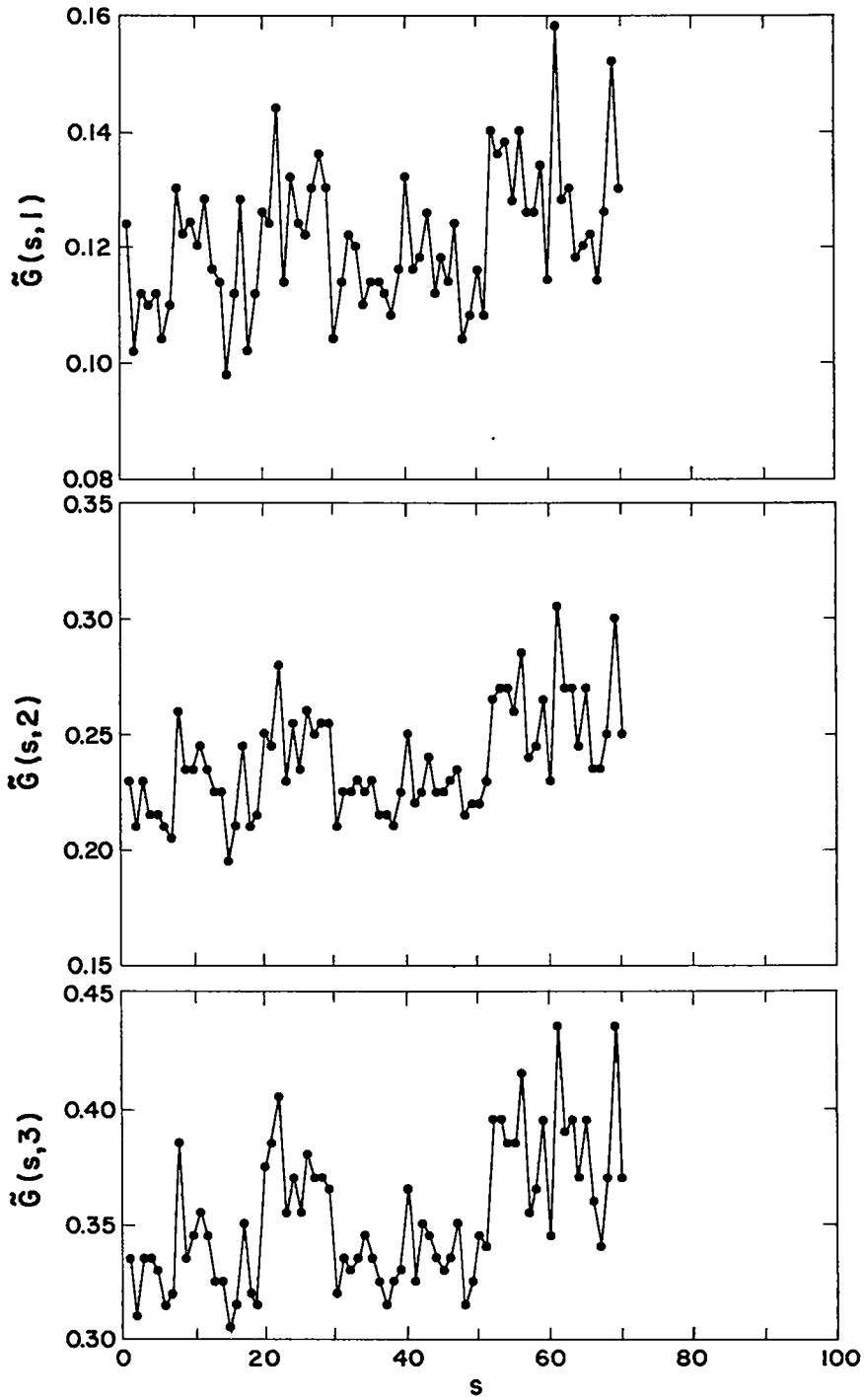

Fig. 6.24 The first three control charts for realization B23 at $\tau = 1.34$; $\Delta t = 38\,400$.

permutation. In the H region similar remarks apply, except that diffusion is, of course, very frequent. In this realization the observed sequences of "7X7" snapshots were frequently interrupted by more irregular appearing ones, in contrast to the long sequence of "7X7" states noticed in the previous realization.

6.1.2.6 Three realizations at $\tau = 1.35$.

At this reduced area we have the three realizations for which sample control charts are given in Fig. 6.25.

The snapshots for the very short realization B24 were all of H type, mostly irregular, except those for s = 1, 2, 3, and 19. Snapshot 1 showed only slight displacements from the regular hexagonal initial configuration. The second snapshot showed a vacancy-interstitial combination similar to those mentioned earlier, while the third snapshot was a quite distorted and permuted structure of regular hexagonal type. Snapshot 19 was also of this type, indicating that the downward excursion in the control chart at this point may have been due to a transient return of the system to the L region of configuration space; it had spent the intervening time s = 4-18 in the H region, as far as our observations indicate. All observations except the first were averaged, with Fig. 6.2 showing that the resulting reduced pressure lies as expected along the "fluid" branch of the equation of state.

Realization B25 gave control charts and snapshots which indicate a number of excursions back and forth between the two regions of configuration space. The snapshot classification was approximately s = 1-14

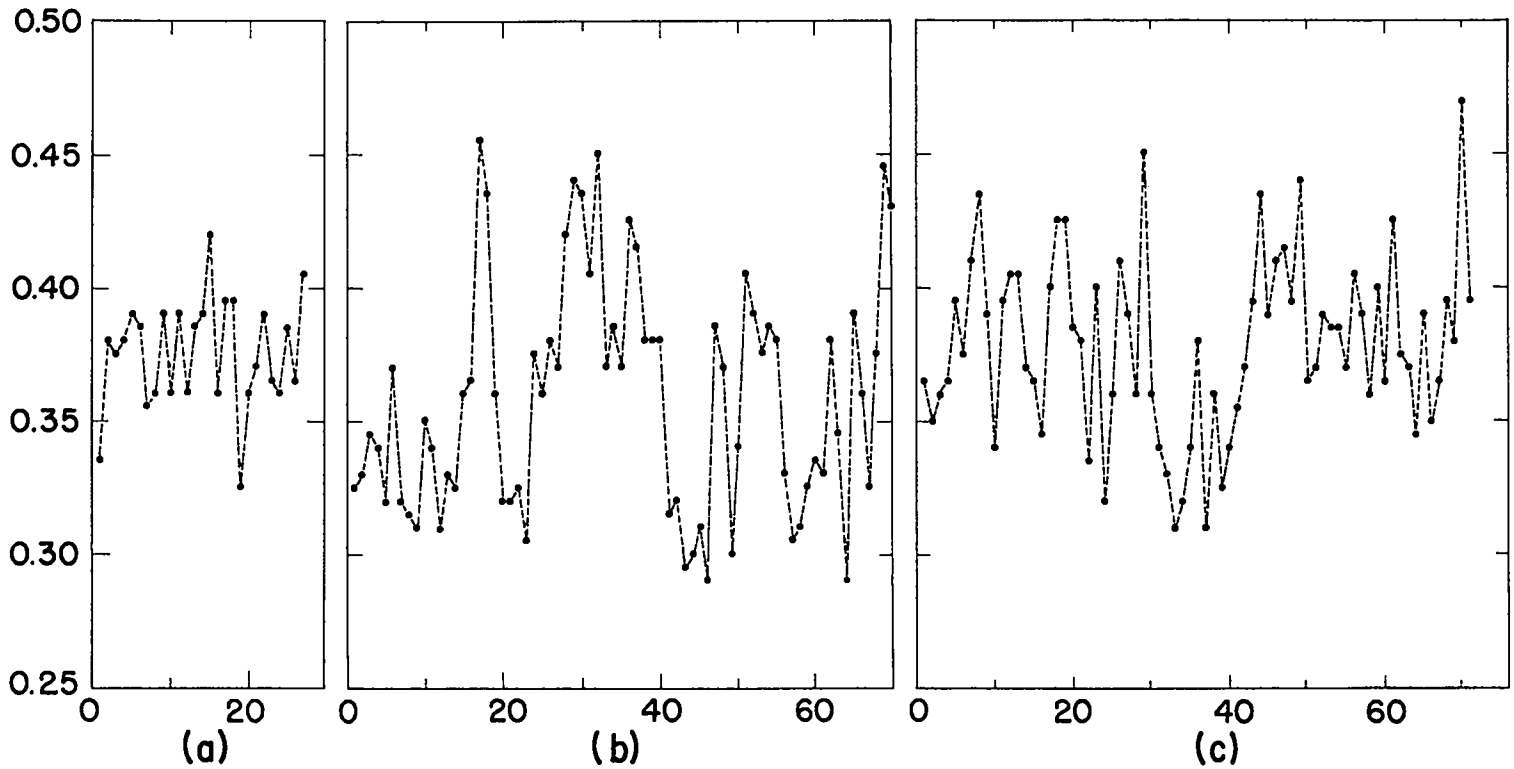

Fig. 6.25 Control charts for $\tau = 1.35$ realizations B24 (a), B25 (b), and B26 (c). In each case $\tilde{G}(s, 3)$ is plotted vs. s, with $\Delta t = 19\ 200$.

as L; 15-18 as H, irregular; 19-23 as L; 24-38 as H, mostly irregular, some "7x7"; 39-49 as L; 50-54 as H, irregular; 55-60 as L; 61-62 as H, irregular; 63-64 as L; 65-70 as H, irregular and "7x7". Even within this rather fine sub-division, configurations of the opposite type were noted in some cases. Only two sequences were averaged, as indicated in Table 6.1. The interval s = 1-16 was selected as a L plateau on the basis of the control charts before the snapshots were obtained. The latter, as already mentioned, indicate that at least some of the configurations included in the last two points of this interval (and also point s = 6) were of H type; this sort of imprecision becomes more or less unavoidable as τ becomes this large. The resulting reduced pressure lies (Fig. 6.2) on the "crystalline" curve, as expected. The sequence s = 28-40 was taken as a H plateau; again the snapshots indicate that some of the states were of the other type. Nevertheless, Fig. 6.2 shows that the estimated reduced pressure is rather higher than would be expected from the neighboring points. This may be taken, in part at least, as illustrative of the bias which can be introduced by the process of plateau classification, particularly for so short a sequence of observations.

The control charts for realization B26, Fig. 6.25c, suggested that the system had spent most of its time in H states, with the low level of s = 30-40 suggesting occurence of L states. This interpretation was largely supported by the snapshots, except that they suggest a somewhat longer residence in L states, since snapshots s = 20-40 were mostly L

type. (The pronounced upward fluctuation at s = 29 appears to have been associated with a vacancy-interstitial combination.) Reduced pressures were calculated from the entire set of observations (except the first), and from the last portion, s = 42-71, which seems to consist entirely of H states. The first estimate is clearly of no particular significance, being a rather arbitrary mixture of L and H contributions. The second estimate, being based on appreciably more observations than the H estimates of the other two realizations, is presumably a somewhat better average over what is evidently, at this density, a rather poorly defined region of configuration space.

Perhaps the most striking feature of these three realizations is the large scatter in the H-plateau estimates which is apparent in Fig. 6.2. It is clear that in the neighborhood of this reduced area, at least, the precision estimates given in Table 6.1 and obtained by methods not yet described, are not reliable. As will be seen, the statistical analysis itself gives warning of this, and furthermore it is clear that the uncertainties and subjective elements inherent in a two-plateau classification process of this kind would be expected to result in such scatter.

The single L-plateau estimate at this reduced area evidently agrees rather better with its adjacent values than ought to be expected, inasmuch as most of the above causes of large H-plateau estimate scatter would also be expected to be operative in this case.

We noticed among snapshot configurations of the H type an apparent decrease in the frequency of well-defined "7X7" configurations, compared

with realizations at slightly higher density.

6.1.2.7 Realization B27 at $\tau = 1.355$.

The control chart for this realization is shown in Fig. 6.26. From a control-chart statistician's viewpoint it shows definite indications of non-randomness, but no suggestion of a well-defined two-plateau structure. We discuss it along with the "jumpy" realizations because its reduced area is so close to that of the preceding set of three realizations. The snapshots were classified as follows: 1-9, mostly L; 10-23, mostly H, both irregular and "7X7"; 24, a very nice regular hexagonal arrangement; 25-42, mostly "7X7"; 43-49, mostly irregular. The very frequent occurence of "7X7" structures, which in a number of cases were quite well-defined, was perhaps the most striking feature of this experiment. The somewhat low control-chart level in the interval s = 31-40 is apparently associated with a predominance of these configurations. Along with the apparent occurrence of L states in points 1-9, this predominance of "7X7" configurations is also evidently responsible for the resulting reduced pressure shown in Fig. 6.2 (the estimated standard deviation is evidently not to be taken very seriously) being somewhat low compared to the H estimates at $\tau = 1.35$.

6.1.2.8 Summary of "jumpy" realizations.

These realizations for reduced areas from 1.3 to 1.355 have been discussed in some detail, in order that the reader can form his own

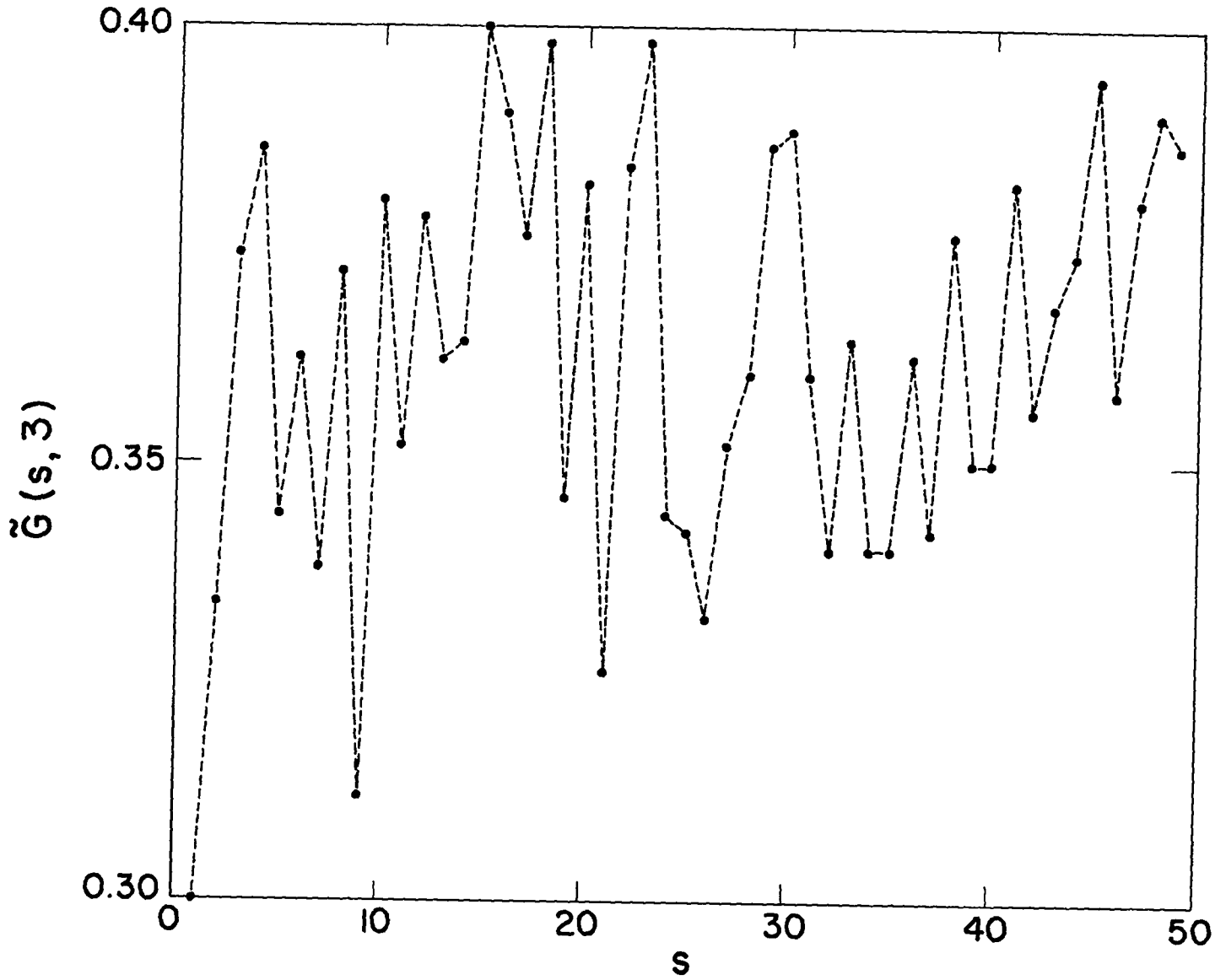

Fig. 6.26 Control chart for realization B27 at $\tau = 1.355$, $\Delta t = 19\ 200$.

judgment of our impressions, which are as follows:

(1) The "hourglass" model of configuration space forms an adequate framework within which to discuss the behavior of these realizations.

(a) L-region states show typically small deviations from the regular hexagonal lattice, very restricted diffusion, and in general seem to merit description as "perfectly crystalline" states.

(b) The H states apparently should be divided into two types, "irregular" and "7X7". The irregular states may, topologically, play the role of connections between L states and "7X7" states, and may have on the average larger values of $\tilde{G}$ than "7X7" states. The latter states have the character of imperfect crystals, their primary characteristic being the presence of a vacancy, with diffusion occurring in the obvious way.

(2) The increasing frequency of transitions between L and H states as τ increases implies a widening of the constricted connection between them.

(3) Not much can be said with respect to the relative volumes of the L and H regions of configuration space, and therefore with respect to the true petit canonical ensemble equation of state, in this interval of reduced areas, and particularly near $\tau = 1.3$. At the upper end of the interval, $\tau \approx 1.35$, the tendency for L

plateaus to disappear suggests that the H region is beginning to dominate.

(4) As τ increases, the L-L connections appear to enlarge, with permutations of the regular hexagonal arrangement occuring without intervention, so far as we can tell, of typical H structures. It is noteworthy that this "diffusion" is first observed to occur at the same reduced area ($\tau = 1.3$) and by the same mechanism (columnar rotation around the torus) as in the 12-molecule system, even though in Section 3.5 we saw that this motion is possible at all $\tau > 1.063$ in the 48-molecule system.

6.1.3 Realizations at $\tau \geq 1.375$.

All of these low density realizations were started from the regular hexagonal lattice. Their behavior leaves no doubt that equivalent results would have been obtained with any other choice of initial configuration.

None of these realizations displayed a two-plateau behavior. Control charts for the two highest density realizations, B28 at $\tau = 1.375$ and B29 at $\tau = 1.4$, are given in Fig. 6.27. As will be seen later, quantitative statistical tests for randomness indicate the presence of significant serial correlation in these two realizations, but their control charts are clearly much more nearly normal than those obtained for $\tau = 1.3$-1.35.

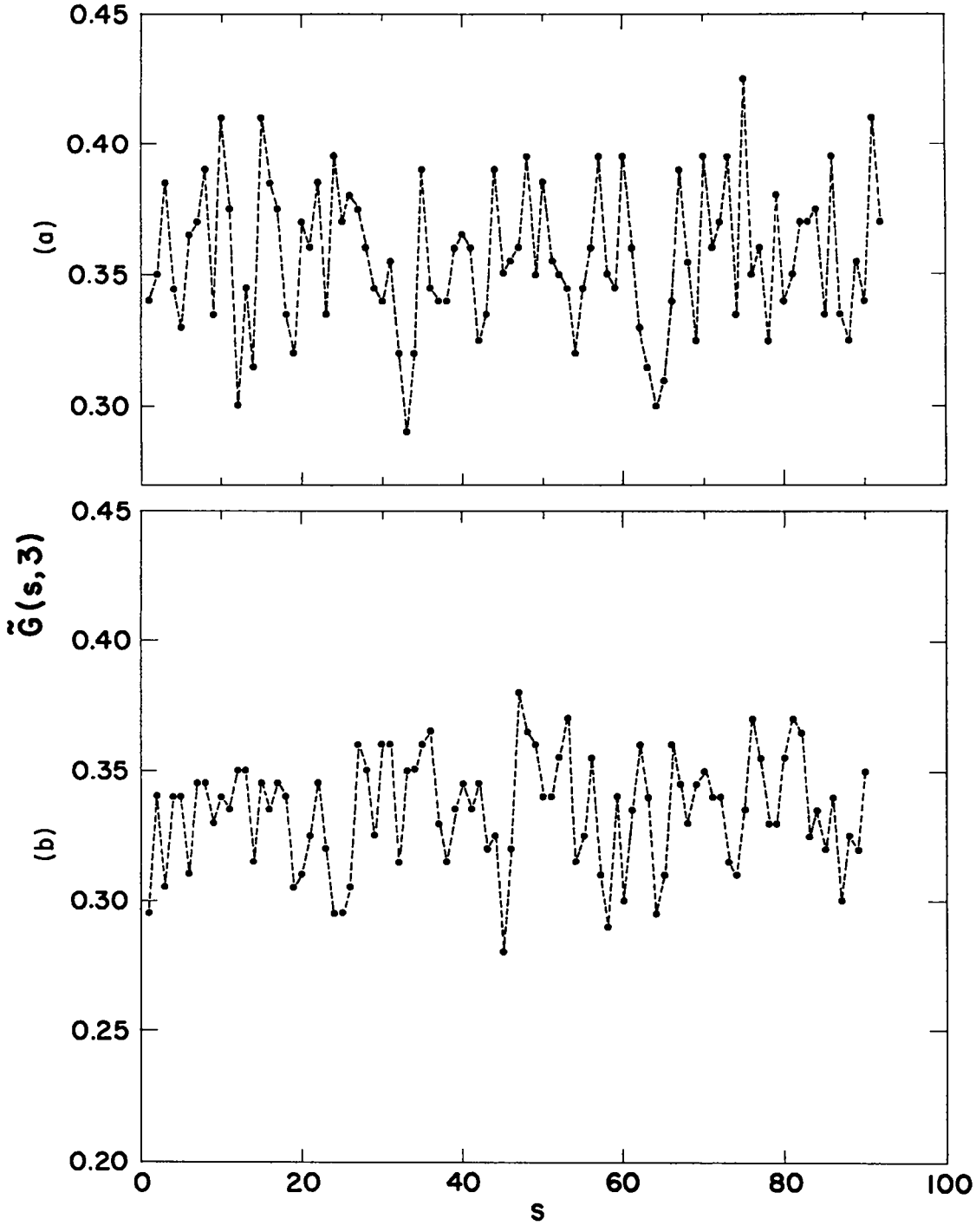

Fig. 6.27 Control charts for (a) realization B28 at $\tau = 1.375$; (b) realization B29 at $\tau = 1.4$; both with $\Delta t = 19\ 200$.

The snapshots show the expected trend away from structures of noticeable regularity of either the hexagonal or "7X7" types. In realizations B28 and B29 the typical structure, in the terminology of the previous subsections, was irregular. In B28 the larger downward fluctuations in the control charts ($s \approx 12, 33, 54, 64$) were accompanied by snapshots of the L type i.e., ones in which the regular hexagonal arrangement could be detected.

It is our opinion, based upon both the statistical and geometrical investigations, that the realizations at $\tau \geq 1.375$ are usefully convergent to the true petit canonical ensemble average for this particular 48-molecule system, although the estimated standard deviations of Table 6.1, particularly for B28 and B29, may perhaps be too small. In Fig. 6.28 we present a typical sequence of 10 consecutive snapshots ($\Delta t = 19\ 200$) from the realization at $\tau = 1.4$, as exhibiting the structure of this 48-molecule system near the high density limit of complete convergence. Our classification of these configurations was: snapshot 59, a somewhat distorted regular hexagonal structure; 60-63, 65, and 66, irregular arrangements in which in some cases suggestions of the presence of both the regular hexagonal and the "7X7" structures are present; 64, 67, and 68, more or less distorted "7X7" structures.

Of the 151 snapshots obtained from the long realization B31 at $\tau = 1.5$, the vast majority were classified as irregular. In only one was any resemblance to the regular hexagonal arrangement noticed, and only two were classified as reasonably regular "7X7" types.

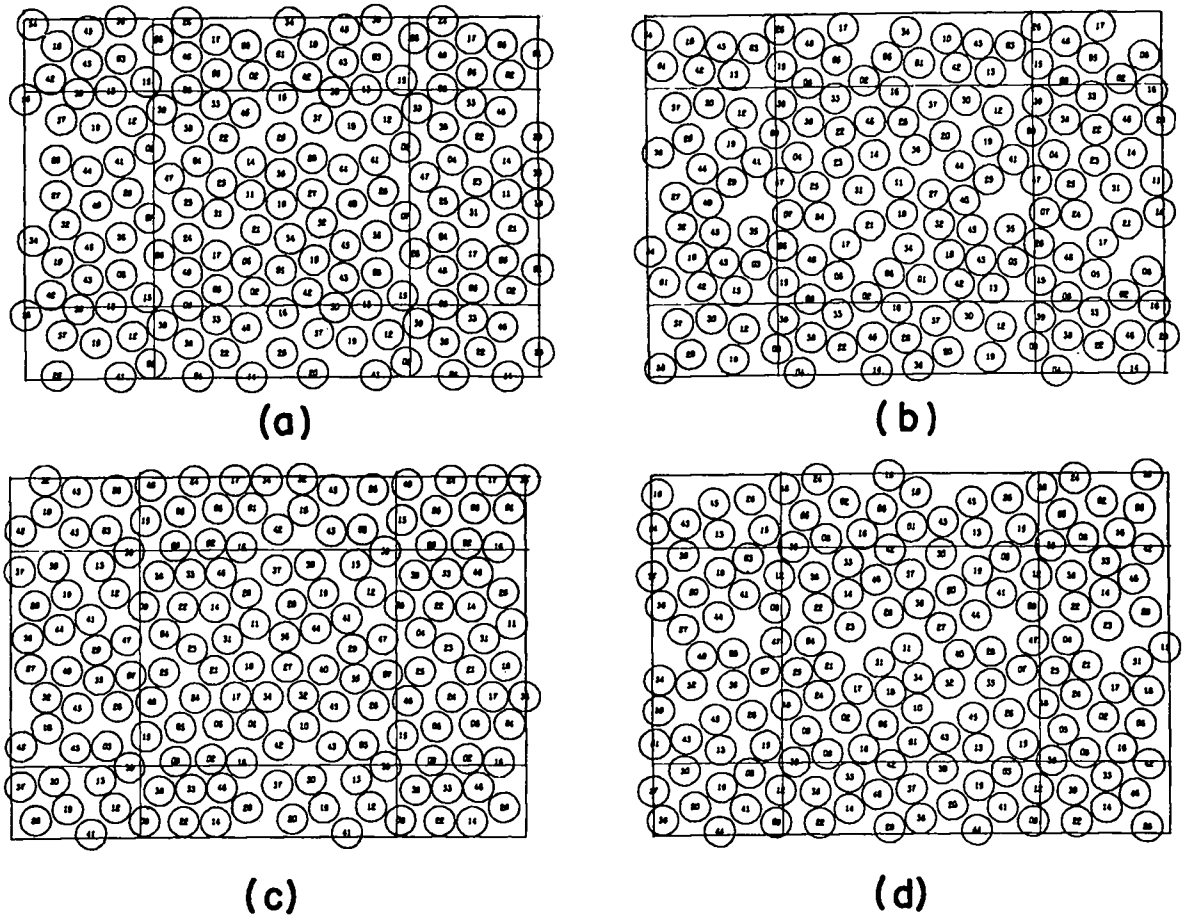

Fig. 6.28 A typical sequence of ten consecutive snapshots from realization B29 at $\tau = 1.4$, $\Delta t = 19\ 200$; (a)-(d), snapshots 59 through 62.

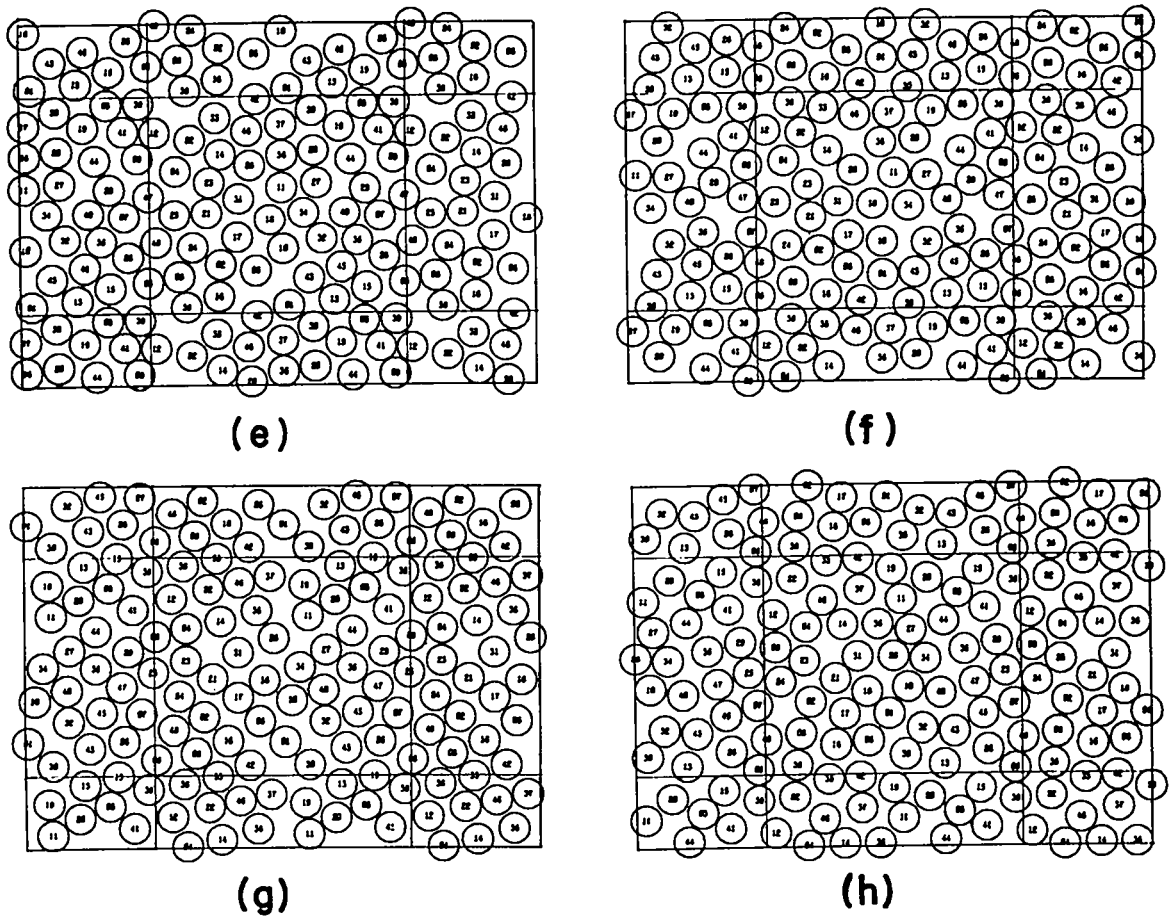

Fig. 6.28 A typical sequence of ten consecutive snapshots from realization B29 at $\tau = 1.4$, $\Delta t = 19\ 200$; (e)-(h), snapshots 63 through 66.

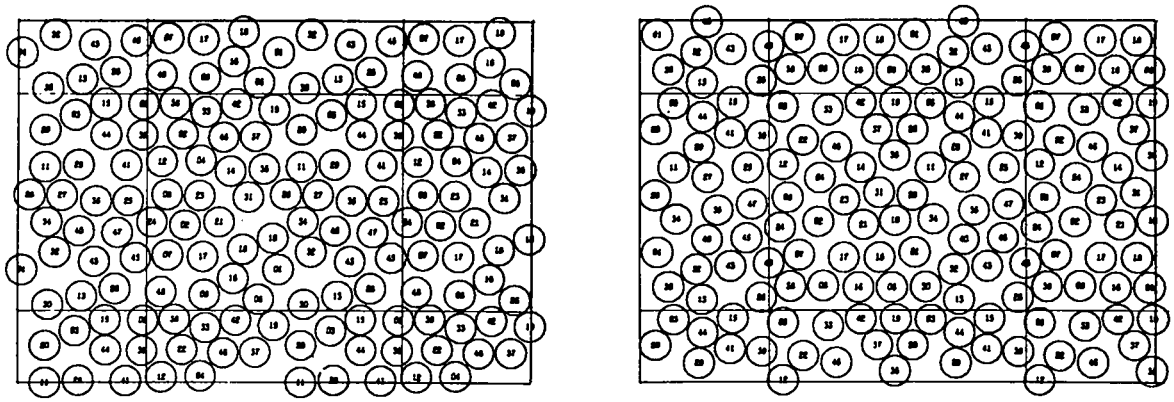

Fig. 6.28 A typical sequence of ten consecutive snapshots from realization B29 at $\tau = 1.4$, $\Delta t = 19\ 200$; (i) and (j), snapshots 67 through 68.

In the twelve other snapshots enough similarity to the latter arrangement was detected to describe them as distorted "7X7" structures, but the amount of subjective judgment being exercised was annoyingly great, with a tendency to make different classifications of the same snapshot when viewing it at different times. The principal impression is of increasingly irregular structure as τ increases.

In the realization at $\tau = 1.65$, all of the 38 snapshots were classed as irregular, as was also the case in a less detailed examination of the snapshots from the realizations at still lower density.

We have already commented upon the convergence of the resulting reduced pressures (Figs. 6.1 and 6.2) toward the approximate virial expansion, as well as their approximate agreement with the scaled-particle

approximation throughout this range of reduced area.

6.2 The "7X7" Arrangement at High Density

As the reader will probably have anticipated from the important role played by the "7X7" states in the H region of configuration space for reduced areas between 1.3 and 1.35, this structure forms the basis of the "extended fluid" branch of the equation of state obtained by the "compressor" technique, as will be described in Section 6.3. Before proceeding to this discussion, however, it is profitable to consider certain requirements which at high density are imposed on the arrangement by the periodic boundary conditions and the shape of the area V, and which can be deduced a priori even though in most cases they were first observed during the calculations.

The basic characteristic of this structure, as already mentioned and indeed implied in the term "7X7", is its arrangement in 7 rows (parallel to the longer edge of V) of 7 molecules each in approximately hexagonal coordination, one molecule being, of course, replaced by a vacancy. We begin, then, by first considering the properties of the 49-molecule system, afterwards describing the modifications which occur when one of them becomes a hole.

6.2.1 The 49-molecule arrangement.

At high density we may expect the molecules to be arranged in as nearly hexagonal close-packed fashion as is compatible with the periodic

boundary condition and the fixed shape of V. We therefore first recall that if a hexagonal close-packed array of hard circles is regarded as being composed of successive rectilinear rows of tangent circles, then there is an A - B - A - B··· alternation in row character: the centers of the circles of the second row (B) must be directly above the osculation points of the first row (A); while the third row, its centers being directly over those of the first row, is again of type A, etc.

Now if we attempt to make such a hexagonal close-packed, seven-rowed structure, designating the first row as type A and indicating the number of the row by a subscript, then the arrangement dictated by the periodicity requirement in the direction perpendicular to the rows is $A_1B_2A_3B_4A_5B_6A_7A_1'B_2'\cdots$, where the primes indicate "image" rows. We see that the A - B character of hexagonal close-packing is incompatible with a periodic structure having an odd number of rows, so that there must be a stacking defect in which two adjacent rows are of the same type (A_7A_1' in the above notation).

The resulting array is shown in Fig. 6.29a, except that the stacking defect has been moved into the interior for convenience. As can be seen from the dimensions given in the figure, with close-packed rows this array has an edge ratio of $\frac{3\sqrt{3}+1}{7}$, and thus cannot fit exactly into the rectangular area V for our 48-molecule system, whose edge ratio is $\sqrt{3}/2$ (Chapter 3):

$$\frac{3\sqrt{3}+1}{7} - \frac{\sqrt{3}}{2} = \frac{2-\sqrt{3}}{14} > 0 \quad .$$

That is, its shorter side is slightly too long.

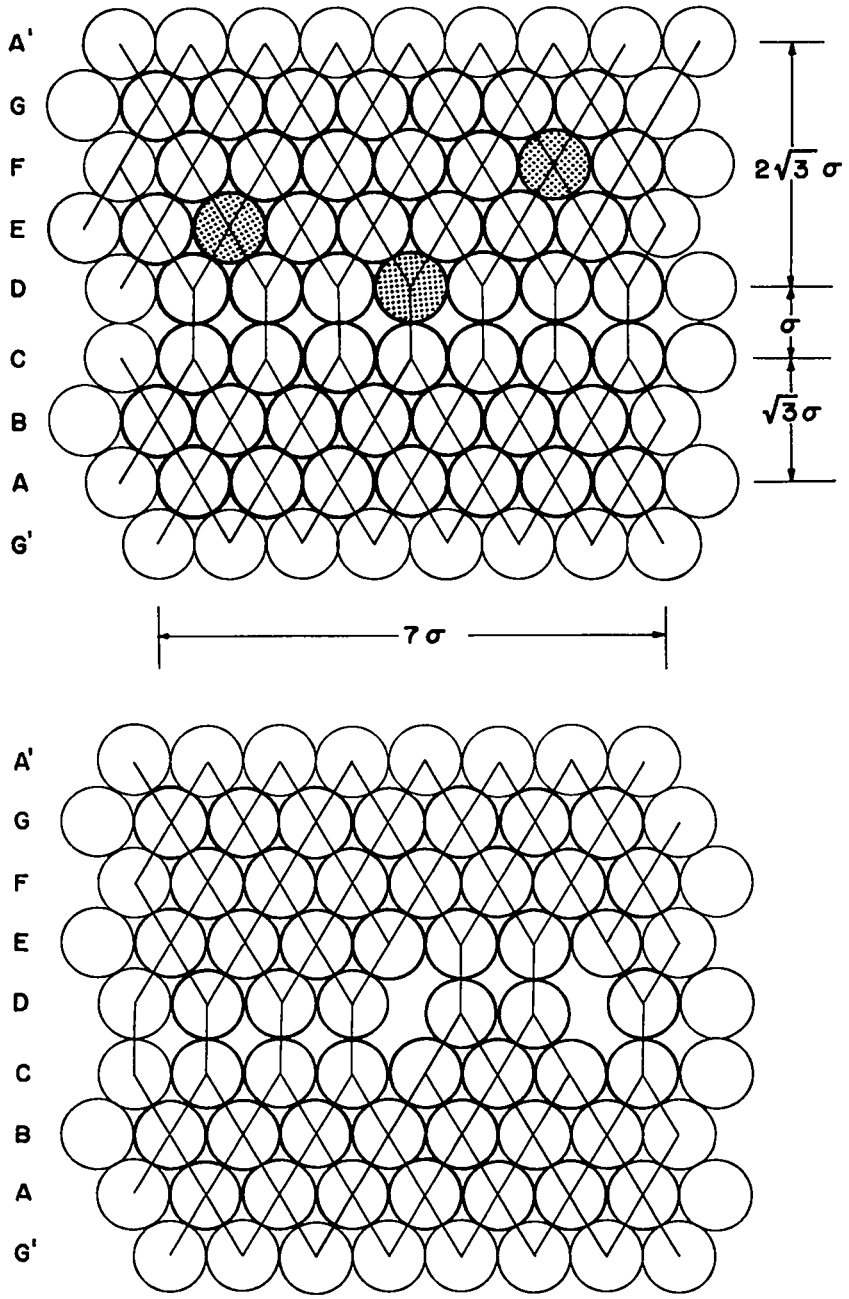

Fig. 6.29 Two idealized "7×7" structures of the 48-molecule system at $\tau = 1.056$. The bonds connect molecules which are in contact after the lattice is deformed in order to fit into the rectangular area V with side ratio $\sqrt{3}/2$. In (a) the dimensions are for the system with close-packed rows, before deformation; the shaded molecules indicate the three types of vacancy location. In (b) is shown an arrangement having two half-vacancies in row D, with the stacking defect being partly between rows C and D, and partly between D and E.

In order to make the system fit, we evidently must squeeze it together from top and bottom, figuratively speaking, while letting it expand slightly laterally. As a result the molecules in the horizontal rows will tend to break contact. If this is done uniformly throughout the structure, these horizontal contacts are all lost, with only the diagonal contacts between nested rows and the vertical contacts along the stacking defect remaining. Only a slight deformation of this sort is required in order to fit the system into the desired rectangle. The calculated change in inclination of the diagonal contact lines is only about $\frac{1}{2}$ degree, and the free distance between circumferences of circles in the horizontal rows is only about 1.6% of the hard-circle diameter. The latter is calculated to be, in units of the long edge of V, $\sigma = 0.14046$. These perturbations are too small to be apparent in a figure, so we continue to use Fig. 6.29a, keeping in mind that now only the bonded circles are in actual contact.

We will shortly discuss the several ways in which one of these molecules can be removed to form the desired system of 48 molecules and one hole, but let us first note that the above value of σ leads with use of $N = 49$ and Eqs. (2.8) and (2.9) to $\tau = 1.034$. That is, this arrangement is an allowable close-packed (i. e., no molecule can be moved if all the others are held fixed) configuration of 49 molecules in V with an area per molecule which is 1.034 times that for the regular hexagonal close-packed configuration. However, it is not a <u>stable</u> limiting

configuration, in the terminology of Salsburg and Wood (see Section 3.3.1.1), because it does not satisfy the contact criterion for stability, Eq. (3.4). Figure 6.29a shows that there are five rows in which each molecule has coordination number 4, and two rows in which the coordination number is 3. The average coordination number is thus 26/7, which fails to satisfy Eq. (3.4). Therefore, according to the Salsburg-Wood analysis, although this 49-molecule state is close-packed, nevertheless a configuration space region of non-vanishing volume is accessible from it, and at $\tau = 1.034$ the corresponding reduced pressure is not infinite. The true limiting configuration and limiting reduced area for this region of configuration space of this system are unknown. They are clearly not the regular hexagonal lattice nor $\tau = 1$, and we surmise that the limiting arrangement and reduced area are not much different from the unstable ones.

6.2.2 The 48-molecule, 1-hole arrangement.

When one of the molecules of the 49-molecule structure described in the preceding sub-section is removed, the reduced area becomes $\tau = 1.056$ [$\sigma = 0.14046$, $N = 48$; Eqs. (2.8) and (2.9)]. There are three different ways in which this can be done, viz., (1) removal of a molecule from one of the two adjacent rows which create the stacking defect (row C or D in the figure); (2) removal of a molecule from a row which is adjacent to one of these defect rows (row B or E); (3) removal from a row both of whose adjacent rows are not defect rows (row A, F, or G). Each case is exemplified by a shaded circle in Fig. 6.29a.

In all three cases creation of the vacancy immediately gives a structure which is no longer close-packed. In case (1) this is obvious since the molecule in the defect row is now free to move back and forth between its own site and the vacancy site. In the terminology of the free-volume theory it has a relatively large free area. In addition, even with all other molecules fixed, two of the molecules adjacent to the vacancy in the non-defect row have much smaller free areas, which moreover can be distributed by way of their neighbors throughout the system. (These two molecules have three contacts after creation of the vacancy, but two of them are diametrically opposite each other, so that these two molecules are not fixed by their neighbors.) The free area created in case (2) or (3) is similar to the small free areas of the last-mentioned two molecules in case (1).

We note that only in case (1) is the vacancy likely to be very mobile. In all three cases, as for the parent 49-molecule system, the exact limiting configuration and reduced area are unknown; the latter is obviously less than 1.056. It is possible that there are different limiting configurations and reduced areas depending on which of the above three types of vacancy is present, since below some critical reduced area the hole may no longer be able to move from one location to another.

We also note from Fig. 6.29a that in some range of expansions a probable mode of defect migration should be movement of the stacking error from rows C and D to D and E, for example, by means of a fluctuation

in which the vacancy row D moves as a unit one-half molecular diameter in the horizontal direction. During such a fluctuation there will also be ample opportunity for horizontal diffusion of the vacancy. By a combination of these two types of motion, the vacancy should be able to reach any position in the 49-site lattice.

We note that if, during a fluctuation of the above type, some, but not all of the molecules of the vacancy row make such displacements, then a configuration is produced in which there are two "half-vacancies" and in which the stacking defect is distributed between two pairs of rows. Figure 6.29b shows an example in which two molecules have been so displaced. This arrangement is also not close-packed; two of the molecules near each half-vacancy have two of their three contacts diametrically opposed, and thus these molecules are free to move slightly, even with their neighbors fixed.

6.2.3 Summary.

The "7X7" configurations of Figs. 6.29a-b evidently correspond to one or more regions of allowable states of the 48-molecule system for $\tau > \tau_o$, with $\tau_o < 1.056$, but its exact value (or values) is unknown. Probably it is only slightly less than 1.056.

It does not seem possible to predict which of these various possible "7X7" arrangements is most likely to occur at high density. Clearly, there will be a range of τ over which well-defined "7X7" structures exist but in which fluctuations are large enough so that the various

sub-types will not be distinguishable; e.g., the "7X7" structures already described at $\tau \geq 1.3$.

In any case, the corresponding region of configuration space is evidently the H region of our hourglass model (or one of several H regions), and is probably inaccessible from the regular hexagonal states over some unknown interval $\tau_o \leq \tau < \tau_m < 1.3$. The last inequality follows from the observed L → H transition in realization B19. However, at $\tau = 1.3$ the L-H connection is evidently quite constricted.

For $\tau \geq 1.056$ the calculated positions of the molecules in any of the versions of Fig. 6.29 could be used as initial configurations for Markov chain realizations intended to investigate the corresponding equations of state, as well as the connectivity with the regular hexagonal configurations. As already indicated, this was not the procedure which we followed. Rather, we came to the above understanding of this type of arrangement by way of observing it in a sequence of "compressions" from lower density, H-type configurations, as well as observing it in the already-described "jumpy" realizations. It is for this reason that we give this discussion here rather than in Section 3.5.

The important point is that the existence of the "7X7" structures at high density is intimately connected with the periodic boundary conditions and with the shape of the area V required by the latter and the value N = 48. There is no corresponding configuration for the 12-molecule system discussed previously, nor is it clear what the behavior of larger systems is likely to be. For example, in the four-times larger

system obtained from the obvious 2X2 replication of the present 48-molecule unit cell, there is, of course, a corresponding "14X14" arrangement in which there are four vacancies and two pairs of defect rows. However, it is not clear that this would necessarily be a preferred arrangement of such a 192-molecule system in any significant range of expansions.

6.3 Realizations Started From "Compressed" Configurations, $\tau \leq 1.254$

The five realizations B6, B9, B10, B13, and B16, which establish our so-called "extended fluid" branch of the equation of state, were all started from configurations selected from what amounts to a single "compression" (Section 1.2.3) process.

The intention, of course, was to select a "fluid" configuration and "compress" it to values of τ less than 1.34 (where realization B23 had given somewhat less pronounced jumps than those to which we had become accustomed for the case of hard spheres), in order to see if the resulting equation of state points would define a locus different from that obtained from the regular hexagonal realizations.

The selected configuration was that at t = 729 600 (s = 38) from realization B29 at τ = 1.4 on the "fluid" branch of the equation of state. (At the time, this happened to be the last configuration of B29, which later was developed further.)

This configuration is shown in Fig. 6.30, and is of the type which we described in the previous discussion as "irregular, with some

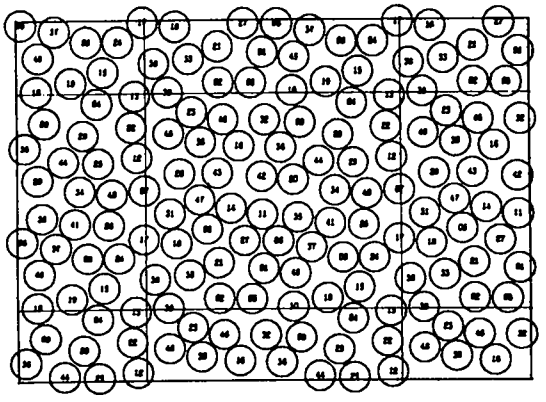

Fig. 6.30 The parent configuration of the "extended fluid" branch of the equation of state, shown as snapshot 38 from realization B29 at $\tau = 1.4$, $\Delta t = 19\ 200$. The initial configurations of the "extended fluid" branch realizations were generated by successive compressions of this configuration.

indications of being a mixture of both structures." Even in hindsight it seems to be a reasonably typical configuration of realization B29.

In discussing these realizations we will follow the compression process from low to high density. The control charts for these realizations were not exceptional, so we will discuss them in terms of their snapshot configurations and their resulting reduced pressures.

6.3.1 Realization B16 at $\tau = 1.254$.

Compression of the configuration shown in Fig. 6.30 to $\tau = 1.254$ produced the one shown in Fig. 6.31a, which was the starting point of the present realization. The configuration is obviously an only slightly distorted "7X7" structure. Figures 6.31b-c show the two subsequent

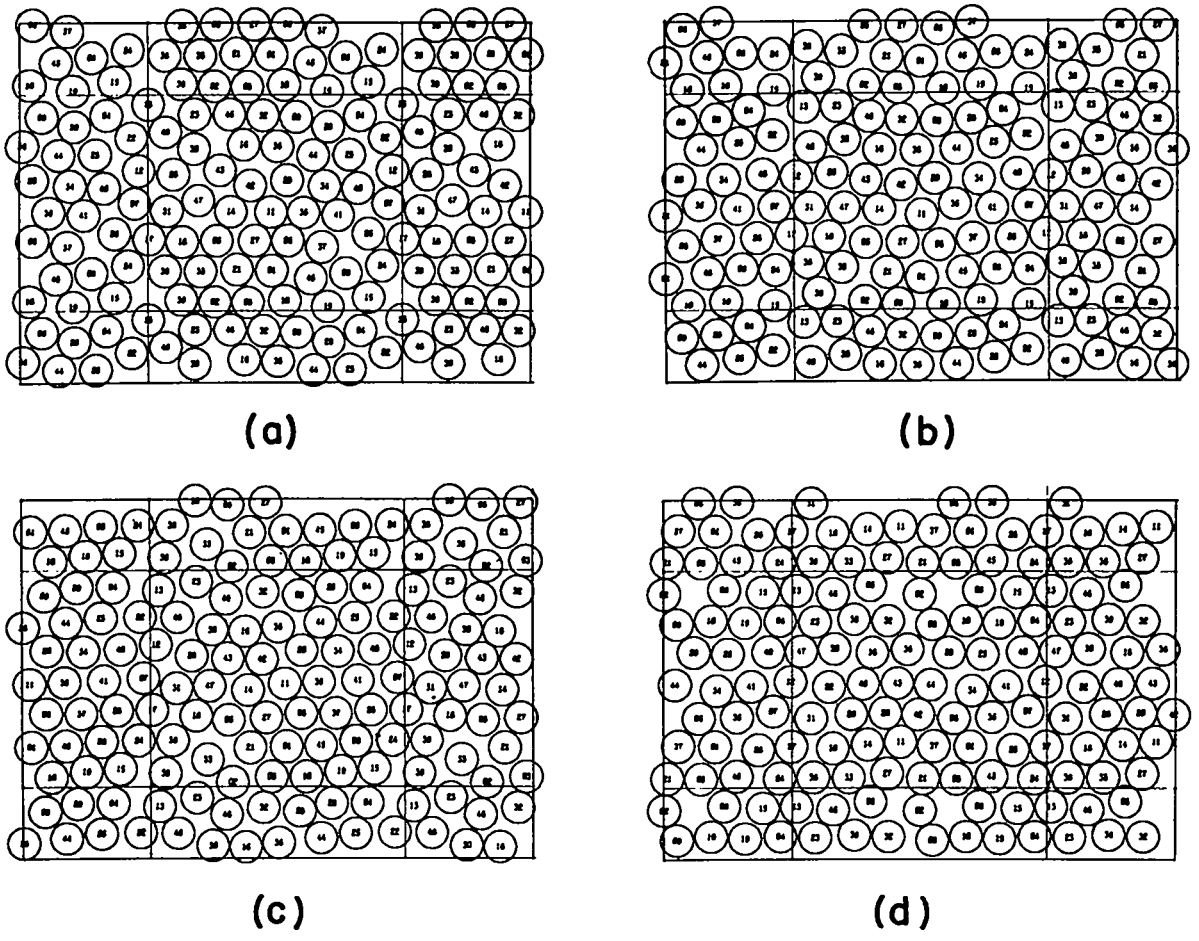

Fig. 6.31 Snapshots s = 0, 1, 2, and 75 (a through d) from "extended fluid" branch realization B16 at $\tau = 1.254$, $\Delta t = 19\ 200$.

snapshots, while Fig. 6.31d shows the last configuration of the run. All are quite well-defined "7X7" structures, as were all the other snapshots. No deviation large enough to suggest description as "irregular" was noted, nor was any snapshot at all suggestive of the regular hexagonal lattice.

The snapshots displayed vacancy migrations of the expected type. They were infrequent enough so that a few (in most cases one; in a single case, five) vacancy-molecule interchanges sufficed to account for the differences between successive snapshots. A total of 85 such vacancy jumps were counted in this way during the 1 440 000 configurations of this realization. Of these, 34 were interchanges of the vacancy with an adjacent molecule in the same row, while 51 involved an interchange with an adjacent molecule of an adjacent row. As Fig. 6.31 illustrates, at this density fluctuations are large enough so that the stacking defect of Section 6.2 is usually not well-defined. Consequently the vacancy cannot usually be classified according to the three types of Fig. 6.29a. There were, of course, a number of examples such as Fig. 6.31b in which the vacancy is more or less distributed over the six-molecule row, but at this density a description in terms of half-vacancies of the Fig 6.29b type did not seem warranted. For the purposes of the above counting of within-row vacancy jumps, in doubtful cases we assigned the location of the hole in such a way as to minimize the number of jumps.

Figures 6.1 and 6.2 show, as already indicated, that the reduced pressure calculated from this realization is indeed much above that for a regular hexagonal realization at this reduced area, as would be

expected from the observed geometrical structure.

In terms of the hourglass description of configuration space, all configurations of this realization are evidently from the H region, which moreover appears to consist entirely of "7X7" states. This H region is apparently effectively disconnected from the L region, and also from the irregular type of H state. The behavior is consistent with our previous conjecture that irregular states form the connection between L and H states, and therefore are probably not very numerous at this density.

6.3.2 Realization B13 at $\tau = 1.169$.

The initial configuration, shown in Fig. 6.32a, was produced by compression of the B16 configuration of Fig. 6.31b. It is thus hardly surprising that the result of the compression process was a nicely regular "7X7" structure. Neither, in view of the behavior of realization B16, is it surprising that all of the 33 subsequent snapshots, the last of which is shown in Fig. 6.32b, were also well-defined "7X7" arrangements.

The qualitative behavior was quite similar to that of B16. At this increased density the structures were more regular, and vacancy jumps less frequent. There was now a noticeable tendency for a more or less well-defined stacking defect to appear. In Fig. 6.32a it is somewhat poorly defined, and appears to be shared between two pairs of rows (7-1 and 1-2, numbering from the lower edge of the cell upwards). In Fig. 6.32b the defect is fairly prominent between rows 3 and 4. In all such

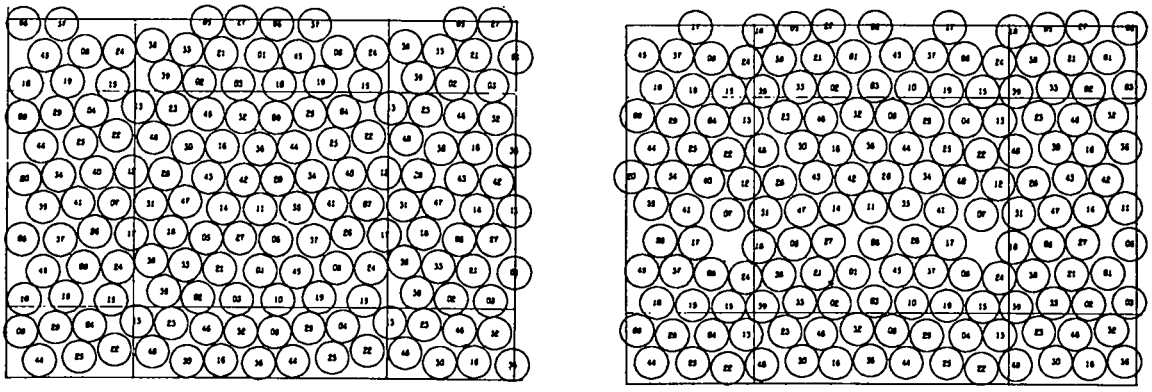

Fig. 6.32 The initial (a; s = 0) and final (b; s = 33) snapshots of "extended fluid" branch realization B13 at τ = 1.169, Δt = 19 200.

cases the vacancy was in one of the defect rows [case (1) of Section 6.2.2]. However, in a number of the snapshots no stacking defect was noticeable, accommodation to the periodic structure being made by a slight deformation of the lattice lines. For the purpose of counting vacancy jumps, therefore, we ignored the half-vacancy cases as with realization B16, and obtained 14 within-row and only 4 between-row jumps. This represents a notable decrease in relative jump frequency, as well as a shift to a preponderance of within-row jumps, when compared with B16. As a result of so few jumps between rows, the vacancy was restricted to rows 1, 2, and 3 throughout the calculation.

6.3.3 Realizations B9 and B10 at $\tau = 1.124$.

As indicated in Table 6.1, these two realizations were identical except that different versions of the machine code were used (see Section 4.2), and B10 had a smaller value of Δr^2 (see Section 2.3.4). The initial configuration, shown in Fig. 6.33, was obtained by compression of the t = 19 200 configuration of realization B13 at $\tau = 1.169$. As would be expected from the previous discussion of the lower-density realizations of the "extended fluid" branch, this configuration and all the other snapshots from both of the present realizations were well-defined "7X7" structures. At rather high density the stacking defect (Section 6.2) was always quite pronounced. It was always adjacent to the six-molecule row [vacancy location case (1) of Section 6.2.2], and in addition the

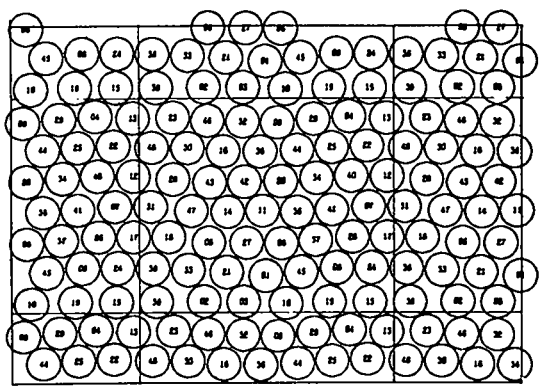

Fig. 6.33 The initial configuration for realizations B9 and B10 at $\tau = 1.124$.

"half-vacancy" configurations discussed in Section 6.2.2 were quite predominant. That is, the typical snapshot from these realizations was one in which the stacking defect was shared between the six-molecule row and both its adjacent rows, and the vacancy was split into two half-vacancies. This observation is the principal qualitative result obtained from these two realizations. In Fig. 6.33, for example, the best idealized description seems to be the following assignment of stacking defect and half-vacancy locations to the six-molecule row:

$$\overline{39},\ \tfrac{1}{2}\text{-hole},\ \underline{2,\ 3,\ 10},\ \tfrac{1}{2}\text{-hole},\ \overline{19,\ 15},$$

where the position of the line above or below the molecule numbers indicates the location of the stacking defect.

Consecutive snapshots ordinarily indicated a few half-lattice-spacing jumps of one or both of the half vacancies. Occasionally the latter, as a result of their more or less random individual motions, met and coalesced into a full vacancy. At these times the stacking defect is necessarily consolidated entirely to one side of the vacancy row, and it is only at these times that a vacancy jump to another row is possible. Thus, the latter were rather rare at this density; in B10, the longer of these two realizations, only three such between-row jumps occurred during 1 113 600 configurations; in the shorter B9, one occurred in 403 200 configurations.

The above described behavior is well illustrated by the last nine snapshots from realization B10, shown in Fig. 6.34. Our idealized description of these configurations is as follows:

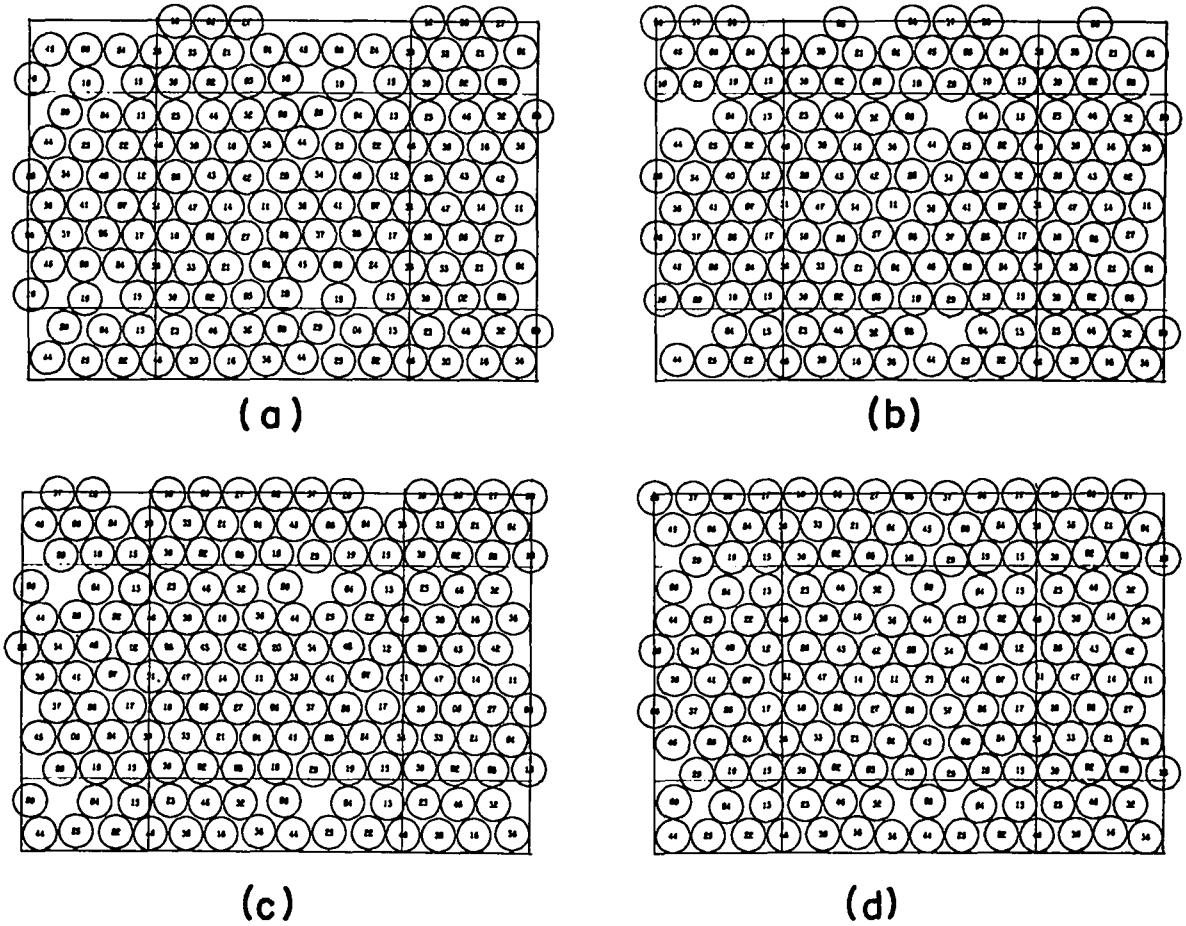

Fig. 6.34a-d Snapshots 50 through 53 from "extended fluid" branch realization B10 at $\tau = 1.124$; $\Delta t = 19\ 200$.

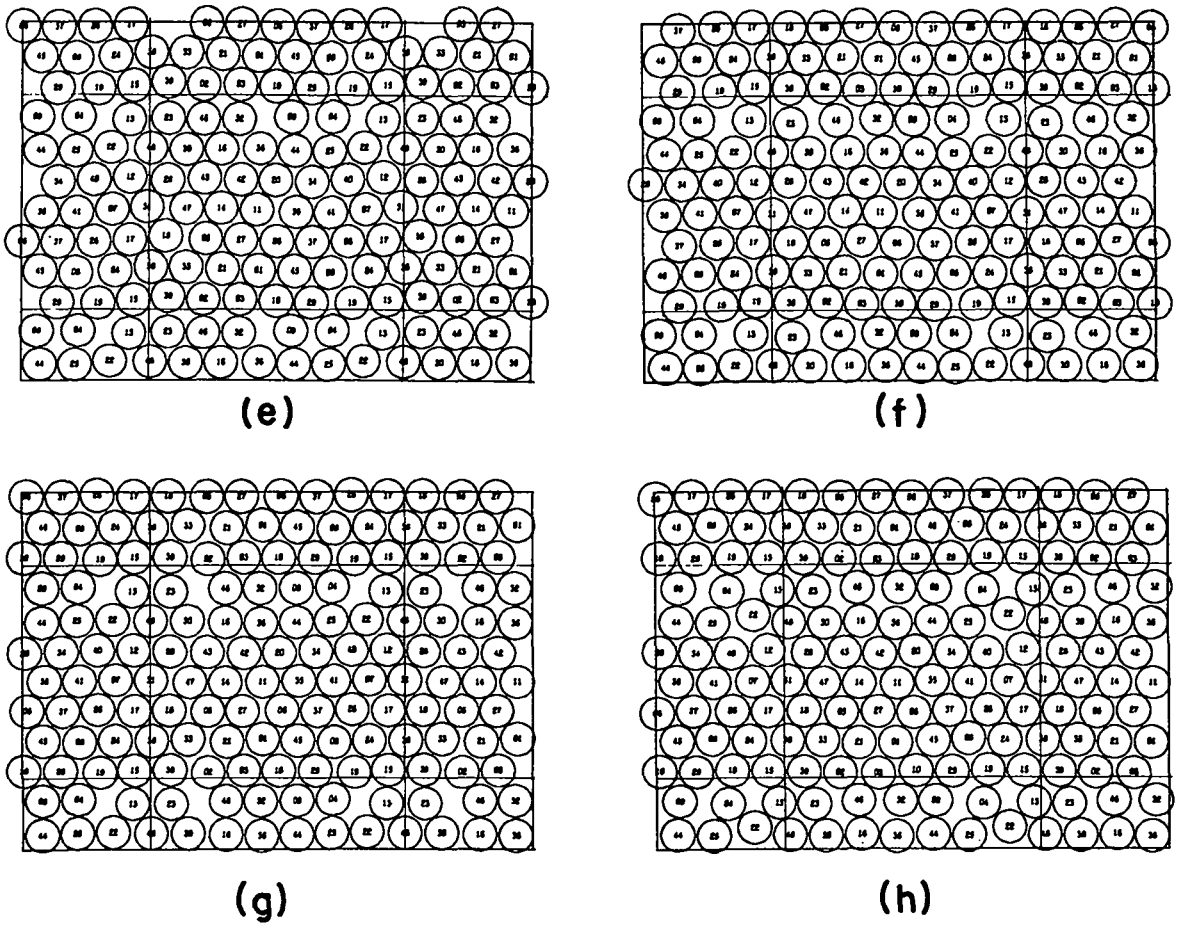

Fig. 6.34e-h Snapshots 54 through 57 from realization B10 at τ = 1.124; Δt = 19 200.

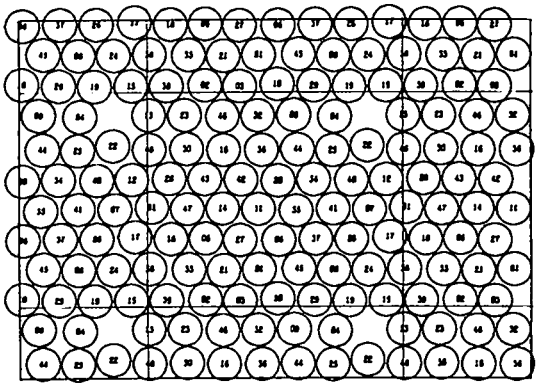

(i)

Fig. 6.34i Snapshot 58 from realization B10 at $\tau = 1.124$.

Snapshot	Six-Molecule Row	Jumps Since Previous Snapshots
50	$\underline{39, 2, 3, 10}$, $\frac{1}{2}$-hole, $\overline{19}$, $\frac{1}{2}$-hole, $\underline{15}$	
51	$\overline{23, 46, 32, 9}$, hole, $\overline{4, 13}$	$19 \rightarrow (\frac{1}{2})$; $29 \uparrow$
52	$\overline{23, 46, 32, 9}$, hole, $\overline{4, 13}$	
53	$\overline{23, 46, 32}$, $\frac{1}{2}$-hole, $\underline{9}$, $\frac{1}{2}$-hole, $\overline{4, 13}$	$9 \rightarrow (\frac{1}{2})$
54	$\overline{23, 46, 32}$, $\frac{1}{2}$-hole, $\underline{9, 4}$, $\frac{1}{2}$-hole, $\overline{13}$	$(\frac{1}{2}) \leftarrow 4$
55	$\overline{23, 46}$, $\frac{1}{2}$-hole, $\underline{32, 9, 4}$, $\frac{1}{2}$-hole, $\overline{13}$	$32 \rightarrow (\frac{1}{2})$
56	$\overline{23}$, $\frac{1}{2}$-hole, $\underline{46, 32, 9, 4}$, $\frac{1}{2}$-hole, $\overline{13}$	$46 \rightarrow (\frac{1}{2})$
57	$\overline{23}$, $\frac{1}{2}$-hole, $\underline{46, 32, 9}$, $\frac{1}{2}$-hole, $\overline{4, 13}$	$4 \rightarrow (\frac{1}{2})$
58	$\underline{23, 46, 32, 9, 4}$, hole, $\underline{13}$	$(\frac{1}{2}) \leftarrow 4$; $23 \rightarrow (\frac{1}{2})$; $13 \rightarrow (\frac{1}{2})$.

Comparison of the above tabulation with Fig. 6.34 will show the reader the extent of the idealizations involved in making such simplified descriptions. Note that at the end of the calculation the configuration would permit a vertical interchange between the vacancy in row 7 and molecule 22 in row 6.

6.3.4 Realization B6 at $\tau = 1.074$.

The initial configuration, Fig. 6.35a, for this, our highest-density realization on the "extended fluid" branch of the equation of state, was obtained by further compression of the $\tau = 1.169$ configuration shown in Fig. 6.32a (the initial configuration of realization B13). As Fig. 6.35a shows, the compression process trapped the system in a split-vacancy

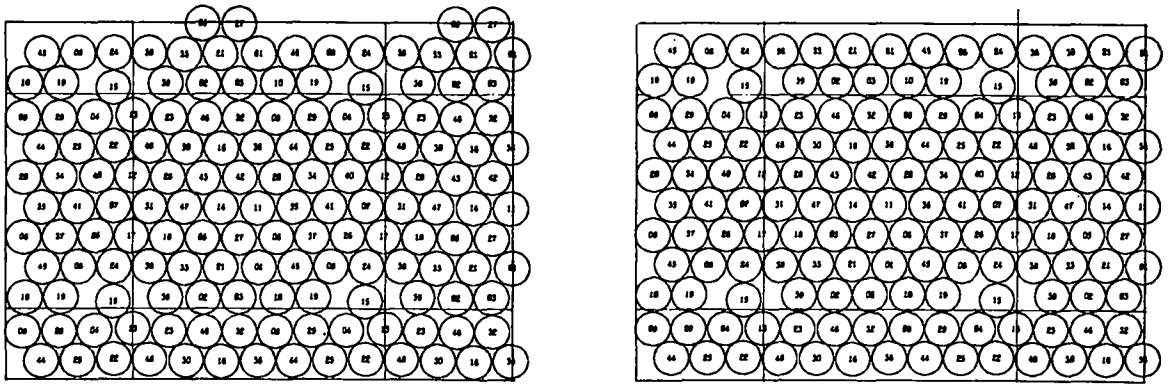

Fig. 6.35 The initial (a) and final (b) configurations of "extended fluid" branch realization B6 at $\tau = 1.074$.

configuration whose six-molecule row we describe, in the notation of the previous subsection, as

$\frac{1}{2}$-hole, 39, 2, 3, 10, 19, $\frac{1}{2}$-hole, $\overline{15}$.

At this density these vacancies appear to be immobile, since after a quite long time (1 900 800 configurations) the last snapshot, Fig. 6.35b, shows the system in a configuration which is almost indistinguishable from the first.

In terms of the Salsburg-Wood analysis discussed in Section 3.3, this suggests that the system is now confined to a region of configuration space associated with a limiting configuration which has developed the extra number of contacts (21 or more) required for stability, in addition to those present in the idealized split-vacancy configuration of Fig. 6.29b. Using Eq. (3.5) we can estimate the reduced area of limiting configuration as $\tau \approx 1.05_2$, which compares not unfavorably with the value 1.056 for the unstable, idealized configuration. In Fig. 6.35b one can see some indication of the extra contacts developing within the horizontal rows, which in the idealized arrangement are not close-packed.

6.3.5 Summary.

From the above discussion of these five realizations which, as shown in Fig. 6.1, establish over the interval $\tau = 1.074$-1.254 an "extended fluid" branch of the equation of state of the 48-molecule system, we see that the underlying geometrical structure is the "7X7"

arrangement first noticed in the "jumpy" realizations for $\tau = 1.3$-1.35 and discussed in Section 6.2. With increasing density the split-vacancy structure of Fig. 6.29b apparently predominates. There appears to be a stable close-packed configuration which has a reduced area $\approx 1.05_2$ and an appearance very similar to Fig. 6.29b, but which has achieved the necessary additional contacts by way of slight deformation.

The term "extended fluid" is, of course, completely inappropriate as a description of states with such a structure, which is clearly of the imperfect-crystal type. The implications of these observations with respect to the over-all behavior of the 48-molecule system will be discussed in Section 6.5. Here we again call attention to the alternative vacancy configurations of Section 6.2.2. The observed behavior at $\tau = 1.074$ makes it likely that one or more of these, particularly the consolidated-vacancy-in-defect-row configuration, corresponds to a region of configuration space which at $\tau = 1.074$ is disconnected (either in the actual sense, or in the sense of a very small transition probability) from the split vacancy region sampled by realization B6. The corresponding reduced pressures are probably not much different. The question could be investigated, as mentioned in Section 6.2.2, by starting from the various configurations of Fig. 6.29a with τ slightly greater than 1.056. This has not been done, since this type of behavior is presumably strongly N-dependent, and since there is clearly some limitation to our interest in the 48-molecule system.

6.4 Realizations Started from the Tetragonal Lattice of Fig. 3.7

As in the case of the 12-molecule system, two realizations were started from the c = 4 configuration of Fig. 3.7, whose close-packed reduced area is 1.116 (Sections 3.4.4 and 3.5).

6.4.1 Realization B12 at $\tau = 1.15$.

The control charts for this realization displayed an initial transient of large $\tilde{G}$ values, which by s = 6 (Δt = 19 200) had decayed. For s = 6-40 the control charts were approximately normal in appearance. The even-numbered snapshots s = 0, 2, 4, and 6 are shown in Fig. 6.36. Note that the control chart transient was associated with a structural change in which the two independent spirals of diagonal lattice lines (see the discussion in Sections 3.4.2 and 3.5) slip along each other until they are approximately nested together on one side and diametrically opposed on the other, with each molecule now having five instead of four close neighbors. This process was essentially complete at s = 6; all subsequent snapshots showed only slight displacement from the latter configuration (no "diffusion").

The observations for s = 6-40 were averaged to obtain the reduced pressure plotted for this realization in Fig. 6.1. Note that it falls about midway between the free-volume curve FV* based on the tetragonal lattice and the locus corresponding to "7X7" structure. This is in

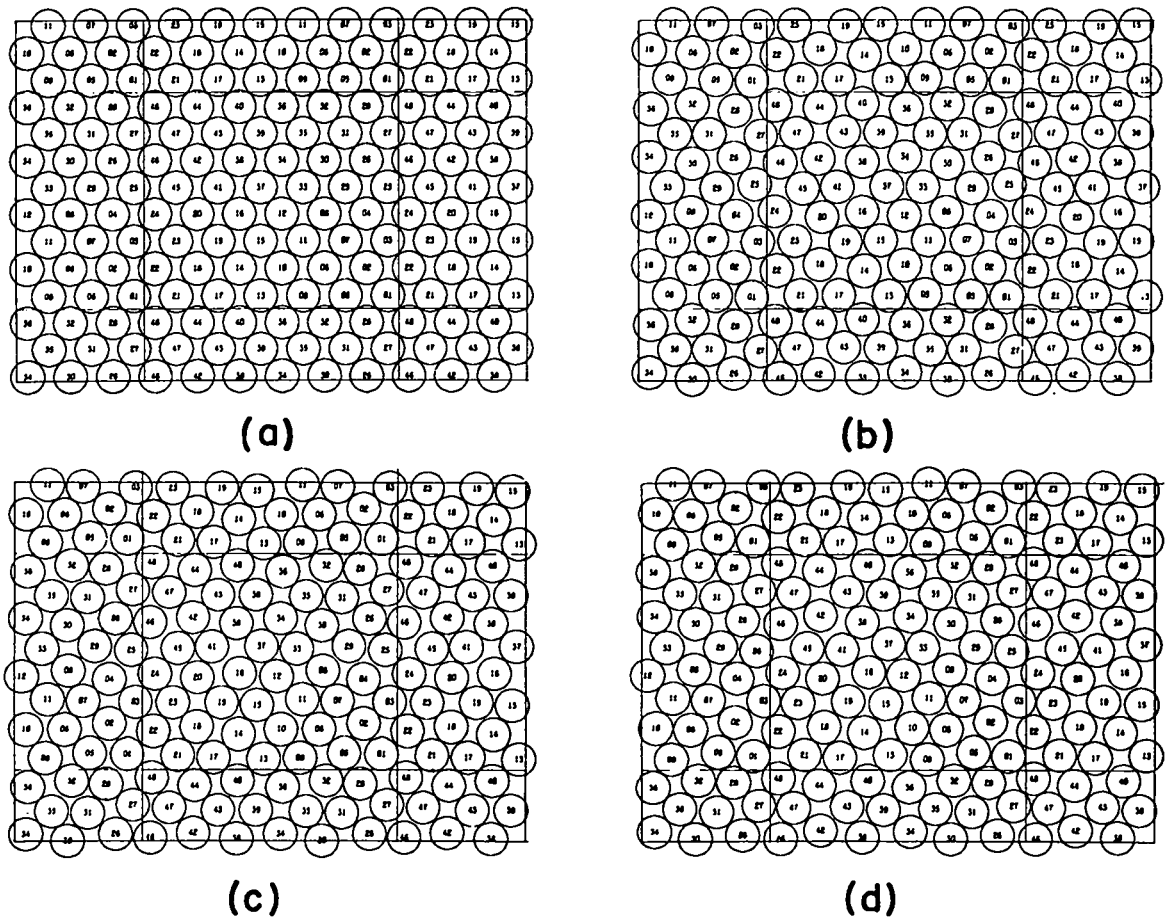

Fig. 6.36 Snapshots s = 0, 2, 4, and 6 (a through d) from realization B12 at $\tau = 1.15$, $\Delta t = 19\ 200$, showing the relaxation from tetragonal to "slipped" structure.

marked contrast to the behavior of the 12-molecule realization at the same density (Section 5.2.4.1), which gave a reduced pressure in approximate agreement with the FV* curve, and in which the tetragonal arrangement was preserved. As discussed in Section 3.4, this can be ascribed to the fact that the smaller system has only one spiral diagonal lattice line.

6.4.2 Realization B15 at $\tau = 1.25$.

This realization also showed a pronounced initial control-chart transient, but the first four snapshots, Fig. 6.37, show a configuration space behavior quite different from that of B12: The system is rearranging to the familiar "7X7" structure. Snapshots 4 to 13 were all of this type, and the realization was not developed further, nor was a reduced pressure calculated, since the result would only duplicate that from realization B16.

For comparison we recall that at this density the 12-molecule system was also unstable in the tetragonal configuration, rearranging to a regular hexagonal structure.

6.4.3 Summary.

These two realizations show that for the 48-molecule system the tetragonal lattice at $\tau = 1.25$ is well connected to the "7X7" states and undoubtedly of no statistical importance. At $\tau = 1.15$ it appears to be disconnected from both the "7X7" and regular hexagonal states, with its

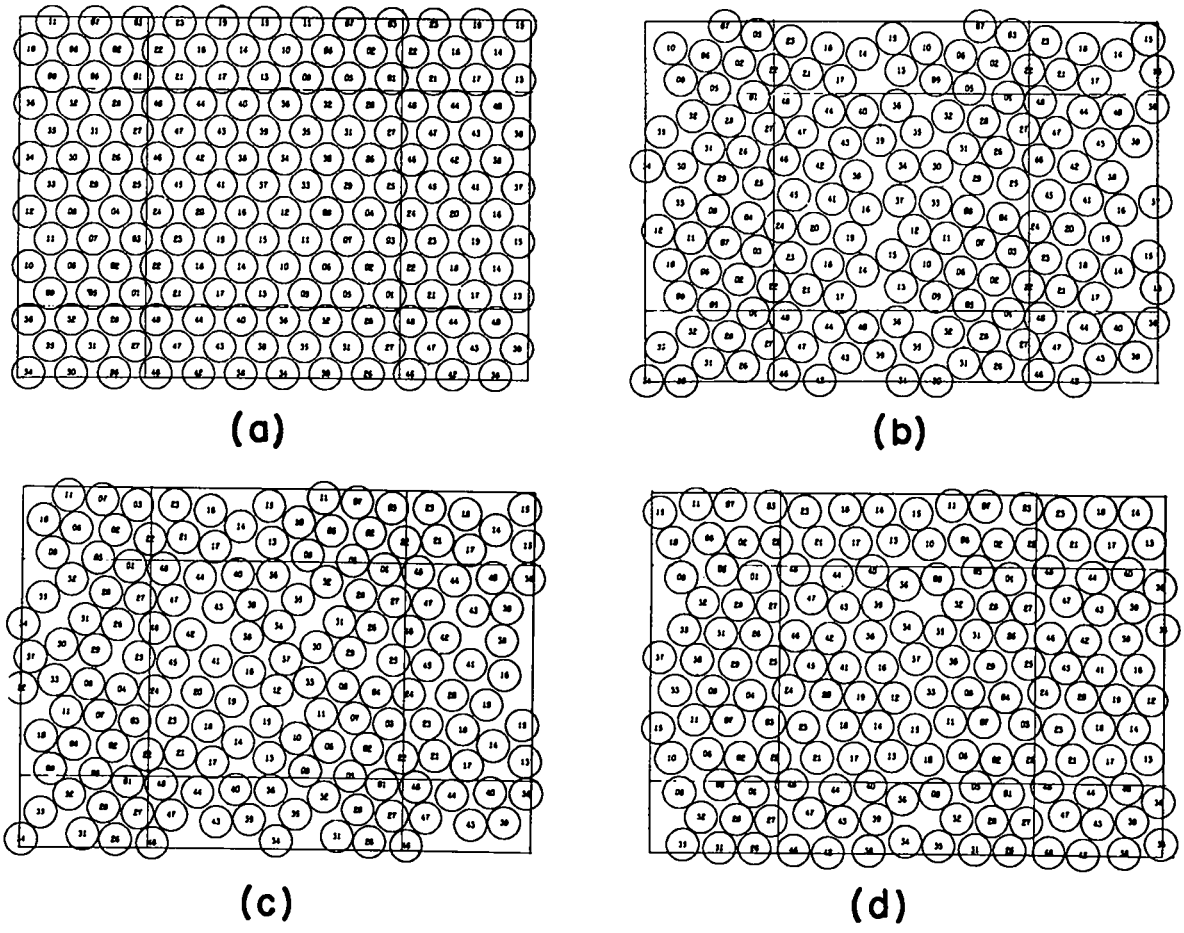

Fig. 6.37 Snapshots s = 0, 1, 2, and 3 (a through d) from realization B15 at $\tau = 1.25$; $\Delta t = 19\ 200$.

own region of configuration space and an equation of state intermediate between FV* (Fig. 6.1) and that of the "7X7" states. At still smaller values of τ, this region of configuration space presumably decomposes into a region associated with the tetragonal lattice (this region disappearing for $\tau < 1.116$) and a larger region associated with a limiting configuration which probably is quite similar to Fig. 6.36d in appearance, and has a limiting reduced area between 1.05 and 1.116.

As mentioned earlier, we believe configurations of this tetragonal type to be of no importance in large systems, and present these calculations mostly as curiosities of interest in connection with the Salsburg-Wood analysis, and as additional evidence, if any be needed, of the peculiarities possible in small periodic systems.

6.5 Summary of the Calculations for the 48-Molecule System

We will summarize our results for the 48-molecule system by following the evolution of the allowed region of configuration space with decreasing density, as deduced from our calculations.

First, however, we make some preliminary remarks in connection with the definition of the term "equation of state" for a small periodic system. We will define the "true" equation of state (i.e., the reduced pressure as a function of reduced area) as being the usual petit ensemble result when averaging is restricted to just those states which are accessible from some specified reference state (e.g., the regular hexagonal lattice).

When all allowable states are mutually accessible, forming a single connected region in configuration space, as will certainly be the case at sufficiently low densities, the "true" equation of state so defined is independent of the reference state. If, however, there are densities for which the allowable states are compartmentalized into two or more disconnected and non-equivalent (by renumbering the molecules) regions, then according to the above definition there is a "true" equation of state for each of these non-equivalent regions.

In so far as the small periodic system is considered as an entity in itself, such a definition is entirely appropriate, leading in either connectivity situation to the usual correspondence (assuming the at least approximate validity of a quasi-ergodic theorem or its equivalent) between the statistical and the dynamical behaviors. It is also, of course, the equation of state to which our Markov chains are convergent, if the initial configuration of the random walk is the reference state of the definition, or is accessible from it.

It should be noted, however, that this "true" equation of state, even with a fixed reference state, may easily have jump discontinuities in its density dependence. Such a discontinuity will appear at a reduced area τ_d at which connections first appear between two non-equivalent regions of configuration space with comparable and non-negligible $2(N - 1)$-dimensional volumes. One of the regions is assumed to contain the reference state in question, and we suppose that for $\tau < \tau_d$ the connection disappears, while for $\tau > \tau_d$ it is present, presumably widening with increasing τ. The "true" equation of state then evidently

jumps at $\tau = \tau_d$ from a value intermediate between the reduced pressures of each region averaged separately to that of whichever region contains the reference point (see Fig. 6.38).

One could remove the discontinuity, obtaining a smooth extension of curve AB to higher densities (see figure), by defining the "true" equation of state to be that obtained by averaging over all allowable states regardless of their accessibility. In so doing one would lose the correspondence with the behavior of a dynamical system, as well as the convergence of the present random-walk Monte Carlo method. Nevertheless one might be tempted to believe that the result would be a better approximation to the behavior of large systems. The assumption here would be that with increasing N the qualitative properties of the two regions remain more or less unchanged, the principal effect of larger N being to supply connections at $\tau < \tau_d$. This may well be the case, since large values of N certainly do lead to increased connectivity; see for example the Salsburg-Wood[18] discussion, where it is just this phenomenon which renders questionable the usefulness of Eq. (3.5) for large N. However, our present limited experience indicates that the qualitative character (even the existence!) of one or more of the regions is likely to depend even more profoundly on N, so that this question, as indeed the entire subject of the behavior of larger systems, is really one for subsequent investigation rather than one which the present investigation can answer. Thus, we will retain our first definition of the "true" equation of state.

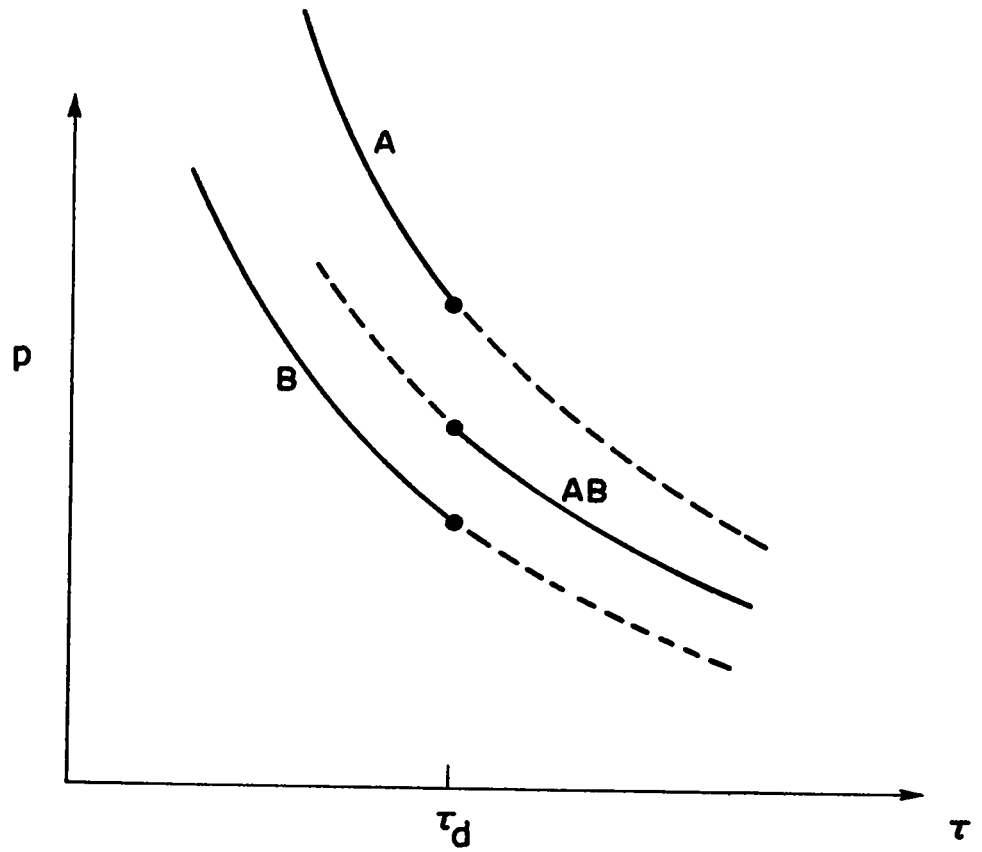

Fig. 6.38 Jump discontinuities in the "true" equations of state (curves A and AB, or B and AB, depending on whether the reference state is in region A or B) of a small finite system in which the two regions are disconnected for $\tau < \tau_d$.

As we remarked above, the present Monte Carlo method is indeed in theory always convergent to the "true" equation of state corresponding to its initial configuration. However, as our calculations for the 48-molecule system abundantly illustrate, the convergence is necessarily very poor at densities where the corresponding region of accessible states is almost compartmentalized, consisting of two or more pockets which are indeed interconnected, but by connections of very small $2(N - 1)$-dimensional volume compared to the volumes of the pockets themselves. As has already been seen in the case of the "jumpy" realizations at $\tau = 1.3$-1.35 (Section 6.1.2), and as will be further discussed below, our calculations indicate that such is indeed the situation with the 48-molecule system over a wide range of reduced areas. For such densities, then, we are unable to estimate effectively the "true" equation of state of the system. Instead we can estimate, by the partial or "plateau" averaging techniques which have been repeatedly mentioned, the extensions to $\tau > \tau_d$ of the two or more "true" equations of state for $\tau < \tau_d$ (dashed curves of Fig. 6.38). This will be the only possibility until a density is reached at which the connections are relatively large and the "true" equation of state (curve AB) can be estimated. It is important to note that not only is the AB curve unknown over this range of densities, but also the value of τ_d itself is not in general known a priori, and so must be inferred from the observations. As we will see, the latter cannot usually be done with any satisfactory precision at all.

Finally, we mention that the behavior just discussed differs somewhat from that discussed in Section 1.2.2 as a mechanism for the production

of a "van der Waals loop". In the latter we supposed that the relative 2(N - 1)-dimensional volumes of the two regions changed very rapidly with density while remaining connected. In the present case we considered the situation where the relative volumes remain comparable and their connection disappears. One can, of course, imagine a situation in which both a discontinuity and a loop would be present.

6.5.1 $\tau = 1.0$ to 1.05.

At $\tau = 1$, the allowable region of $2(N - 1) = 94$ dimensional configuration space reduced to the $47!$ isolated points corresponding to the various permutations of molecule numbers. Its volume is, of course, zero, and the pressure infinite.

At τ slightly greater than one, each of these points becomes a region of accessible states, which will clearly be of the regular hexagonal (L) type. If τ is not too large these $47!$ pockets will be disconnected from each other. In Section 3.5 we calculated that some of these pockets are certainly connected at $\tau > 1.063$, by paths corresponding to columnar rotations around the torus. This may, in fact, be the smallest τ at which any L-L connection appears. If so, it is interesting that before these occur, there appear allowable regions of the "7X7" type, which in Section 6.2 we saw to be present at $\tau = 1.056$, and even at very slightly smaller values.

However, in the interval $\tau = 1.0$ to 1.05 presently under discussion we will assume, as is consistent with our observations and a priori

calculations, that the allowable region consists solely of the 47! disconnected L pockets, all of which are of course equivalent. Thus, in this density range the Monte Carlo method is convergent to the unique "true" equation of state, and the latter in turn, according to the Salsburg-Wood theory, is asymptotically, as $\tau \to 1$ and neglecting $O(N^{-1})$ terms, convergent to the free volume Eq. (3.6) with $\tau^* = 1$. A quantitative comparison has been postponed to Chapter 10, but we have already noticed (Section 6.1.1) that realizations B1 through B5 at $\tau = 1.025$ and 1.04 are indeed in qualitative agreement with the free volume equation of state. This is perhaps best regarded as evidence of the over-all reliability of the calculator programs involved in these calculations.

The question as to whether these results (at $\tau = 1.025$ and 1.04) approximate, with neglect of terms of $O(N^{-1})$, the equation of state of larger systems at the same reduced areas is essentially the same as the fundamental question of whether the Salsburg-Wood derivation of Eq. (3.5) can somehow be extended so as to be valid in the presence of the L-L connections which will exist for $\tau \to 1$ as $N \to \infty$. Here we refer the reader to the Salsburg-Wood discussion itself,[18] as well as to related comments on the 12-molecule results in Sections 5.2.3, 5.2.5, and 5.3, and to subsequent remarks with respect to the 48-molecule system.

6.5.2 $\tau = 1.05$ to 1.1.

As mentioned in the previous subsection, at a value of τ known to be less than 1.056 but probably only very slightly less, the estimated

value being 1.05_2 (Section 6.3.4), pockets of "7X7" ("H") states appear. As far as is known, these "7X7" pockets and the regular hexagonal ("L") pockets are the only allowable regions of configuration space, aside from certain connections to be discussed below, in the interval $\tau = 1.05\text{-}1.10$. As was mentioned in Section 6.5.1, at $\tau > 1.063$ some L-L connections between the regular hexagonal pockets are known to exist. However, it will be recalled (Section 6.1.2.1) that not until $\tau = 1.30$ was the system actually observed to traverse a L-L connection. We may thus safely infer that these connections are very constricted indeed at $\tau < 1.10$. However, this behavior is also a convenient warning that it is not safe to infer the absence of connections of any particular type from a failure to observe traversals between the corresponding pocket of states.

Thus, although realization B6 at $\tau = 1.074$ (Section 6.3.4) exhibited no excursions between different "7X7" pockets, neither with respect to permutations of the molecules nor with respect to different half-vacancy configurations, it would be rash to assert that at this density the "7X7" pockets are disconnected from each other. Presumably such will be the case at some reduced area above $\tau \approx 1.05_2$.

Similar remarks apply also with respect to the existence of connections between the "7X7" and the regular hexagonal pockets. No traversal between these two regions was observed in the present density interval. Indeed, as will be seen in Section 6.5.3.2, the smallest reduced area at which such L-H connections are known to be present is 1.25. They may well be present at smaller reduced areas, the exact point of their

appearance being unknown in the interval τ = 1.05-1.25.

Thus, we can not be certain whether our quite precise equation of state results from realization B6 in the "7X7" region at τ = 1.074 and from realizations B7 and B8 in the L region at τ = 1.075 are accurate estimates of two different "true" equations of state, or are only partial averages over pockets which are actually connected. In the latter case one might suppose the regular hexagonal pockets to have the larger 94-dimensional volume at τ = 1.074-1.075, since this density is only slightly lower than that at which the "7X7" pockets contract to zero volume. If so, the L branch of the equation of state would approximate the "true" equation of state.

This uncertainity with regard to the significance of the two main branches of our equation of state results (Fig. 6.1) will be present from τ = 1.05 to 1.25. Moreover, since the significance of the "7X7" structure in larger systems is an open question, the present calculations provided little information about the equation of state of such systems. We would, of course, be rather surprised if for τ = 1.05-1.1 it was not close to the L branch of Fig. 6.1.

6.5.3 τ = 1.1 - 1.25.

In this section we will mention the additional topological features of configuration space which accompany the L (regular-hexagonal) and H ("7X7") pockets, keeping in mind the remarks of the last section with respect to uncertain significance of the two main branches of the

equation of state over the interval τ = 1.05-1.25.

6.5.3.1 τ = 1.1 - 1.15.

In this interval two new pockets appear in configuration space, namely, one associated with the tetragonal lattice of Fig. 3.7, and one associated with the related but more stable configuration which developed from this tetragonal lattice during realization B12 at τ = 1.15 (Section 6.4.1 and Fig 6.36). We will call this second pocket the "slipped tetragonal pocket", and the first-mentioned one the "tetragonal pocket". The latter is surmised to exist as an entity disconnected from the slipped tetragonal pocket (and also from the L and H pockets) over a small interval of reduced area whose lower end point is its close-packed value τ = 1.116. As realization B12 demonstrates, at τ = 1.15 these two pockets are certainly connected, the behavior suggesting that the connection is comparable in volume to the tetragonal pocket. The reduced pressure obtained from the realization (Table 6.1), in conjunction with the Salsburg-Wood theory, suggests that the slipped tetragonal pocket may have a limiting configuration with $\tau \approx 1.10$.

At τ = 1.15 we do not know whether or not the combined tetragonal - slipped tetragonal pockets are connected to either the L or H pockets.

As has been emphasized repeatedly, both of these regions are artifacts of the 48-molecule system, in the sense that we are quite certain that they are of no importance in large systems, as contrasted with the "7x7" states about whose significance in larger systems we are uncertain.

Finally, we recall that realizations B9 and B10 at $\tau = 1.124$ demonstrate that at that density the various "7X7" pockets are connected with each other.

6.5.3.2 $\tau = 1.15 - 1.25$.

At the lower reduced areas of this interval our 48-molecule system appears to have three well-defined types of pockets, viz. the L, H, and slipped tetragonal pockets. At $\tau = 1.25$, realization B15 (Section 6.4.2) demonstrates that the slipped tetragonal region is connected to the "7X7" region, the behavior suggesting that the former pocket is no longer very well defined.

More interestingly, comparison with the 12-molecule realization A6 (Section 5.2.4.1) at the same density permits us to deduce the existence in the 48-molecule system of L-H connections which at this density have not been directly observed. The argument is as follows: The 12-molecule system relaxed to L-type states, while the 48-molecule system relaxed to the H-type ("7X7") states, both starting from the tetragonal lattice of Fig. 3.7. Now any allowable state of the 12-molecule system corresponds to the essentially identical and allowable 48-molecule state obtained by a 2X2 array of the 12-molecule configuration. Therefore, the 48-molecule system could have relaxed to the L pocket, by simply following the sequence of 12-molecule states realized in A6. Thus, the 48-molecule combined tetragonal - slipped tetragonal pocket is connected at $\tau = 1.25$ to both the L and H pocket systems, so that the latter are themselves

connected, at least by the way of the probably poorly defined tetragonal pockets.

As remarked earlier, L-L connections are known to be present, though not observed, while realizations B13 and B16 show the presence of fairly frequently traversed H-H connections.

6.5.4 $\tau = 1.25$ to 1.30.

As discussed in the previous section, at $\tau = 1.25$ configuration space appears to consist principally of L (regular hexagonal) and H ("7X7") regions which are known to be connected. Thus, for $\tau = 1.25$ to 1.375, where the L-H connections begin to become large enough for the random walk to estimate the over-all "true" average, the two branches of our equation of state definitely correspond to extensions to lower density of different "true" high density equations of state (Fig. 6.38).

At $\tau = 1.30$ we first observed directly the L-H connections, by virtue of the "jumpy" behavior of realization B19 (Section 6.1.2.1). At the same time there also appear the type of states which we described as "irregular". These have not been observed at higher densities, except possibly for the transient states during the relaxation of realization B15 at $\tau = 1.25$ (Section 6.4.2) from the tetragonal lattice to "7X7" states. As described in Sections 6.1.2 and 6.1.3, irregular states become increasingly prominant at lower densities. Their fate at $\tau < 1.3$ constitutes one of the most important questions left unanswered by the present investigation. As mentioned in Section 6.1.2, there are some

indications that these states may actually be connecting states between the L (regular hexagonal) and H ("7X7") pockets. In this case they probably indeed effectively disappear at $\tau < 1.30$, as the L-H connections contract and apparently become negligibly small in comparison with the L and H pockets themselves. See however, the qualifications discussed in Section 5.2.3 (particularly Fig. 5.6), which apply as well to the 48-molecule system. The question could be investigated to some extent by means of a number of compression experiments starting from irregular configurations obtained at $\tau \geq 1.3$. This has not been done, mostly owing to our desire to terminate this long drawn out investigation of the 48-molecule system.

6.5.5 $\tau > 1.3$

As discussed in detail in Section 6.1.2.8, in the interval $\tau = 1.3$-1.35, configuration space appears to consist of regular hexagonal (L) pockets, "7X7" (H) pockets, and irregular states. The irregular states possibly constitute the L-H connection, and in any case are numerous enough to have appreciable statistical weight. Whatever the nature of the L-H connection, however, it is still too constricted to allow the "true" equation of state to be determined, although at $\tau = 1.35$ it seems likely that it will be in the vicinity of the H or "fluid" branch (Figs. 6.1 and 6.2).

At $\tau \geq 1.375$, as described in Section 6.1.3, we believe that our realizations estimate the "true" or over-all equation of state of the

48-molecule system. As Table 3.1 shows, for these densities the virial coefficient up to and including the coefficient of τ^{-6} in the expansion of the compressibility factor pV/NkT will have their "normal" N-dependence according to the analysis of Lebowitz and Percus.[17] However, as we shall see in Chapter 10, from $\tau = 1.375$ to at least 1.5, terms of $O(\tau^{-6})$ and beyond probably make appreciable contributions to the compressibility factor, so that only perhaps beyond $\tau = 1.5$ can we be reasonably certain that the 48-molecule results estimate the thermodynamic equation of state within a few per cent.

6.5.6 Final remarks and comparison with Alder and Wainwright's 870-molecule dynamical results.

It is quite clear that the above-described Monte Carlo results for the 48-molecule system are such as to prevent one from drawing any conclusion whatever with respect to the presence or absence of a first-order, fluid-crystalline phase transition. At $\tau = 1.35$ the frequently occurring "irregular" states, whose contributions are included in the "H" or "fluid" branch of the equation of state for $\tau > 1.3$ in Figs. 6.1 and 6.2, are suggestive of a fluid phase, but by $\tau = 1.30$ the "7X7" or vacancy-defect structures are predominant on this branch of the equation of state, whose statistical weight relative to the "crystalline" or "L" branch can no longer even be guessed.

Thus, it is clear that if the existence of a hard-circle phase transition is to be further investigated by the present numerical technique, larger systems will have to be employed. As mentioned in

Chapter 1, Alder and Wainwright have already investigated a system of 870 hard circles. In Fig. 6.39 we compare their results for this large system, as well as their results for a system of 72 molecules, with our 48-molecule points from Fig. 6.2. There is rough agreement between the two small-system points, the 48-molecule Monte Carlo points tending to lie somewhat below the 72-molecule dynamical points, but the principal point of interest is of course the van der Waals loop in the 870-molecule system. It is noteworthy that it lies nicely between the L and H curves for the smaller systems, the solid terminus of the horizontal tie line being approximately on the L curve, its fluid terminus on the H curve. It would be interesting to know if any analogue of the 48-molecule, "7X7" or vacancy-defect structure appears in the large system.

In the near future we hope to investigate a similarly large system by the Monte Carlo method.

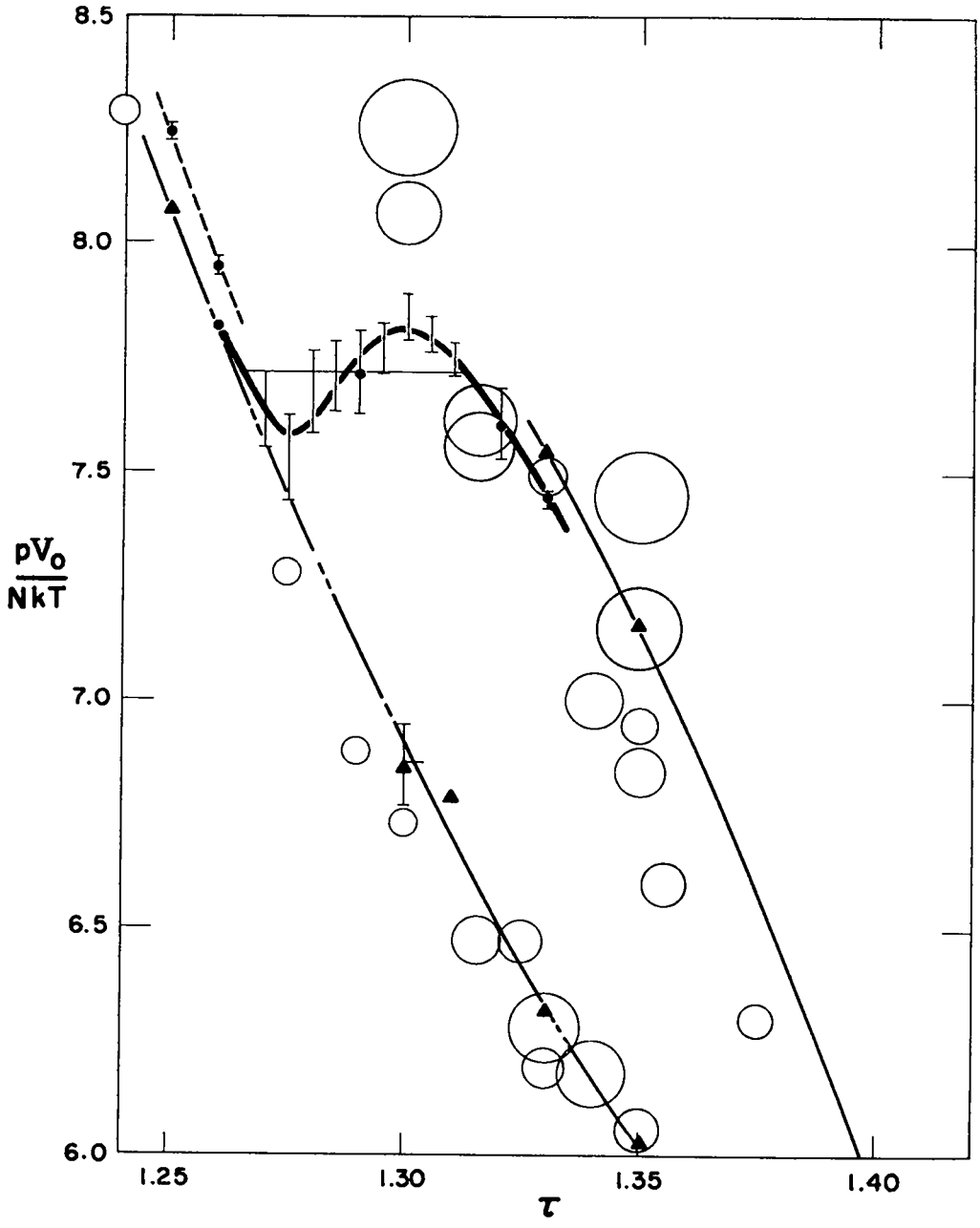

Fig. 6.39 Comparison of the 48-molecule Monte Carlo results (o) with the 72 (Δ) and 870 (bars) molecule dynamical results.[15] The figure is adapted, except for the Monte Carlo points, from Ref. 15. The heavy curve and tie line are Alder and Wainwright's[15] phase transition interpretation of their data, the light curves their L and H (in our terminology) branches for the 72-molecule system. Their dashed curve indicates a branch of the 870-molecule equation of state corresponding to a "glassy" region of configuration space.

Chapter 7

OUTLINE OF THE DATA REDUCTION PROBLEM

The remaining chapters of this report will be mainly devoted to a description of the statistical techniques which we have used to reduce our "experimental observations" to the equation of state estimates already given in Tables 5.1 and 6.1. Here we will outline the over-all data reduction process, reserving detailed discussion of the various steps for Chapters 8 and 9.

7.1 The "Experimental Observations"

It is convenient to regard a single realization of a particular Markov chain for a given molecular system as constituting a single "experiment." The parameters which define a particular Markov chain, as well as those which determine a particular pseudostochastic realization of such a chain, were discussed in Sections 2.3.2 and 2.3.3.

The "experimental observations" are then the set of values $\tilde{G}(s, \alpha)$, $s = 1(1)n$, $\alpha = 1(1)K$, of the time-smoothed or coarse-grained cumulative pair distribution function, as defined in Section 2.3.4. The parameters K and Δr^2 determine the spatial range and spatial resolution of these

observations; the parameter Δt (time-smoothing interval, see Section 2.3.4) determines the time-resolution of the observations; and the parameter n reflects the duration of the random walk or Markov chain realization constituting the experiment.

The n values $\bar{G}(s, \alpha)$ for each α are of course ultimately averaged, according to Eq. (2.14), to obtain the over-all estimate $\overline{G}_{n\Delta t}(\zeta_\alpha)$ of $G(\zeta_\alpha)$, the theoretical or "true" cumulative pair-distribution function of the system at $\zeta = \zeta_\alpha = \sqrt{\sigma^2 + \alpha\Delta r^2}$. However, it is not these quantities which we wish to estimate, but rather the derivative $G'(\sigma)$ from which the compressibility factor of the system is obtained by Eq. (2.6). Our basic data reduction problem is thus that of numerically differentiating the observed averages $\overline{G}_{n\Delta t}(\alpha)$. This leads us to inquire as to the sampling distribution of these quantities.

7.2 The Central Limit Theorem for Markov Chains

The quantity $\overline{G}_{n\Delta t}(\zeta_\alpha)$, which henceforth we will write as $\overline{G}_{n\Delta t}(\alpha)$, is the average value of the state function $G(\zeta_\alpha)$ over $n\Delta t$ consecutive states of a particular stochastic realization of a Markov chain. According to the central limit theorem for ergodic Markov chains,[21] such an average has a sampling distribution which is asymptotically (i.e., as $n\Delta t \to \infty$) independent of the initial ($t = 0$) state of the system, and which is asymptotically normal with a mean equal to the theoretical value $G(\zeta_\alpha)$ and a variance $D^2\left[\overline{G}_{n\Delta t}(\alpha)\right]$ which decreases as $(n\Delta t)^{-1}$:

$$D^2\left[\overline{G}_{n\Delta t}(\alpha)\right] = \tilde{\sigma}_\alpha^2/n\Delta t \quad . \tag{7.1}$$

No simple expression is known for the multiplicative factor $\tilde{\sigma}_\alpha^2$, which must be non-zero in order for asymptotic normality to hold.[21]

Considering the set of values $\overline{G}_{n\Delta t}(\alpha)$, $\alpha = 1(1)K$, as a vector stochastic variable, its sampling distribution[22] is asymptotically multivariate-normal with the mean vector $G(\zeta_\alpha)$, $\alpha = 1(1)K$, and a covariance matrix which decreases as $(n\Delta t)^{-1}$.

7.3 Testing for Approximate Normality and Time-Independence

The central limit theorem outlined in the previous section shows that if $t = n\Delta t$ is "large enough" then the values $\overline{G}_t(\alpha)$, $\alpha = 1(1)K$, from a given experiment will be approximately multivariate-normally distributed, so that the usual methods of applied statistics become available (though not, as we shall see, without certain difficulties) for the estimation of the equation of state. We know of no way of selecting an a priori "large enough" value of t, so that it seemed to us worthwhile to devote some effort to an empirical statistical investigation of this question. (The behavior of the "jumpy" realizations described in Section 6.1.2 was adequate warning that under some conditions, at least, even very large values were by no means adequate.)

This phase of the data analysis requires then, in the terminology of Chapter 2, values of $\overline{G}_t(\alpha)$ from a number of independent realizations of a given Markov chain, each realization being of length t. We wish to test the "null hypothesis" that they are each an independent sample

from a normal distribution with unknown mean $G(\zeta_\alpha)$ and unknown variance $\sigma^2(\alpha)$. As discussed in Section 2.3.3, different realizations of a given chain can be obtained by varying the random number sequence or the initial configuration. Such realizations will be statistically independent, however, only if t is again "large enough".

The simplest procedure, then, appears to be to decompose a given realization of length $n\Delta t$ into a number n' of shorter "sub-realizations" of equal length, and apply standard statistical tests for "time-independence" of the resulting n' values $\overline{G}_{\frac{n\Delta t}{n'}}(\alpha)$. If these tests are satisfactory, the values are then tested for approximate normality. Both types of tests will be described in detail in Chapter 8. Here we should perhaps mention that in practice the tests for time-independence and normality of distribution are not independent of each other (i.e., some of the more convenient tests of the null hypothesis of time-independence assume a normal sampling distribution as well); nor are either of these tests completely independent of the presence of the spatial correlations to be mentioned in the following section.

The statistical tests for absence of time-correlation and normality of distribution are, of course, more powerful the larger the number n' of supposedly independent samples. This naturally suggests trying $n' = n$, that is, taking the largest number of time-smoothed observations available from the magnetic tape output of the main Monte Carlo code. Thus, we begin with the null hypothesis that the value Δt (in most cases, 19 200) is "large enough" according to the central limit theorem, for the

observations $\tilde{G}(s, \alpha)$ (see Eq. 2.13) to be approximately s-independent and normally distributed. This is manifestly not the case for some of our experiments (the "jumpy" realizations), and in Chapter 8 we will see that the quantitative tests show this null hypothesis to be untenable in other, less obvious, cases as well.

7.4 Spatial Correlation and Transformation of the Observed Data

The numerical differentiation required to obtain the equation of state will be done, naturally, by least squares techniques, which will be described in preliminary fashion in the next section. The appropriate type of least squares technique, however, depends upon whether or not the observations $\overline{G}_{n\Delta t}(\alpha)$, assumed to be sampled from a normal distribution, are correlated for different values of $\alpha = 1(1)K$. If such spatial correlation is present, that is, if the covariance matrix of the theoretical sampling distribution is non-diagonal, then a somewhat more complicated than usual least squares procedure should be used (see Chapter 9). Alternatively, one can attempt to remove or reduce the spatial correlation by an appropriate transformation of the observations.

Both a visual inspection of the control charts, examples of which have been given in Chapters 5 and 6, and quantitative statistical tests for spatial correlation (to be discussed in Chapter 8) show that indeed the $\tilde{G}(s, \alpha)$ values are strongly α-correlated throughout the density range of our calculations. On physical grounds it seemed likely that

transformation to the "shell populations"

$$Y_{s\alpha} = \tilde{G}(s, \alpha) - \tilde{G}(s, \alpha - 1),$$
$$\tilde{G}(s, 0) \equiv 0 , \tag{7.2}$$

would lead to a considerable reduction in the apparent α-correlation, as indeed turns out to be the case (Chapter 8). The variables $Y_{s\alpha}$, being linear combinations of the variables $G(s, \alpha)$, are of course normally distributed and time-independent if the latter are.

In addition to simplifying the numerical differentiation procedures, the transformation is also helpful in the statistical tests for time-independence and normality, in the following way. Suppose that some test of the hypothesis of time-independence, say, is applied to each of the K sets of observations $\left\{Y_{s\alpha},\ s = 1(1)n\right\}$, so that we obtain a test statistic T_α for each set $\alpha = 1(1)K$. If the $Y_{s\alpha}$ are α-uncorrelated, then the K statistics T_α are independent of each other. This simplifies the interpretation of the test, since we do not know of a convenient test for time-independence within a sequence of vector stochastic variables with correlated components.

Accordingly, throughout our statistical analysis we will take as the fundamental observational variables the set $Y_{s\alpha}$, rather than the set $\tilde{G}(s, \alpha)$. The corresponding "theoretical" or "true" shell population, to which the observations $Y_{s\alpha}$ converge stochastically, independently of s, as $\Delta t \to \infty$, will be denoted by

$$\eta_\alpha = G(\zeta_\alpha) - G(\zeta_{\alpha-1}) \quad . \tag{7.3}$$

In addition to their indicated dependence on the index α, and on the

system parameters such as N, τ, etc., the variables η_α depend upon the observational parameter Δr^2.

7.5 Numerical Differentiation by Least Squares Regression Analysis

In order to use Eq. (2.6) to estimate the compressibility factor, we must estimate the derivative $G'(\sigma)$ by numerical differentiation of the observations. The usual procedure envisages that the functional dependence of $G(\zeta)$ on ζ is known, except for certain coefficients which appear linearly in $G(\zeta)$. These coefficients, along with their respective variances, would then be estimated by least squares regression of the observations $\tilde{G}(s, \alpha)$ onto the known functional form. Substitution of these estimated coefficients into the analytical expression for $G'(\sigma)$ [obtained, of course, by differentiating the given functional form of $G(\zeta)$] then yields the desired estimate of the derivative, as well as an estimate of its variance.

In the present case the dependence of $G(\zeta)$ on ζ is, of course, not known. Since $K\Delta r^2$ is always chosen to be small compared to σ^2, it seems reasonable to assume that in the interval $\sigma^2 \leq \zeta^2 \leq \sigma^2 + K\Delta r^2$, $G(\zeta)$ has a convergent power series expansion in $\zeta^2 - \sigma^2$, which can be truncated after some small number of terms with an error which is small, or at least not large, compared to the statistical scatter of the observations. In other words, our regression procedure will be based upon the hypothesis that $G(\zeta)$ is adequately represented by a polynomial of unknown degree

$\nu + 1$ in $\zeta^2 - \sigma^2$. (Note that the value of ν will itself depend on the experimental data: the smaller the statistical spread of the data, other things being equal, the larger will be the necessary value of ν.) Using Eq. (2.12) this assumption can be written

$$G(\zeta_\alpha) = \sum_{i=1}^{\nu+1} \gamma_i \alpha^i \quad , \tag{7.4}$$

the coefficients γ_i being unknown.

Introducing the statistically more convenient shell populations by use of Eq. (7.2), an equivalent assumption is that

$$\eta_\alpha = \sum_{i=0}^{\nu} \beta_i \alpha^i \quad . \tag{7.5}$$

The relations between the two sets of coefficients are readily found to be

$$\gamma_i = \frac{1}{i}\beta_{i-1} + \frac{1}{2}\beta_i + \sum_{j=1}^{J(\nu,i)} \frac{(-1)^{j+1}(i - 1 + 2j)!}{(2j)!\, i!} B_j \beta_{i-1+2j}, \tag{7.6}$$

where $J(\nu,i)$ denotes the integer part of $\frac{1}{2}(\nu + 1 - i)$, and B_j is the j^{th} Bernoulli number.[23] The summation is to be omitted if $J(\nu,i) = 0$, and the term $\frac{1}{2}\beta_i$ is to be omitted when $i = \nu + 1$.

The derivative $G'(\sigma)$ is given by

$$G'(\sigma) = 2\sigma\gamma_1 \Delta r^2 \quad , \tag{7.7}$$

so that Eq. (2.6) becomes

$$\frac{pV}{NkT} = 1 + \frac{\gamma_1 \sigma^2}{2\Delta r^2} \quad . \tag{7.8}$$

The regression analysis accordingly proceeds as follows. The value of ν and the corresponding coefficients β_i are estimated by least squares techniques. A corresponding estimate of γ_1 is then calculated from Eq. (7.6), and finally the compressibility factor is calculated from Eq. (7.8).

The most important difficulty in the above program is, as will be seen, the necessity of determining the degree ν of the regression polynomial from the data. In addition the choice of the appropriate least squares technique (see Chapter 9) requires information about the unknown covariance matrix of the sampling distribution of the observations $Y_{s\alpha}$, which also can only be obtained from the observations themselves.

Chapter 8

TESTS OF DISTRIBUTION

This chapter is devoted to a description of the statistical tests which we carried out prior to the least squares reduction of the data. As outlined in the previous chapter we are concerned here with the credibility of the "null hypothesis" that the observations $Y_{s\alpha}$ are random (i.e., s-independent), spatially-uncorrelated (i.e., α-independent) samples from a normal distribution (of unknown mean vector and unknown, but diagonal, covariance matrix). We will, for the sake of brevity and precision call this "hypothesis A".

8.1 Control Charts

The simple process of inspection of control charts such as were presented in Chapters 5 and 6, in which $\bar{G}(s, \alpha)$, or $Y_{s\alpha}$, is plotted against s for one or more values of α, constitutes a crude statistical test of hypothesis A, especially the assumption of time-independence.

For example, the control charts of Fig. 6.3, for the 48-molecule realization B19 at $\tau = 1.3$, are sufficient to show the hypothesis to be

untenable. Our only reason for applying more quantitative statistical tests to such jumpy realizations (Section 6.1.2) was to gain experience with their performance in such obviously ill-behaved situations in order the better to interpret their results in more borderline cases.

8.2 Testing the Assumption of Time-Independence

Of the available tests for s-independence of a sequence of observations $Y_{s\alpha}$, $s = 1(1)n$, for given α, we chose two: the number of runs above and below the sample median,[24] and the mean-square successive-difference ratio test of von Neumann.[25] The runs test has the advantage of an exactly known distribution which is independent of the distribution of the samples (providing of course that they are really random). It seems especially appropriate in view of the abrupt "jumps" or shifts in level which characterize some of our experiments.

The mean-square successive-difference ratio test is simple to apply, and the distribution of the test statistic is known approximately when the sampling distribution of the observations $Y_{s\alpha}$ is normal. It seems to be one of the most widely used tests of randomness.

8.2.1 The runs test.

We followed essentially the procedure of Ref. 24, concentrating mostly on the total number $R^{(\alpha)}$ of runs above and below the sample median, but examining also the numbers $R_k^{(\alpha)}$ of runs of length k for $k > 5$, for each set of shell population observations $Y_{s\alpha}$. For convenience in interpreting the results, we extended Olmstead's tables[26] of the

probabilities $P_a(k; n) = P_b(k; n)$, $P_{a+b}(k; n)$, and $P_{a \cdot b}(k; n)$ of observing one or more runs of a specified side, on either side $(a + b)$, and on both sides $(a \cdot b)$ of the median, of length k or greater in a series of n independent observations, up to $n = 200$, and up to $k = k^*(n)$ such that $P_{a+b}[k^*(n); n] < 10^{-5}$. We also tabulated the cumulative distribution $P(R^*; n)$, giving the probability of observing a total number of runs $R \leq R^*$ in a sequence of $n \leq 200$ independent observations. This was done simply as a matter of convenience; the distribution $P(R^*; n)$ is very nearly normal for $n \geq 20$.[24]

Table 8.1 shows the application of the runs test to the observed shell populations $Y_{s\alpha}$ of realization B34, with $s = 2(1)50$, $\alpha = 1(1)8$. Note that in this realization the first time-smoothed observation $(s = 1)$ was omitted from the statistical analysis; for most realizations it was included, but in some of the earlier experiments it was omitted. Note also that following the procedures of Ref. 24, the sample median is omitted when the number of observations is odd, so that in the runs test n is always even. Finally, we mention at this point that throughout our statistical analysis we will use the notations $E(x)$, $D^2(x) = E(x^2) - E^2(x)$, and $D(x) = \sqrt{D^2(x)}$ for the expected value (i.e., the theoretical mean), the theoretical variance, and the theoretical standard deviation of a stochastic variable x. From Hald[24] we have

$$E(R) = \tfrac{1}{2}(n + 2) \quad , \qquad D^2(R) = \frac{n(n - 2)}{4(n - 1)} \quad , \tag{8.1}$$

TABLE 8.1 RUNS TEST FOR REALIZATION B34

$s = 2(1)50; \qquad n = 48; \qquad K = 8$

$E(R) = 25$

$D^2(R) = 11.75; \qquad D(R) = 3.43$

Shell α	Observed Total Number of Runs $R^{(\alpha)}$
1	29
2	25
3	29
4	25
5	29
6	20
7	26
8	22

$$\overline{R} = \frac{1}{K}\sum_{\alpha=1}^{K} R^{(\alpha)} = 25.625$$

$$s^2 = \frac{1}{K}\sum_{\alpha=1}^{K}\left[R^{(\alpha)} - E(R)\right]^2 = 10.375$$

$$\chi^2(K = 8) = \frac{Ks^2}{D^2(R)} = 7.06; \qquad 0.50 \le P(\chi^2) \le 0.60$$

$$u = \frac{[\overline{R} - E(R)]n^{\frac{1}{2}}}{D(R)} = 0.52; \qquad P(u) \approx 0.70$$

for the theoretical mean and variance of the total number of runs in a series of n independent observations.

In Table 8.1 we note that the eight observed values of $R^{(\alpha)}$ scatter about the theoretical mean $E(R) = 25$ in a fashion which is qualitatively, at least, in accord with the theoretical standard deviation $D(R) \approx 3.43$. As we have already mentioned, the detailed interpretation of such a set of values $R^{(\alpha)}$ depends upon whether the eight series of observations $\{Y_{s\alpha},\ s = 1(1)n\}$ for $\alpha = 1(1)8$ are independent, i.e., on whether the observations are spatially uncorrelated. Our procedure is to assume tentatively, subject to subsequent correlation tests, that the observations are indeed α-independent. The runs test, as we apply it, is then really a test of the combined assumptions of s- and α-independence. Thus, we wish now to test the hypothesis that the eight values $R^{(\alpha)}$ given in Table 8.1 are independent samples from the known distribution of R for a series of n independent observations.

For this purpose we compare the sample variance s^2 (see Table 8.1) of these eight values R_α about their known theoretical mean E(R) with the known theoretical variance $D^2(R)$ by means of the chi-squared test.[27] We also compare the deviation of the sample mean $\overline{R}$ (see Table 8.1) from the theoretical mean with the known theoretical standard deviation, using the "u-test", i.e., the normal deviate test.[28] These tests are appropriate since the distribution of R is very nearly normal for $n > 20$.

As shown in Table 8.1, the χ^2-test gives a value $\chi^2 = 7.06$. with 8 degrees of freedom, which falls in the 50 to 60 percentile of the χ^2

distribution.[29] The u-test gives u = 0.52, for which P(u), the cumulative probability density of the standardized normal distribution, is about 0.70 (i.e., the chance of observing $u \leq 0.52$ is approximately 70%). These values are evidently unexceptionable, and the hypothesis of s- and α-independence is evidently consistent with this test.

We may also examine the occurrence of runs of unusual length; considering the number of observations n in a typical realization, we usually considered runs of 6 or more to be "unusual". In realization B34 there were 3 runs of length 6, one below the median in the sequence Y(s, 6), and one above the median for both $\alpha = 7$ and $\alpha = 8$. There were no runs of greater length. From our tabulations we find $P_{a+b}(6, 48) = 0.4273$; i.e., the probability of observing one or more runs of length 6 or longer, on either side of the median, in a single series of 48 observations, is 0.4273, or 42.73%. Under our assumption of α-independence we have 8 independent such series of 48 observations each, and it is clear that 3 occurrences of the event "one or more runs of 6 or more" in 8 trials, with a probability of 0.4273 in a single trial, is certainly not exceptionable.

Conversely, we can ask whether we perhaps have a dearth of long runs? Our tables give $P_{a+b}(7, 48) = 0.2077$. The probability of observing <u>no</u> successes in 8 independent trials of an event for which the probability of a success in a single trial is 0.2077, is $(1 - 0.2077)^8 \approx 0.155$, according to the binomial distribution. This value is small, but not exceptionable (unless other realizations should show a consistent tendency to have

similarly small numbers of longer runs). Thus, the runs test applied to realization B34 suggests that the hypothesis of s- and α-independence is not unreasonable.

The number of "unusually" long runs and the total number of runs are not independent statistics. Thus, in Table 8.2, where we summarize the entire statistical analysis of the 48-molecule realizations, for the runs test we report the above-mentioned statistic P(u) (see Table 8.1), as being the best representative of the various runs test statistics for each realization. We postpone discussion of these results until after we have outlined the mean-square successive-difference ratio test, and the α-correlation test.

8.2.2 The mean-square successive-difference ratio test.

We use the definitions of Bennett and Franklin,[30] so that if $r^{(\alpha)}$ denotes von Neumann's mean-square successive-difference ratio statistic for a series of observations $Y_{s\alpha}$, $s = 1(1)n$,

$$r^{(\alpha)} = \frac{1}{(n-1)s_\alpha^2} \sum_{\alpha=1}^{n-1} (Y_{s,\alpha+1} - Y_{s\alpha})^2 \quad ,$$

$$E(r^{(\alpha)}) = 2 \quad , \tag{8.2}$$

$$D^2(r_\alpha) = \frac{4(n-2)}{n^2-1} \quad ,$$

where s_α^2 is the usual unbiased estimate of the variance of the sampling distribution,

TABLE 8.2 STATISTICAL ANALYSIS OF THE 48-MOLECULE REALIZATIONS

Class	Reduced Area τ	Realization	Observations[e] n	Runs Test[f] P(u)	MSSDR Test[g] P(u)	α-Correlation Tests[h] C-E(C)/D(C)	E(C)/D(C)	P(u)	Skewness Test[i] P(u)
A	1.025	B 1	157	0.27	0.40	- 6.56	8.60	0.9975	0.66
		B 2	100	0.08	0.16	- 1.92	5.32	0.12	0.92
		B 3	121	0.65	0.25	+ 0.22	6.53	0.78	0.88
		B 4	100	0.78	0.98	- 0.33	5.32	0.54	0.94
	1.040	B 5	100	0.24	0.62	- 1.01	5.32	0.54	0.99
	1.074	B 6	99	0.76	0.56	+ 0.03	5.61	0.11	0.98
	1.075	B 7	37	0.14	0.75	- 1.00	2.77	0.80	0.03
		B 8	50	0.08	0.12	+ 0.55	2.22	0.81	0.98
	1.124	B 9	20	0.09	0.19	- 0.26	1.15	0.85	0.06
		B10	58	0.48	0.42	+ 0.68	2.68	0.69	0.98
	1.125	B11	33	0.54	0.32	- 0.71	2.40	0.79	0.97
	1.169	B13	32	0.81	0.26	+ 0.06	2.59	0.28	0.98
	1.240	B14	100	0.38	0.61	- 2.98	9.16	0.60	1.00
B	1.254	B16	75	0.02	0.01	- 0.88	6.77	0.64	
	1.275	B17	101	0.17	0.18	- 2.34	7.71	0.9993	
	1.290	B18	50	0.68	0.05	- 1.09	3.58	0.945	
	1.300	B19[a]	80	0.22	0.53	- 1.14	4.44	0.975	
		[b]	70	0.04	0.01	- 2.47	3.82	0.9997	
	1.316	B20[c]	20	0.26	0.31	- 0.53	0.98	0.87	
		[d]	43	0.22	0.03	- 2.19	3.00	0.9871	
	1.325	B21	95	0.01	<.0001	- 8.36	8.68	>.9999	
	1.330	B22	95	<.0001	<.0001	- 9.44	9.64	>.9999	
	1.340	B23	141	<.0001	<.0001	-14.15	14.51	>.9999	
	1.350	B24	27	0.76	0.43	- 1.30	1.84	0.86	
		B25	70	<.0001	<.0001	- 5.68	5.70	>.9999	
		B26	71	0.012	0.0003	- 4.66	5.79	(not calc.)	
	1.355	B27	49	0.10	0.02	- 3.02	3.84	0.9939	
	1.375	B28	92	0.07	0.006	- 4.57	7.63	0.9989	
	1.400	B29	90	0.26	0.01	- 3.97	10.2	0.9978	
C	1.500	B30	46	0.82	0.58	- 1.48	3.97	0.67	0.99s
		B31	151	0.64	0.48	- 0.38	10.8	0.67	1.00
	1.650	B32	38	0.42	0.06	- 0.53	3.58	0.52	0.98
	1.750	B33	41	0.70	0.44	- 0.06	4.42	0.46	0.87
	2.000	B34	49	0.70	0.77	- 0.87	6.16	0.98	0.99s
	2.400	B35	22	0.08	0.29	+ 1.14	2.47	0.60	0.99
	3.000	B36	51	0.26	0.23	+ 0.17	7.48	0.96	0.80
	3.900	B37	27	0.56	0.15	- 0.65	3.74	0.91	0.91
		B38	50	0.50	0.49	0.00	3.27	0.06	0.99s
		B39	50	0.08	0.38	0.43	3.27	0.19	0.99s

a The "L plateau", s = 1(1)80, see Section 6.1.2.1.1.
b The "H plateau", s = 81(1)150, see Section 6.1.2.1.2.
c The "L plateau", s = 20(1)39, see Section 6.1.2.2.2.
d The second "H plateau", s = 40(1)82, see Section 6.1.2.2.3.
e The column gives the number n of coarse-grained observations (Δt = 19 200) included in the statistical analysis.
f Section 8.2.1
g The mean-square successive-difference ratio test, see Section 8.2.2.
h Section 8.3.
i Section 8.5

$$s_\alpha^2 = \frac{1}{n-1}\sum_{s=1}^{n}(Y_{s\alpha} - \overline{Y}_\alpha)^2 \quad ,$$

$$\overline{Y}_\alpha = \frac{1}{n}\sum_{s=1}^{n} Y_{s\alpha} \quad . \tag{8.3}$$

As already mentioned, this statistic tests the assumption that the observations $Y_{s\alpha}$ are sampled randomly from a normal distribution. Tables of the approximate percentage points of the distribution of $r^{(\alpha)}$ are available,[30,31] while for $n > 20$ its distribution is approximately normal, with mean and variance as given in Eq. (8.2). In most cases we have used the normal approximation.

Our procedure is exemplified in Table 8.3, again for realization B34. Just as with the runs test, we make now the additional assumption that the observations are α- as well as s-independent, so that we are actually testing here our over-all hypothesis A, since the present test assumes normality. Thus, the eight values of $r^{(\alpha)}$ given in Table 8.3 should be independent samples from an approximately normal distribution with mean and variance given by Eq. (8.2). We again test this assumption by means of the χ^2- and u-tests, as shown in Table 8.3. The results are consistent with the null hypothesis, χ^2 falling in its 80 percentile, and u at about its 77 percentile.

Table 8.3 suggests a systematic decrease of $r^{(\alpha)}$ with increasing α, which, however, does not appear in neighboring realizations and is believed to be coincidental. The largest value, $r^{(1)} = 2.6935$, is evidently

TABLE 8.3 MEAN-SQUARE SUCCESSIVE-DIFFERENCE RATIO TEST FOR REALIZATION B34

$n = 49, \qquad K = 8$

$E(r) = 2$

$D^2(r) = 0.07833 \qquad D(r) = 0.2799$

α	$r^{(\alpha)}$
1	2.6935
2	2.1225
3	2.0916
4	1.9849
5	2.3922
6	1.9714
7	1.7503
8	1.5693

$$\overline{r} = \frac{1}{K}\sum_{\alpha=1}^{K} r^{(\alpha)} = 2.0720$$

$$s^2 = \frac{1}{K}\sum_{\alpha=1}^{K} [r^{(\alpha)} - E(r)]^2 = 0.1134$$

$$\chi^2(K = 8) = \frac{Ks^2}{D^2(r)} = 11.58; \qquad 0.80 \le P(\chi^2) \le 0.90.$$

$$u = \frac{[\overline{r} - E(r)]n^{\frac{1}{2}}}{D(r)} = 0.73; \qquad P(u) \approx 0.77.$$

somewhat exceptional, but not markedly so; from the normal approximation we find that the probability of obtaining so large a value, in a single sequence of 49 independent observations, is about 0.0066. Using the binomial distribution we find the probability of obtaining, out of 8 independent sequences, one or more values so large is $1 - (1 - 0.0066)^8 \approx 0.052$. The latter is not, in itself, especially exceptionable, particularly in a two-sided situation.

As with the runs test, we select as the best single representative statistic from the von-Neumann test the fractile value P(u) obtained from the mean of the values $r^{(\alpha)}$, $\alpha = 1(1)K$. In Table 8.2 this statistic is tabulated for most of the 48-molecule realizations. Again we postpone further discussion until the α-correlation tests have been described.

8.3 Testing for α-Correlation

As mentioned several times previously, the question of the existence of spatial correlation is of importance in two respects; it affects our tests for time-independence, as discussed in Sections 8.2.1 and 8.2.2; and it also affects the type of regression analysis which is appropriate in the numerical differentiation.

All α-correlation tests of which we are aware assume that the observations are s-independent, and indeed that they are samples from a multivariate normal distribution. Consequently the tests which we are about to describe are really tests of our over-all hypothesis A. In the cases in which the tests make the hypothesis appear to be doubtful, it

will not necessarily be obvious which of the three constituent assumptions may be at fault.

Even within these restrictions we are not aware of any simple and direct quantitative test of our hypothesis. Since the latter can be stated as the assumption that the sampling distribution is multivariate normal with unit correlation matrix, it seems natural to seek a test based on the K × K sample correlation matrix

$$C_{\alpha\beta} = \frac{1}{(n-1)\sqrt{s_\alpha s_\beta}} \sum_{s=1}^{n} (Y_{s\alpha} - \overline{Y}_\alpha)(Y_{s\beta} - \overline{Y}_\beta) \quad . \tag{8.4}$$

The simplest single test statistic would appear to be the determinant

$$C = \det(C_{\alpha\beta}) \quad , \tag{8.5}$$

which is discussed by Cramér.[32] The distribution of C on the interval (0, 1) is unknown (except for the case K = 2, where it is related to the known distribution of the bivariate correlation coefficient), but Cramér gives the following exact expressions for its mean and variance:

$$\begin{aligned} E(C) &= \frac{(n-2)!}{(n-K-1)!\,(n-1)^{K-1}} \quad , \\ D^2(C) &= E^2(C)\left[\frac{n(n-1)}{(n+1-K)(n-K)} \; \frac{(n-1)^{K-1}}{(n+1)^{K-1}} - 1\right] \quad . \end{aligned} \tag{8.6}$$

If $[C - E(C)]/D(C)$ is, say, smaller than unity in absolute value, then we may reasonably expect that the observations are consistent with hypothesis A, provided that $E(C)/D(C)$ is at least several times larger than unity. The latter will be the case when n is large compared to K;

otherwise D(C) and E(C) become comparable, and since $C \geq 0$ the test is then of little value. Large values of $[C - E(C)]/D(C)$ can sometimes be shown to be exceptionable by means of the Tchebycheff criterion.[33]

In order to have a somewhat more quantitative test for α-correlation we made use of the fact that each element $C_{\alpha\beta}$ of the sample correlation matrix has the distribution of the familiar bivariate correlation coefficient. In general the elements are not independent of each other, but it is easy to see that a set $\{C_{\alpha_1\beta_1}, C_{\alpha_2\beta_2}, \cdots\}$ in which no subscript repeats is independent. We chose alternate next-to-the-diagonal elements $(C_{12}, C_{34}, C_{56}\cdots)$ and then used Fisher's normalizing z-transformation,[34] testing the assumption that the variables $(u_{12}, u_{34}, \cdots)$,

$$u_{\alpha,\alpha+1} = \tfrac{1}{2}(n - 3)^{\frac{1}{2}} \ln \frac{1+C_{\alpha,\alpha+1}}{1-C_{\alpha,\alpha+1}} \quad , \tag{8.7}$$

are independent samples from the standardized normal distribution. For this purpose we again used the χ^2- and u-tests, with

$$\chi^2(f) = \sum_{\alpha=1,3,\cdots} u^2_{\alpha,\alpha+1} \quad ,$$

$$u = f^{\frac{1}{2}} \sum_{\alpha=1,3,\cdots} u_{\alpha,\alpha+1} \quad , \tag{8.8}$$

where $f = \frac{1}{2}K$ if K is even, $\frac{1}{2}(K - 1)$ if K is odd. The defect of this procedure is that it uses so little of the available data, so that other choices of an internally independent sub-set of the elements $C_{\alpha\beta}$, such as $(C_{23}, C_{45}\cdots)$, can give, in any given case, a different result.

Tables 8.4a and 8.4b give the observed α-correlation matrices for the cumulative pair-distribution functions $G(s, \alpha)$ and the shell populations $Y_{s\alpha}$ of realization B34. The matrices are of course symmetric; the below-diagonal elements have been omitted. We note immediately the presence of strong α-correlation among the cumulative pair-distribution function observations; all the off-diagonal elements of the correlation matrix are positive and most are greater than one half. The correlation matrix for the shell populations, on the other hand, shows off-diagonal elements of variable sign and smaller magnitude, the situation which we anticipated in Chapter 7.

Table 8.5 exemplifies the above tests as applied to both of the sample correlation matrices of Table 8.4. We note that the determinant C lies within one theoretical standard deviation of its expected value in the case of the shell populations, while for the cumulative pair distribution functions it is nearly zero, the deviation being more than six times the standard deviation. The first result can be interpreted as being consistent with the hypothesis of negligible α-correlation among shell populations, while the second merely confirms the strong correlations apparent by inspection of Table 8.4a. However, Table 8.5 shows that the χ^2- and u-tests of Eq. (8.8) give somewhat exceptional results when applied to the shell population correlation matrix, Table 8.4b. This is probably more indicative of the procedural defect already mentioned, than of the presence of appreciable α-correlation in realization B34. For example, the alternative set (C_{23}, C_{45}, C_{67}) gives

TABLE 8.4 OBSERVED α-CORRELATION MATRICES

FOR REALIZATION B34

(a) Cumulative Pair-Distribution Function $\tilde{G}(s, \alpha)$

α \ β	1	2	3	4	5	6	7	8
1	1.00	0.69	0.46	0.41	0.39	0.27	0.20	0.26
2		1.00	0.77	0.65	0.65	0.58	0.55	0.56
3			1.00	0.91	0.86	0.79	0.74	0.71
4				1.00	0.93	0.85	0.79	0.75
5					1.00	0.96	0.89	0.86
6						1.00	0.94	0.92
7							1.00	0.96
8								1.00

(b) Shell Populations $Y_{s\alpha}$

α \ β	1	2	3	4	5	6	7	8
1	1.00	-0.03	-0.15	0.11	0.09	-0.25	-0.17	0.23
2		1.00	0.08	0.02	0.19	0.31	0.14	-0.03
3			1.00	0.28	0.03	0.17	-0.07	-0.15
4				1.00	-0.00	0.06	-0.11	-0.03
5					1.00	0.43	-0.02	0.17
6						1.00	0.06	0.04
7							1.00	-0.12
8								1.00

TABLE 8.5 SPATIAL CORRELATION TESTS FOR REALIZATION B34

$n = 49, \quad K = 8$

$E(C) = 0.5399$

$D(C) = 0.0877$

$\frac{E(C)}{D(C)} = 6.158$

	Table	C	$\frac{C-E(C)}{D(C)}$	$\chi^2(4)$ Eq. (8.8)	$P(\chi^2)$	u Eq. (8.8)	P(u)
Cumulative pair distribution	8.4a	2.4×10^{-6}	-6.158	—	—	—	—
Shell populations	8.4b	0.464	-0.87	14.3	0.990-0.995	2.026	0.9786

$P[\chi^2(3)] = 0.05\text{-}0.10$, $P(u) = 0.70$. Thus, we feel entitled to accept the hypothesis of negligible α-correlation among shell populations, on the basis of the general appearance of the sample correlation matrix, Table 8.4b, as well as the reasonable value of its determinant C, unless subsequent investigation of neighboring realizations should for some unexplained reason show a tendency towards strong correlations within the set $(C_{12}, C_{34}, \cdots)$.

In Table 8.2 we display, for most of the 48-molecule realizations, the statistic $[C - E(C)]/D(C)$, along with the value $E(C)/D(C)$ for comparison, as well as the statistic $P(u)$ corresponding to Eq. (8.8).

8.4 Survey of the Randomness and Correlation Tests for the 48-Molecule Realizations; Division Into Classes A, B, and C

Although there still remained the desirability of making more direct tests for approximate normality of the distribution of the coarse-grained observations, we paused at this point to assess the results of the tests already described, which are directed primarily at the assumptions of s- and α-independence.

Inspection of Table 8.2 immediately shows that the combined assumptions are certainly untenable for realizations in the mid-range of $\tau = 1.254$ to $\tau = 1.4$ inclusive (the exact limits being, of course, rather arbitrary). The exceptional character of these realizations is particularly obvious in the column of normal deviate fractiles $[P(u)]$ for the

correlation test; all of the 15 tabulated values exceed 0.5, and all but three are greater than 0.9. The values for the randomness tests are almost equally striking: In the runs test all but 2 out of 16 values are less than 0.3. The probability, under hypothesis A, that more than two values should exceed 0.3 is greater than 0.9995.

These results were not unexpected, particularly in the case of realizations with $\tau = 1.3$ to 1.355, whose "jumpy" control chart behavior was sufficient warning of the inadequacy of hypothesis A. Our quantitative tests verify this, and further indicate that the anomaly persists to reduced areas appreciably to either side of the jumpy interval.

From this point on we divided the 48-molecule realizations into classes A, B, and C as indicated in Table 8.2. There is, of course, a considerable element of arbitrariness in the classification, since it is based primarily upon the statistics themselves. However, it seems likely that the classification does indeed reflect in a rough way the changes in the topology of the configuration space of the system which take place with increasing τ.

8.4.1 Class A, $\tau = 1.0 - 1.24$.

For each test of the hypothesis of s- and α-independence we have in Table 8.2 a value P(u) from each of the 13 realizations in this class. Under our assumptions, within a given type of test each of the 13 values of P(u) should be a random sample from the uniform distribution on the interval (0, 1).

Considering first the correlation test, we note that P(u) for realization B1 is somewhat exceptionally large. However, the binomial distribution shows that the probability of obtaining one or more values ≥ 0.9975 in 13 independent samples is about 3.2%. The latter, though small, is not extremely so. Considering the set of 13 values as a whole, we find that their average $\overline{P}$ is ≈ 0.61. The theoretical average is, of course, 0.50, while the theoretical variance of such a mean of 13 randomly sampled values from the uniform distribution is $(\frac{1}{13}) \cdot (\frac{1}{12}) = 0.00641$, corresponding to a theoretical standard deviation of about 0.080. Thus, we conclude that the observed set of P(u) values is reasonably consistent with the hypothesis of negligible s- and α-correlation.

Applying the same considerations to the runs test and the mean-square successive-difference ratio test statistics in Table 8.2 for class A, we find $\overline{P} = 0.41$ and 0.43, respectively. These values are again quite consistent with our assumptions. Thus, we conclude that for the realizations of class A, time-smoothed shell populations with $\Delta t = 19\ 200$ are approximately s- and α-independent, subject to further tests of the normality of their sampling distributions.

8.4.2 Class B, $\tau = 1.254 - 1.4$.

We have already mentioned that Table 8.2 shows the combined hypotheses of s- and α-independence to be untenable for these realizations. The presence of s-correlation is, of course, especially noticeable

in the case of the "jumpy" realizations. However, the statistics in Table 8.2 also suggest the presence of less obvious types of serial correlation, since the values of P(u) from the runs and m.s.s.d.r. tests tend to be small both for non-jumpy realizations such as B16, B17, B28, and B29, as well as for different "plateaus" of jumpy realizations such as B19 and B20. The presence of serial correlation can also be argued in the following way. If the observations were s-independent but positively α-correlated, then the runs or m.s.s.d.r. statistics P(u) for independent realizations (or independent plateaus within a given realization) would be independent samples from a distribution which would no longer be uniform on (0, 1), but which would still be symmetric about P(u) = 0.5. In such a case, the 16 values of P(u) given in Table 8.2 for either of these randomness tests would be expected to be approximately evenly divided above and below 0.5. Such is far from the case, so that we conclude that for realizations of this class the value $\Delta t = 19\ 200$ is not nearly large enough for consecutive time-smoothed observations to be time-independent.

As might be expected, investigation of larger values of Δt yielded some, but not sufficient, improvement. (The upper limit of Δt is in practice limited for a realization of a given length t by the practical worthlessness of the above statistical tests when the sample size decreases much below n = 20.)

8.4.3 Class C, τ = 1.5 - 3.9

Applying the procedure used for class A to the 10 realizations in class C, we find the average $\bar{P}$ for the correlation, runs, and m.s.s.d.r. statistics to be 0.60, 0.48, and 0.39, respectively. These compare favorably with their theoretical value 0.5 and theoretical standard deviation 0.091.

Thus, we conclude that the Δt = 19 200 coarse-grained observations on these realizations may be regarded as temporally and spatially independent, again subject to further tests for approximate normality.

8.5 Tests of Normality

It remains to inquire as to whether the observations for the class A and C realizations with Δt = 19 200 can be reasonably regarded as being sampled from uncorrelated multivariate normal distributions. The negative results from the correlation and randomness tests on the class B realizations make it superfluous to test them for normality.

For this purpose we examined only the marginal distribution of each shell population sample. Of the various tests for approximate normality we chose the coefficients of skewness G_1 and excess G_2 defined by Cramér,[35]

$$G_{1\alpha} = \frac{n}{(n-1)(n-2)s_\alpha^3} \sum_{s=1}^{n} (Y_{s\alpha} - \bar{Y}_\alpha)^3 \ ,$$

$$G_{2\alpha} = \frac{(n-1)}{(n-2)(n-3)} \left\{ \frac{n(n+1)}{(n-1)^2 s_\alpha^2} \left[\sum_{s=1}^{n} (Y_{s\alpha} - \bar{Y}_\alpha)^4 \right] - 3(n-1) \right\} \qquad (8.9)$$

These statistics have a disadvantage in that their exact distributions are unknown. Cramér[35] gives the following exact expressions for their means and variances:

$$E(G_1) = E(G_2) = 0 \quad ,$$

$$D^2(G_1) = \frac{6n(n-1)}{(n-2)(n+1)(n+3)} \quad , \tag{8.10}$$

$$D^2(G_2) = \frac{24n(n-1)^2}{(n-3)(n-2)(n+3)(n+5)} \quad .$$

The distribution of G_1 is symmetric; that of G_2 is not. For large values of n, of course, the distributions will tend towards normality by virtue of the central limit theorem.

Approximate values of the 0.01, 0.05, 0.95, and 0.99 fractiles of the statistic

$$\sqrt{b_1} = \frac{(n-2)}{\sqrt{n(n-1)}} G_1$$

for $n \geq 25$ are tabulated by Pearson and Hartley,[36] based on Pearson-type distributions having the correct first four moments. These values for sample sizes of interest here are compared with those of the asymptotic normal distribution in Table 8.6, from which it is seen that for our purposes the normal approximation is adequate.

The same authors[36] also give similar approximations for the statistic

$$b_2 = \frac{(n-2)(n-3)}{(n-1)(n+1)} G_2 + \frac{3(n-1)}{n+1} \quad ,$$

but only for $n \geq 200$. The distributions of these coefficients of excess apparently approach normality much more slowly with n than do those of

TABLE 8.6 APPROXIMATE FRACTILES[a] OF $\frac{G_1}{D(G_1)}$

Sample Size	Fractiles	
n	0.95	0.99
25	1.63_3	2.43_7
30	1.63_1	2.42_3
40	1.63_2	2.41_7
50	1.63_3	2.41_1
100	1.63_6	2.38_5
∞ (normal)	1.645	2.32_6

[a] From reference 36. The 0.01 and 0.05 fractiles follow from the tabulated fractiles and the symmetry of the distribution.

the coefficients of skewness. Approximations of uncertain validity for n = 40 and 100 recently discussed by Pearson[37] are compared with their asymptotic normal distribution in Fig. 8.1. The deviations are quite large, with marked skewness even for n = 100.

Table 8.7 shows our analysis of the observed coefficients of skewness of the shell populations sampled in realization B34. Under hypothesis A, each value of $G_{1\alpha}$ is an independent sample from a distribution which is approximately normal with zero mean and standard deviation given by Eq. (8.10) The preponderance of positive values makes it clear that the hypothesis is doubtful. As with the other statistical tests, a more quantitative measure is obtained by comparing the sample mean $\overline{G}_1$ of these K = 8 values with its theoretical standard deviation

$$D(\overline{G}_1) = \frac{D(G_{1\alpha})}{\sqrt{K}} \quad .$$

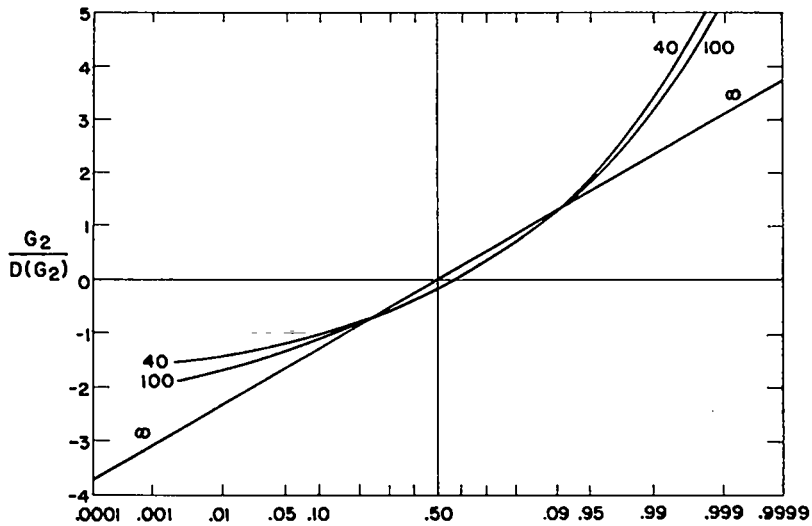

Fig. 8.1 Pearson approximations to the distributions of the coefficient of excess G_2, for sample sizes n = 40 and 100, compared with the asymptotic (n = ∞) normal distribution.

TABLE 8.7

SKEWNESS TEST FOR REALIZATION B34

$n = 49$

$K = 8$

$D(G_{1\alpha}) = 0.340$

α	$G_{1\alpha}$
1	-0.141
2	+0.110
3	0.959
4	0.674
5	0.426
6	0.642
7	0.274
8	-0.079

$$\overline{G}_1 = 0.358$$

$$u = \frac{\sqrt{K}\,\overline{G}_1}{D(G_{1\alpha})} = 2.98$$

$$P(u) = 0.9986$$

Under our hypothesis and approximations, the statistic

$$u = \frac{\overline{G}_1}{D(\overline{G}_1)} \tag{8.11}$$

should be a standardized normal deviate. The fractile value 0.9986 for realization B34 makes hypothesis A doubtful, particularly the assumption of normality of the sampling distribution.

The coefficients of excess $G_{2\alpha}$ from the same set of observations were analyzed as shown in Table 8.8. An approximate fractile $P(G_{2\alpha})$ was obtained graphically from Fig. 8.1 for each shell. Under hypothesis A, each of these eight values should be an independent sample from the rectangular distribution on the interval (0, 1). The mean $\overline{P}$ of these eight values should then be approximately normally distributed[38] with mean 0.5 and standard deviation $(8 \cdot 12)^{-\frac{1}{2}}$. Thus, the normal deviate

$$u = \frac{\overline{P} - 0{\cdot}5}{\sqrt{\frac{1}{8{\cdot}12}}}$$

tests the hypothesis. For realization B34 the fractile value obtained is 0.957, which would make the hypothesis of normality somewhat doubtful, considering this realization in isolation from the others.

Because of the somewhat uncertain validity of the Pearson approximation to the distribution of the coefficient of excess, we restrict ourselves to reporting in Table 8.2 the fractile value P(u) obtained by applying Eq. (8.11) to the coefficients of skewness of the shell populations sampled by the 48-molecule realizations of classes A and C.

TABLE 8.8

EXCESS TEST FOR REALIZATION B34

$$n = 49$$

$$K = 8$$

$$D(G_{2\alpha}) = 0.668$$

α	$G_{2\alpha}$	$G_{2\alpha}/D(G_{2\alpha})$	$P(G_{2\alpha})$
1	-0.224	-0.335	0.42
2	-0.488	-0.730	0.22
3	+2.045	+3.061	0.98_8
4	-0.082	-0.123	0.52
5	-0.018	-0.027	0.57
6	+0.583	+0.873	0.84
7	+0.796	+1.191	0.89
8	+1.420	+2.125	0.96

$$\overline{P} = 0.676$$

$$u = \frac{0.676 - 0.5}{\sqrt{\frac{1}{8 \cdot 12}}} = 1.72$$

$$P(u) = 0.957$$

Note that in Table 8.2 all but two out of 23 values of the skewness statistic are greater than 0.5, and indeed 17 are greater than 0.90. These results, particularly in view of the known symmetry of the distribution of G_1 under the null hypothesis, leave little doubt that with $\Delta t = 19\ 200$ the sampling distributions of the time-smoothed shell populations are appreciably positively skewed. Indeed, the control charts had given some prior indication of this.

Larger values of Δt would presumably tend to reduce the skewness, but an investigation of class C with $\Delta t = 38\,400$ showed only slight improvement. Still larger values would result in unsatisfactorily small values of n.

The coefficients of excess, not reported in detail here, were somewhat better behaved, in particular yielding P(u) values scattering somewhat better above and below 0.5. By themselves, they might indeed be consistent with the hypothesis of normality.

8.6 Conclusion

The results of the preceding section indicate that even for the realizations of classes A and C, for which the time- and space-correlation statistics were reasonably well behaved, hypothesis A is not strictly valid. However, the presence of a moderate amount of skewness is not likely to seriously invalidate the tests for the two types of correlation, so that we feel justified in carrying out by more or less standard techniques the numerical differentiation which is required in order to reduce the data to values of the compressibility factor.

In class B, on the other hand, the results of the two varieties of correlation tests strongly indicate a somewhat modified procedure.

Chapter 9

NUMERICAL DIFFERENTIATION BY LEAST SQUARES REGRESSION ANALYSIS

9.1 Introduction

According to the procedure briefly outlined in Section 7.5, the basic assumption underlying the regression analysis is that the theoretical shell populations η_α for a given realization can be represented by a truncated power series

$$\eta_\alpha = \sum_{i=0}^{\nu} \beta_i \alpha^i , \qquad \alpha = 1(1)K \quad , \tag{9.1}$$

the omitted terms being assumed to be in some sense small compared to the statistical fluctuation of the observations. In Eq. (9.1) both the degree ν of the polynomial and its coefficients β_i are unknown and are to be estimated from the data.

Let us suppose that ν is known, and outline the familiar problem of estimating the coefficients β_i from data consisting of a single observation Y_α of η_α at each value $\alpha = 1(1)K$. The general minimum variance solution to this problem was given by Aitken,[39] and can be written as

follows

$$b = (x^{\dagger}\varphi^{-1}x)^{-1}x^{\dagger}\varphi^{-1}Y \quad , \tag{9.2}$$

where b is the column matrix $(b_o, b_1 \cdots b_\nu)^{\dagger}$ of the estimates b_i of the unknown coefficients β_i, and the superscript dagger indicates the transposed matrix. The matrix x of K rows and $\nu + 1$ columns is

$$x = \begin{pmatrix} 1 & 1 & 1 & \cdots & 1 \\ 1 & 2 & 4 & \cdots & 2^{\nu} \\ 1 & 3 & 9 & \cdots & 3^{\nu} \\ \vdots & \vdots & \vdots & \vdots & \vdots \\ 1 & K & K^2 & \cdots & K^{\nu} \end{pmatrix} \quad , \tag{9.3}$$

while Y denotes the column matrix $(Y_1, Y_2, \cdots Y_K)^{\dagger}$ of the observations, and φ is the theoretical K-square covariance matrix of observations Y_α:

$$\varphi_{\alpha\alpha'} = \mathrm{cov}(Y_\alpha Y_{\alpha'}) \quad , \qquad \alpha,\alpha' = 1(1)K. \tag{9.4}$$

The covariance matrix of the estimates b_i, $i = 0(1)\ \nu+1$, is

$$\mathrm{cov}\ b = \left\{\mathrm{cov}\ b_i b_{i'}\right\} = (x^{\dagger}\varphi^{-1}x)^{-1} \quad . \tag{9.5}$$

The estimate b given by Eq. (9.2) is unbiased, i.e., the average of b in the sampling distribution of the observations Y is β. It is the <u>minimum variance</u> estimate, in the sense that of all linear unbiased estimates it minimizes the variance of any arbitrary linear function of β.

Equation (9.2) is seldom directly applicable, since it assumes that the theoretical covariance matrix φ is known, except for a perhaps unknown

scalar multiplier. In the latter case one writes

$$\varphi = \sigma^2\tilde{\varphi} \quad , \tag{9.6}$$

where $\tilde{\varphi}$ is a known matrix and σ^2 an unknown scalar. The estimate b given by Eq. (9.2) is evidently independent of σ^2, but Eq. (9.5) for its covariance requires an estimate s^2 of σ^2, which can be shown to be appropriately (in the sense that the ensemble average of s^2 is σ^2) taken in the form

$$s^2 = \frac{1}{K-\nu-1}(y - Y)^\dagger\tilde{\varphi}^{-1}(y - Y) \quad . \tag{9.7}$$

Here

$$y = xb \tag{9.8}$$

denotes the least squares estimate $(y_1, y_2 \cdots y_K)$ of the theoretical shell population column matrix η. The covariance matrix of b is then estimated as

$$\text{cov } b = \frac{(y-Y)^\dagger\tilde{\varphi}^{-1}(y-Y)}{K-\nu-1}(x^\dagger\varphi^{-1}x)^{-1} \quad . \tag{9.9}$$

Only in exceptional cases, of course, is the theoretical covariance matrix known to within a scale factor.

The above equations are usually encountered in one of two specialized forms. The next most general form is for the case of uncorrelated observations, φ being a known diagonal matrix, again aside from a possibly unknown scalar. This is just the well-known "weighted least squares" case. Finally, if φ is just the unknown scalar σ^2 times the unit matrix, the general equations reduce to the usual unweighted least squares procedures. In all cases the only requirement upon the distribution from which the

observations Y_α are sampled is that its covariance matrix φ be positive definite.

When more than one independent observation is available at each value of α, say n observations $Y_{s\alpha}$, s = 1(1)n, the above equations are unchanged, except that Y_α is replaced by $\overline{Y}_\alpha$ [Eq. (8.3)], and φ is the covariance matrix $\left\{\text{cov } \overline{Y}_\alpha \overline{Y}_{\alpha'}\right\}$, equal to n^{-1} times $\text{cov}(Y_{\alpha s} Y_{\alpha' s})$.

The advantage of a numer of independent observations at each α lies in the possibility of testing assumptions about the covariance matrix φ, as in Chapter 8, where we tested the assumption that φ is diagonal, finding it tenable in classes A and C. Multiple observations also lead to the possibility of making certain "goodness of fit" tests, as will be described.

We should perhaps also mention that if a wrong assumption concerning the form of φ is made, the estimate b is still unbiased, but the estimate of its covariance matrix given by Eq. (9.9) becomes incorrect, and in extreme cases may be grossly so.

The above discussion makes clear the role played in the regression analysis by our assumptions of s- and α-independence. We note that the third constituent of hypothesis A, the assumption of normal sampling distributions, enters only if one wishes to obtain confidence interval estimates from the estimated standard deviations.

The above procedures do not completely solve our data reduction problem, since we must also estimate the degree ν of the regression polynomial. We are not aware of any systematic statistical treatment of this type of estimation problem. Our ad hoc procedure consists in

calculating a sequence of regression vectors $b^{(\nu)}$ for increasing values of ν, and taking as the "correct" degree ν^* the value at which the high order coefficients $b_i^{(\nu)}$, $i > \nu^*$, become statistically indistinguishable from zero for $\nu > \nu^*$. The detailed procedure will be described in Section 9.2.2.2. A similar statistical problem arises in the estimation of virial coefficients from experimental p,V,T data, and has received a somewhat different treatment by Michels and his coworkers.[40]

9.2 Realizations in Classes A and C

9.2.1 Preliminary calculation of smoothed weights.

In Chapter 8 we saw that the hypothesis that the time-smoothed shell populations $Y_{s\alpha}$ (Δt = 19 200) were time-independent and spatially uncorrelated was reasonably consistent with the observations for realizations in classes A and C. In terms of the discussion of the previous section, we may thus assume that the unknown theoretical covariance matrix φ is diagonal, and that each observation $Y_{s\alpha}$ is an independent estimate of the theoretical value η_α.

It remains to inquire whether or not φ can be reasonably assumed to be a scalar times the unit matrix. Somewhat to our surprise we found that in both class A and class C the sample variances s_α^2 given by Eq. (8.3) showed a systematic decrease with increasing α. This is shown for realizations B2 and B34 in Fig. 9.1. This dependence was strongest for the high density realizations of class A, but noticeable for all realizations except B35, B36, and B37 at low density and small K.

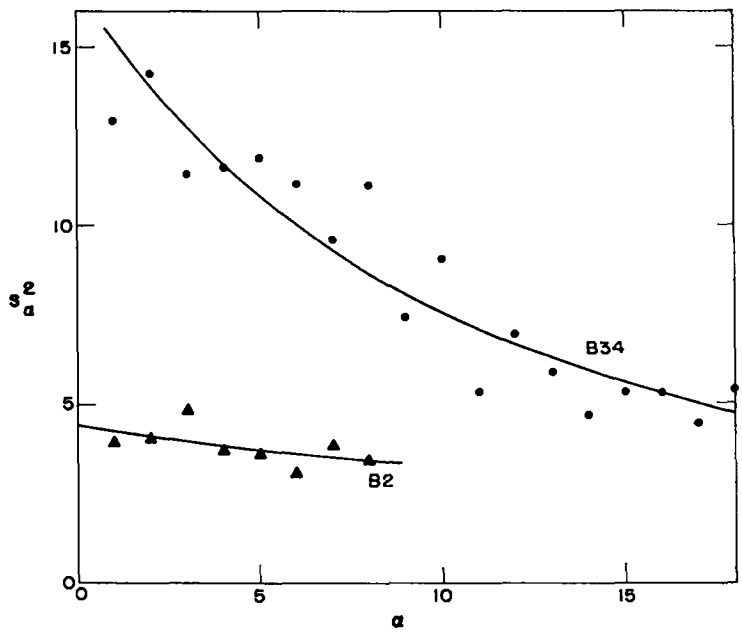

Fig. 9.1 Dependence of the shell population variances s_α^2 on the shell number α, for realizations B2 and B34.

Thus, it seemed desirable to use a weighted least squares procedure in estimating the compressibility factor. The most direct method would have been to take the diagonal terms of the matrix $\tilde{\varphi}$ [see Eq. (9.6)] to be

$$\tilde{\varphi}_{\alpha\alpha} = n^{-1} s_\alpha^2 \quad .$$

However, we decided to perform the following preliminary least squares smoothing of the sample variances (which in retrospect seems overly elaborate).

The standard deviation s_α of a set of n independent observations from a normal distribution with variance σ_α^2 is itself approximately normally distributed[41] with

$$E(s_\alpha) \approx \sigma_\alpha \quad ,$$

$$D^2(s_\alpha) \approx \frac{\sigma_\alpha^2}{2(n-1)} \quad . \tag{9.10}$$

Since it was somewhat more convenient to smooth s_α^{-1} , and since by the usual approximation

$$D^2(s_\alpha^{-1}) \approx \left(\frac{ds_\alpha^{-1}}{ds_\alpha}\right)^2 D^2(s_\alpha) \approx \frac{1}{2(n-1)\sigma_\alpha^2} \quad , \tag{9.11}$$

we carried out a linear least squares smoothing of the observed reciprocal standard deviations by minimizing the sum of squares

$$\chi^2(K-2) = \sum_{\alpha=1}^{K} w'_\alpha (s_\alpha^{-1} - \hat{s}_\alpha^{-1})^2 \quad , \tag{9.12}$$

with weight factors

$$w'_\alpha = 2(n-1)s_\alpha^2 \quad , \tag{9.13}$$

and smoothed reciprocal standard deviations

$$\hat{s}_\alpha^{-1} = a_0 + a_1\alpha \quad . \tag{9.14}$$

The curves in Fig. 9.1 are drawn through the corresponding smoothed values $\hat{s}_\alpha^2$. A crude goodness of fit test of this smoothing procedure is obtained by comparing the value of $\chi^2(K-2)$ given by Eq. (9.12) with the fractiles of the standard chi-square distribution with K - 2 degrees of freedom. The value for realization B2 falls in the interval 0.5-0.6, that for B34 in the interval 0.05-0.10; both are regarded as satisfactory.

9.2.2 Shell population regression analysis.

Our data reduction program carried out the least squares calculation of Section 9.1 with the observational vector Y equal to the mean vector $(\overline{Y}_1, \overline{Y}_2, \cdots \overline{Y}_K)$ for a given realization or a specified portion (plateau) thereof, and with a number of options with regard to the covariance matrix $\tilde{\varphi}$. We will here be concerned with three of these alternatives. The first and most commonly used one is that in which the matrix is diagonal, with the diagonal elements determined by the linear smoothing procedure of the previous section:

$$\tilde{\varphi}_{\alpha\alpha'} = n^{-1}\hat{s}^2_\alpha \, \delta_{\alpha\alpha'} \quad . \qquad \text{(option 1)} \qquad (9.15)$$

The second alternative was simply the usual unweighted least squares procedure with

$$\tilde{\varphi}_{\alpha\alpha'} = \delta_{\alpha\alpha'} \quad , \qquad \text{(option 2)} \qquad (9.16)$$

while the third method took $\tilde{\varphi}$ proportional to the unsmoothed, non-diagonal sample covariance matrix,

$$\tilde{\varphi}_{\alpha\alpha'} = \frac{1}{n(n-1)} \sum_{s=1}^{n} (Y_{s\alpha} - \overline{Y}_\alpha)(Y_{s\alpha'} - \overline{Y}_{\alpha'}) \quad . \qquad \text{(option 3)} \qquad (9.17)$$

The last procedure corresponds, for the general case of correlated observations, to the commonly encountered weighted least squares practice of using weight factors computed from the sample variances, i.e., using in Eq. (9.15) the sample variances s^2_α instead of the smoothed values $\hat{s}^2_\alpha$.

In all three options the subsequent analyses of variance and goodness of fit tests are approximate only, since they proceed by way of assumptions about the true theoretical covariance matrix φ. In options 1 and 3, the approximation consists in the first place in assuming that φ is an unknown scalar σ^2 times the known matrix $\tilde{\varphi}$, which in the second place depends stochastically upon the observations $Y_{s\alpha}$. In option 2 the approximation consists in ignoring the apparent inhomogeneity of the true variances σ_α^2.

The matrix inversions required in the calculation of the estimate b given by Eq. (9.2) were carried out by a row-by-row Gram-Schmidt orthogonalization process carried out in double-precision floating-point arithmetic on the IBM 704 calculator. In options 1 and 2 this process was checked for numerical accuracy by an independent single-precision least squares method based on orthogonal polynomials.

9.2.2.1 Analysis of variance and goodness of fit.

We will describe our procedure in detail for the most used case, option 1; the procedures for the other alternatives were obvious modifications. The general method, as already mentioned, is based upon standard procedures[42] for the situation in which φ is known aside from a multiplicative scalar; in the present case φ is assumed to be given by Eq. (9.6), with $\tilde{\varphi}$ given by Eq. (9.15). Since φ is defined as the covariance matrix of the sample mean vector $(\overline{Y}_1, \overline{Y}_2, \cdots \overline{Y}_K)$, under the above approximation and for a given value of ν there are available two

statistically independent estimates of the scalar σ^2 . The first of these, which we will designate as $s^{(2)^2}$, is calculated from the residual deviations by means of Eq. (9.7),

$$s^{(2)^2} = (K - \nu - 1)^{-1}(y - Y)^{\dagger}\tilde{\varphi}^{-1}(y - Y) \quad , \tag{9.18}$$

and has

$$f^{(2)} = K - \nu - 1 \tag{9.19}$$

degrees of freedom. The second, designated as $s^{(1)^2}$, is obtained from the internal variances of the K sets of observations $Y_{s\alpha}$,

$$s^{(1)^2} = \frac{1}{K} \sum_{\alpha=1}^{K} \frac{s_\alpha^2}{\hat{s}_\alpha^2} \quad , \tag{9.20}$$

and has

$$f^{(1)} = K(n - 1) \tag{9.21}$$

degrees of freedom.

Since the approximate "true" variances $\hat{s}_\alpha^2$ were obtained by smoothing the observed sample variances s_α^2 , the value of $s^{(1)^2}$ calculated from Eq. (9.20) is always close to unity. Indeed, our statistical analysis could equally well be carried out, with no significant change in our conclusions, under the assumption that the "true" value of σ^2 is exactly 1; the F-test to be discussed in the next paragraph would then be replaced by a chi-squared comparison of $s^{(2)^2}$ with its theoretical value 1.

If the given value of ν is exactly correct, that is, if the theoretical shell populations η_α are exactly representable by a polynomial of degree ν, then, subject to all our other statistical assumptions and

approximations, the ratio

$$F(f^{(2)}, f^{(1)}) = \frac{s^{(2)^2}}{s^{(1)^2}} \tag{9.22}$$

is a random sample from the F-distribution[43] with parameters $f^{(2)}$ and $f^{(1)}$. Comparison of the calculated value with the tabulated fractiles of the distribution thus affords an approximate goodness of fit test of the given value of ν.

If this test indicates that the observations are compatible with a theoretical polynomial of degree ν, an improved (in principle, at least) estimate of the unknown scalar σ^2 can be obtained by the usual pooling of the two independent estimates:

$$s^{(12)^2} = \frac{f^{(1)}s^{(1)^2} + f^{(2)}s^{(2)^2}}{f^{(1)} + f^{(2)}} \quad ,$$

$$f^{(12)} = f^{(1)} + f^{(2)} \quad . \tag{9.23}$$

The estimate $s^{(12)^2}$ of σ^2 is then used, in conjuction with Eqs. (9.5), (9.6), and (9.15) to obtain an estimate (with $f^{(12)}$ degrees of freedom) of the covariance matrix of the estimate b:

$$\text{cov } b = s^{(12)^2}(x^{\dagger}\tilde{\varphi}^{-1}x)^{-1} \quad . \tag{9.24}$$

These procedures as applied to realization B34 are illustrated in Table 9.1 for $\nu = 1$, 2, and 3. We note that all three of the resulting goodness of fit statistics F have non-exceptionable values. This indicates

TABLE 9.1 GOODNESS AND DEGREE OF FIT TESTS FOR REALIZATION B34, UNDER WEIGHT OPTION # 1

$s = 2(1)\ 50; \quad n = 49, \quad K = 8$

$s^{(1)^2} = 0.9971, \quad f^{(1)} = 384$

ν	$f^{(2)}$	$s^{(2)^2}$	$F(f^{(2)},384)$	P(F)	$s^{(12)^2}$	$f^{(12)}$	$t(f^{(12)})$	P(t)
1	6	0.718	0.72	0.3-0.5	0.993	390	-4.68	< 0.0005
2	5	0.799	0.80	0.3-0.5	0.995	389	-0.56	0.2-0.3
3	4	0.999	1.00	0.5-0.7	0.997	388	+0.00	0.5

that polynomials of degree one through three can adequately represent the observed α-dependence of the mean shell populations $\overline{Y}_\alpha$ (an abnormally large value of F would indicate a polynomial of too low a degree to follow the indicated variation of η with α) with no apparent tendency to reproduce the statistical fluctuations in the $\overline{Y}_\alpha$ (as may be indicated by too small a value of F). This insensitivity is typical of the behavior of the F statistic, which is not adequate to select the appropriate degree of fitting polynomial in cases such as ours, precisely because it does not include any test of our convergence assumption that contributions of higher order terms of the power series are in some sense negligible. The test is usually of use only in showing that a particular value of ν is too low. This would have been the case, for example if we had included in Table 9.1 the value $\nu = 0$.

Thus, we see that in order to select a particular value of ν we need a test which explicitly involves an examination of the smallness of the higher order terms of the power series.

9.2.2.2 Degree of fit test.

Let us suppose that a polynomial of degree ν^* exactly represents the theoretical shell populations η_α, $\alpha = 1(1)K$ for a given system. Obviously a polynomial of degree K - 1 will certainly represent these K discrete points; we require the much stronger condition that the corresponding [by Eqs. (7.4) and (7.6)] polynomial of degree $\nu^* + 1$ and zero constant term exactly represents the theoretical cumulative pair-distribution function $G(\zeta_\alpha)$ for all α, particularly non-integral values, in the interval (0, K). Consider then a regression analysis carried out with $\nu = \nu^* + 1$ on the observations obtained from a realization appropriate to the system in question, and suppose that hypothesis A is satisfied. Then the highest order theoretical coefficient β_{ν^*+1} is zero. Its estimated value b_{ν^*+1} will, of course, not usually be exactly zero, but upon replication of our over-all experiment (which consists of generating an independent realization of given length n with the given observational parameters, then carrying out the least squares data reduction as described in the previous sections, with $\nu = \nu^* + 1$) the estimate should fluctuate about zero with a variance which is estimated by Eq. (9.24). Thus, the usual t-test[44] with

$$t(f) = \frac{b_{\nu^*+1}}{s^2[(x^\dagger \tilde{\varphi}^{-1} x)^{-1}]_{\nu^*+1,\ \nu^*+1}} , \qquad (9.25)$$

which tests the hypothesis $\beta_{\nu^*+1} = 0$, is a test of the hypothesis that a polynomial of degree ν^* represents exactly the theoretical shell populations. In Eq. (9.25) s^2 is any estimate with f degrees of freedom of the scalar σ^2 of Eq. (9.6) which is statistically independent of b_{ν^*+1}. Following the discussion of the previous section, it will usually be the pooled variance $s^{(12)^2}$ with $f = f^{(12)}$ obtained from the regression analysis with $\nu = \nu^* + 1$, but either $s^{(1)^2}$ or $s^{(2)^2}$ with $f = f^{(1)}$ or $f^{(2)}$ could be used.

It can be shown that the above test utilizes all the information obtainable by comparison of the lower order coefficients of the two fits of degree ν^* and $\nu^* + 1$. Futhermore, if the hypothesis $\nu = \nu^*$ is correct, it is easy to show that the "best" (i.e., minimum variance) estimates of the coefficients β_i are the values b_i obtained with $\nu = \nu^*$. The b_i obtained with $\nu = \nu^* + 1$ are, of course, unbiased estimates of β_i, but have inherently greater variability [which variability is, of course, correctly estimated by Eq. (9.24)]. On the other hand, if the hypothesis $\nu = \nu^*$ is incorrect, i.e., if we make an "error of the second kind,"[45] the estimates obtained from the $\nu = \nu^*$ regression are in general biased. Thus, it would appear to be desirable, in applying the above test, to use rather wide rejection zones (for example rejecting the hypothesis $\nu = \nu^*$ when $P(t) < 0.05$ or > 0.95, corresponding to making an "error of the first kind," i.e., rejecting the hypothesis when it is true, on the average in one experiment in ten).

The test as outlined makes no allowance for information obtainable by comparing still higher degrees of fitting polynomial, e.g. $\nu = \nu^* + 2$, etc. Since the largest value of ν^* which we encountered in this investigation (see below) was 3, with the most common values being 1 and 2, this defect does not seem particularly serious. The test also makes no allowance for the fact that a polynomial of finite degree cannot and need not exactly represent the theoretical shell populations. Again, since the observational parameters were chosen with the intention that ν^* should be small, this does not seem to be a serious defect.

A far more serious deficiency in the procedure as outlined is that the resulting degree ν of the fitting polynomial is a stochastic variable whose choice has a considerable effect on the estimates b_1 (and therefore on the estimate of γ_1 and on the final estimated compressibility factor), but whose uncertainty is not taken into account in our estimate Eq. (9.24) of the uncertainty of the estimated regression coefficients. We have tried to reduce this extra uncertainty by taking into consideration, during the data reduction for a particular realization, the indicated behavior of ν for other realizations at the same or nearby values of τ.

The above-described procedure is illustrated for realization B34 in Table 9.1. The very small value of the fractile P(t) for $\nu = 1$ indicates that the regression polynomial of degree $\nu = 0$ (not computed) is in all likelihood inconsistent with the observations. On the other hand the values of this statistic for $\nu = 2$ and $\nu = 3$ are quite consistent with the hypothesis $\nu^* = 1$, a value which is also in agreement with other

realizations with similar parameters. Therefore, we take as our "best" estimate of the theoretical shell populations the polynomial of degree 1, whose coefficients are displayed in Table 9.2 along with those for $\nu = 2$ and 3. The tabulated uncertainties are the estimated standard deviations given by Eq. (9.24); the covariance terms are not given.

In Fig. (9.2) the observed mean shell populations $\overline{Y}_\alpha$ are compared graphically with the above linear regression function.

9.2.3 Estimating the compressibility factor.

From Eq. (7.8) we see that for the estimation of the compressibility factor pV/NkT we require an estimate of the first coefficient γ_1 of the truncated power series expansion, Eq. (7.4), of the cumulative pair distribution function. Equation (7.6) shows that γ_1 is just a linear combination of the shell population coefficients β_i, so that the appropriate estimate is just the same linear combination of the estimates b_i:

$$\gamma_1 \approx b_o + \tfrac{1}{2}b_1 + \sum_{j=1}^{I\left(\frac{\nu}{2}\right)} (-1)^{j+1} B_j b_{2j} \quad . \tag{9.26}$$

We use the approximately equal symbol $\approx$ to indicate that the quantity on the right is a statistical estimate of that on the left, rather than introduce a special symbol for the estimate of γ_1. In matrix notation this equation can be written

$$\gamma_1 \approx \lambda^\dagger b \quad , \tag{9.27}$$

TABLE 9.2 REGRESSION POLYNOMIALS FOR REALIZATION B34

SHELL POPULATIONS UNDER WEIGHT OPTION # 1

ν	$\left(b_0 \pm s_{b_0}^{(12)}\right)\cdot 10^2$	$\left(b_1 \pm s_{b_1}^{(12)}\right)\cdot 10^4$	$\left(b_2 \pm s_{b_2}^{(12)}\right)\cdot 10^5$	$\left(b_3 \pm s_{b_3}^{(12)}\right)\cdot 10^7$
1	5.6189 ± 0.0702	-6.372 ± 1.350		
2	5.5599 ± 0.1266	-2.917 ± 6.312	-3.785 ± 6.755	
3	5.5589 ± 0.2237	-2.810 ± 19.92	-4.063 ± 49.42	2.046 ± 359.6

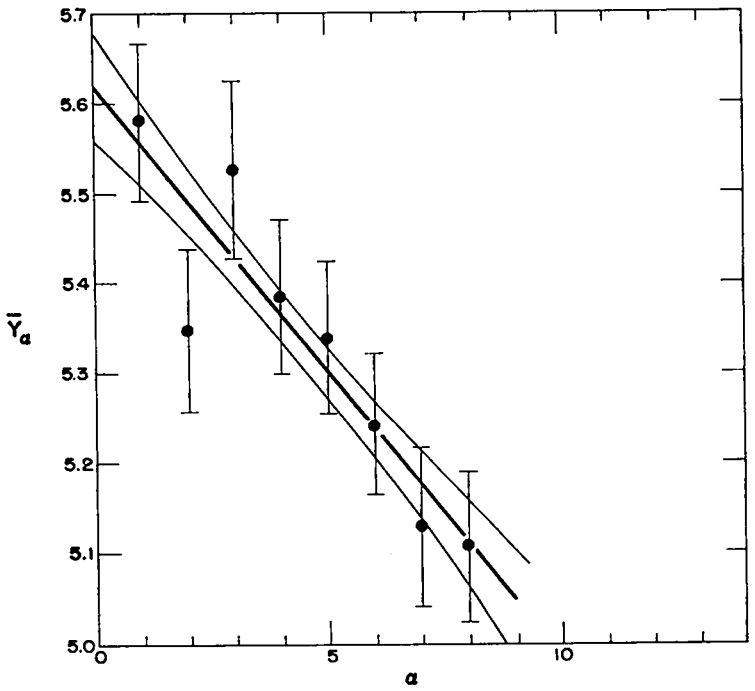

Fig. 9.2 Comparison of the observed shell population $\bar{Y}_\alpha$ of realization B34 with the least squares straight line computed for weight option # 1. The vertical flags indicate one estimated standard deviation, $s_{\bar{Y}_\alpha} = n^{-1}s_\alpha$, to either side of $\bar{Y}_\alpha$. The light curves are error hyperbolas drawn one estimated standard deviation $s_{y_\alpha}^{(12)}$ around the regression line. The variation of the regression line with the different weight options is not perceptible on this graph.

where λ is the column vector with components

$$\left.\begin{aligned} \lambda_0 &= 1 \\ \lambda_1 &= \tfrac{1}{2} \\ \lambda_{2j} &= (-1)^{j+1} B_j \\ \lambda_{2j+1} &= 0 \end{aligned}\right\} \quad j = 1,2,\cdots I\left(\frac{\nu}{2}\right), \text{ if } \nu > 1; \text{ zero otherwise.}$$

Then the estimated variance of the estimate Eq. (9.27) of γ_1 is

$$s^2_{\gamma_1} = s^{(12)^2} \lambda^\dagger (x^\dagger \tilde{\varphi}^{-1} x)\lambda \quad . \tag{9.28}$$

Finally, this estimate of γ_1 is used in Eq. (7.8) to obtain an estimate of the compressibility factor $\varkappa = pV/NkT$, the estimated variance of which is

$$s^2_{\varkappa} = (\sigma^2/2\Delta r^2)^2 s^2_{\gamma_1} \quad . \tag{9.29}$$

In this equation σ is the hard-sphere diameter, not the theoretical scalar of Eq. (9.6).

Table 9.3 shows these estimates as obtained for realization B34, using the three different weight options; the degree of fit test of Section 9.2.2.2 indicated the linear fit $\nu = 1$ in all three cases. The degrees of freedom associated with these estimated standard deviations are so large ($f^{(12)} = 390$) that for purposes of assigning confidence intervals, etc., the t-factors for $f = \infty$ can be used, providing one is willing to accept the various approximations and assumptions involved, particularly the uncertainty and possible bias introduced by the degree of fit

TABLE 9.3 ESTIMATED CUMULATIVE DISTRIBUTION FUNCTIONS AND COMPRESSIBILITY FACTORS FOR REALIZATION B34

Weight Option	$\gamma_1 \cdot \Delta r^2 \cdot 10^2$	$\gamma_2 \cdot (\Delta r^2)^2 \cdot 10^4$	$\frac{pV}{NkT}$
# 1	5.587 ± 0.064	-3.186 ± 0.675	3.384 ± 0.027
# 2	5.585 ± 0.062	-3.162 ± 0.676	3.383 ± 0.027
# 3	5.579 ± 0.063	-3.052 ± 0.628	3.380 ± 0.027

selection, Section 9.2.2.2.

The rather close agreement of the estimated standard deviations given in Table 9.3 for the different weighting procedures is due primarily to the use in Eq. (9.28) of the pooled estimate $s^{(12)^2}$ of σ^2. Owing to the large value of $f^{(1)}$ compared to $f^{(2)}$, $s^{(12)^2}$ is dominated by $s^{(1)^2}$, the within-shell estimate of σ^2, which is essentially common to all three weighting procedures. If we had chosen to base our estimates instead on $s^{(2)^2}$, the estimate of σ^2 obtained from the variance of the average shell populations about the regression curve, the standard deviations given for this particular realization in Table 9.3 would have been slightly smaller, and for all realizations would have tended to vary more with the weight option. Confidence interval estimates, if made, would then, of course, use the t-factors for $f^{(2)} = 6$ degrees of freedom.

Such a procedure would have the advantage that the basic statistical assumption would then be hypothesis A, but with Δt equal to the entire

length of the realization. The assumption that the sampling distribution of $\overline{Y}_\alpha$ is normal with mean η_α is certainly better than the assumption that the ($\Delta t = 19\ 200$) $Y_{s\alpha}$ are s-independent samples from a normal distribution, also with mean α. The assumption of negligible α-correlation, on the other hand, is not necessarily improved by increasing Δt (though it is not likely to become worse).

In any case, in classes A and C the analysis of Chapter 8 indicates that the stronger assumption is reasonably tenable, and we have chosen to use it.

9.2.4 Survey of regression analysis results.

In Table 9.4 are displayed the goodness of fit and degree of fit statistics for the realizations of classes A and C, and the estimates of the compressibility factor and reduced pressure as well as their standard deviations. In each case, except for realization B12, the number of degrees of freedom associated with the standard deviation estimates is so large as to be effectively infinite so far as the t-test and confidence interval estimates are concerned.

The fractile values for the goodness and degree of fit tests are seen to be more or less reasonably distributed over the unit interval. For the goodness of fit test this can be interpreted as additional support for the pooling of $s^{(1)^2}$ and $s^{(2)^2}$. For the degree of fit statistic it can be taken as an indication that our procedure has not led to a systematic bias for all realizations, but it does not exclude the

TABLE 9.4 REGRESSION ANALYSIS RESULTS FOR CLASS A AND CLASS C REALIZATIONS

Class	τ	Realization	Weight Option	$n^{(b)}$	ν	Goodness of Fit F	Goodness of Fit P(F)	Degree of Fit P(t)	Compressibility Factor and Standard Deviation pA/NkT	Reduced Pressure and Standard Deviation pA_o/NkT
A	1.025	B 1	1	159	3	2.29	0.995 - 0.999	0.65	80.399 ± 0.292	78.438 ± 0.285
		B 2	1	99	3	0.89	0.3 - 0.5	0.10	80.315 ± 0.366	78.356 ± 0.357
		B 3	1	120	2	0.49	0.05 - 0.10	0.70	80.644 ± 0.354	78.696 ± 0.346
		B 4	1	99	2	1.64	0.95 - 0.975	0.61	80.962 ± 0.388	78.987 ± 0.378
	1.040	B 5	1	99	1	1.07	0.5 - 0.7	0.08	50.995 ± 0.215	49.034 ± 0.206
	1.074	B 6	1	98	2	0.89	0.3 - 0.5	0.34	97.199 ± 0.737	90.502 ± 0.686
	1.075	B 7	1	37	2	0.13	0.001	0.58	28.216 ± 0.158	26.247 ± 0.147
		B 8	1	49	1	0.79	0.3	0.28	28.301 ± 0.146	26.326 ± 0.136
	1.124	B 9	1	20	2	1.17	0.5 - 0.7	0.19	29.042 ± 0.208	25.838 ± 0.185
		B10	1	57	2	0.74	0.1 - 0.3	0.46	29.388 ± 0.237	26.146 ± 0.211
	1.125	B11	1	32	2	1.80	0.9 - 0.95	0.63	17.666 ± 0.084	15.703 ± 0.074
	1.150	B12[a]	2	35	2	—	—	0.3 - 0.4	42.587 ± 0.254	37.032 ± 0.220
	1.169	B13	1	32	1	2.45	0.975 - 0.99	0.86	18.545 ± 0.104	15.864 ± 0.089
	1.124	B14	1	99	1	0.73	0.3 - 0.5	0.92	10.277 ± 0.039	8.288 ± 0.032
C	1.500	B30	1	46	2	0.94	0.5 - 0.7	0.15	6.675 ± 0.065	4.450 ± 0.044
		B31	1	150	2	1.17	0.5 - 0.7	0.86	6.545 ± 0.032	4.363 ± 0.022
	1.650	B32	1	37	1	0.92	0.5 - 0.7	0.29	5.099 ± 0.042	3.090 ± 0.025
	1.750	B33	1	40	1	1.39	0.7 - 0.9	0.58	4.427 ± 0.036	2.530 ± 0.021
	2.000	B34	1	49	1	0.72	0.3 - 0.5	0.29	3.384 ± 0.027	1.692 ± 0.014
	2.400	B35	2	21	1	0.083	0.001 - 0.005	0.43	2.597 ± 0.026	1.082 ± 0.011
	3.000	B36	2	50	1	0.94	0.5 - 0.7	0.66	2.063 ± 0.012	0.6877 ± 0.0041
	3.900	B37	2	26	1	1.05	0.5 - 0.7	0.76	1.6766 ± 0.0103	0.4299 ± 0.0026
		B38	1	49	1	0.36	0.01 - 0.025	0.70	1.6976 ± 0.0056	0.4353 ± 0.0014
		B39	1	49	1	1.10	0.5 - 0.7	0.38	1.6960 ± 0.0055	0.4349 ± 0.0014

[a] For this realization, $s^{(2)}$ with $f^{(2)} = 15$ was used in the degree of fit tests, and in obtaining the estimated standard deviation of the compressibility factor and reduced pressure.

[b] The number of coarse-grained ($\Delta t = 19\,200$) observations included in the least squares data reduction.

possibility that we have chosen a polynomial of too low degree for any particular realization.

At five reduced areas we have more than one realization, the replicates being regarded as statistically independent either by virtue of having different values of the displacement parameter δ, or by virtue of the presence of low order noise introduced by code A (see Section 4.2). Comparison of the individual estimates of the equation of state obtained from such replicate realizations is of interest as an additional check upon the reliability of the internal precision estimates.

Comparison of realizations having the same observational parameters Δr^2 and K can be regarded as primarily a test of the more straightforward of our statistical procedures, since the same degree of regression polynomial would be expected to be more or less appropriate to both realizations, unless one should happen to be much longer than the other. Comparison of realizations with different values of these observational parameters can be regarded as more directly testing the reliability of the degree of fit criterion of Section 9.2.2.2.

The pairs (B1, B2), (B3, B4), and (B38, B39) have within each pair common values of Δr^2 and K. It is immediately evident from an inspection of the entries for these pairs in Table 9.4 that the between-realization differences of the compressibility factor estimates are consistent with their internally estimated standard deviations. Furthermore, the degrees of freedom associated with the latter are so large that inclusion of the between-realization differences would change the estimated standard

deviations only trivially.

All three of these pairs also enter into the comparison of realizations with different values of Δr^2 and K, so that it is convenient to pool each of these pairs into a single value of pV/NkT and an associated standard deviation. This is appropriately done by weighting the individual values by their number of observations n, it having been noted that there was no apparent dependence of the sampling variances σ_α^2 upon δ, even in the case of the pair (B38, B39) in which the two members had radically different values of this parameter. The pooled results are given in Table 9.5.

Turning now to the comparison of realizations with different values of Δr^2 and/or K, we will designate the individual results by $\kappa_1 \pm s_1$ and $\kappa_2 \pm s_2$, where $\kappa \equiv pV/NkT$, with the convention that subscript 1 designates the realization with larger Δr^2, if the values of this parameter are different, or that with larger K if the values of Δr^2 are the same. Be-

TABLE 9.5 POOLED RESULTS FOR REPLICATE REALIZATIONS HAVING COMMON VALUES OF Δr^2 AND K

Pair	$\frac{pV}{NkT}$	$\frac{pV_o}{NkT}$
B1, B2	80.367 ± 0.228	78.407 ± 0.222
B3, B4	80.798 ± 0.261	78.828 ± 0.255
B38, B39	1.6968 ± 0.0039	0.4351 ± 0.0010

cause of the large numbers of degrees of freedom involved, the simple u-test (u = standardized normal deviate) is appropriate:

$$u = \frac{\kappa_1 - \kappa_2}{\sqrt{s_1^2 + s_2^2}} \quad . \tag{9.30}$$

If the hypothesis of a common theoretical mean is acceptable (we regard the test as really being more a test of the reliability of the estimates s_1 and s_2), then the individual values can be pooled into a single estimate

$$\kappa_{12} = \frac{\kappa_1 s_1^{-2} + \kappa_2 s_2^{-2}}{s_1^{-2} + s_2^{-2}} \quad ,$$

$$s_{12} = \sqrt{[s_1^{-2} + s_2^{-2}]^{-1}} \quad .$$

This analysis is displayed in Table 9.6. The values of P(u) obtained by use of Eq. (9.30), and shown in the table, can be best described as only marginally in accord with expectations based upon the validity of the internally estimated standard deviations.

It is, of course, possible to make a direct comparison of the observed average shell populations $\overline{Y}_\alpha$ and the corresponding sample variance s_α^2 for replicate realizations, grouping shells to obtain common values of ζ_α when Δr^2 is different. The procedure is illustrated in Table 9.7 for the 11 shells which are common to realizations B30 and B31 at $\tau = 1.5$,

TABLE 9.6 COMPARISON OF REPLICATE REALIZATIONS HAVING DIFFERENT VALUES OF Δr^2 AND K

τ	Realizations	pV/NkT $\varkappa \pm \beta$	P(u) (Eq. 9.30)
1.025	B1, B2 (pooled)	80.367 ± 0.228	
	B3, B4 (pooled)	80.798 ± 0.261	
	All pooled	80.553 ± 0.172	0.107
1.075	B7	28.216 ± 0.158	
	B8	28.301 ± 0.146	
	Pooled	28.262 ± 0.107	0.346
1.124	B9	29.042 ± 0.208	
	B10	29.388 ± 0.237	
	Pooled	29.192 ± 0.158	0.136
1.500	B30	6.6747 ± 0.0654	
	B31	6.5450 ± 0.0324	
	Pooled	6.5706 ± 0.0290	0.038
3.900	B37	1.6766 ± 0.0103	
	B38, B39 (pooled)	1.6968 ± 0.0039	
	All pooled	1.6943 ± 0.0036	0.967

the value of Δr^2 being the same in the two experiments. We first test the assumption that for given α the internal variances σ_α^2 are the same in the two sampling distributions, by means of the F-ratio fractiles given in the fourth column of the table. These 11 values of $P[F_\alpha(45, 149)]$ are seen to scatter reasonably well over this unit interval. Under the null hypothesis their sum should be approximately[38] normally distributed with mean K/2 and variance K/12, so that an appropriate over-all statistic is the normal deviate

TABLE 9.7 COMPARISON OF AVERAGE SHELL POPULATIONS OF REALIZATIONS B30 AND B31

	Internal Variances $s^2_\alpha \cdot 10^4$			Pooled Variance	Shell Populations $\bar{Y}_\alpha \cdot 10^2$		
	Realization B30	Realization B31		$s^{(p)2}_\alpha$	B30	B31	
α	f_α=45	f_α=149	$P[F_\alpha(45,149)]$	f_α=194	n_α=46	n_α=150	$t_\alpha(194)$
1	0.4374	0.8321	0.01	0.7405	0.98151	0.95634	1.736
2	0.8035	0.8746	0.38	0.8581	0.96654	0.95080	1.008
3	0.7993	0.6780	0.76	0.7062	0.91173	0.91730	-0.393
4	0.7182	0.6673	0.63	0.6791	0.90523	0.89077	1.041
5	0.8273	0.6443	0.86	0.6867	0.88236	0.88133	0.074
6	0.6615	0.6544	0.53	0.6560	0.84402	0.85921	-1.113
7	0.4237	0.5840	0.11	0.5468	0.84365	0.84814	-0.360
8	0.5851	0.5341	0.66	0.5460	0.81794	0.81833	-0.031
9	0.4651	0.5731	0.21	0.5480	0.81683	0.80261	1.140
10	0.5994	0.5538	0.64	0.5643	0.80526	0.79256	1.003
11	0.3361	0.4473	0.13	0.4216	0.77293	0.77612	-0.292
	sum = 4.92					sum = 3.813	
	u = -0.61					u = 1.15	
	P(u) = 0.27					P(|u|) = 0.75	

$$u = \left(\frac{K}{12}\right)^{-\frac{1}{2}} \left[\left(\sum_{\alpha=1}^{K} P(F_\alpha)\right) - \frac{K}{2}\right] \quad .$$

For the example of Table 9.7, u = - 0.61, and P(u) = 0.27, so that the assumption of common theoretical variances σ_α^2 is reasonable. Accordingly, the two sets of values s_α^2 were pooled to obtain the values $s_\alpha^{(p)^2}$ given in the fifth column. The assumption of common theoretical means η_α is next examined for each shell by means of the t-test:[46]

$$t_\alpha(194) = \frac{\overline{Y}_\alpha^{(B30)} - \overline{Y}_\alpha^{(B31)}}{s_\alpha^{(p)}\left(\frac{1}{n_\alpha^{(B30)}} + \frac{1}{n_\alpha^{(B31)}}\right)} \quad .$$

The 11 values of this statistic are shown in the last column of Table 9.7. For so many degrees of freedom the t-distribution is well approximated by the standardized normal distribution, so an appropriate over-all statistic is the normal deviate

$$u = K^{-\frac{1}{2}} \sum_{\alpha=1}^{K} t_\alpha(194) = 1.15 \quad .$$

Since the above equation for $t_\alpha(194)$ could equally well have been written with the opposite sign, the appropriate fractile is $P(|u|)$, equal in the present example to 0.75. Thus, the agreement between realizations B30 and B31 is certainly statistically reasonable, which may be interpreted as additional support for our over-all hypothesis A for these realizations.

The analysis could be continued further, pooling the two sets of $\overline{Y}_\alpha$ to form a single set

$$\overline{Y}_\alpha^{(p)} = \frac{n_\alpha^{(B30)}\overline{Y}_\alpha^{(B30)} + n_\alpha^{(B31)}\overline{Y}_\alpha^{(B31)}}{n_\alpha^{(B30)} + n_\alpha^{(B31)}} \quad ,$$

then carrying out a regression analysis and calculating a compressibility factor using the set $\overline{Y}_\alpha^{(p)}$ according to the procedures of Sections 9.2.2 and 9.2.3. For the realizations at $\tau = 1.5$ we did not do so, but in the case of the four realizations at $\tau = 1.025$, for example, we first performed the above comparison and pooling (but not the subsequent regression analysis) of realization B1 with B2 (which have a common value of Δr^2), and also of B3 and B4. (B3 and B4 have one-half of the Δr^2 value of B1 and B2, so that their shells were first grouped in pairs to obtain shells of width equal to those in B1 and B2). The pooled data from B1 and B2 were then compared as outlined above with those from B3 and B4. The comparison statistics $P(|\mu|)$ so obtained are shown in Table 9.8 along with those from other replicate realizations in classes A and C. The values scatter reasonably well over the unit interval, which tends to support hypothesis A for these classes.

Our final statistical conclusion for classes A and C is that while the statistical errors in the average shell populations $\overline{Y}_\alpha$ are reasonably well estimated by standard techniques, our estimated compressibility factors have an additional unestimated component of variation, and a possible bias, arising from the stochastic nature of the degree of fit

TABLE 9.8 COMPARISON OF AVERAGE SHELL POPULATIONS IN REPLICATE REALIZATIONS

Reduced Area τ	Realizations	$-\log_2 \frac{\Delta r^2}{48a^2}$	K	P(μ)
1.025	B1 - B2	15	9	0.95
	B3 - B4	15	9	0.74
	(B1 - B2) - (B3 - B4)	15	9	0.69
1.075	B7 - B8	13	4	0.55
1.124	B9 - B10	13	4	0.30
1.5	B30 - B31	13	11	0.75
3.90	B38 - B39	13	14	0.62
	(B38 - B39) - B37	13	7	0.16

parameter ν. Intuitive considerations suggest that arbitrarily doubling the estimated standard deviations tabulated for the compressibility factor would result in an ample allowance for these uncertainties.

9.3 Class B Realizations

As discussed in detail in Chapter 6, there are serious uncertainties in the physical significance of our Monte Carlo calculations in the interval τ = 1.254-1.40. However, some of the realizations, particularly those near the end points of the reduced area interval, are reasonably well-behaved and possibly represent averages over physically reasonably well-defined regions of configuration space. Therefore, it seemed

desirable to make some attempt to apply the systematic data reduction procedures described in the preceding sections.

As was seen in Chapter 8, our basic statistical hypothesis A is not valid for realizations in this class. Thus, the procedures of Section 9.2 must be modified to take account of the circumstance that the internal, $\Delta t = 19\ 200$ shell population "variances" $s_\alpha^{(1)^2}$ no longer have their previous significance, since the $\Delta t = 19\ 200$ coarse-grained observations $Y_{s\alpha}$ from which they are calculated are evidently appreciably s-correlated. Consequently the goodness of fit test discussed in Section 9.2.2.1 is for the most part ignored, and the degree of fit criterion of Section 9.2.2.2 is modified to use only the variance $s^{(2)^2}$ of the average shell populations $\overline{Y}_\alpha$ (the average being taken either over the entire realization, or over a portion thereof; see below) about the estimated regression curve. Similarly the estimated standard deviation of the resulting compressibility factor is calculated from $s^{(2)^2}$.

As indicated in Section 9.2.3, this procedure is based on the untestable assumption of s-independence with $\Delta t = \hat{t}$, where $\hat{t}$ is the number of elementary Markov chain steps included in the averages $\overline{Y}_\alpha$. Furthermore, neither the presence of α-correlation nor the homoscedasticity of the variances σ_α^2 can be examined for $\Delta t = \hat{t}$ with the available data. Thus, the choice of the appropriate weighting procedure for the least squares data reduction is somewhat uncertain. As was mentioned in Section 9.1, a wrong weighting choice does not in itself introduce bias into the compressibility factor estimate, but in general leads to erroneous

estimates of its precision. The $\Delta t = 19\ 200$ variance s^2_α displayed the same systematic dependence on α that was noted in classes A and C, and since this behavior might well persist at larger values of Δt, we for the most part used linearly smoothed weight factors obtained from these $\Delta t = 19\ 200$ internal variances, as described in Section 9.2.1. It should be kept in mind that the precision estimates so obtained may be considerably in error due to α-correlation among the $\overline{Y}_\alpha$.

The results obtained in this way are summarized in Table 9.9. For those realizations in which no apparent "jumps" occurred, the averages $\overline{Y}_\alpha$ were taken over the entire run (with the usual omission of the first coarse-grained point). In the "jumpy" realizations, the averages were taken over "plateaus" which in some cases are reasonably well-defined, but in other cases were rather arbitrarily chosen. Clearly, this subjective element introduces still further uncertainty into both the significance of the quoted average and the associated precision estimate. These points have already been discussed in Chapter 6, particularly in Section 6.1.2. Here we simply emphasize again that such results should be regarded as only qualitative at best.

TABLE 9.9 REGRESSION ANALYSIS RESULTS FOR CLASS B REALIZATIONS

τ	Realization	Plateau[a]	Weight Option	n[b]	Degree of Fit ν	Degree of Fit P(t)	Compressibility Factor ± Standard Deviation pV/NkT	Reduced Pressure and Standard Deviation pV_o/NkT
1.254	B16	(H)	1	74	1	0.9	11.645 ± 0.051	9.286 ± 0.041
1.275	B17	(L)	1	100	2	0.6 - 0.7	9.280 ± 0.035	7.278 ± 0.027
1.290	B18	(L)	1	49	1	0.5 - 0.6	8.886 ± 0.039	6.888 ± 0.030
1.300	B19	2 - 80 (L)	1	79	1	0.8 - 0.9	8.747 ± 0.036	6.728 ± 0.028
		81 - 150 (H)	1	70	2	0.1 - 0.2	10.484 ± 0.089	8.065 ± 0.068
		120 - 150 (H)	1	31	2	0.2	10.732 ± 0.137	8.255 ± 0.105
1.316	B20	2 -19 (H)	1	18	1	0.6 - 0.7	10.017 ± 0.100	7.612 ± 0.076
		20 - 39 (L)	1	20	1	0.8 - 0.9	8.520 ± 0.068	6.474 ± 0.052
		40 - 82 (H)	1	43	2	0.6 - 0.7	9.941 ± 0.094	7.554 ± 0.071
1.325	B21	(L)	1	94	2	0.1 - 0.2	8.583 ± 0.061	6.478 ± 0.046
1.330	B22	1 - 14 (L)	2	14	1	0.7 - 0.8	8.359 ± 0.102	6.285 ± 0.077
		15 - 26 (H)	2	12	1	0.7 - 0.8	9.964 ± 0.056	7.492 ± 0.042
		86 - 95 (L)	2	10	1	0.8 - 0.9	8.236 ± 0.060	6.192 ± 0.045
1.340	B23	58 - 78 (L)	2	21	1	0.1 - 0.2	8.282 ± 0.098	6.181 ± 0.073
		102 - 141 (H)	1	20	1	0.8 - 0.9	9.370 ± 0.082	6.993 ± 0.061
1.350	B24	(H)	1	26	1	0.5 - 0.6	9.238 ± 0.075	6.843 ± 0.056
	B25	1 - 16 (L)	2	16	1	0.9 - 0.95	8.174 ± 0.065	6.055 ± 0.048
		28 - 40 (H)	2	13	2	0.2 - 0.3	10.050 ± 0.136	7.444 ± 0.101
	B26	(H?)	1	70	2	0.5 - 0.6	9.374 ± 0.056	6.944 ± 0.041
		42 - 71 (H)	1	30	2	0.6 - 0.7	9.674 ± 0.122	7.166 ± 0.090
1.355	B27	(H)	1	48	2	0.7 - 0.8	8.941 ± 0.064	6.599 ± 0.047
1.375	B28	(H)	1	91	2	0.2 - 0.3	8.667 ± 0.047	6.303 ± 0.034
1.400	B29	(H)	1	89	2	0.05 - 0.1	8.080 ± 0.053	5.771 ± 0.038

[a] If no numerical entry is given, the entire realization, with omission of the first Δt = 19 200 coarse-grained observation, was averaged. The entry n_1-n_2 means that the Δt = 19 200 coarse-grained observations $Y_{s\alpha}$, $s = n_1(1)n_2$, were averaged. The letter H or L in parentheses indicates that the result is believed to estimate a restricted average in the H or L region of configuration space (see Section 1.2.1).

[b] The number of coarse-grained (Δt = 19 200) observations included in the least squares data reduction.

Chapter 10

COMPARISON OF EQUATION OF STATE RESULTS FOR N = 12 AND 48

The most striking difference between the 12- and 48-molecule systems, namely, the qualitatively different topologies suggested for their configuration spaces by the behavior of the Monte Carlo calculations at intermediate (class B) reduced areas, has already been sufficiently discussed (Chapters 5 and 6). In this chapter we wish to make a somewhat more quantitative comparison of the calculated equations of state for the two systems at the high and low density extremes, where at least a modicum of theory is available.

10.1 High and Medium Densities

In comparing the N = 12 and N = 48 results at high densities we will make use of the Salsburg-Wood asymptotic analysis already discussed at some length in Chapter 3. For $\tau^* = 1$, corresponding to systems in which the accessible region of configuration space is a pocket surrounding the regular hexagonal configuration, Eq. (3.5) can be written

$$\pi(\tau; N) \equiv pV/NkT = \frac{1}{\tau^{\frac{1}{2}} - 1}\left[\tau^{\frac{1}{2}} - N^{-1} + \tfrac{1}{2}b(N)\ (\tau - 1) + O(\tau - 1)^2\right], \qquad (10.1)$$

where the coefficient b(N) is unknown. We define

$$\varkappa^*(\tau;\ N) = \frac{\tau^{\frac{1}{2}} - N^{-1}}{\tau^{\frac{1}{2}} - 1} \quad , \tag{10.2}$$

so that we can write

$$\Delta\varkappa_N(\tau) \equiv \varkappa(\tau;\ N) - \varkappa^*(\tau;\ N) = b(N) + O(\tau - 1); \tag{10.3}$$

note that $\varkappa^*(\tau;\ N)$ can be regarded as the "free-volume" equation of state (3.6) with an N^{-1} correction term appended.

We see that $\Delta\varkappa_N(\tau)$ should approach the unknown constant b(N) as $\tau \to 1$. In Fig. 10.1 we have plotted the values $\Delta\varkappa_N(\tau)$ obtained by substituting our Monte Carlo estimates (Tables 5.1 and 6.1) for $\varkappa(\tau;\ N)$ in Eq. (10.3), for both N = 12 and N = 48. The trend of the observations near $\tau = 1$ is somewhat obscured by their large scatter at $\tau = 1.025$. This is believed to be due mostly to the circumstance that $\varkappa$ is becoming rather large (≈ 80 at $\tau = 1.025$), with the result that quite small percentage errors in $\varkappa$ become large ones in $\Delta\varkappa_N$. The low N = 12, $\tau = 1.05$ point is believed to be due to a rather too large value of the observational parameter Δr^2 (Section 2.3.4) having been used in this realization. As a result the degree of fit criterion (Section 9.2.2.2) required use of a fourth degree regression polynomial, the highest encountered in this investigation. The abnormally high value of $\Delta\varkappa_N$ for N = 12, $\tau = 1.025$ is not understood.

Considering the $\tau \leq 1.25$ points, Figure 10.1 suggests, though it certainly does not establish, a value $b(N) \approx 0.6$ for both N = 12 and 48.

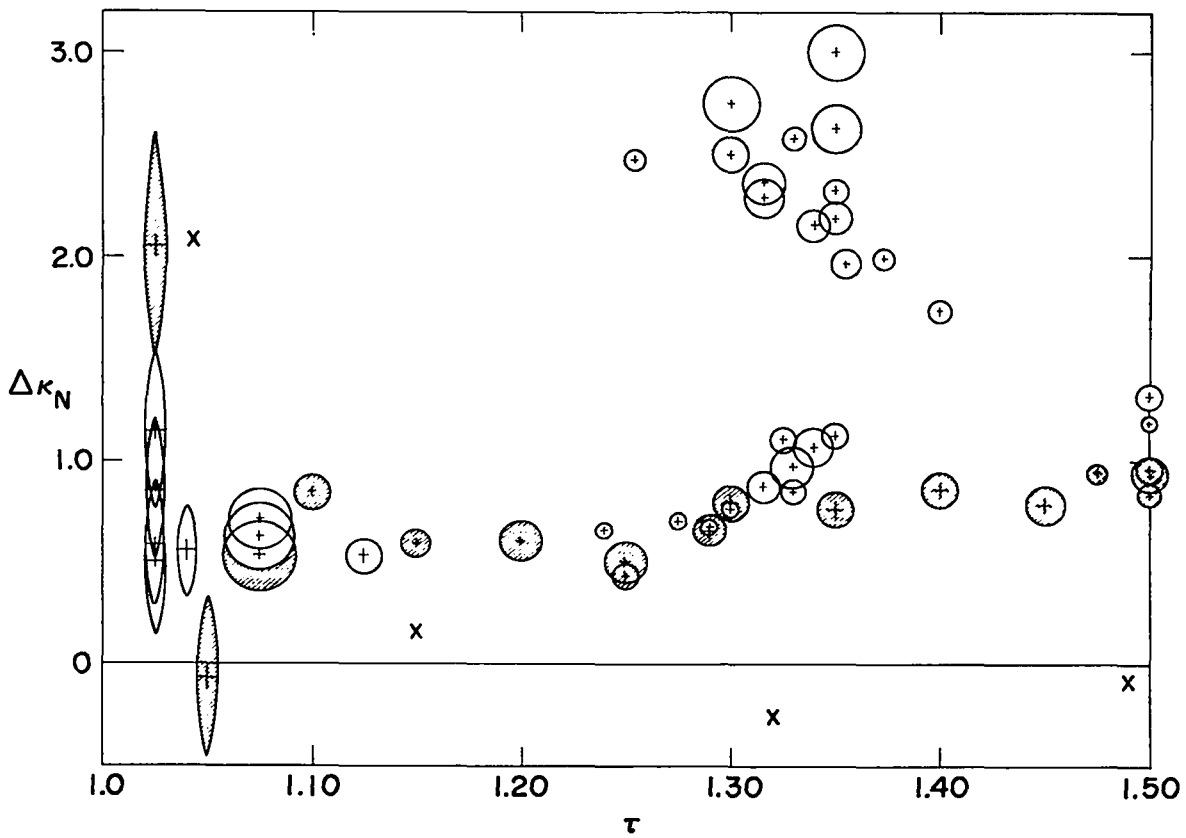

Fig. 10.1 Comparison of N = 12 (cross-hatched symbols) and N = 48 (open symbols) results at high and medium densities: $\Delta\kappa_N(\tau)$ vs. τ, Eq. (10.3). The vertical extent of the plotting symbols is one estimated standard deviation on both sides of the estimated mean; see Table 5.1 and 6.1. Also shown (x) are the points obtained by Metropolis et al.[1] for their 224-molecule system.

It should be noted, however, that in making this estimate we are using points well beyond the upper limits ($\tau = 1.136$ for $N = 12$, 1.063 for $N = 48$; see Sections 3.4 and 3.5) of reduced areas within which the asymptotic validity of Eq. (10.1) was rigorously established. Alternatively, as mentioned in earlier chapters, one can interpret Fig. 10.1 as suggesting that the asymptotic expression may be a useful approximation outside the rigorously established reduced area interval.

Figure 10.1 also affords a convenient comparison of the $N = 12$ and 48 results in the intermediate or class B density range. We should perhaps recall here that the large scatter of "fluid-branch" points for $N = 48$, $\tau = 1.35$ arises not so much from the inherent variability of the observations, as from the subjective uncertainties introduced in an attempt to estimate plateau averages in realizations in which such plateaus are at best very poorly defined.

Finally, it is probably worth observing that Fig. 10.1 supplies a graphical indication that our estimates of precision tend to be somewhat too small, at least in some density regions.

The 224-molecule points obtained by Metropolis et al.,[1] are also shown in Fig. 10.1. Here we again used Eq. (10.3), with $\varkappa^*(\tau; N)$ given by Eq. (10.2), even though this system does not, strictly speaking, have a close-packed reduced area per molecule corresponding to $\tau^* = 1$. Metropolis et al., chose to use a square area V for numerical convenience, whereas their initial configuration when hexagonally close-packed requires a rectangular cell of height $4\sqrt{3}/7 \approx 0.98974343$ and unit width. As a result the stable limiting configuration (in the sense of Salsburg-Wood,[18]

presuming one to exist) of this 224-molecule system has a reduced area somewhere in the interval $1.0 < \tau^* < 7/4\sqrt{3} \approx 1.010363$. The large value (Fig. 10.1) of $\Delta\mu_N$ at $\tau = 1.04269$, the highest density investigated by Metropolis et al., is presumed to be due to our use of $\tau^* = 1$ instead of the unknown correct value, in calculating $\Delta\mu_N$.

At lower densities these early Monte Carlo points lie below the present ones (Fig. 10.1). This could be due to a significant N-dependence of the coefficient b(N) in Eq. (10.1) (leaving aside the additional τ^*-dependence already mentioned, which would tend to make the early points fall still lower in Fig. 10.1), or, as suggested previously in Chapters 5 and 6 as being perhaps more likely, these points may be low because of insufficiently long realizations. Definitive resolution of this question must await further Monte Carlo investigation of larger two-dimensional systems than the present ones. The molecular dynamical results of Alder and Wainwright for their 870-molecule system can, of course, be regarded as supporting the latter conjecture.

10.2 Low Densities

In the low density region the analysis by Lebowitz and Percus (Chapter 3) of the N-dependence of the virial coefficients affords a theoretical framework for our discussion. They express the "normal" N-dependence, that is to say, the N-dependence at an area per molecule large enough so that the corresponding cluster integrals cannot wind

around the torus, of the ν-th virial coefficient in terms of the lower order (2 through ν - 1) virial coefficients of an infinite system. For two-dimensional hard spheres, the N = ∞ virial coefficients are known, from the second through the fifth, from the work of Metropolis et al.[1] If we write the virial expansion in the form

$$\varkappa(\tau;\ N) \equiv \frac{pV}{NkT} = 1 + \sum_{i=2}^{\infty} C_i(N)\tau^{-(i-1)} \quad , \tag{10.4}$$

and for convenience abbreviate

$$C_i(\infty) = C_i \quad , \tag{10.5}$$

then the values given by Metropolis et al., are

$$\begin{aligned} C_2 &= \pi 3^{-\frac{1}{2}} = 1.813799 \quad , \\ C_3 &= \frac{4}{9}\pi^2\left(1 - \frac{3\sqrt{3}}{4\pi}\right) = 2.57269 \quad , \\ C_4 &= 3.179 \quad , \\ C_5 &= 3.38 \pm 5\% \quad . \end{aligned} \tag{10.6}$$

In the calculation of C_4 these authors evaluated one of the three four-particle cluster integrals by an independent-sampling Monte Carlo technique, while for C_5 all the five-particle cluster integrals were so estimated.

Lebowitz and Percus give the "normal" N-dependence of $C_2(N)$ and $C_3(N)$. Using their equations we calculated similar expressions for the next two coefficients, obtaining

$$C_2(N) = C_2 - C_2N^{-1} \quad , \tag{10.7}$$

$$C_3(N) = C_3 + (2C_2^2 - 3C_3)N^{-1} + (-2C_2^2 + 2C_3)N^{-2} \quad , \tag{10.8}$$

$$\begin{aligned} C_4(N) = C_4 &+ (-4C_2^3 + 9C_2C_3 - 6C_4)N^{-1} \\ &+ (16C_2^3 - 27C_2C_3 + 11C_4)N^{-2} \\ &+ (-12C_2^3 + 18C_2C_3 - 6)N^{-3} \quad , \end{aligned} \tag{10.9}$$

$$\begin{aligned} C_5(N) = C_5 &+ (-24C_2^2C_3 + 9C_3^2 + 16C_2C_4 - 10C_5 + 8C_2^4)N^{-1} \\ &+ (192C_2^2C_3 - 51C_3^2 - 96C_2C_4 + 35C_5 - 80C_2^4)N^{-2} \\ &+ (-408C_2^2C_3 + 90C_3^2 + 176C_2C_4 - 50C_5 + 192C_2^4)N^{-3} \\ &+ (240C_2^2C_3 - 48C_3^2 - 96C_2C_4 + 24C_5 - 120C_2^4)N^{-4} \end{aligned} \tag{10.10}$$

In passing it is interesting to note two sum rules for the numerical coefficients in the above relations. First, if we set N = 1 we obtain $C_i(1) = 0$ for all i, corresponding to the obvious requirement that a 1-molecule periodic system must have the ideal gas equation of state. Second, if we set all $C_i \equiv c^{i-1}$, where c is any constant, corresponding to an equation of state

$$\varkappa(\tau, \infty) = \frac{\tau}{\tau - c} \quad ,$$

then we have $C_i(N) = (1 - N^{-1})C_i$. It is not clear to us why this last sum rule holds, and therefore, it may in fact not hold for $i > 5$. However, the validity of these two relations for Eqs. (10.7-10.10) affords

some assurance that the latter are correct, in spite of their derivations being somewhat tedious.

In principle, Eqs. (10.7 - 10.10) give the normal N-dependence for all the virial coefficients whose numerical values for $N = \infty$ are known. However, the quoted 5% uncertainty for C_5 combined with the varying signs and rather large magnitudes of the numerical coefficients in Eq. (10.10) result in the $O(N^{-1})$ coefficient in $C_5(N)$ being of uncertain sign. Thus we obtain

$$C_2(N) = 1.813799 - 1.813799N^{-1} \quad , \tag{10.11}$$

$$C_3(N) = 2.57269 - 1.13834N^{-1} - 1.43435N^{-2} \quad , \tag{10.12}$$

$$C_4(N) = 3.179 - 0.946N^{-1} + 4.45N^{-2} - 6.69N^{-3} \quad , \tag{10.13}$$

$$C_5(N) = 3.38 \pm 5\% - O(N^{-1}). \tag{10.14}$$

For comparison purposes it is convenient to define

$$\varkappa_{N,i}(\tau) = 1 + \sum_{j=1}^{i} C_{j+1}(N)\tau^{-j} \quad ; \tag{10.15}$$

that is, $\varkappa_{N,i}$ is the "normal" virial expansion for a system of N molecules, truncated to a polynomial of degree i in τ^{-1}. In Fig. 10.2 the difference $\varkappa_{N,i} - \varkappa_{\infty,4}$ is plotted for N = 12, 48, and ∞, and for i = 1(1)4, as well as the difference $\varkappa_{N,MC} - \varkappa_{\infty,4}$ for the Monte Carlo results, N = 12 and 48. In calculating $\varkappa_{N,4}$ we used $C_5(\infty) = 3.38$, $C_5(48) = 3.31$, $C_5(12) = 3.10$; the effect of a 5% change in this coefficient was in all cases small compared to the difference $\varkappa_{N,4} - \varkappa_{N,3}$.

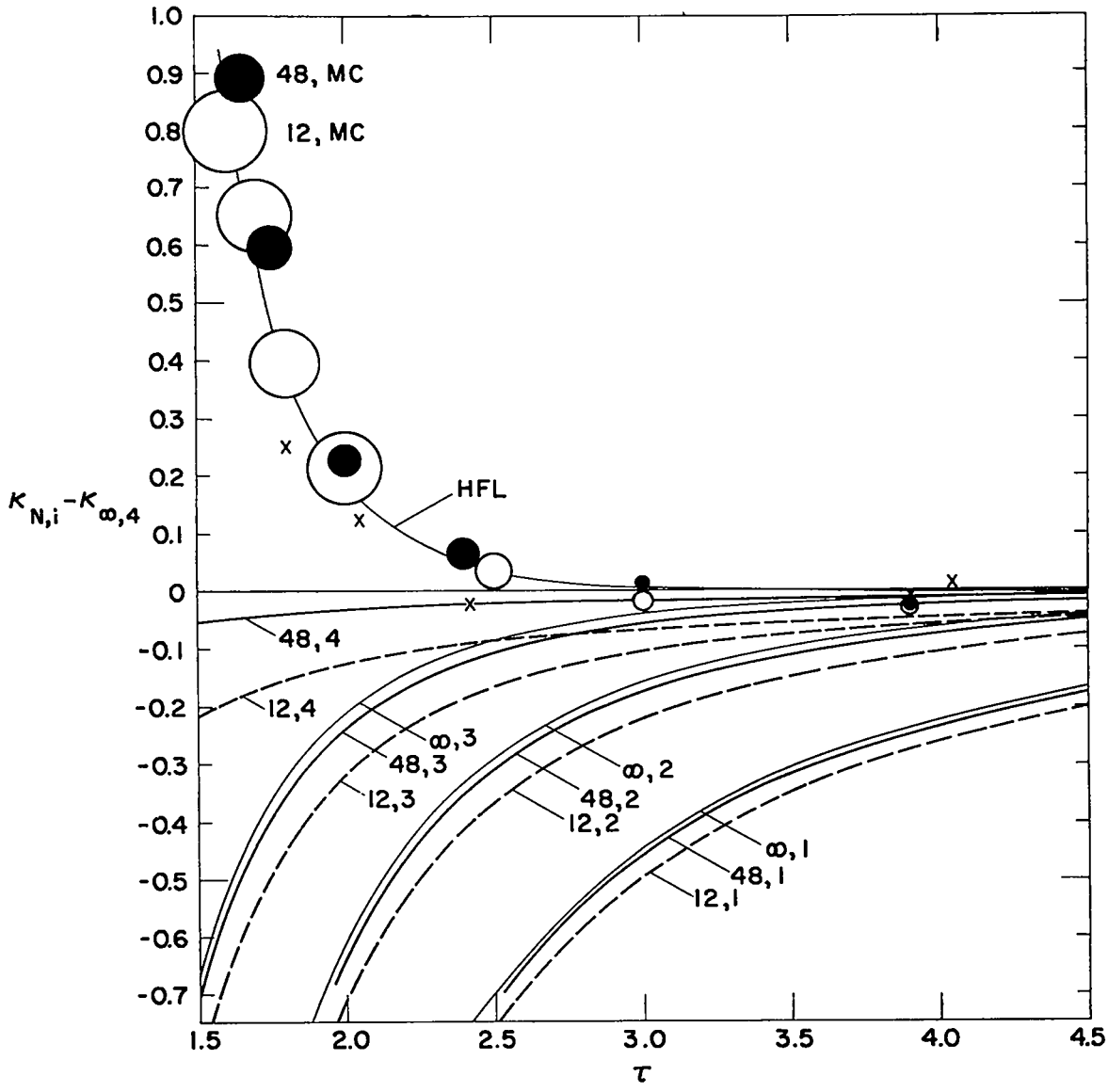

Fig. 10.2 Comparison of N = 12 (open circles) and N = 48 results (solid circles) at low density, with virial expansions to $O(\tau^{-i+1})$ for i = 1(1)4. The radii of the circles are the standard deviation estimates of Tables 5.1 and 6.1. The curves are the truncated virial expansions for the indicated values of N and i, all compressibility factors being plotted relative to that of an infinite system correct to $O(\tau^{-5})$. The finite-N virial coefficients include the "normal" N-dependence only; for N = 12 "anomalous" contributions to the fourth virial coefficient are present (and neglected in the $\kappa_{N,i}$ curves) below τ = 1.78, and to the fifth virial coefficient below τ = 2.78. The "scaled-particle" approximation HFL of Ref. 14 is also shown, as well as the original Monte Carlo results (x) of Metropolis et al.[1]

We note that the Monte Carlo points conform to our expectations in that the N = 12 points tend, on the whole, to fall below those for N = 48. In addition we note that, except for the point obtained from the short realization B37 at $\tau = 3.9$, all the points lie above the corresponding $\varkappa_{N,4}$ curve, in accordance with the widely held expectation that at least the next few (perhaps all) virial coefficients are positive. Finally, the trend of the $\varkappa_{N,i}$ curves for fixed N with increasing i is such as to suggest that only at $\tau = 3.9$ is the virial expansion to $O(\tau^{-5})$ reasonably convergent within the apparent statistical uncertainty of the Monte Carlo values.

Thus, we conclude that the calculations appear to be in qualitative agreement with the theoretical, low-density N-dependence. A more quantitative comparison would evidently require much more extensive calculations, particularly at $\tau > 4$.

The Metropolis et al.[1] points for N = 224 are also displayed in Fig. 10.2, and lie somewhat below the present N = 12 and N = 48 points except at the lowest density. For this large system all virial coefficients C_ν of order $\nu \leq 13$ have a "normal" N-dependence, which itself is rather small. Insofar as this normal N-dependence is concerned, the points for the larger system would be expected to lie above those for the smaller ones, although we are not aware of a proof of this conjecture. The contrary behavior of the 224-molecule points in Fig. 10.2 may possibly be due to the "anomalous" N-dependence of the 48-molecule virial coefficients of order $\nu \geq 5$, but may also be due, as mentioned repeatedly, to the early Monte Carlo calculations being somewhat too short.

Chapter 11

CONCLUSION

11.1 Necessity for Larger Systems

The implications of the small system results presented in this report with respect to the behavior of a macroscopic system of hard circles have been discussed in some detail in Section 6.5. Here we will simply remark that the necessity for studying systems of considerably more molecules is clearly evident. This is especially the case as regards the question of a phase transition; the present results are not conclusive either for or against this possibility. However, we again call attention to Alder and Wainwright's recent paper[15] (see Section 6.5.6) reporting a van der Waals loop in the molecular dynamical equation of state of a system of 870 hard circles.

Leaving aside for the moment the existence of these latter calculations, one might well be inclined to question the feasibility of machine calculations with $N \approx 1000$, in view of the increase in complexity noted in passing from $N = 12$ to $N = 48$ (or $N = 72$, in the case of the dynamical method).

In Section 6.5 we indicated how, in some respects, the topology of configuration space might perhaps be expected to become again less complex than for N = 48, at N >> 48, particularly at reduced areas in the "jumpy" range. In addition, the present results contain some suggestion that the number of Markov chain steps required for a given statistical accuracy in pV/NkT may increase somewhat more slowly than linearly with N. For example, Tables 5.1 and 6.1, as well as Fig. 10.2, show that for $\tau > 1.5$ the estimated standard deviations for N = 12 are in general appreciably larger than those for N = 48, in spite of the fact that, in terms of the number t/N of time steps per molecule, the 12-molecule realizations are longer than those for the 48-molecule system.

11.2 Faster Calculators

Calculations on larger systems are now more feasible than before, owing to the laboratory's acquisition of faster computing machinery than the IBM-704 machines used in these investigations. Using essentially the existing programs, the IBM-7090 is expected to roughly seven times as fast as the IBM-704, while the IBM-7094 (expected within a few months) will be still faster, but probably not by so much as a factor of 2.

Speed ratios between the IBM-7030 and the IBM-7090 are quite sensitive to the nature of the program, being larger for programs involving much "floating point" arithmetic (especially multiplications) than for programs consisting primarily of logical or "red-tape" work. The Monte Carlo calculations, especially for hard spheres or circles, are

unfortunately of the latter type, so that the IBM-7030 is likely to be no more than twice as fast as the IBM-7090 at values of N small enough to permit both machines to retain all the data in internal memory. The larger IBM-7030 memory is, of course, advantageous in the latter regard.

11.3 Improvements in Programming and in Choice of Parameters

In the paper[5] describing some of the computational details, we mentioned that a significant increase in speed could be obtained if it were proved adequate to represent the molecular coordinates (x_i, y_i) by few enough bits to allow the Pythagorean computation of squared intermolecular distances,

$$r_{ij}^2 = (x_i - x_j)^2 + (y_i - y_j)^2 \quad ,$$

to be carried out by table-look-up of $(x_i - x_j)^2$ rather than by multiplication. Some preliminary investigations of this possibility were carried out on the N = 32 hard-sphere system, with results suggesting that it was feasible at least in the "jumpy" region around $\tau = 1.55$. Considerably more calculations would be required in order to be certain that adequate space resolution was being provided over the complete range of interesting densities. Also, as faster computing machines appear, their multiply-time to add-time ratio tends to decrease, so that the speed improvement obtainable by this device decreases. Finally the required number of bits must eventually increase as N increases, simple considerations indicating proportionability to $N^{\frac{1}{2}}$. Consequently we

will probably not use this technique in future calculations. Some increase in speed is obtainable, however, by incorporating some of the other program improvements mentioned in Ref. 5.

There are also various other areas in which the calculation can perhaps be improved. For example, only at $\tau = 3.9$ and for $N = 48$ have we made any statistical examination of the effect of the displacement parameter δ upon the rate of convergence of the Markov chains. The machine time per step and the observed shell population variances s_α^2 (Eq. 8.3) changed only slightly with large changes in δ indicating that at least at this low density the convergence rate is not strongly dependent on δ. This comparison was also useful in showing that at this low density, at least, our previous[5] rate-of-convergence criterion involving the root-mean-square displacement

$$\ell = \left\{\frac{1}{t}\sum_{t'=1}^{t}\left[\vec{r}_{i(t')}(t') - \vec{r}_{i(t')}(t'-1)\right]^2\right\}^{\frac{1}{2}} ,$$

in the notation of Section 2.3.2, is actually a very unreliable measure of convergence rate, at least at low density. This is evident from the fact that realization B39 had a value of ℓ about 17 times that of B38, whereas our statistical tests indicate the two realizations to be about equally convergent.

Other areas in which more investigation might possibly be worthwhile are the optimum values of the parameters Δr^2, K, and Δt, as well as further statistical tests on the pseudo random number sequence. In the latter connection it would be desirable to have several independent

sequences, rather than to use the same sequence for all realizations.

11.4 Constant Pressure Ensemble

In Chapters 7 through 9 we saw that the numerical differentiation required for the equation of state calculation is the source of considerable difficulty in the data-reduction process, in particular being responsible for the questionable validity of our estimated standard deviations. Evidently, it would be desirable to calculate the pressure directly as the simple average of a configuration function, rather than as the derivative of such an average. Unfortunately, no such expression is known for the petit ensemble pressure of a system of hard spheres (or circles). However, the Markov chain method is not restricted to the petit ensemble, and in fact we have made some fairly extensive, but unpublished, calculations for a system of 32 hard spheres in the isothermal, isobaric ensemble,[47] usually called the constant-pressure ensemble for brevity. In this ensemble the variables p, T, and N are fixed, while the other variables, in particular the volume V, fluctuate. The equation of state is calculated from the ensemble average of this fluctuating volume,

$$\kappa = p\langle V\rangle/NkT \quad ,$$

$$\tau = \frac{\langle V\rangle}{Nv_o} \quad .$$

The resulting $\kappa(\tau; N)$ relation differs from that obtained with the petit ensemble by terms of $O(N^{-1})$, which is, of course, not serious since the

petit ensemble equation of state deviates by the same order from the thermodynamic equation of state. Since no numerical differentiation is required, the constant-pressure ensemble data-reduction problem is considerably simplified.

The motivation for the unpublished hard-sphere calculations in this ensemble was not, however, the easier data reduction, but rather the hope that the fluctuation in configuration space topology produced by the volume fluctuation would materially increase the transition probability between different configuration space regions, e.g., regions L and H in terms of the hourglass description. In this ensemble, strictly speaking, all state points are accessible from each other, i.e., there are no isolated pockets of configuration space, due to the always non-vanishing (but no doubt very small, at high pressure) probability of occurrence of arbitrarily large values of V. Most of the calculations were carried out in the so-called "transition region" in the vicinity of $\tau = 1.5$ to 1.6, see Fig. 1.1. Here it will suffice to mention that the results agreed quite well with those of the petit ensemble method. In particular, "jumps" still occurred, now of course, at constant pressure between different levels of the fluctuating volume, indicating that at these densities configuration space is still rather effectively compartmentalized. The "jumps" were perhaps slightly more frequent in terms of Markov time steps than in comparable petit ensemble realizations, as expected. However, the computing time per step is also somewhat increased due to certain additional complexities inherent in the constant-pressure formulation.

Thus, the two methods appear to be roughly equally effective in coping with the difficult topology of hard-sphere (or circle) configuration spaces. The greater simplicity of the data-reduction problem in the constant-pressure ensemble then makes it quite attractive for use in future investigations. There is, however, an important difference in the two equations of state. Whereas in the petit ensemble, so far as is known, the exact equation of state for a finite system may possess a "Van der Waals loop," in the constant-pressure ensemble, $\langle V \rangle$ is known to be a monotonically decreasing function of P. Thus, the manifestation, at finite N, of a first-order phase transition would presumably be a p-V isotherm having a nearly horizontal portion in the vicinity of the thermodynamic ($N = \infty$) coexistence region.

However, it is possible to obtain the petit ensemble equation of state, as well as the constant-pressure ensemble equation of state, from a Monte Carlo calculation based on the latter ensemble, if the probability density $P_{N\hat{p}T}(V)$ of the fluctuating volume can be estimated sufficiently accurately.[48] To avoid confusion, in the remainder of this section we will use the notation $\hat{p}$ for the non-fluctuating pressure parameter of the isobaric-isothermal ensemble, and $p = p(V)$ for the corresponding (same N, T) petit ensemble pressure at any fixed volume V. The probability density $P_{N\hat{p}T}(V)$ is defined as

$$P_{N\hat{p}T}(V) = \frac{Z_N(V)e^{-\hat{p}V/kT}}{\hat{Z}_N(\hat{p})} \quad , \tag{11.1}$$

with

$$\hat{Z}_N(\hat{p}) = \int_0^\infty Z_N(V) e^{-\hat{p}V/kT} dV \quad ,$$

and with $Z_N(V)$ given by Eq. (2.1). From Eq. (2.3) one then readily finds the petit canonical ensemble pressure $p(V)$ to be given by

$$p = \hat{p} + kT \left(\frac{\partial \ell n \, P_{N\hat{p}T}(V)}{\partial V} \right)_{N,\hat{p},T} \quad . \tag{11.2}$$

From this relation we see that there is a one-to-one correspondence between the presence of a van der Waals loop in the petit canonical ensemble equation of state on the one hand, and a bimodal probability density $P_{N\hat{p}T}(V)$ on the other. The latter function can, of course, be estimated by the Monte Carlo method. We note, however, that subsequent estimation of the petit ensemble equation of state requires a numerical differentiation in which we may expect many of the same statistical difficulties as we encountered with the petit ensemble method. Nevertheless, the above discussion lends further encouragement to use of a constant-pressure ensemble Monte Carlo method, since a bimodal $P_{N\hat{p}T}(V)$ should be an at least as easily detected qualitative indication of a possible first-order phase transition as is a loop in the equation of state.

11.5 A Word of Caution

We would like to emphasize that the finite system effects which have been described for systems of 12 and 48 hard circles almost surely have analogues in the previous investigations of three-dimensional

hard-sphere and Lennard-Jones molecules, which were mostly done with 32- and 108-molecule systems. Thus these results, particularly any interpretation in terms of the existence and location of a phase transition, should be regarded with some skepticism until such time as it appears feasible to examine considerably larger three-dimensional systems. With present equipment, systems of 1000-2000 molecules would be feasible, though time consuming. Even at these values of N, however, "surface" effects would be expected to be of considerable importance in three dimensions, so that it seems preferable to first verify the behavior reported by Alder and Wainwright for two-dimensional systems of such a size.

11.6 Is It Worthwhile?

It is clear that the Monte Carlo method is certainly not a quick and easy way of determining exact equations of state. It requires large amounts of computing time, especially for the large values of N which seem to be required, and the results require careful interpretation. The latter tends to be expensive in terms of personnel time.

On the other hand, in spite of the many recent advances in statistical mechanics, reliable analytical equations of state covering the entire density range seem to be as far in the future as ever; in particular, a theoretical proof of the existence or non-existence of a hard-sphere phase transition is completely lacking. The only comparable equation of state tool seems to be the Alder and Wainwright dynamical

method. For systems of hard spheres (or circles), the two methods seem to be of comparable efficiency; we regret the slow pace of our investigation, which is not due to inherent difficulties of the technique, but to the frequent diversion of our attention to other problems. For continuous inter-molecular potentials the Monte Carlo method appears to be advantageous. Furthermore, given the difficulties of interpretation and the different theoretical foundations of the two methods, it appears to be desirable to investigate the same or similar systems by both techniques, at least for the present.

Thus, it appears to us to be worthwhile to continue these investigations. One of the purposes of this long report was to make it possible to solicit the informed opinion of others. Comments by the reader who has persevered to this point will, accordingly, be appreciatively received.

REFERENCES

1. N. Metropolis, A. W. Rosenbluth, M. N. Rosenbluth, A. H. Teller, and E. Teller, J. Chem. Phys. 21, 1087 (1953).

2. W. W. Wood and F. R. Parker, J. Chem. Phys. 27, 720 (1957).

3. W. W. Wood and J. D. Jacobson, J. Chem. Phys 27, 1207 (1957).

4. W. W. Wood, F. R. Parker, and J. D. Jacobson, Nuovo Cimento (Suppl.) 9, 133 (1958).

5. W. W. Wood and J. D. Jacobson, Proceedings of the Western Joint Computer Conference, San Francisco, Institute of Radio Engineers, New York (1959), p. 261.

6. M. N. Rosenbluth and A. W. Rosenbluth, J. Chem. Phys. 22, 881 (1954).

7. B. J. Alder and T. E. Wainwright, J. Chem. Phys. 31, 459 (1959).

8. A brief summary of the present state of this question has been given recently by G. Birkhoff and R. E. Lynch, Los Alamos Scientific Laboratory (Los Alamos, New Mexico) report LA-2618, pp. 31-33, September 1961.

9. B. J. Alder and T. E. Wainwright, J. Chem. Phys. 27, 1208 (1957).

10. B. J. Alder and T. E. Wainwright, J.Chem. Phys. 33, 1439 (1960).

11. W. W. Wood, J. Chem. Phys. 20, 1334 (1952).

12. T. L. Hill, Statistical Mechanics (McGraw-Hill Book Company, Inc., New York, 1956), Appendix IX, p. 413.

13. G. D. Scott, Nature 188, 908 (1960), and other references cited therein.

14. E. Helfand, H. L. Frisch, and J. S. Lebowitz, J. Chem. Phys. 34 1037 (1961).

15. B. J. Alder and T. E. Wainwright, Phys. Rev. 127, 359 (1962).

16. C. A. Rogers, Proc. London Math. Soc. (3) 8, 609 (1958).

17. J. L. Lebowitz and J. K. Percus, Phys. Rev. 124, 1673 (1961).

18. Z. W. Salsburg and W. W. Wood, J. Chem. Phys. 37, 798 (1962).

REFERENCES

19. N. Metropolis, Proceedings of the Symposium on Monte Carlo Methods, H. A. Meyer, editor, (John Wiley and Sons, Inc., New York, 1956) pp. 29-36.

20. J. D. Bernal, Nature 183, 141 (1959).

21. J. L. Doob, Stochastic Processes (John Wiley and Sons, Inc., New York, 1953) pp. 221-232.

22. J. G. Kemeny and J. L. Snell, Finite Markov Chains (D. Van Nostrand Co., Inc., Princeton, New Jersey, 1960) p. 89.

23. H. B. Dwight, Tables of Integrals and Other Mathematical Data (The Macmillan Co., New York, 1947) p. 10.

24. A. Hald, Statistical Theory with Engineering Applications (John Wiley and Sons, Inc., New York 1952) pp. 342-349.

25. Ibid., pp. 357-358, and the paper cited in ibid., p. 373.

26. F. Mosteller, Ann. Math. Stat. 12, 228 (1941).

27. Hald, op. cit., pp. 280-285.

28. Hald, op. cit., pp. 224-239.

29. A. Hald, Statistical Tables and Formulas (John Wiley and Sons, Inc., New York, 1952).

30. C. A. Bennett and N. L. Franklin, Statistical Analysis in Chemistry and the Chemical Industry (John Wiley and Sons, Inc., New York, 1954) pp. 677-684.

31. B. I. Hart, Ann. Math. Stat. 13, 445 (1942). It should be noted that Hart defines $r^{(\alpha)}$ according to Eq. (8.2), but with n - 1 in Eq. (8.3) replaced by n.

32. H. Cramér, Mathematical Methods of Statistics (Princeton University Press, 1946) p. 411. Cramér gives the variance $D^2(C)$ only to $O(n^{-3})$; the exact expression, our Eq. (8.6), is easily derived following the procedure outlined by Cramér.

33. Ibid., p. 183.

REFERENCES

34. Hald, Ref. 24, pp. 609-611.

35. Cramér, op. cit., pp. 386-387.

36. E. S. Pearson and H. O. Hartley, Biometrika Tables for Statisticians, Vol. 1 (Cambridge University Press, England, 1954) Table 34B, p. 183.

37. E. S. Pearson, Properties of Higher Moments and Cumulants. Technical Report No. 47 of the Statistical Techniques Research Group, Department of Mathematics, Princeton University, December 1961.

38. Cramér, op. cit., p. 245.

39. A. C. Aitken, Proc. Roy. Soc. Edinburgh 55, 42 (1934).

40. A. Michels, J. C. Abels, C. A. Ten Seldam, and W. de Graaff, Physica 26, 381 (1960).

41. Hald, Ref. 24, p. 300.

42. See, for example, the procedure of Hald, Ref. 24, pp. 551-557, for weighted least squares. The discussion is easily generalized to any regression function in which the unknown parameters appear linearly.

43. See Ref. 42, but note that the distribution usually named the "F distribution" by American writers is there called the "v^2-distribution."

44. Hald, Ref. 24, p. 540.

45. Hald, Ref. 24, p. 226.

46. Hald, Ref. 24, p. 394.

47. Hill, op. cit.

48. Hill, op. cit., p. 415. A similar relation, between petit-ensemble variables and the grand canonical ensemble probability density $P_{\mu VT}(N)$ of the fluctuating number of molecules has been used by Professor Z. W. Salsburg in Monte Carlo calculations for lattice gases. I am indebted to him for discussion of this work, which suggested use of the constant-pressure ensemble relations outlined here.